SPECTRAL INVESTIGATION AND CRYSTAL STRUCTURES OF SOME TRANSITION METAL COMPLEXES OF AROYLHYDRAZONES

Thesis submitted to

Cochin University of Science and Technology

in partial fulfillment of the requirements

for the award of the degree of

Doctor of Philosophy

Under the Faculty of Science

by

YAMUNA S. NAIR

Department of Chemical Oceanography
Cochin University of Science and Technology
Kochi 682 016

March 2016

Spectral investigation and crystal structures of some transition metal complexes of aroylhydrazones

Ph. D. Thesis under the Faculty of Science

Author:

Yamuna S. Nair
Research Fellow, Department of Chemical Oceanography
Cochin University of Science and Technology
Kochi 682 016
India
Email: *yamuna.nair@christuniversity.in*

Supervising guides

Dr. M.R. Prathapachandra Kurup
Professor
Department of Applied Chemistry
Cochin University of Science and Technology
Kochi 682 022
India
Email: mrp@cusat.ac.in

Dr. S. Muraleedharan Nair
Professor and Head
Department of Chemical Oceanography
Cochin University of Science & Technology
Kochi 682 016
India
Email: muralis@cusat.ac.in

Department of Chemical Oceanography
School of Marine Sciences
Cochin University of Science and Technology
Kochi 682 016
India

March 2016

Front cover: Hydrogen bonding interactions of $[Co(HFPB)_2]Br_2 \cdot 2H_2O$

Back cover: C–H$\cdots$O hydrogen bonding interactions connecting adjacent molecules in $[Ni(FPB)_2]$

Om Namah Shivaya

The universe bows to Lord Shiva.
I bow to Lord Shiva

Dedicated to my family

Certificate

Certified that the thesis entitled *"Spectral investigation and crystal structures of some transition metal complexes of aroylhydrazones"* submitted by *Ms. Yamuna S. Nair* in partial fulfillment of the requirements for the degree of Doctor of Philosophy, to the Cochin University of Science and Technology, Kochi-22, is an authentic record of the original research work carried out by her under our guidance and supervision in the Department of Chemical Oceanography, School of Marine Sciences, Cochin University of Science and Technology. The results embodied in this thesis, in full or in part, have not been submitted for the award of any other degree. All the relevant corrections and modifications suggested by the audience and recommended by the doctoral committee of the candidate during the presynopsis seminar have been incorporated in the thesis.

Dr. M.R. Prathapachandra Kurup
Professor
Department of Applied Chemistry
Cochin University of Science and Technology
Kochi-682022

Dr. S. Muraleedharan Nair
Professor and Head
Department of Chemical Oceanography
School of Marine Sciences
Cochin University of Science and Technology
Kochi-682016

Declaration

I hereby declare that the work presented in this thesis entitled *"Spectral investigation and crystal structures of some transition metal complexes of aroylhydrazones"* is entirely original and was carried out independently under the supervision of **Prof. M.R. Prathapachandra Kurup**, Department of Applied Chemistry, Cochin University of Science and Technology and has not been included in any other thesis submitted previously for the award of any other degree.

01-03-2016   **Yamuna S. Nair**
Kochi-22

Acknowledgement

Completion of this research work was possible only with the support of several others. I would like to express my sincere gratitude to all of them.

First and foremost I am deeply grateful to my supervising guide Prof. (Dr.) M.R. Prathapachandra Kurup, Department of Applied Chemistry, CUSAT for his valuable guidance, scholarly inputs, consistent encouragement and unconditional support throughout my research work. I consider it as a great opportunity to do my doctoral programme under his guidance and to learn from his research expertise.

I express my sincere gratitude to my co-guide Prof. (Dr.) S. Muraleedharan Nair, Department of Chemical Oceanography, CUSAT for the academic support and facilities provided to carry out my research work at Department of Chemical Oceanography, CUSAT.

I also thank Prof. (Dr.) Sujatha and Prof. (Dr.) N. Chandra Mohanakumar for their concern and good wishes. I am thankful for the support received from all the non-teaching staff of the Department of Chemical Oceanography, CUSAT.

I am indebted to all the staff of SAIF, Kochi, IIT Madras and IIT Bombay for the services rendered for sample analyses.

This work would not have come to conclusion without the help I received from my research colleagues Ambili, Mridula, Sajitha, Dr. Bibitha, Dr. Jinsa, Nisha, Lincy, Movitha, Baiju, Rajesh and Karthik.

▐▐▐ Preface ▐▐▐

Aroylhydrazones and their metal complexes have been extensively studied over past few decades. These types of complexes have been vigorously explored in recent years and such studies have been the subject of many papers and reviews. Aroylhydrazones offer a versatile and flexible series of ligands able to bind with various metal ions to give complexes with suitable properties for theoretical and practical applications. Hydrazones derived from aromatic acid hydrazides and aromatic or heterocyclic aldehydes have a wide variety of applications in many fields, *e.g.*, biological, inorganic and analytical chemistry.

The present interest in the coordination chemistry of aroylhydrazones stems from their ligational behavior. This versatility in ligand design provides the straightforward modulation of the sterics, electronics, and chirality at the central metal ion. This in turn allows for the investigation of structure-function relationships in diverse areas from catalysis to material chemistry. In the current work, we chose two novel aroylhydrazones as principal ligands. The hydrazones under investigation were characterized by IR, UV and NMR spectral studies. The molecular structure of both the hydrazones was solved by single crystal XRD studies. In the present study copper(II), nickel(II), cobalt(II), iron(III), manganese(II), zinc(II) and cadmium(II) complexes were synthesized and characterized by various spectroscopic techniques, molar conductivity and magnetic susceptibility measurements. Single crystals of some of the complexes were isolated and characterized by single crystal X-ray diffraction.

The work embodied in this thesis was carried out by the author in the Department of Chemical Oceanography, CUSAT, Kochi, during the period 2010-2016. The thesis is divided into seven chapters. Chapter 1 gives an introduction on hydrazones, diversity in their chelating behavior and their application in various fields. This chapter also describes different analytical techniques employed for the characterization of hydrazones and their metal complexes. Chapter 2 includes the synthesis and characterization of two novel NNO donor aroylhydrazones. Chapters 3-7 discuss the synthesis and characterization of some transition metal complexes derived from the aroylhydrazones under study. A brief summary and conclusion of the work is also included in the last part of the thesis.

▌▌▌ Contents ▌▌▌

Chapter-3
SYNTHESES, SPECTRAL CHARACTERIZATION AND CRYSTAL STRUCTURE OF COPPER(II) CHELATES OF TRIDENTATE AROYLHYDRAZONES

Chapter-4
SYNTHESES, SPECTRAL CHARACTERIZATION AND CRYSTAL STRUCTURE OF NICKEL(II) CHELATES OF TRIDENTATE AROYLHYDRAZONES

CURRICULUM VITAE

List of Abbreviations

HFPB·H$_2$O	3-Fluoropyridine-2-carbaldehyde benzoylhydrazone monohydrate
HFPN·2H$_2$O	3-Fluoropyridine-2-carbaldehyde nicotinoylhydrazone dihydrate
DMF	N,N-dimethylformamide
Complex **1**	[Cu$_2$(FPB)$_2$(μ-NCS)$_2$]
Complex **2**	[Cu(HFPB)(SO$_4$)]·H$_2$O
Complex **3**	[Cu(FPB)(ClO$_4$)]
Complex **4**	[Cu(FPB)(OAc)(H$_2$O)]
Complex **4a**	[Cu(FPB)(OAc)(H$_2$O)]·H$_2$O
Complex **5**	[Cu(FPB)(N$_3$)(H$_2$O)$_2$]
Complex **6**	[Cu(FPB)$_2$]
Complex **7**	[Cu(FPN)$_2$]
Complex **8**	[Cu(FPN)(OAc)(H$_2$O)]
Complex **9**	[Ni(FPB)(NO$_3$)]·2H$_2$O
Complex **10**	[Ni(HFPB)(FPB)]Cl
Complex **11**	[Ni(FPB)(OAc)(DMF)]
Complex **12**	[Ni(FPB)(ClO$_4$)]·DMF
Complex **13**	[Ni(FPB)$_2$]
Complex **14**	[Ni(FPN)(ClO$_4$)]
Complex **15**	[Co(HFPB)$_2$]Br$_2$·2H$_2$O
Complex **16**	[Co(HFPB)(FPB)](OAc)·DMF
Complex **17**	[Co(FPB)$_2$]
Complex **18**	[Co(HFPN)Br$_2$]
Complex **19**	[Co(FPN)$_2$]
Complex **20**	[Co(FPN)(OAc)]
Complex **21**	[Mn(FPB)$_2$]
Complex **22**	[Mn(FPB)(OAc)(H$_2$O)$_2$]·H$_2$O
Complex **23**	[Fe(FPB)$_2$]FeCl$_4$·H$_2$O
Complex **24**	[Fe(FPN)$_2$]FeCl$_4$
Complex **25**	[Zn(HFPB)$_2$](ClO$_4$)$_2$
Complex **26**	[Zn(HFPB)(SO$_4$)]
Complex **27**	[Zn(HFPB)Cl$_2$]
Complex **28**	[Zn(HFPN)Cl$_2$]
Complex **29**	[Cd(FPB)(ClO$_4$)]·DMF

…..�808…..

AN OVERVIEW ON AROYLHYDRAZONES

1.1. Introduction

Coordination complexes have been known since the beginning of modern chemistry. The coordination chemistry was pioneered by Nobel Prize winner Alfred Werner (1866-1919). He received the Nobel Prize in 1913 for his coordination theory of transition metal-amine complexes. At the start of the 20th century, inorganic chemistry was not a prominent field until Werner studied the metal-amine complexes such as $[Co(NH_3)_6Cl_3]$.

The applications of coordination compounds in chemistry and technology are many and varied. The brilliant and intense colors of many coordination compounds, such as Prussian blue, render them of great value as dyes and pigments. Coordination compounds also cover a large area in

the field of metallurgy, analytical and medicinal chemistry. A technological and scientific development of major significance was the discovery in 1954 that certain metal complex catalysts bring about the polymerization of organic compounds under mild conditions to form polymers of high molecular weight and highly ordered (stereoregular) structures.

Metal complexes play a variety of important roles in biological systems. Many enzymes, the naturally occurring catalysts that regulate biological processes, are metal complexes (metalloenzymes). Hemoglobin also contains iron-porphyrin complexes, its role as an oxygen carrier being related to the ability of the iron atoms to coordinate oxygen molecules reversibly. Other biologically important coordination compound is chlorophyll (a magnesium-porphyrin complex) which is an extremely important and critical biomolecule in the photosynthesis.

The formation of coordination compounds should satisfy the essential properties such as the number and arrangement of the ligands attached to the central metal atom or ion-that is, the coordination number and the coordination geometry, respectively. The coordination number of a particular complex is determined by the relative sizes of the metal atom and the ligands, by spatial (steric) constraints governing the shapes (conformations) of polydentate ligands, and by electronic factors, most notably the electronic configuration of the metal ion. Although coordination numbers from 1 to 16 are known, those below 3 and above 8 are rare. Possible structures and examples of species for the various coordination numbers are as follows: three for trigonal planar, four for tetrahedral or square planar, five for trigonal bipyramid or square pyramid,

six for octahedral or trigonal prismatic, seven for pentagonal bipyramid or capped trigonal prism or capped octahedron, eight for square antiprism or dodecahedron and nine for capped square antiprism or tricapped trigonal prism.

The ligand systems containing different donor sites produce diverse coordination compounds with interesting properties and this makes the selection of ligands as an important step. A ligand system containing electronegative atoms like nitrogen, oxygen and sulfur increases the denticity and thus enhances the coordination possibilities. Among nitrogen-oxygen donor ligands, hydrazones possess a special place due to their widespread applications and interesting coordination capability with transition metal ions [1-5].

1.2. Aroylhydrazones

Aroylhydrazones are a group of compounds having –C=N– linkage and are marked as ligands in coordination chemistry. They have played an important role in the development of coordination chemistry because of their simple synthetic strategy, easily tunable steric, electronic properties and denticity, and formation of wide variety of complexes with immense applications [1,3]. Over the few decades, aroylhydrazones and their metal complexes have attracted the researchers due to their preparative accessibility and structural variety to act as the most important stereo-chemical models in transition metal coordination chemistry. The present interest in the coordination chemistry of aroylhydrazones stems from their ligational behavior. They can act as a neutral or monoanionic bidentate or tridentate ligand depending on the substituents and the reaction conditions.

Hydrazones contain two nitrogen atoms of different nature connected to each other and a C=N group that is conjugated with a lone electron pair of the terminal nitrogen atom. These structural fragments are mainly responsible for the physical and chemical properties of hydrazones (Fig. 1). Both nitrogen atoms of the hydrazone group are nucleophilic, although the amino type nitrogen is more reactive. The carbon atom of hydrazone group has both electrophilic and nucleophilic character [6]. General formula for a substituted aroylhydrazone is shown in Fig. 1.1. The structural diversity of the hydrazone is shown in Fig. 1.2.

Fig. 1.1. General formula for a substituted aroylhydrazone.

Fig. 1.2. The structural and functional diversity of the hydrazone group.

Aroylhydrazones are the condenzation products of aromatic acid hydrazides (aroyl hydrazides) with carbonyl compounds and are of special interest as a ligand, as it offers a combination of amide oxygen and imine nitrogen as donor atoms, the imine nitrogen being involved in formation of an N–N bond reminiscent of a doubly reduced azo functionality [7]. The electron density of the amide oxygen and imine nitrogen, involved in the metal complexation process can be controlled by protonation-deprotonation of the amide nitrogen. The protonation-deprotonation equilibrium of the amide nitrogen also affects the crystal field strength of the hydrazone ligand, which in turn can be used to control the stereochemistry and spin state of the corresponding metal complexes. The interesting amido-iminol tautomerism (Fig. 1.3) has an important role in determining the overall charge on the ligands. The amido-iminol equilibrium depends on the nature of the substituents present in the hydrazide moiety, pH of the medium used for reaction and the metal salts employed [8].

Amido form　　　　　　**Iminol form**
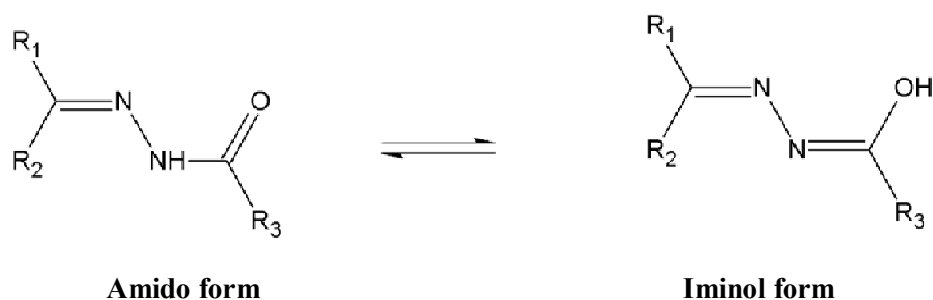
Fig. 1.3. Tautomerism in aroylhydrazones.

1.3. Coordination versatility of hydrazones

The coordination chemistry of aroylhydrazones are quite interesting as it presents a combination of donor sites such as protonated/ deprotonated amide oxygen, an imine nitrogen of hydrazone moiety and additional donor site (usually N or O) provided from the aldehyde or ketone forming the hydrazone moiety. The coordinating ability of aroylhydrazones is attributed to the extended delocalization of electron density over the R–CO–NH–N=CHR system. Generally in the simple aroylhydrazone, the basic coordination sites are carbonyl oxygen and azomethine nitrogen (Structure I) [7,9]. The chelating behavior depends on different factors like amido-iminol tautomerism, reaction conditions and the type of substituents attached to the hydrazone skeleton.
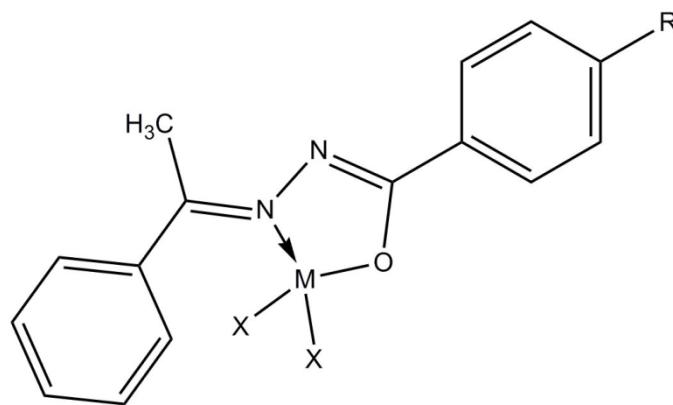
Structure I

Coordination sites can be further improved by suitable substituents on the hydrazide part as well as on carbonyl part. Moreover, these ligands exhibit amido-iminol tautomerism and can coordinate in either

neutral, monoanionic, dianionic or tetraanionic form bearing unusual coordination numbers such as six and seven in some mononuclear or binuclear species [10]. For example, if we take a hydrazone having a heterocyclic ring like pyridine moiety on the carbonyl part, it can coordinate to the central metal by adopting an NNO coordination mode, either through neutral amido form (Structure II) or through the deprotonated iminolate form (Structure III) [11].
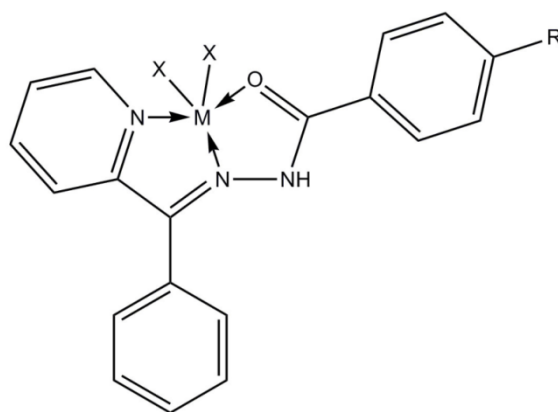
Structure II
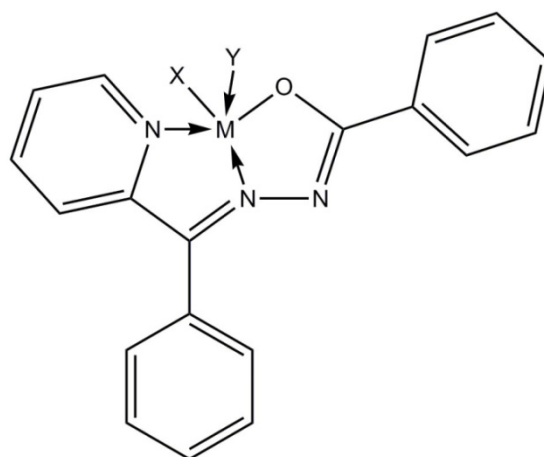
Structure III

The actual ionization state of the hydrazone moiety depends upon the pH of the medium and the metal salts employed [12,13]. In basic media, amide oxygen gets deprotonated and coordinates to the metal ion in the iminolate form whereas strongly acidic conditions favor neutral form of the ligand. Usually in hydrazone type ligands, the C=O and N–C bond lengths are indicative of the type of coordination. When the hydrazone ligand coordinates to the metal ions in the amido form, HN–C and C=O bond lengths are around 1.34 and 1.27 Å respectively [14] while their bond lengths in the iminolate form are found to shifted to the value of about 1.28 and 1.34 Å respectively [15].

Another possibility is the formation of a bis-ligated six-coordinated metal complex with two deprotonated ligands (Structure IV) [16]. These types of complexes have extra stability due to increased chelation.
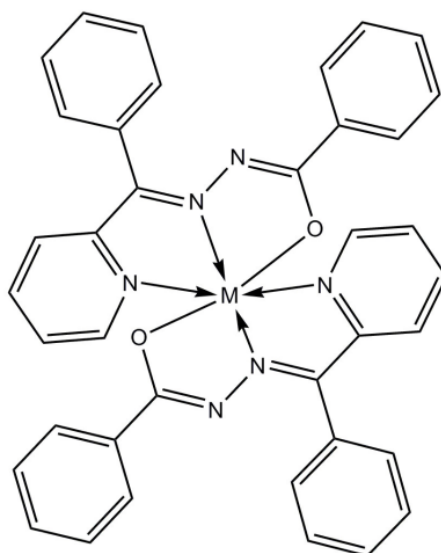
Structure IV

There are cases in which hydrazones form bridged complexes. Anions present in the metal salts or pseudohalide ions like azide or thiocyanate can act as a bridging ligand resulting in the formation of a dimeric structure (Structure V) [17]. In ONO donor type hydrazones containing phenolic group, the phenolate oxygen atom can form a bridge between the metal centers and thus forming a dimer (Structure VI) [18].
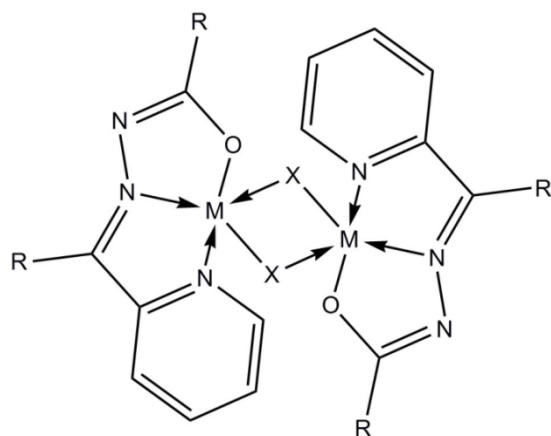
Structure V
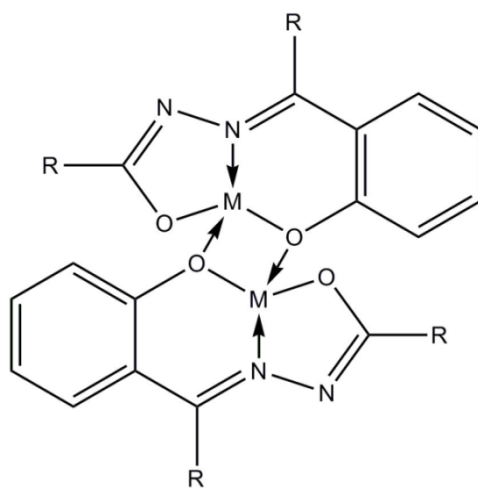
Structure VI

The presence of additional donor sites in the carbonyl part offers further coordination sites resulting in multinuclear complexes. If additional donor sites like –OMe group are present in the carbonyl compound, the dianionic hydrazone can act as a tetradentate ligand resulting in the formation of multinuclear complexes (Structure VII) [19]. Hydrazones can act as potential multifunctional ligands with interesting coordination modes. There are cases in which hydrazones form coordination polymers [20].
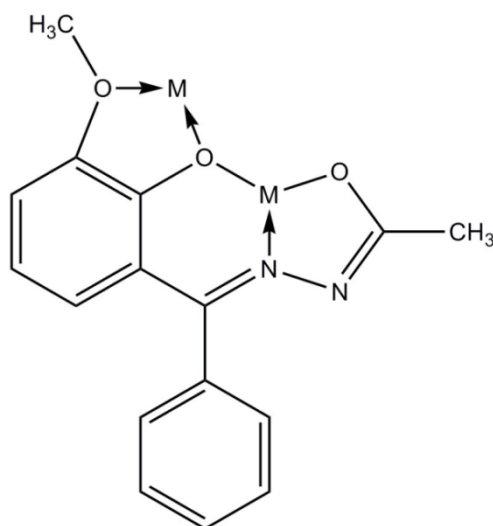
Structure VII

1.4. Applications of hydrazones

A great deal of work has been carried out on the syntheses and characterization of transition metal compounds with these ligands, mainly due to their variety of applications in in biological, clinical and analytical fields [21,22]. Hydrazones find applications in the treatment of diseases such as cancer, schizophrenia, tuberculosis, leprosy and mental disorder [23]. Formation of stable chelates with transition metals present in the

cell is responsible for the tuberculostatic activity of the hydrazones [23]. Thus many vital enzymatic reactions catalyzed by these transition metals cannot take place in presence of hydrazones [24]. Hydrazones can be used as plasticizers and stabilizers for polymers, polymerization initiators, antioxidants etc. Hydrazones also found to have application in analytical chemistry and can be used as indicators and spot test agents [23].

1.4.1. Hydrazones in nonlinear optics

Materials that exhibit nonlinear optical (NLO) properties are very useful because they allow manipulation of the fundamental properties of laser light beams, and are hence of great technological importance in areas such as optical data processing and storage. The most readily understood amongst NLO effects are frequency doubling or tripling second- or third-harmonic generation SHG/THG, respectively. In recent years, investigations into the nonlinear optical properties of different materials have attracted considerable attention, because they provide valuable information for the structural analysis of these materials and for their practical use in optoelectronic devices [25]. Among a large number of materials with a pronounced nonlinear optical response, the compounds whose refractive indices change significantly with the intensity of light are of prime importance. This property provides a means of controlling the optical propagation in a medium. Nonlinear optical (NLO) materials play a major role in fast developing fields like photonics and optoelectronics. One of the ways in which an organic molecule can have a large optical nonlinearity is by possessing a conjugated system of bonds which gives rise to a strong π-electron delocalization. The delocalization of the π electrons can be

further enhanced by the addition of donor and acceptor groups at the opposite ends of the conjugated system [26]. The strong charge transfer between such groups operating across the entire extended system markedly adds to the optical nonlinearity of the structure [27].

The design strategy, used by many with success, involves connecting donor and acceptor groups at the terminal position of a π bridge to create highly polarized molecules, which could exhibit large molecular nonlinearity. Hetero rings due to their relatively lower aromatic stabilization energy than benzene, are reported to provide more effective π conjugation between D and A, resulting in larger nonlinearities. Various aromatic donors and acceptors have been used to tune electronic factor and understand the origin of nonlinearity in these molecules. Excellent optical limiting responses have been reported in many substituted hydrazones [28,29]. They possess extensive two-dimensional π electron delocalization and hence have been shown to be as promising NLO materials.

There is currently a considerable effort to develop new organic materials with large nonlinear optical (NLO) properties because of their potential applications in optical signal processing. Particularly, the research has been focused on the third-order NLO properties of organic molecules, which are promising materials for all-optical photonic switching and optical limiting devices. The study of linear and NLO coefficients is very important to tune the NLO properties by the appropriate design of organic systems at the molecular level. Aroylhydrazones have recently been identified as class of organic molecule for nonlinear optics since these molecules typically have delocalized π electrons [25]. The possible

charge transfer interactions in aroylhydrazone is in between aromatic rings through –C=N–N– linker [30,31].

1.4.2. Hydrazones: Biological and medicinal applications

Hydrazones are important synthons for several transformations and have gained importance due to their diverse biological and clinical applications [32]. Hydrazone linkage provides a suitable system for pH-dependent release of anticancer drugs from drug-conjugates [32,33]. Several studies have been devoted to the anticancer activity of aroylhydrazone derivatives [34,35]. Hydrazone derivatives containing an –CO–NH–N=CH– group have been shown to exhibit antiproliferative activities and act as cytotoxic agents with the ability to prevent cell progression in cancerous cells through different mechanisms [36].

A number of hydrazone derivatives have been reported to exert notably antimicrobial [37], antihypertensive, anticonvulsant, analgesic, anti-inflammatory, antituberculosis, antitumoral, antiproliferative and antimalarial activities [38-40]. It had been observed with several experimental results that the metal complexes had better biological activity than their parent ligands [41,42].

The iron coordination and biological chemistry of a series of hetero-aroylhydrazones is reported with regard to their activity as Fe chelators for the treatment of Fe overload and also cancer. The potentially tridentate ligand 2-pyridinecarbaldehyde isonicotinoylhydrazone (HPCIH) and its analogues are an emerging class of orally effective Fe chelators that show great promise for the treatment of Fe overload diseases [43,44].

Investigations on the interactions of DNA with transition metal complexes provide leads for rational drug design, as well as means for the development of sensitive chemical probes for DNA [45-48].

Lin and co-workers reported that DNA binding properties of a series of aroylhydrazone ligands and their transition metal complexes [49]. Cancer is the growth of abnormal cells in the body in an uncontrolled manner. There are many different kinds of cancer. It can be developed in almost any organ or tissue, such as lung, colon, breast, skin, bones, or nerve tissues. Chemotherapy is the most common way of treatment of different kinds of malignant tumors. The need for new promising antitumor agents is increasing worldwide. Hydrazone ligands and their complexes have wide applications as anti-tumour, anti-cancer, anti-neoplastic and anti-proliferative agents [50].

1.4.3. Analytical applications of hydrazones

Hydrazones are an important class of known analytical reagents. They have been extensively used in detection and determination of several metals, such as the micro determination of gold by N-cyanoacylacetaldehyde hydrazone, lanthanides by arylhydrazones, molybdenum by 2,4-dihyroxyacetophenone benzoylhydrazone [5]. They are used in sensitive determination of uranium(VI) by *o*-hydroxy-1-naphthaldehyde isonicotinoylhydrazone or *o*-hydroxypropiophenone isonicotinoylhydrazone. Hydrazones are also used in the spectrophotometric determination of titanium in mineral or rock using 1,2-cyclohexanedione bis-benzoylhydrazone. They are also used in photometric determination of sub-nanograms level of cobalt(II), chromium(III) and iron(III) and in

direct, rapid and derivative spectrophotometric determination of thorium, titanium and zinc in potable water or pharmaceutical formulations. Substituted quinolyl and benzothiazolylhydrazones used as metallochromic indicators in the EDTA titration of copper(II). Complexes of hydrazones are used also in radiometric determination of metals such as determination of copper and iron by labeled cobalt (^{60}Co) complexes of *o*-hydroxybenzaldehyde isonicotinoylhydrazone. Some hydrazone ligands are used in the extraction of metals, hydrazone are also used in liquid-liquid extraction of copper(II), nickel(II) and cobalt(II). Poly-acrolein isonicotinic acid hydrazone resin was used for separation and concentration of palladium and platinum in the road dust. The hydrazone derivatives of dialdehyde cellulose were used in sewage wastewater treatment. They act as good and active coagulants for removing the total suspended solids (TSS), chlorine, iron and chromium [5].

Singh *et al.* have reviewed critically for the potential analytical applications of hydrazone derivatives [51]. Hydrazones are very important group of analytical regents for the determination of various metal ions by using various analytical techniques as they react with metal ions and form colored precipitates or solutions. Since the state of protonation of amide nitrogen also affects the extent of electron delocalization in the hydrazone backbone, a sharp color change of the hydrazone and its complexes often accompanies deprotonation and this property has led to search for its possible applications in analytical chemistry for ultra trace determination of metal ions and the development of sensors and acid–base indicators based on such complexes. Organic

reagents containing the atomic arrangement –CO–NH–N=CH– namely aroylhydrazones have been widely used for the spectrophotometric determination of metal ions because of their great complexing capability to form colored complexes with transition metal ions. The ability of these reagents to undergo conformational transformations in the reaction between their ionized particles and metallic ions leads to the formation of complexes with co-planar structure. This allows the formation of rigid structures that facilitate the fluorescent emission from the complex. Studies show that the CO–NH$_2$ group has a relevant participation in the formation of fluorogenic-chelates. On the other hand, the possibility of amido-iminol tautomerism, which increases the conjugation of the molecule in the iminolic form, and also the ability to coordinate with metal ions, contributes greatly to the production of fluorescent phenomena with the coordination process. Recently, Mukherjee and co-workers investigated two new luminescent hydrazones for selective and sensitive fluorescent recognition of Cu^{2+} in aqueous medium [52].

Recently, Rai and co-workers have developed a new rhodamine hydrazone as OFF-ON-OFF type selective sequential sensor of Al^{3+} and N^{3-} ions [53]. Said *et al.* have developed a chemosensor for Cu^{2+} determination in alkaline aqueous solutions [54]. Mukherjee *et al.* also have reported two novel hydrazone type ligands for the selective fluorescent recognition of Al^{3+} ions in aqueous medium [55]. Wu *et al.* have developed a dual colorimetric and fluorescent sensor for lead ion based on naphthalene hydrazone derivative [56]. Hu *et al.* have developed a highly sensitive and selective colorimetric naked-eye

detection of Cu^{2+} in aqueous medium using a hydrazone chemosensor [57]. Yang *et al.* have developed a Cu(II)-benzoylhydrazone based fluorescent probe for lipopolysaccharides [58].

The broad range of the chemical and supramolecular reactivities of the hydrazone functional group enables their use in the detection of anions. Two novel biologically active hydrazones were synthesized and characterized as colorimetric sensors for the recognition of cyanide and acetate ions in DMSO/H_2O [59].

1.4.4. Catalytic and corrosion inhibition applications

Catalysis is an important field in both academic and industrial research because it leads to more efficient reactions in terms of energy consumption and waste production. The common feature of these processes is a catalytically active species which forms reactive intermediates by coordination of an organic ligand and thus decreases the activation energy. Formation of the product should occur with regeneration of the catalytically active species. The efficiency of the catalyst can be described by its turnover number, providing a measure of how many catalytic cycles are passed by one molecule of catalyst. For efficient regeneration, the catalyst should form only labile intermediates with the substrate. This concept can be realized using transition metal complexes because metal-ligand bonds are generally weaker than covalent bonds.

Coordination chemistry of hydrazones has been a subject of competitive research since they exhibit a wide range of catalytic activities in some polymerization as well as oxidation processes. The

combination of heterocyclic ring and azomethine moiety exerts potential catalytic activities in aroylhydrazones. Aroylhydrazone complexes with a variety of metals have been extensively used as efficient catalysts [60-66]. Selvamurugan *et al.* demonstrated the transition metal complexes of bidentate 2-oxo-1,2-dihydroquinoline-3-carbaldehyde hydrazone ligands as efficient catalysts for catalytic amidation reaction [67]. Prakash and co-workers have reported a series of bis(hydrazone) complexes derived from 1,3,4-oxadiazoles and their catalytic application in N-alkylation reactions [68].

The design and synthesis of new families of chiral ligands has been the starting task for the many particular pieces of research that have contributed to the spectacular growth of asymmetric catalysis during the last 30 years. Aroylhydrazones and their metal complexes are efficient catalysts in carrying out asymmetric reduction of dialkyl ketones. Yolanda *et al.* have reported a novel class of chiral pyridine-hydrazone ligands served as catalysts in the 1,2-addition of arylboronic acids to saccharin-derived cyclic ketimines, affording products in high yields and enantioselectivities [69].

Among the several corrosion protection technologies, the use of inhibitors is one of the most practical methods especially in acidic media. The choice of the inhibitor is based on two considerations: first it could be synthesized conveniently from relatively cheap raw materials, secondly, it should contain an electron cloud on the aromatic ring or, the electronegative atoms such as nitrogen and oxygen in the relatively long chain compounds [70]. Due to the presence of $-C=N-$ group in

the aroylhydrazone molecules, they are likely to be good corrosion inhibitors [71]. Aroylhydrazones are adsorbed on the surface of mild steel and spontaneously form a monolayer on the surface, therefore, act as effective corrosion inhibitor. The metal complexes of Co(II), Ni(II) and Zn(II) with different ligands have shown good corrosion inhibition property for steel in different acidic media at room as well as elevated temperatures [72]. The transition metal complexes of aroylhydrazone ligands are expected to provide better efficiency due to their larger size and compactness, and the synergistic action of metal-organic blends. It has also been reported that the metal complexes show greater inhibition efficiency than the free ligands [73].

1.5. Scope and objectives of the present work

Aroylhydrazones and their complexes of first row transition series metal ions has been the subject of enthusiastic research since they show a wide range of applications in various fields especially those derived from heterocyclic aldehydes or ketones. In order to pursue the interesting coordinating properties of hydrazones, complexes with different types of ligand environments are essential. The coordination properties of hydrazones can be tuned by the appropriate choice of parent aldehyde or ketone and hydrazide and the substituents attached to them.

So in the present investigation, we selected two different NNO donor hydrazones as pro-ligands. 3-Fluoropyridine-2-carbaldehyde was selected as the carbonyl part in both the ligands since it can provide a further binding site for the metal ion which in turn increases the denticity.

The choice of nicotinoylhydrazide as the hydrazide part in one of the hydrazones was based on the fact that the nitrogen present in the ring can coordinate to the metal center and is capable of forming polymeric structures, eventhough this type of complexes are not reported in this thesis. Hence it is interesting to explore the coordinating capabilities of the synthesized hydrazones and to study the spectral properties and structures of hydrazones and their metal complexes.

The objectives of our present work includes

- To synthesize some NNO donor aroylhydrazones

- To characterize the synthesized aroylhydrazones by different physico-chemical techniques.

- To synthesize different transition metal chelates using the synthesized aroylhydrazones.

- To study the coordination modes of different aroylhydrazones in transition metal chelates using different physico-chemical methods like partial elemental analyses, thermogravimetry and different spectroscopic techniques.

- To establish the structure of the compounds by isolating single crystals of the compounds and by collecting and refining single crystal X-ray diffraction data.

In the present work, two new tridentate aroylhydrazones were synthesized and characterized. The molecular and crystal structures of these aroylhydrazones were established by single crystal X-ray diffraction

studies. The metals selected for the preparation of the complexes are copper, nickel, cobalt, iron, manganese, zinc and cadmium.

1.6. Physical measurements

The physico-chemical methods adopted for the present study are discussed below.

1.6.1. Elemental analyses

Elemental analyses of carbon, hydrogen and nitrogen present in all the compounds were done on a Vario EL III CHNS elemental analyzer at the Sophisticated Analytical Instrument Facility, Cochin University of Science and Technology, Kochi-22, Kerala, India. This information is important to determine the purity of synthesized compounds.

1.6.2. Molar conductivity measurements

The molar conductivities of the complexes in DMF (10^{-3} M) at 298 K were measured using a Systronic model 303 direct reading conductivity meter at the Department of Applied Chemistry, Cochin University of Science and Technology, Kochi-22, Kerala, India.

1.6.3. Magnetic susceptibility measurements

The magnetic susceptibility measurements of the complexes were carried out on a Vibrating Sample Magnetometer using Hg[Co(SCN)$_4$] as a calibrant at the Sophisticated Analytical Instrument Facility, Indian Institute of Technology, Madras.

1.6.4. Infrared spectroscopy

Infrared spectra of the compounds were recorded on a Perkin Elmer Spectrum 100 model Spectrometer using KBr pellets at the Department of Chemical Oceanography, School of Marine Sciences, Cochin University of Science and Technology, Kochi, India.

1.6.5. Electronic spectroscopy

The electronic spectra of the compounds were recorded on a Thermo Scientific Evolution 220 UV-Vis Spectrophotometer in the 200-900 nm range at the Department of Applied Chemistry, Cochin University of Science and Technology, Kochi-22, Kerala, India.

1.6.6. NMR spectroscopy

^{1}H NMR spectra of hydrazones were recorded using Bruker AMX 400 FT-NMR Spectrometer with deuterated DMSO as the solvent and TMS as internal standard at the Sophisticated Analytical Instrument Facility, Cochin University of Science and Technology, Kochi-22, Kerala, India.

1.6.7. Thermogravimetric analyses

TG-DTG analyses of the complexes were carried out in a Perkin Elmer Pyris Diamond TG/DTA analyzer under nitrogen at a heating rate of 10 °C min^{-1} in the 50-700 °C range at the Sophisticated Analytical Instrument Facility, Cochin University of Science and Technology, Kochi-22, Kerala, India.

1.6.8. EPR spectroscopy

The EPR spectra of the complexes in the solid state at 298 K and in DMF at 77 K were recorded on a Varian E-112 spectrometer using TCNE as the standard with 100 kHz modulation frequency, 2 G modulation amplitude and 9.5 GHz microwave frequency at the Sophisticated Analytical Instrument Facility, IIT Bombay, India. EPR spectra of complexes are simulated using EasySpin software package [74].

1.6.9. Single crystal X-ray diffraction studies

Single crystal X-ray diffraction studies of the compounds were carried out using Bruker SMART APEXII CCD diffractometer equipped with a graphite crystal, incident-beam monochromator and a fine focus sealed tube with Mo Kα (λ=0.71073 Å) as the X-ray source at the Sophisticated Analytical Instrument Facility, Cochin University of Science and Technology, Kochi-22, Kerala, India. The unit cell dimensions were measured and the data collections were performed. Bruker SMART software was used for data acquisition and Bruker SAINT software for data integration [75]. Absorption corrections were carried out using SADABS based on Laue symmetry using equivalent reflections [76]. The structure was solved by direct methods using SHELXS97 and refined by full-matrix least-squares refinement on F^2 using SHELXL97 [77]. The molecular and crystal structures were plotted by ORTEP-3 [78] and DIAMOND version 3.2g [79].

References

[1]   L. Pan, C. Wang, K. Yan, K. Zhao, G. Sheng, H. Zhu, X. Zhao, D. Qu, F. Niu, Z. You, J. Inorg. Biochem. 159 (2016) 22.

[2]   B. Shaabani, A.A. Khandar, H. Mobaiyen, N. Ramazani, S.S. Balula, L.C. -Silva, Polyhedron 80 (2014) 166.

[3]   S. Mondal, S. Naskar, A.K. Dey, E. Sinn, C. Eribal, S.R. Herron, S.K. Chattopadhyay, Inorg. Chim. Acta 398 (2013) 98.

[4]   B.F. Ali, Z. Judeh, K. Ayub, Polyhedron 101 (2015) 118.

[5]   M.M.E. Shakdofa, M.H. Shtaiwi, N. Morsy, T.M.A. Adel-rassel, Main Group Chem. 13 (2014) 187.

[6]   X. Su, I. Aprahamian, Chem. Soc. Rev. 43 (2014) 1963.

[7]   S. Mondal, C. Das, B. Ghosh, B. Pakhira, A.J. Blake, M.G.B. Drew, S.K. Chattopadhyay, Polyhedron 80 (2014) 272.

[8]   M. Sutradhar, M.V. Kirillova, M.F.C.G. da Silva, C.M. Liu, A.J.L. Pombeiro, Dalton Trans. 42 (2013) 16578.

[9]   N. Mohan, S. Muthumari, R. Ramesh, J. Organomet. Chem. 807 (2016) 45.

[10]   B. Jeragh, M.S. Ali, A.A. El-Asmy, Spectrochim. Acta 145A (2015) 295.

[11]   S.P. Dash, A.K. Panda, S. Pasayat, S. Majumder, A. Biswas, W. Kaminsky, S. Mukhopadhyay, S.K. Bhutia, R. Dinda, J. Inorg. Biochem. 144 (2015) 1.

[12]   M.F. Iskander, T.E. Khalil, R. Werner, W. Haase, I. Svoboda, H. Fuess, Polyhedron 19 (2000) 949.

[13]   B. Samanta, J. Chakraborty, S. Shit, S.R. Batten, P. Jensen, J.D. Masuda, S. Mitra, Inorg. Chim. Acta 360 (2007) 2471.

[14] H.H. Monfared, M. Vahedpour, M.M. Yeganeh, M. Ghorbanloo, P. Mayer, C. Janiak, Dalton Trans. 40 (2011) 1286.

[15] R. Bikas, H.H. Monfared, L. Sieron, A. Gutierrez, J. Coord. Chem. 66 (2013) 4023.

[16] N.A. Mangalam, S.R. Sheeja, M.R.P. Kurup, Polyhedron 29 (2010) 3318.

[17] M.C. Vineetha, M. Sithambaresan, J.M. Jacob, M.R.P. Kurup, Acta Cryst. E68 (2012) 1086.

[18] S. Pal, Proc. Indian Acad. Sci. (Chem. Sci.) 114 (2002) 418.

[19] J. Chakraborty, S. Thakurta, G. Pilet, D. Luneau, S. Mitra, Polyhedron 28 (2009) 819.

[20] M.M. Wang, H. Wang, G.Q. Gan, Y. Qu, H. Chen, Z.D. Lin, J. Macromol. Sci. A 49 (2012) 355.

[21] R. Laurinaviciute, V. Mimaite, J. Ostrauskaite, J.V. Grazulevicius, V. Jankauskas, Synthetic Metals 197 (2014) 1.

[22] A. Kolesnicenko, T. Malinauskas, E. Kasparavicius, R. Send, V. Gaidelis, V. Jankauskas, H. Wonneberger, I. Bruder, V. Getautis, Tetrahedron 71 (2015) 8162.

[23] M. Shakir, A. Abbasi, J. Chem. Pharma. Res. 7 (2015) 375.

[24] B. Murukan, K. Mohanan, J. Enzyme Inhib. Med. Chem. 22 (2007) 65.

[25] S. Urnikaite, M. Daskeviciene, R. Send, H. Wonneberger, A. Sackus, I. Bruder, V. Getautis, Dyes Pigment 14 (2015) 175.

[26] B. Zhao, W.Q. Lu, Z.H. Zhou, Y. Wu, J. Mater. Chem. 10 (2000) 1513.

[27] G.A. Babu, R.P. Ramasamy, P. Ramasamy, S. Natarajan, J. Cryst. Growth 311 (2009) 3461.

[28] R.N. Singh, P. Rawat, S. Sahu, Spectrochim. Acta 135A (2015) 1162.

[29] P. Rawat, R.N. Singh, J. Mol. Struct. 1097 (2015) 214.

[30] G.S. He, T.C. Lin, J. Dai, P.N. Prasad, R. Kannan, A.G. Dombroskie, R.A. Vaia, L.S. Tan, J. Chem. Phys. 120 (2004) 5275.

[31] C. Ravikumar, I.H. Joe, V.S. Jayakumar, Chem. Phys. Lett. 460 (2008) 552.

[32] B. Narasimhan, P. Kumar, D. Sharma, Acta. Pharm. Sci. 52 (2010) 169.

[33] K. Ulbrich, V. Subr, Adv. Drug Del. Rev. 56 (2004) 1023.

[34] S. Vogel, D. Kaufmann, M. Pojarová, C. Müller, T. Pfaller, S. Kühne, P.J. Bednarski, E. Angerer, Bioorg. Med. Chem. 16 (2008) 6436.

[35] W.Y. Liu, H.Y. Li, B.X. Zhao, D.S. Shin, S. Lian, J.Y. Miao, Carbohydr. Res. 344 (2009) 1270.

[36] V. Onnis, M. T. Cocco, R. Fadda, C. Congiu, Bioorg. Med. Chem. 17 (2009) 6158.

[37] S.Y. Ebrahimipour, I. Sheikhshoaie, J. Simpson, H. Ebrahimnejad, M. Dusek, N. Kharazmi, V. Eigner, New J. Chem. (2016) DOI: 10.1039/c5nj02594j

[38] K. Padmini, P. Jaya Preethi, P. Divya, M. Rohini, K. Lohita, P. Swetha, M. Kaladar, Int. J. Pharma Res. Rev. 2 (2013) 43.

[39] V.F.S. Pape, D. Türk, P. Szabó, M. Wiese, E.A. Enyedy, G. Szakács, J. Inorg. Biochem. 144 (2015) 18.

[40] T. Mukherjee, J.C. Pessoa, A. Kumar, A.R. Sarkar, Dalton Trans. 42 (2013) 2594.

[41] M. Shebl, Spectrochim. Acta 117A (2014) 127.

[42] B.M. Kalshetty, S.S. Karabasannavar, R.S. Gani, M.B. Kalashetti, Drug Invention Today 5 (2013) 105.

[43] P.V Bernhardt, P. Chin, P.C. Sharpe, D.R. Richardson, Dalton Trans. 30 (2007) 3232.

[44] M.T. Basha, J.D. Chartres, N. Pantarat, M.A. Ali, A.H. Mirza, D.S. Kalinowski, D.R. Richardson, P.V. Bernhardt, Dalton Trans. 41 (2012) 6536.

[45] K.R.S. Gowda, H.S.B. Naik, B.V. Kumar, C.N. Sudhamani, H.V. Sudeep, T.R.R. Naik, G. Krishnamurthy, Spectrochim. Acta 105A (2013) 229.

[46] R. Kaplánek, M. Havlík, B. Dolenský, J. Rak, P. Džubák, P. Konečný, M. Hajdúch, J. Králová, V. Král, Bioorg. Med. Chem. 23 (2015) 1651.

[47] F. Wang, H. Yin, J. Cui, Y. Zhang, H. Geng, M. Hong, J. Organomet. Chem. 759 (2014) 83.

[48] J. Eswaran, K. Sivalingam, V.P. Viswanatha, S.P.B. Nattamai, D. Nallasamy, Inorg. Chim. Acta 429 (2015)148.

[49] W.J. -Lin, Z.Y. -Qin, Y.B. -Sheng, Inorg. Chim. Acta 409 (2014) 484.

[50] R. Kaplánek, M. Jakubek, J. Rak, Z. Kejík, M. Havlík, B. Dolenský, I. Frydrych, M. Hajdúch, M. Kolář, K. Bogdanová, J. Králová, P. Džubák, V. Král, Bioorg. Chem. 60 (2015) 19.

[51] R.B. Singh, P. Jain, R.P. Singh, Talanta 29 (1982) 77.

[52] S. Mukherjee, P. Mal, H.S. -Evans, J. Lumin. 155 (2014) 185.

[53] A. Rai, N. Kumari, A.K. Srivastava, S.K. Singh, S. Srikrishna, L. Mishra, J. Photochem. Photobiol. Chem. 78A (2016) 319.

[54] A.I. Said, N.I. Georgiev, V.B. Bojinov, J. Photochem. Photobiol. Chem. 311A (2015) 16.

[55] S. Mukherjee, P. Mal, H.S. -Evans, J. Lumin. 172 (2016) 124.

[56] F.-Y. Wu, H. Zhang, M. Xiao, B.-X. Han, Spectrochim. Acta 109A (2013) 221.

[57] S. Hu, J. Song, F. Zhao, X. Meng, G. Wu, Sens. Actuators B215 (2015) 241.

[58] J. Yang, L. Huang, Z. Guo, W. Ren, Q. Wang, J. Lumin. 172 (2016) 290.

[59] V.K. Gupta, A.K. Singh, N. Gupta, Sens. Actuators B204 (2014) 125.

[60] K.C. Gupta, A.K. Sutar, Coord. Chem. Rev. 252 (2008) 1420.

[61] D.P. Singh, B.K. Allam, K.N. Singh, V.P. Singh, RSC Adv. 4 (2014) 1155.

[62] L. Chen, J. Hou, W.-H. Sun, Appl. Catal. 246 (2003) 11.

[63] M.S. Niasari, A. Amiri, Appl. Catal. 290 (2005) 46.

[64] A. El-Motaleb, M. Ramadan, Transit. Met. Chem. 30 (2005) 471.

[65] H.H.-Monfared, N.A.-Lalami, A. Pazio, K. Wozniak, C. Janiak, Inorg. Chim. Acta 408 (2013) 109.

[66] M. Ghorbanloo, R. Bikas, G. Małecki, Inorg. Chim. Acta 445 (2016) 8.

[67] S. Selvamurugan, R. Ramachandran, G. Prakash, P. Viswanathamurthi, J.G. Malecki, A. Endo, J. Organomet. Chem. 803 (2016) 119.

[68] G. Prakash, R. Ramachandran, M. Nirmala, P. Viswanathamurthi, J. Sanmartin, Inorg. Chim. Acta 427 (2015) 203.

[69] Y. Álvarez-Casao, D. Monge, E. Álvarez, R. Fernández, J.M. Lassaletta, Org. Lett. 17 (2015) 5104.

[70] P. Mourya, S. Banerjee, R.B. Rastogi, M.M. Singh, Ind. Eng. Chem. Res. 52 (2013) 12733.

[71] K.S. Jacob, G. Parameswaran, Corros. Sci. 52 (2010) 224.

[72] K.F. Khaled, K.B. -Samardzija, N. Hackerman, Corros. Sci. 48 (2006) 3014.

[73] P. Singh, A.K. Singh, V.P. Singh, Polyhedron 65 (2013) 73.

[74] S. Stoll, Spectral Simulations in Solid-State Electron Paramagnetic Resonance, Ph. D. thesis, ETH, Zurich, 2003.

[75] SMART and SAINT, Area Detector Software Package and SAX Area Detector Integration Program, Bruker Analytical X-ray; Madison, WI, USA, 1997.

[76] Bruker, *SADABS*, APEX2, XPREP and *SAINT*, Bruker AXS Inc., Madison, Wisconsin, USA, 2004.

[77] G.M. Sheldrick, Acta Cryst. 64A (2008) 112.

[78] L.J. Farrugia, J. Appl. Cryst. 45 (2012) 849.

[79] K. Brandenburg, Diamond Version 3.2g, Crystal Impact GbR, Bonn, Germany, 2010.

.....ജരു.....

Chapter **2**

SYNTHESES, SPECTRAL CHARACTERIZATION AND CRYSTAL STRUCTURES OF SOME AROYLHYDRAZONES

2.1. Introduction

Hydrazones are compounds derived from the condenzation of hydrazides with carbonyl compounds, namely aldehydes and ketones. Hydrazones have proved to be strong chelating agents for transition metals and are attractive ligands from the structural point of view [1,2]. These compounds contain –C=N– bond, which is conjugated with a lone pair of electrons of the functional nitrogen atom. The nitrogen atoms of the hydrazones are nucleophilic and the carbon atom has both electrophilic and nucleophilic nature. These structural fragments are mainly responsible for the physical and chemical properties of hydrazones. The combination of hydrazones with other functional group leads to compounds with unique physical and chemical character [3].

The coordination chemistry and biochemistry of aroylhydrazones, R–CO–NH–N=CH–R′, have attracted increasing interest due to their chelating ability and their pharmacological applications. Hydrazone ligands create environment similar to biological systems coordinating through oxygen and nitrogen atoms [4]. Hydrazone moiety is found in natural and synthetic products of biological interest. Furthermore, hydrazones have wide spread applications in fields such as coordination chemistry [5,6], analytical chemistry [7,8], bioinorganic chemistry [9-11], and also as magnetic, electronic, nonlinear optically active, and fluorescent [12] compounds. Literature studies revealed that hydrazones and various substituted hydrazones are associated with a broad spectrum of biological activities such as antioxidant, antibacterial, antiviral, analgesic, antimicrobial, and anticancer activities etc [10]. The ease of preparation, increased hydrolytic stability and tendency toward crystallinity are all desirable characteristics of hydrazones.

Compared to the simple hydrazone, aroyl or hetero-aroylhydrazones have additional donor sites which introduce a wider range of properties for these substances. The study of ligands involving such hydrazones is interesting as they demonstrate versatility in coordination, a tendency to yield stereochemistry [13] of higher coordination number, an ability to behave as neutral or deprotonated ligands, and flexibility in assuming different conformations. The reaction of aroylhydrazones with transition metal ions can proceed according to two pathways attaining the amido or iminolic structure for the hydrazide part of the molecule. The mode of bonding depends on the nature of both the ligand and metal ions, the

anion of the metal salt and the solvent used. Their ease of synthesis, easily tunable steric and electronic properties and good solubility in common solvents enhances research interest in this area.

Interest in coordination chemistry of benzohydrazide has been a subject of enthusiastic research since their complexes show a wide range of applications in different areas such as catalysis [14] and biological applications such as protein binding and DNA binding or cleavage interactions [15]. Benzohydrazone derivatives are also important due to their wide spectrum of biological activities [13]. Hydrazones containing a halo atom in α- or β-positions have been explored for many years as ways to generate nitrile imines and 1,2-diaza-1,3-butadienes that are active intermediates in cycloaddition chemistry [16].

The above mentioned facts guided us for the development of some transition metal complexes using aroylhydrazones as the ligand system. The chapter deals with the synthesis and characterization of two novel aroylhydrazones. The proligands were chosen to probe and examine the effect of the following:

(i) nature of donor atoms

(ii) chelate ring size

(iii) rigidity of the structure caused by the presence of the benzene/pyridine ring and

(iv) presence of halogen (F) on the parent alehyde

The synthesized aroylhydrazones consisting of NNO donor atoms are given below.

- 3-Fluoropyridine-2-carbaldehyde benzoylhydrazone monohydrate (HFPB·H_2O)

- 3-Fluoropyridine-2-carbaldehyde nicotinoylhydrazone dihydrate (HFPN·2H_2O)

As a part of our research in the study of coordinating capabilities of aroylhydrazones and their coordination compounds, we have selected 3-fluoropyridine-2-carbaldehyde benzoylhydrazone and 3-fluoropyridine-2-carbaldehyde nicotinoylhydrazone as pro-ligands to synthesize and characterize some transition metal complexes. The choice of nicotinoyl hydrazide in one of the ligand systems is mainly due to the fact that this heteroatomic moiety can provide a further binding site for metal cations [17]. These aroylhydrazones of HL type (H represents dissociable amide proton) can coordinate a given metal ion *via* pyridine-N, azomethine-N and amide or iminolate O centers.

2.2. Experimental
2.2.1. Materials

3-Fluoropyridine-2-carbaldehyde (Sigma-Aldrich), benzhydrazide (Sigma-Aldrich), nicotinic hydrazide (Sigma-Aldrich) were of analytical reagent grade and used as received. Solvent used was ethanol.

2.2.2. Syntheses of aroylhydrazones

Hydrazones are generally prepared by refluxing the stoichiometric amounts of the appropriate hydrazine and a carbonyl compound of high

purity dissolved in suitable solvent. On cooling, the compound usually crystallizes out. The hydrazones of our interest were synthesized by adapting the reported procedure [15], *via* condenzation between appropriate aldehyde/ketone with the corresponding aroylhydrazide. Detailed account of their preparation is given below. To validate the utility of this methodology, the reaction was also performed with different stoichiometric ratios of the reactants. The chemical structures and abbreviations for the hydrazones are given in Fig. 2.1.

HFPB

HFPN
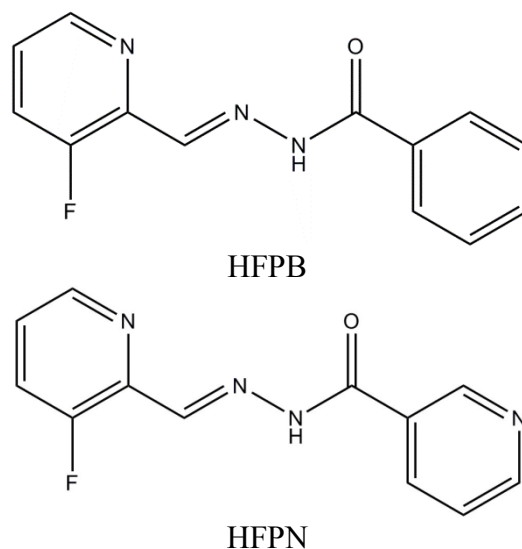
Fig. 2.1. Chemical structures and abbreviations for the aroylhydrazones.

2.2.2.1. 3-Fluoropyridine-2-carbaldehyde benzoylhydrazone monohydrate (HFPB·H₂O)

3-Fluoropyridine-2-carbaldehyde (0.1250 g, 1 mmol) in ethanol (10 mL) was mixed with an ethanolic solution (10 mL) of benzhydrazide (0.1360 g, 1 mmol). The mixture was boiled under reflux for 12 hours

after adding few drops of glacial acetic acid and then cooled to room temperature. Colorless block shaped crystals, suitable for single-crystal analysis, were obtained in 61.8% yield after slow evaporation of the solution in air for a few days (Scheme 2.1)

3-Fluoropyridine-2-carbaldehyde   Benzhydrazide   3-Fluoropyridine-2-carbaldehyde benzhydrazone monohydrate
(HFPB·H₂O)
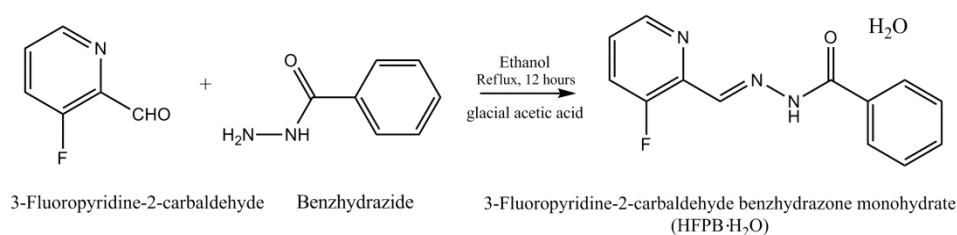
Scheme 2.1. Synthesis of HFPB·H₂O.

Yield: 61.8%, M.P.: 156 °C, Elemental Anal. Found (Calcd.) (%): C: 59.61 (59.77); H: 4.84 (4.63); N: 16.10 (16.08).

2.2.2.2. 3-Fluoropyridine-2-carbaldehyde nicotinoylhydrazone dihydrate (HFPN·2H₂O)

A solution of 3-fluoropyridine-2-carbaldehyde (0.1250 g, 1 mmol) in ethanol (10 mL) was mixed with an ethanolic solution (10 mL) of nicotinic hydrazide (0.1370 g, 1 mmol). The mixture was boiled under reflux for 12 hours after adding few drops of glacial acetic acid and then cooled to room temperature. Colorless needle shaped crystals, suitable for single-crystal analysis, were obtained after slow evaporation of the solution in air for a few days (Scheme 2.2).

3-Fluoropyridine-2-carbaldehyde   Nicotinoylhydrazide   3-Fluoropyridine-2-carbaldehyde nicotinoylhydrazone dihydrate
(HFPN·2H₂O)

Scheme 2.2. Synthesis of HFPN·2H$_2$O.

Yield: 64%, M.P.: 173 °C, Elemental Anal. Found (Calcd.) (%): C: 51.57 (51.43); H: 4.58 (4.68); N: 20.04 (19.99).

2.3. Results and discussion

2.3.1. Elemental analyses

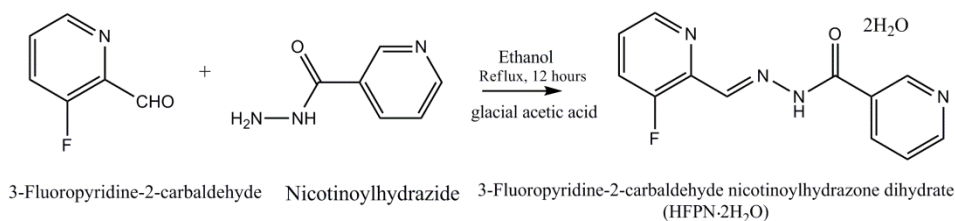C, H, N analyses of the synthesized hydrazones are given in Section 2.2. The results of elemental analyses are found to be in good agreement with the proposed formulae.

2.3.2. Infrared spectral studies

IR spectroscopy measures the vibrations of atoms, and based on this it is possible to determine the functional groups [18]. The characteristic bands of different functional groups provide valuable information regarding the structure of the compounds. FT-IR spectra of the synthesized hydrazones were collected on a Perkin Elmer Spectrum 100 model spectrometer using KBr pellets. The main bands from the IR spectra are presented in Table 2.1. FT-IR spectral data of the compounds are found to be in accordance with their molecular structure.

Table 2.1. Selected infrared spectral data (cm^{-1}) of the aroylhydrazones

Compound	ν(N–H)	ν(C=O)	ν(C=N)
HFPB·H$_2$O	3059	1683	1597
HFPN·2H$_2$O	3058	1682	1590

Aroylhydrazones present a combination of donor sites, such as protonated/deprotonated amide oxygen and the imine nitrogen of hydrazone moiety. These ligands are capable of undergoing amido-iminol tautomerism [1,19]. The IR spectrum of HFPB·H$_2$O contains a strong bands at 1683 and 3059 cm^{-1} corresponds to the ν(C=O) and ν(N–H) stretching modes respectively. These two observations suggest that the hydrazone exists in the amido form in the solid state [20]. A band is observed at 3484 cm^{-1} which is due to the presence of lattice water in the molecule and further confirmed by single crystal X-ray diffraction studies. A prominent band at 1597 cm^{-1} observed in the spectrum corresponding to azomethine ν(C=N) linkage, which confirms the condenzation between hydrazide and aldehyde moiety of carbonyl compound and it is in agreement with the literature reports of aroylhydrazones [21,22]. Fig. 2.2 depicts the infrared spectrum of the HFPB·H$_2$O.
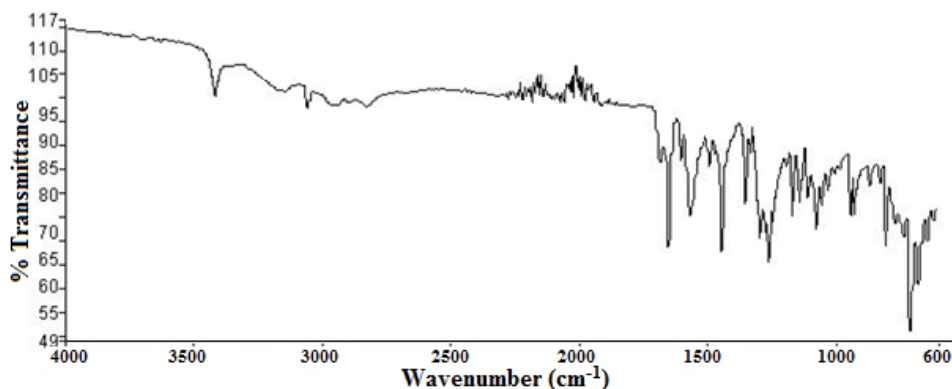
Fig. 2.2. FT-IR spectrum of HFPB·H$_2$O.

The IR spectrum of HFPN·2H$_2$O showed very strong bands at 3058 and 1682 cm^{-1} which are attributed to the ν(N–H) and ν(C=O) stretching vibrations respectively [23] indicating that hydrazone exists in the amido form in the solid state. The broad absorption band at 3330 cm^{-1} is due to the ν(O–H) stretching mode of lattice water and it is confirmed by single crystal X-ray diffraction studies. The azomethine band observed at 1590 cm^{-1} in the spectrum indicate that the reaction between the keto group of the carbonyl compound and corresponding hydrazide has taken place resulting in the formation of desired ligand HFPN·2H$_2$O. Fig. 2.3 depicts the infrared spectrum of the HFPN·2H$_2$O.
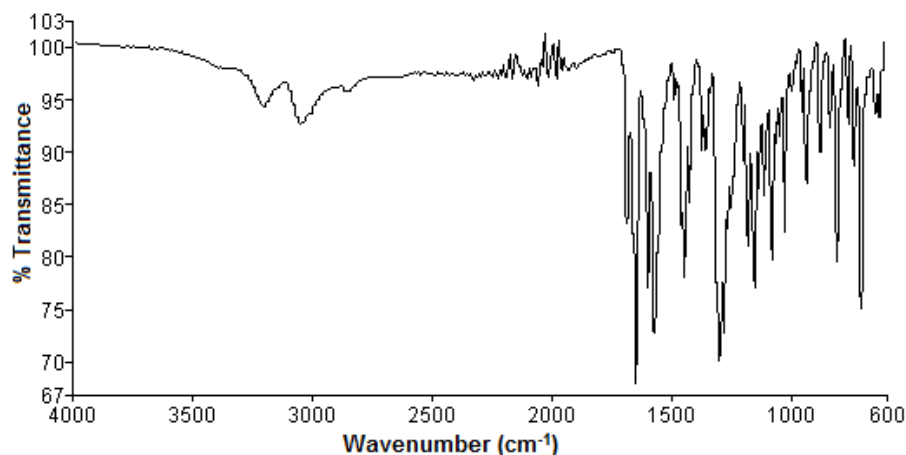
Fig. 2.3. FT-IR spectrum of HFPN·2H₂O.

2.3.3. Electronic spectral studies

DMF solutions of the aroylhydrazones have been used to record electronic spectra. Important bands observed are listed in Table 2.2. The electronic absorption spectra of the hydrazones showed an intense broad band corresponding to n→π* and π→π* transitions associated with azomethine chromophore (–C=N–NH–CO–) and the pyridyl rings of the hydrazones (Fig. 2.4) [24,25].

Table 2.2. Electronic spectral assignments (cm⁻¹) of aroylhydrazones

Compound	n→π*/π→π*
HFPB·H₂O	32400
HFPN·2H₂O	32630
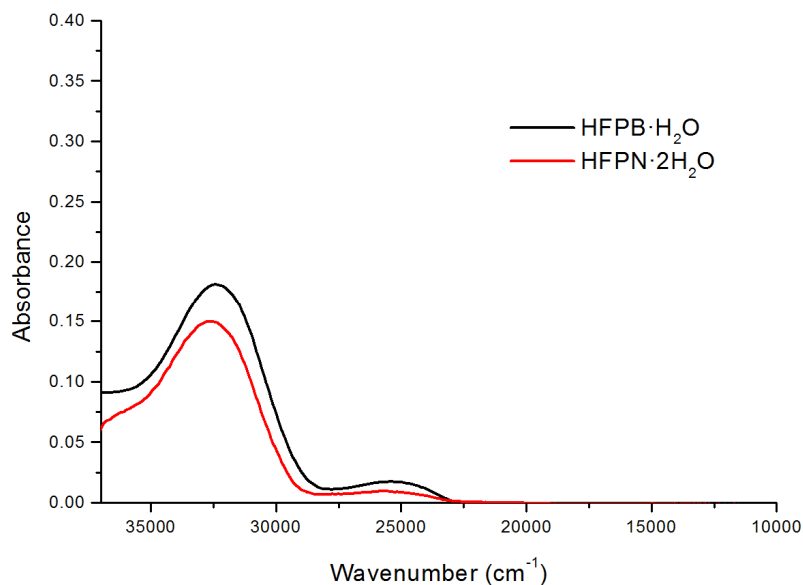
Fig. 2.4. Electronic spectra of aroylhydrazones.

2.3.4. NMR spectral studies

NMR or nuclear magnetic resonance spectroscopy is a technique used to determine a compound's unique structure. It identifies the carbon-hydrogen framework of an organic compound. ^{1}H-NMR spectra of the synthesized aroylhydrazones were recorded in $CDCl_3$ on a Bruker AMX 400 spectrometer and TMS as standard and are found in agreement with their suggested structures [26].

The ^{1}H-NMR spectrum of HFPB·H_2O is given in Fig. 2.5. The sharp signal at 12.12 ppm in the downfield region of the spectrum is due to existence of the hydrazone in the iminol form in the solution state. On D_2O exchange, the intensity of this signal is found to be considerably decreased (Fig. 2.6). The azomethine singlet is observed at 8.66 ppm. Aromatic protons appear as multiplets in the 7.54-7.95 ppm range.
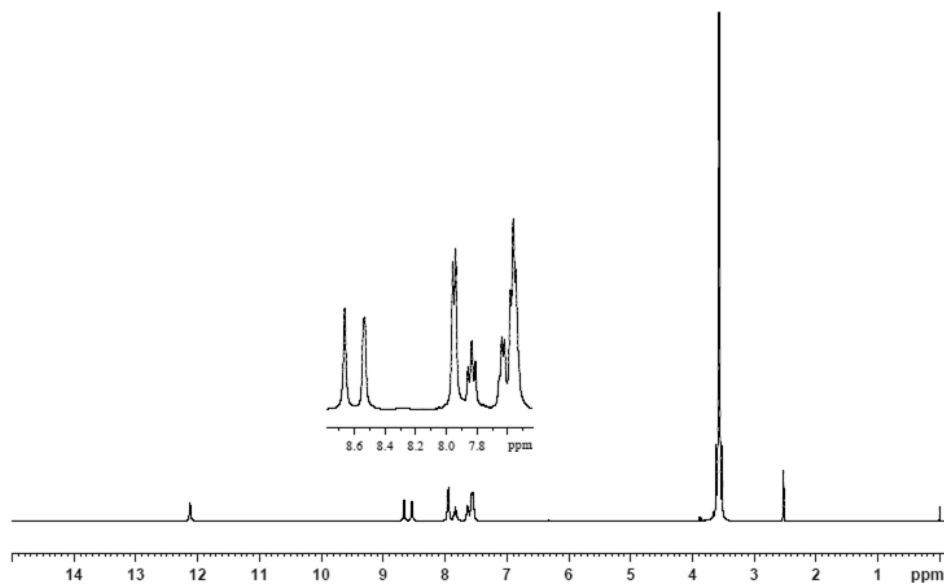
Fig. 2.5. ^{1}H-NMR spectrum of HFPB·H$_2$O.
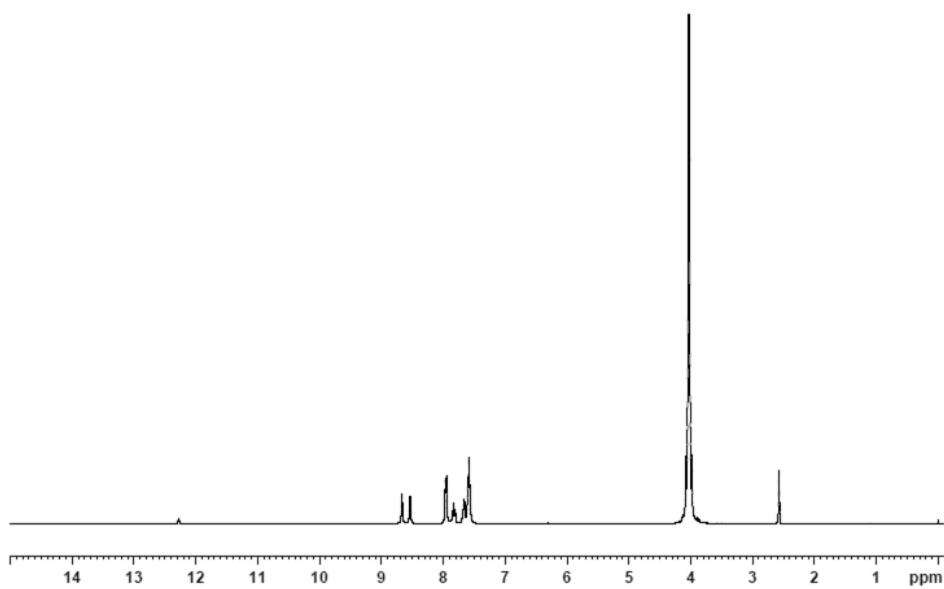
Fig. 2.6. ^{1}H-NMR spectrum of HFPB·H$_2$O-D$_2$O exchange.

The ^{1}H NMR spectrum of HFPN·2H$_2$O is given in Fig. 2.7. Here the singlet in the downfield region of the spectrum at 12.19 ppm is due to the iminolic proton. This peak is found to disappear upon the addition of D$_2$O to the solution, since this proton exchange with deuterium in the D$_2$O [27]. The azomethine proton resonates at 9.09 ppm as a singlet. Aromatic protons appear as multiplets in the 7.54-7.86 ppm range.
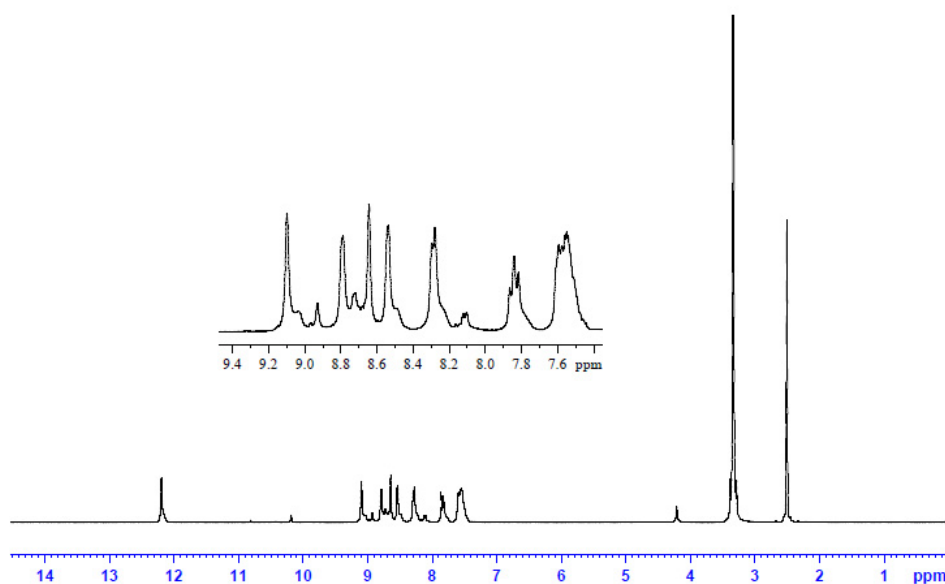
Fig. 2.7. ^{1}H-NMR spectrum of HFPN·2H$_2$O.

2.3.5. X-ray crystallography

Single crystal X-ray diffraction studies of the synthesized aroylhydrazones were carried out using a Bruker SMART APEXII CCD diffractometer equipped with graphite monochromated Mo Kα (λ = 0.71073 Å) radiation at the Sophisticated Analytical Instrument

Facility, Cochin University of Science and Technology, Kochi-22, Kerala, India. Bruker SMART software was used for data acquisition and Bruker SAINT software for data integration [28]. Absorption corrections were carried out using SADABS based on Laue symmetry using equivalent reflections [28]. The cell refinement was done using APEX2 and SAINT [28]. The data was reduced using SAINT and XPREP [28]. The structure was solved by direct methods using SHELXS97 [29] and refined by full-matrix least-squares refinement on F^2 using SHELXL97 [29]. The molecular and crystal structures were plotted using molecular graphics like ORTEP-3 [30] and DIAMOND version 3.2g [31].

In HFPB·H$_2$O, the atoms H3′, H1A and H1B were located from a difference Fourier map and refined isotropically. The remaining hydrogen atoms were placed in geometrically idealized positions and constrained to ride on their parent atoms, with C–H distances of 0.93 Å, and with isotropic displacement parameters 1.2 times that of the parent carbon atoms. The reflections (0 0 2) and (1 0 2) were omitted owing to bad disagreement.

In HFPN·2H$_2$O, the atoms H3′, H1A, H1B, H2A and H2B were located from a difference Fourier map and refined isotropically. The N3–H3′ bond distance was restrained to 0.88 ± 0.01 Å. The O–H distances of water were restrained to 0.86±0.01 Å and H···H distances to 1.36±0.02 Å. The remaining hydrogen atoms were placed in geometrically idealized positions and constrained to ride on their parent atoms, with C–H distances of 0.93 Å, and with isotropic displacement parameters 1.2 times that of the parent carbon atoms.

2.3.5.1. Crystal structure of HFPB·H₂O

Single crystals of HFPB·H₂O suitable for X-ray diffraction studies were obtained by slow evaporation of the mother liquor at room temperature. The compound crystallizes in orthorhombic, *P*bca space group with Z = 8. Molecular structure and the atom numbering scheme for the hydrazone are depicted in Fig. 2.8.
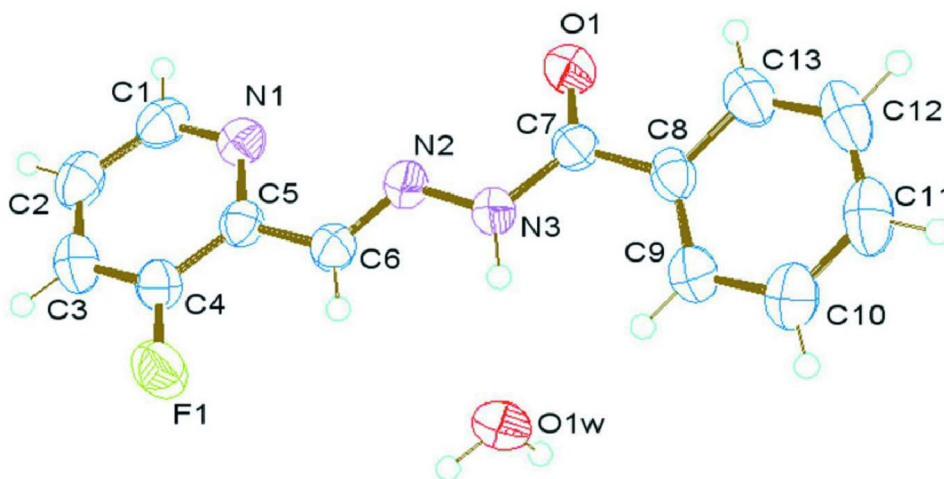
Fig. 2.8. ORTEP diagram of HFPB·H₂O with 50% probability ellipsoids.

The crystallographic data and structure refinement parameters of the compound are given in Table 2.3. The selected bond lengths and bond angles are given in Table 2.4 and the torsion angles in Table 2.5.

Table 2.3. Crystal data and structure refinement parameters for HFPB·H$_2$O

Parameters	HFPB·H$_2$O
Empirical formula	C$_{13}$H$_{12}$FN$_3$O$_2$
Formula weight	261.26
Crystal system	Orthorhombic
Space group	*Pbca*
Unit cell dimensions	
	a = 8.2540(4) Å α = 90°
	b = 11.5489(4) Å β = 90°
	c = 26.1962(11) Å γ = 90°
Volume (Å^3)	2497.14(18)
Z	8
Density (calculated) (mgm^{-3})	1.390
Absorption coefficient (mm^{-1})	0.106
F(000)	1088
Crystal size	0.35 × 0.30 × 0.25 mm^3
θ range for data collection	3.11 to 24.99°
Limiting indices	-9≤ h ≤ 9, -13≤ h ≤ 13, -31≤ h ≤ 31
Reflections collected / unique	34264 / 2192 [R(int) = 0.0265]
Completeness to θ	24.99 99.9%
Absorption correction	Semi-empirical from equivalents
Max. and min. transmission	0.9739 and 0.9637
Refinement method	Full-matrix least-squares on F^2
Data / restraints / parameters	2190 / 0 / 185
Goodness-of-fit on F^2	1.068
Final R indices [I>2σ(I)]	R$_1$ = 0.0319, wR$_2$ = 0.0855
R indices (all data)	R$_1$ = 0.0408, wR$_2$ = 0.0962
Extinction coefficient	0.0073(8)
Largest diff. peak and hole	0.181 and -0.131 e.A^{-3}

$R_1 = \Sigma||F_o| - |F_c|| / \Sigma|F_o|$ $wR_2 = [\Sigma w(F_o^2 - F_c^2)^2 / \Sigma w(F_o^2)^2]^{1/2}$

Table 2.4. Selected bond lengths [Å] and angles [°] for HFPB·H$_2$O

Bond lengths		Bond angles	
N2–C6	1.2721 (18)	C6–N2–N3	116.90 (12)
N2–N3	1.3736 (16)	N2–C6–C5	119.67 (12)
N3–C7	1.3582 (18)	N3–C7–C8	116.67 (13)
O1–C7	1.2258 (17)	O1–C7–N3	122.14 (13)
		O1–C7–C8	121.16 (13)
		C7–N3–N2	117.28 (12)

Table 2.5. Selected torsion angles [°] for HFPB·H$_2$O

Torsion angles	
N1–C5–C6–N2	5.7(2)
C4–C5–C6–N2	-175.10(14)
N3–N2–C6–C5	-179.18(11)
C6–N2–N3–C7	176.10(12)
N2–N3–C7–C8	177.81(11)
N2–N3–C7–O1	-0.4(2)
O1–C7–C8–C9	-166.31(14)
N3–C7–C8–C9	15.5(2)
O1–C7–C8–C13	13.8(2)
N3–C7–C8–C13	-164.45(13)

The molecule adopts an *E* conformation with respect to the C6=N2 bond and it exists in the amido form with a C7=O1 bond length of 1.2258(17) Å which is very close to the reported C=O bond length of a similar structure [32]. The O1 and N2 atoms are in a *Z* conformation with respect to C7–N3 having a torsion angle of -0.4(2)°. The molecule is almost planar with a maximum deviation of 0.286(2) Å for the atom C12 from its least square plane. The pyridyl ring is essentially coplanar with

the central $-C(=O)N_2C-$ unit (dihedral angle 2.02(3)°), the phenyl ring exhibits a dihedral angle of 14.41(10)° with respect to the central unit. The pyridyl ring makes a dihedral angle of 16.41(7)° with the phenyl ring.

Table 2.6. Interaction parameters present in HFPB·H$_2$O

Hydrogen bonding interactions				
D–H···A	**D–H (Å)**	**H···A (Å)**	**D···A (Å)**	**∠D–H···A (°)**
N3–H3′···O1W	0.901(18)	1.914(18)	2.7917(17)	164.3(16)
O1W–H1A···O1[a]	0.84(3)	2.08(3)	2.9187(19)	172(2)
O1W–H1A···N2[a]	0.84(3)	2.48(2)	2.9494(17)	116.1(19)
O1W–H1B···N1[a]	0.89(2)	1.95(3)	2.8420(18)	178(2)
C9–H9···O1W	0.93	2.30	3.209(2)	165

Symmetry code: (a) -x+3/2, y-1/2, z.

The water molecule forms six hydrogen bonds with two different benzohydrazone molecules. The interaction parameters are shown in Table 2.6. Hydrogen bond interactions such as O–H···N, O–H···O, N–H···O and C–H···O are present in the crystal system between the H atoms attached to the O1W atom and N1, N2, N3, C9 and O1 atoms of two adjacent molecules with D···A distances of 2.842(2), 2.9495(17), 2.7917(17), 3.209(2) and 2.9188(18) Å respectively as shown in Table 2.6. Both H-atoms of the water molecule form bifurcated hydrogen bonds with the azomethine nitrogen, the pyridyl nitrogen and the carbonyl oxygen atoms of one neighboring molecule (Fig. 2.9). The water molecule acts as a hydrogen bond acceptor towards another benzohydrazone molecule through an N–H···O hydrogen bond. Through these interactions the molecules are interconnected through the water molecule to form infinite chains parallel to the *b* axis of the unit cell (Fig. 2.9).
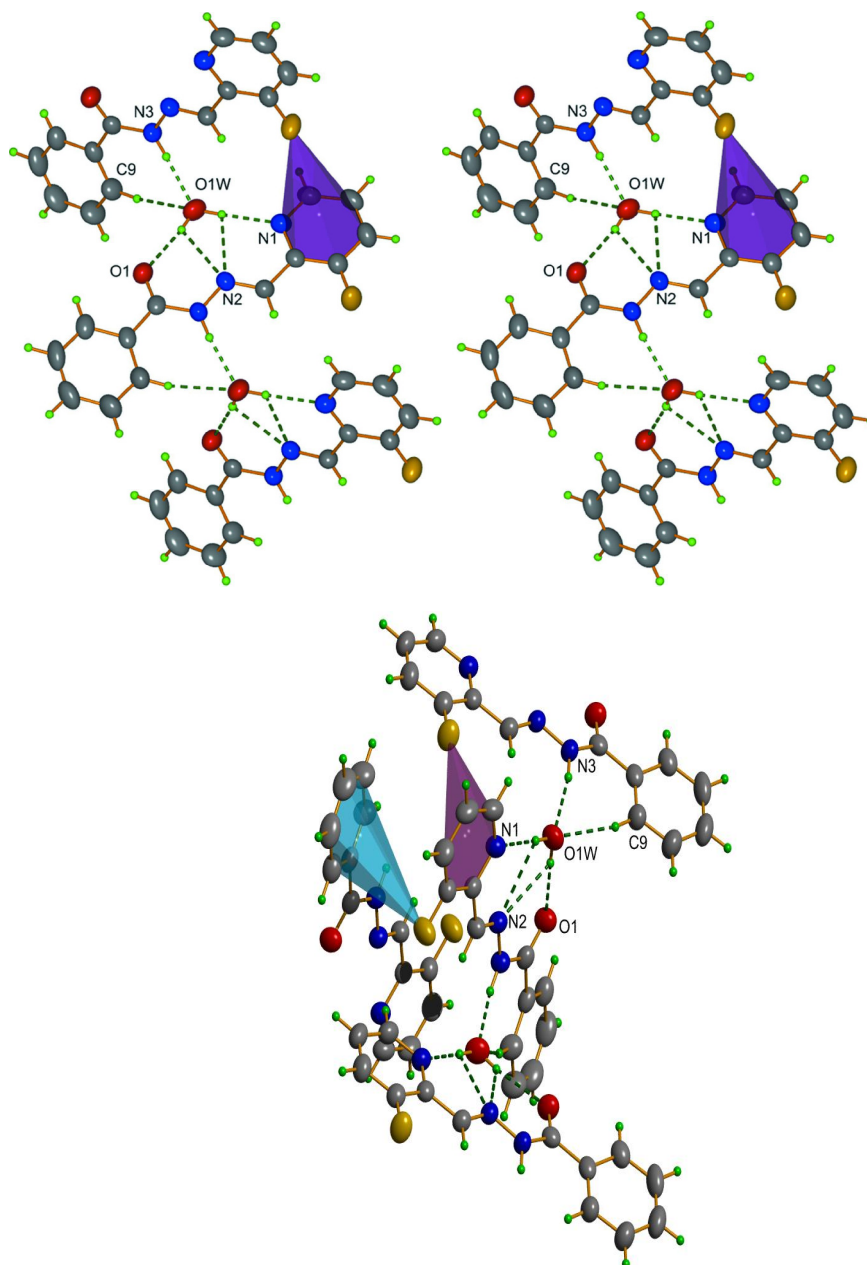
Fig. 2.9. **Hydrogen-bonding interactions showing an infinite chain in the crystal structure of HFPB·H₂O and the interconnection of the chains *via* weak C–F···π interactions.**

Benzohydrazone molecules within these chains also interact through weak C–F⋯π [3.0833(18) Å] interactions (Fig. 2.9) that augment the stronger O–H⋯N, O–H⋯O and N–H⋯O hydrogen bonds.

2.3.5.2. Crystal structure of HFPN·2H$_2$O

X-ray quality crystals of HFPN·2H$_2$O were obtained by slow evaporation of the compound from mother liquor at room temperature. A single crystal with approximate dimensions of 0.33 x 0.30 x 0.28 mm^3 was selected for collecting the data. A view of the molecule showing the crystallographic numbering scheme is given in Fig. 2.10 and structural refinement parameters are given in Table 2.7.
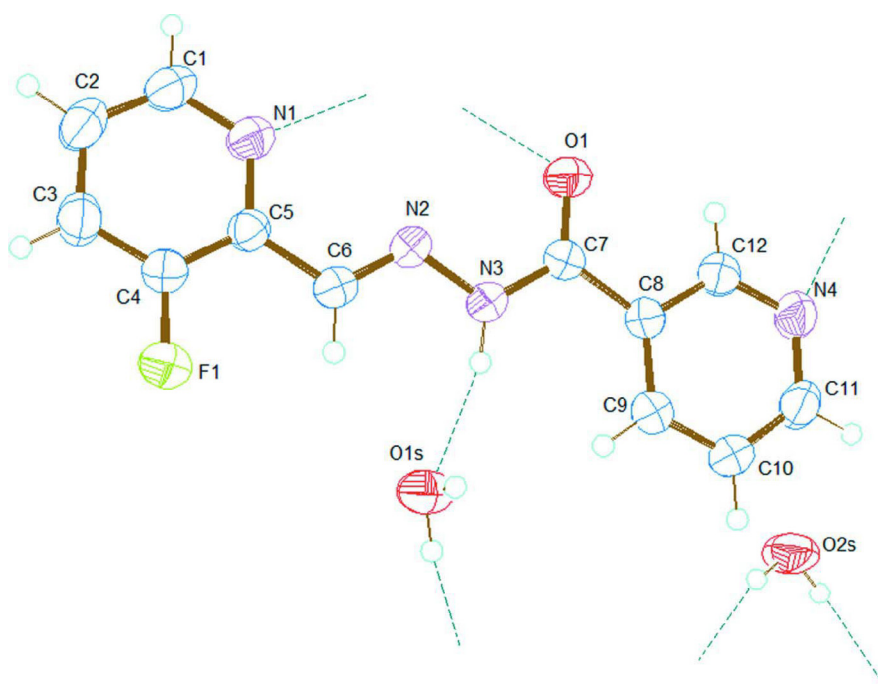
Fig. 2.10. ORTEP diagram of HFPN·2H$_2$O with 50% probability ellipsoids.

Table 2.7. Crystal data and structure refinement parameters for HFPN·2H₂O

Parameters	HFPN·2H₂O
Empirical formula	$C_{12}H_{13}FN_4O_3$
Formula weight	280.26
Crystal system	Monoclinic
Space group	$P2_1/c$
Unit cell dimensions	
	a = 7.3023(7) Å α = 90°
	b = 14.4031(17) Å β = 94.842(3)°
	c = 12.6422(13) Å γ = 90°
Volume (Å³)	1324.9(2)
Z	4
Density (calculated) (mgm⁻³)	1.405
Absorption coefficient (mm⁻¹)	0.113
F(000)	584
Crystal size	0.33 x 0.30 x 0.28 mm³
θ range for data collection	2.8 to 28.0°
Limiting indices	-9≤ h ≤ 9, -17≤ h ≤ 19, -16≤ h ≤ 16
Reflections collected / unique	9779 / 3237 [R(int) = 0.0301]
Completeness to θ	28.18 99.1%
Absorption correction	Semi-empirical from equivalents
Max. and min. transmission	0.969 and 0.963
Refinement method	Full-matrix least-squares on F^2
Data / restraints / parameters	3237 / 7 / 202
Goodness-of-fit on F^2	1.040
Final R indices [I>2σ(I)]	$R_1 = 0.0481$, $wR_2 = 0.1302$
R indices (all data)	$R_1 = 0.0677$, $wR_2 = 0.1490$
Extinction coefficient	0.079(6)
Largest diff. peak and hole	0.290 and -0.195 e.A⁻³

$$R_1 = \Sigma ||F_o| - |F_c|| / \Sigma |F_o| \qquad wR_2 = [\Sigma w(F_o^2 - F_c^2)^2 / \Sigma w(F_o^2)^2]^{1/2}$$

The compound crystallizes in monoclinic space group, $P2_1/c$ with Z=4. This molecule adopts an *E* configuration with respect to the C6=N2 bond and it exists in the amido form with a C7=O1 bond length of 1.2211(18) Å which is very close to the reported C=O bond length of similar structure of benzene analogue [33]. The O1 and N2 atoms are in a *Z* configuration with respect to C7–N3 having a torsion angle of -0.6(3)°. The molecule is almost planar with maximum deviation of 0.117(1) Å for the atom O1 from the mean plane of the molecule (r.m.s. deviation, 0.0513). The pyridyl ring having F atom is essentially coplanar with the central C(=O)N$_2$C unit (dihedral angle 5.71(8)°), the other pyridyl ring exhibits a torsion angle of 1.99(7)°. The pyridyl ring lies in the almost same plane making a dihedral angle of 3.78(7)° with other pyridyl ring of hydrazide part. The selected bond lengths and angles are given in Table 2.8 and torsion angles in Table 2.9.

Table 2.8. Selected bond lengths [Å] and angles [°] for HFPN·2H$_2$O

Bond lengths		Bond angles	
N2–C6	1.267 (2)	C6–N2–N3	117.37 (13)
N2–N3	1.3707 (17)	N2–C6–C5	119.32 (13)
N3–C7	1.3534 (19)	N3–C7–C8	117.29 (13)
O1–C7	1.2211 (18)	O1–C7–N3	122.44 (14)
		O1–C7–N8	120.26 (14)
		C4–C5–C6	120.63 (13)
		C7–N3–N2	117.32 (12)

Table 2.9. Selected torsion angles [°] for HFPN·2H₂O

Torsion angles	
N2–C6–C5–N1	6.6 (2)
N2–C6–C5–C4	-173.62 (15)
C5–C6–N2–N3	-179.37 (13)
C6–N2–N3–C7	179.03 (14)
N2–N3–C7–C8	179.54 (13)
N2–N3–C7–O1	-0.6 (3)
O1–C7–C8–C9	177.57 (17)
N3–C7–C8–C9	-2.5 (2)
O1–C7–C8–C12	-2.0 (2)
N3–C7–C8–C12	177.88 (14)

Whilst one of the water molecules connects two adjacent molecules through two O–H···N and N–H···O hydrogen bonding interactions with D···A distances of 2.946(2) and 2.882(1) Å respectively, the other water molecule forms two O–H···N and O–H···O hydrogen bonds with D···A distances of 2.965(2) and 2.816(2) Å with the same molecule (Fig. 2.11 and Table 2.10).
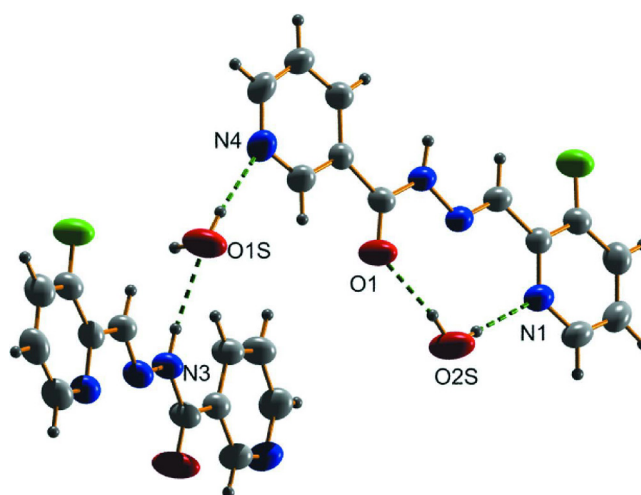
Fig. 2.11. Hydrogen-bonding interactions showing the interconnection of the molecules *via* one of the water molecules in the lattice.

Table 2.10. Interaction parameters present in HFPN·2H$_2$O

Hydrogen bonding interactions				
D–H⋯A	**D–H (Å)**	**H⋯A (Å)**	**D⋯A (Å)**	**∠D–H⋯A (°)**
N3–H3′⋯O1S	0.88(1)	2.04(1)	2.8821(19)	160(2)
O2S–H2A⋯N1[a]	0.87(1)	2.10(1)	2.965(2)	177(2)
O1S–H1A⋯N4[a]	0.87(1)	2.09(1)	2.946(2)	170(3)
O2S–H2B⋯O1[a]	0.86(1)	1.97(1)	2.816(2)	172(2)
π⋯π interactions				
Cg(I)⋯Cg(J)	**Cg⋯Cg (Å)**	**α (º)**	**β (º)**	**γ (º)**
Cg(1)⋯Cg(2)[b]	3.7099(10)	3.78(7)	22.19	19.71
Cg(1)⋯Cg(2)[c]	3.6322(10)	3.78(7)	18.09	14.41
Cg(2)⋯Cg(1)[b]	3.7099(10)	3.78(7)	19.71	22.19
Cg(2)⋯Cg(1)[c]	3.6322(10)	3.78(7)	14.41	18.09
C–F⋯π interactions				
C–F⋯Cg	**X⋯Cg (Å)**	**C–F⋯Cg (°)**	**C⋯Cg (Å)**	
C(4)–F(1)⋯Cg(2)[c]	3.7574(14)	66.84(8)	3.4569(16)	

Symmetry code: (a) x, -y+3/2, z+1/2; (b) 1-x,2-y,-z; (c) 2-x,2-y,-z

D = Donor, A = acceptor, Cg = Centroid of the ring

Cg(1) = N(1), C(1), C(2), C(3), C(4), C(5)

Cg(2) = N(4), C(11), C(10), C(9), C(8), C(12)

α(°) = Dihedral Angle between planes I and J

β(°) = Angle between Cg(I)⋯Cg(J) and Cg(J) perp.

γ(°) = Angle between Cg(I)⋯Cg(J) vector and Cg(I) perp.

One of the water molecules acts as both a hydrogen bond acceptor as well as a donor towards another carbohydrazide molecule while the other acts only as hydrogen bond donor. By means of these interactions,

the molecules are chained through one of the water molecules to form infinite chains parallel to the *c* axis of the unit cell (Fig. 2.12).
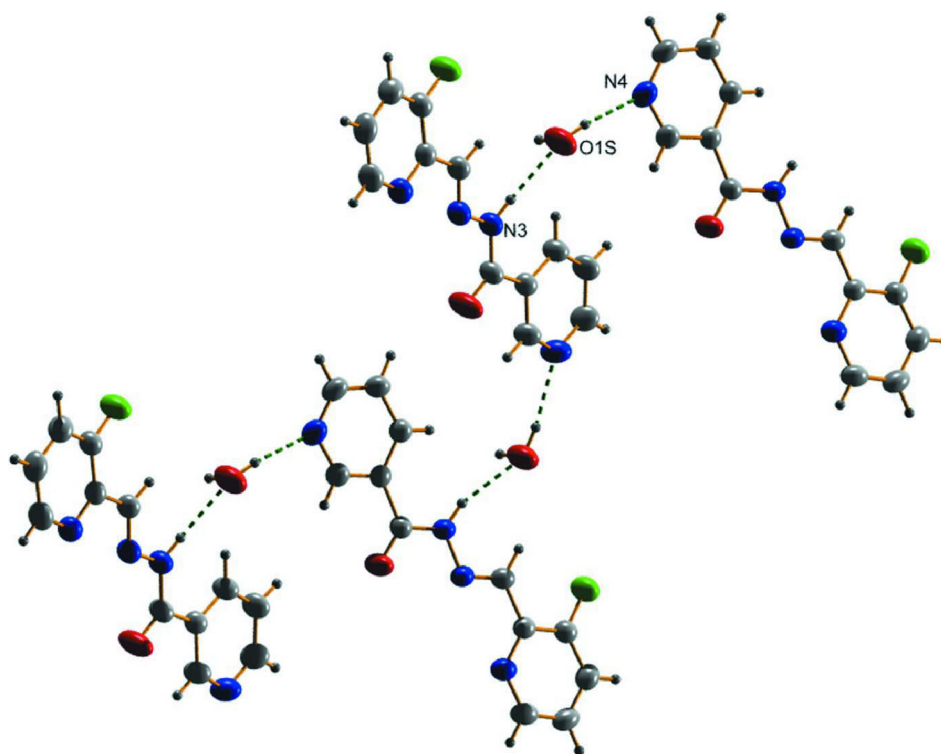
Fig. 2.12.   Hydrogen bonding interactions showing the chain progressing along *c* axis.

These parallel chains are stacked one over the other by means of two π···π interactions between the two aromatic rings of the neighbouring anti parallel molecules (Fig. 2.13) with centroid-centroid distances of 3.7099(10) and 3.6322(10) Å (Table 2.10). Fig. 2.14 shows the stacked packing of the molecules along *a* axis in the unit cell.

Fig. 2.13.   Hydrogen bonding and π···π interactions in the lattice.

Fig. 2.14.   Packing diagram showing the stacked packing arrangement of the molecules along *a* axis.

References

[1] M. Sutradhar, E.C.B.A. Alegria, K.T. Mahmudov, M.F.C.G. da Silva, A.J.L. Pombeiro, RSC Adv. 6 (2016) 8079.

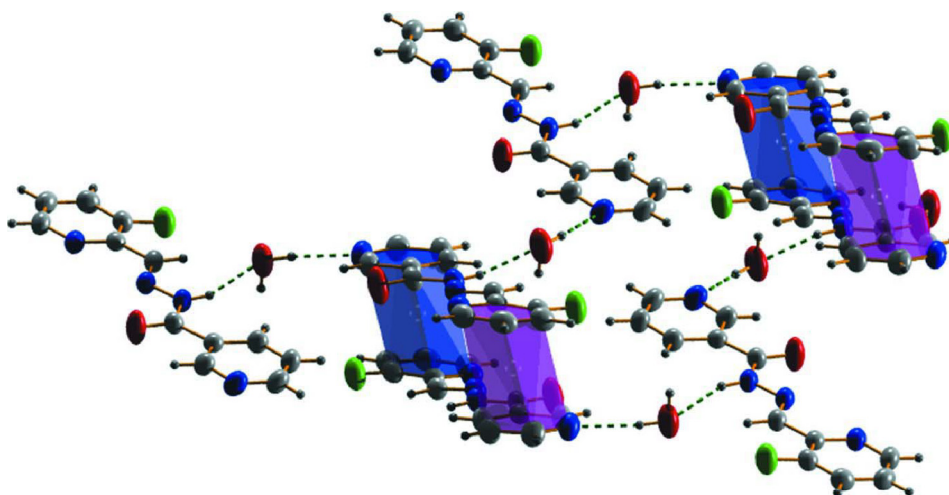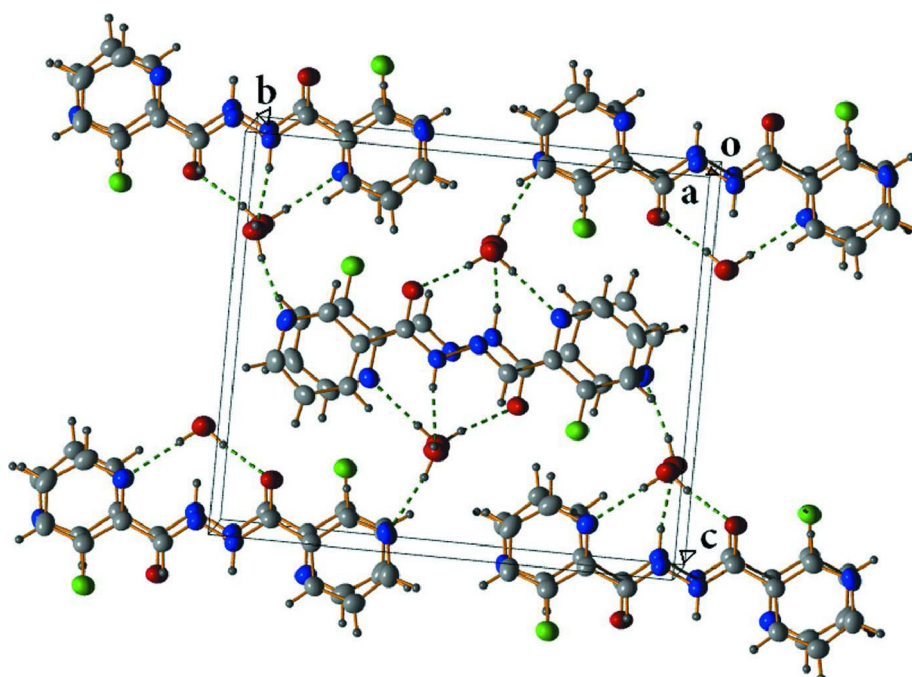[2] S. Naskar, S. Naskar, S. Mondal, P.K. Majhi, M.G.B. Drew, S.K. Chattopadhyay, Inorg. Chim. Acta 371 (2011) 100.

[3] L. Li, Y.Z. Zhang, E. Liu, C. Yang, J.A. Golen, A.L. Rheingold, G. Zhang, J. Mol. Struct. 15 (2016) 180.

[4] M. Kuriakose, M.R.P. Kurup, E. Suresh, Spectrochim. Acta 66A (2007) 353.

[5] S. Das, S. Pal, J. Mol. Struct. 741 (2005) 183.

[6] M. Carcelli, S. Ianelli, P. Pelagatti, G. Pelizzi, D. Rogolino, C. Solinas, M. Tegoni, Inorg. Chim. Acta 358 (2005) 903.

[7] M.G. -Vargas, M.C. Belizón, M. Milla, J.A. Pérez-Buatamante, Analyst 110 (1985) 51.

[8] M. Bakir, C. Gyles, J. Mol. Struct. 753 (2005) 35.

[9] D. Sriram, P. Yogeeswari, K. Madhu, Bioorg. Med. Chem. Lett. 15 (2005) 4502.

[10] J. Patole, U. Sandbhor, S. Padhye, D.N. Deobagkar, C.E. Anson, A. Powell, Bioorg. Med. Chem. Lett. 13 (2003) 51.

[11] J.L. Buss, E. Arduini, P. Ponka, Biochem. Pharmacol. 64 (2002) 1689.

[12] B.N.B. Raj, M.R.P. Kurup, Spectrochim. Acta 66A (2007) 898.

[13] P.B. Sreeja, M.R.P. Kurup, A. Kishore, C. Jasmin, Polyhedron 23 (2004) 575.

[14] J. Hou, W.-H. Sun, D. Zhang, L. Chen, W. Li, D. Zhao, H. Song, J. Mol. Catal. A: Chem. 231 (2005) 221.

[15] P. Krishnamoorthy, P. Sathyadevi, A.H. Cowley, R.R. Butorac, N. Dharmaraj, Eur. J. Med. Chem. 46 (2011) 3376.

[16] N.P. Belskaya, W. Dehaen, V.A. Bakulev, Arkivoc (i) (2010) 275.

[17] T.A. Reena, E.B. Seena, M.R.P. Kurup, Polyhedron 27 (2008) 1825.

[18] K.P.C. Vollhardt, N.E. Schore, Organic Chemistry: Structure and Function, 5th Edn., W. H. Freeman and Company, New York (2007).

[19] S. Sinha, A.K. Srivastava, S.K. Sengupta, O.P. Pandey, Transit. Met. Chem. 33 (2008) 563.

[20] N. Mathew, M. Kuriakose, E.B. Seena, M.R.P. Kurup, Acta Cryst. E63 (2007) o2190-o2191.

[21] M.M. Al-Ne'aimi, M.M. Al-Khuder, Spectrochim. Acta 105A (2013) 365.

[22] P.B. Sreeja, A. Sreekanth, C.R. Nayar, M.R.P. Kurup, A. Usman, I.A. Razak, S. Chantrapromma, H.-K. Fun, J. Mol. Struct. 645 (2003) 221.

[23] F. Hueso-Ureña, N.A. Illan-Cabeza, M.N. Moreno-Carretero, A.L. Peñas-Chamorro, R. Faure, Polyhedron 19 (2000) 689.

[24] W. Kemp, Organic Spectroscopy, 3rd Edn., Macmillan, Hampshire (1996).

[25] D.L. Pavia, G.M. Lapman, G.S. Kriz, J.R. Vyvyan, 3rd Edn., Introduction to spectroscopy, Harcourt College Publishers, Orlando (2004).

[26] R.A.-El-Halawa, M. Al-Nuri, F. Mahmoud, Asian J. Chem. 19 (2007) 1658.

[27] B.N.B. Raj, M.R.P. Kurup, E. Suresh, Spectrochim. Acta 71A (2008) 1253.

[28] Bruker, *APEX2, SAINT, XPREP and SADABS*, Bruker AXS Inc., Madison, Wisconsin, USA (2004).

[29] G.M. Sheldrick, SHELXL97 and SHELXS97, University of Göttingen, Germany, 1997.

[30] G.M. Sheldrick, Acta Cryst. A64 (2008) 112.

[31] L.J. Farrugia, J. Appl. Cryst. 45 (2012) 849.

[32] K. Brandenburg, Diamond Version 3.2g, Crystal Impact GbR, Bonn, Germany, (2010).

[33] N.A. Mangalam, S. Sivakumar, S.R. Sheeja, M.R.P. Kurup, E.R.T. Tiekink, Inorg. Chim. Acta 362 (2009) 4191.

[34] Y. Nair, M. Sithambaresan, M.R.P. Kurup, Acta Cryst. E68 (2012) o2709.

.....ഇരു.....

SYNTHESES, SPECTRAL CHARACTERIZATION AND CRYSTAL STRUCTURE OF COPPER(II) CHELATES OF TRIDENTATE AROYLHYDRAZONES

3.1. Introduction

Copper was one of the first metals used widely because the metal is fairly plentiful (among the 25 most abundant elements in the earth's crust) and can be found in its metallic state. In addition, this metal and its alloys have a number of beneficial qualities including ductility, malleability, strength, corrosion resistance, and high thermal and electrical conductivity, combined with an attractive appearance. Copper is also an essential trace nutrient for organisms ranging from bacteria to mammals. Copper is essential to all living organisms as a trace dietary mineral because it is a key constituent of the respiratory enzyme complex cytochrome c oxidase. The main areas where copper is found in humans are liver, muscle and bone. Copper compounds are used as bacteriostatic substances.

Copper exhibits rich coordination chemistry with complexes known in oxidation states ranging from 0 to +4, although the +2 (cupric) and the +1 (cuprous) oxidation states are by far the most common, with +2 predominating. Compounds of copper have found extensive practical usage, including as catalysts in both homogeneous and heterogeneous reactions, as fungicides, pesticides, and wood preservatives, as pigments for paints and glasses, and in the so-called high-temperature superconductors.

The coordination numbers and geometries of copper complexes vary with oxidation state. The structural diversity of the copper(II) complexes is largely related to Cu(II) d^9 system. It enables a variety of coordination polyhedra with significantly different geometries. Copper(II) is found in many reported compounds of diverse structures, generally in mononuclear, binuclear, and polynuclear species [1]. For the spherically symmetric d^{10} Cu(I) ion, the common geometries are two-coordinate linear, three-coordinate trigonal planar, and four-coordinate tetrahedral. Cu(I) compounds are diamagnetic and colorless, except where color results from charge-transfer bands or a counter ion; these complexes are often fairly readily oxidized to Cu(II) compounds. Cu(III) complexes are typically square planar and diamagnetic.

Cu(II) species in various coordination environments are of interest to many researchers primarily due to their structural, magnetic, electron transfer and catalytic properties and also due to their biological potential and EPR features [2,3]. Copper is one of the transition elements frequently found at the active site of proteins. The copper containing

enzymes and proteins constitute an important class of biologically active compounds. The biological functions of copper enzymes/proteins include electron transfer, dioxygen transport, oxygenation, reduction, oxidation and disproportionation that exploit the easy interconversion of Cu(I) and Cu(II). Because of their biological relevance a large number of copper(II) complexes have been synthesized with different perspectives [4,5].

Cu(II) complexes of diverse drugs have been the subject of a large number of research studies, presumably due to the biological role of Cu(II) and its synergetic activity with the drug. The antifungal and antibacterial properties of a range of Cu(II) complexes have been evaluated against several pathogenic fungae and bacteria *Escherichia coli*, *Pseudomonas aeruginosa*, *Staphylococcus aureus*, *Bacillus subtilis*, *Enterococcus faecalis* and *Streptococcus pyogenes* and fungi *Candida albicans*, *Aspergillus niger* and *Aspergillus clavatus*. The activity data show that the metal complexes have a promising biological activity comparable with the parent ligand against all bacterial and fungal species [6-8].

Metal complexes of substituted hydrazones have been found to hold therapeutic activity. The complexes could bind and cleave the DNA strands *via* different mechanisms under different physiological conditions. DNA is an important cellular receptor. Many chemicals exert their antitumor effects through binding with DNA, thereby changing the replication of DNA and further inhibiting the growth of the tumor cells. Based on it, new and more efficient antitumor drugs are

designed. Their effectiveness depends on the mode and affinity of the binding. Some aroylhydrazones (AH) have been widely investigated as one of the orally effective tridentates iron chelators [9]. Aroylhydrazone complexes of transition metals are used as models for elucidation the mechanism of enzyme inhibition [10]. Aroylhydrazones on complexation with Cu(II) have also been proposed as anticancer drug analogues. Recently, Gup *et al.*, reported self-activating nuclease activity (DNA cleavage) of copper(II) aroylhydrazone complexes of the type $[CuL]_n$. The experimental results suggest that the copper complexes bind significantly to calf thymus DNA by both groove binding and intercalation modes and cleavage effectively pBR322 DNA [11].

Proteasome inhibition is a desirable target for controlling the aberrant growth of tumor cells. Dou *et al.*, have shown that copper complex of 8-hydroxyquinoline can potently and selectively inhibit the chymotrypsin-like activity of the proteasome *in vivo* [12]. Highly elevated levels of copper can be tumor-specific and use of copper chelators might be one of the useful strategies for cancer therapies. The role of copper metal in the ubiquitin-proteasome pathway is as yet undetermined. Although copper alone has been known to inhibit the activity of purified proteasome and copper complexes are able to inhibit the cellular proteasome activity, the exact mechanism remains to be explored [13]. The EPR and magnetic studies of Cu(II) complexes have attracted the eyes of various research groups [14-16].

With all these facts in the mind here we report the syntheses and spectral characteristics of eight novel Cu(II) complexes of two

NNO donor aroylhydrazones with special emphasis to EPR spectral properties.

3.2. Experimental
3.2.1. Materials

All reagents for the synthesis were commercially available and were used as received without further purification. 3-Fluoropyridine-2-carbaldehyde (Sigma-Aldrich), benzhydrazide (Sigma-Aldrich), nicotinic hydrazide (Sigma-Aldrich), copper(II) acetate monohydrate (Merck), copper(II) perchlorate hexahydrate (Aldrich), copper(II) sulphate pentahydrate (Merck), sodium azide (Reidel-De Haen) and potassium thiocyanate (Merck) were of Analar grade and were used as received. Solvents used were methanol, ethanol, DMSO and DMF.

3.2.2. Syntheses of aroylhydrazones

3-Fluoropyridine-2-carbaldehyde benzoylhydrazone monohydrate (HFPB·H$_2$O) and 3-fluoropyridine-2-carbaldehyde nicotinoylhydrazone dihydrate (HFPN·2H$_2$O) were synthesized as discussed in Chapter 2.

3.2.3. Syntheses of Cu(II) complexes
3.2.3.1. [Cu$_2$(FPB)$_2$(μ-NCS)$_2$] (1)

To the methanolic solution of HFPB·H$_2$O (0.2612 g, 1 mmol), aqueous solution of KSCN (0.0970 g, 1 mmol) was added drop wise and stirred for half an hour. This was followed by the addition of aqueous solution of copper(II) acetate monohydrate (0.1990 g, 1 mmol) and again stirred for 2 hours and the resulting solution was refluxed for 4 hours. The green colored complex separated was filtered, washed

thoroughly with methanol followed by ether and dried over P_4O_{10} *in vacuo.*

$[Cu_2(FPB)_2(\mu\text{-}NCS)_2]$ (**1**): Yield: 71%, λ_m (DMF): 9 ohm^{-1} cm^2 mol^{-1}, μ_{eff} (B.M.): 1.32, Elemental Anal. Found (Calcd.) (%): C: 46.73 (46.21); H: 2.81 (2.49); N: 15.91 (15.40).

3.2.3.2. $[Cu(HFPB)(SO_4)]\cdot H_2O$ (2)

To the methanolic solution of $CuSO_4\cdot5H_2O$ (0.2490 g, 1 mmol), methanolic solution of the hydrazone, $HFPB\cdot H_2O$ (0.2612 g, 1 mmol) was added drop wise and the mixture was stirred for 10 minutes. The resulting deep green solution was then refluxed for 4 hours, the light green color product separated was filtered, washed thoroughly with methanol followed by ether and dried over P_4O_{10} *in vacuo.*

$[Cu(HFPB)(SO_4)]\cdot H_2O$ (**2**): Yield: 66%, λ_m (DMF): 66 ohm^{-1} cm^2 mol^{-1}, μ_{eff} (B.M.): 1.81, Elemental Anal. Found (Calcd.) (%): C: 37.82 (37.10); H: 3.01 (2.87); N: 10.39 (9.98).

3.2.3.3. $[Cu(FPB)(ClO_4)]$ (3)

To a methanolic solution of $Cu(ClO_4)_2\cdot6H_2O$ (0.3700 g, 1 mmol), methanolic solution of $HFPB\cdot H_2O$ (0.2612 g, 1 mmol) was added and the reaction mixture was refluxed for 3 hours. The green color product separated was filtered, washed thoroughly with methanol followed by ether and dried over P_4O_{10} *in vacuo.*

$[Cu(FPB)(ClO_4)]$ (**3**): Yield: 62%, λ_m (DMF): 42 ohm^{-1} cm^2 mol^{-1}, μ_{eff} (B.M.): 1.63, Elemental Anal. Found (Calcd.) (%): C: 39.15 (38.53); H: 2.56 (2.24); N: 10.82 (10.37).

3.2.3.4. [Cu(FPB)(OAc)(H₂O)] (4)

Cu(CH₃COO)₂·H₂O (0.1990 g, 1 mmol) dissolved in ethanol was refluxed with an ethanolic solution of HFPB·H₂O (0.2612 g, 1 mmol) for 2 hours. The resulting solution was then chilled overnight and the green color crystals separated were collected, washed thoroughly with methanol followed by ether and dried over P_4O_{10} *in vacuo.*

[Cu(FPB)(OAc)(H₂O)] (**4**): Yield: 65%, λ_m (DMF): 1.4 ohm^{-1} cm^2 mol^{-1}, μ_{eff} (B.M.): 1.78, Elemental Anal. Found (Calcd.) (%): C: 47.77 (47.06); H: 4.09 (3.69); N: 11.59 (10.98).

3.2.3.5. [Cu(FPB)(N₃)(H₂O)₂] (5)

Cu(CH₃COO)₂·H₂O (0.1990 g, 1 mmol) dissolved in methanol was added to a solution of HFPB·H₂O (0.2612 g, 1 mmol) in methanol and stirred for 10 minutes. A solution of NaN₃ (0.0650 g, 1 mmol) in minimum volume of water-methanol mixture was then added to the solution followed by a further stirring of 3-4 hours. The green product formed was filtered, washed thoroughly with methanol followed by ether and dried over P_4O_{10} *in vacuo.*

[Cu(FPB)(N₃)(H₂O)₂] (**5**): Yield: 71%, λ_m (DMF): 4 ohm^{-1} cm^2 mol^{-1}, μ_{eff} (B.M.): 1.73, Elemental Anal. Found (Calcd.) (%): C: 40.03 (40.68); H: 3.05 (3.41); N: 22.41 (21.9).

3.2.3.6. [Cu(FPB)₂] (6)

Cu(CH₃COO)₂·H₂O (0.0990 g, 0.5 mmol) dissolved in ethanol was added to ethanolic solution of HFPB·H₂O (0.2612 g, 1 mmol). The resulting dark brown solution was then refluxed for 3-4 hours and then cooled at room temperature. The dark brown product formed was filtered,

washed thoroughly with methanol followed by ether and dried over P_4O_{10} *in vacuo.*

[Cu(FPB)$_2$] (**6**): Yield: 61%, λ_m (DMF): 60 ohm^{-1} cm^2 mol^{-1}, μ_{eff} (B.M.): 1.68, Elemental Anal. Found (Calcd.) (%): C: 57.39 (56.98); H: 3.69 (3.31); N: 15.05 (15.34).

3.2.3.7. [Cu(FPN)$_2$] (7)

Cu(CH$_3$COO)$_2$·H$_2$O (0.0990 g, 0.5 mmol) dissolved in ethanol was added to ethanolic solution of HFPN·2H$_2$O (0.2802 g, 1 mmol). The resulting green color solution was then refluxed for about 5 hours and then cooled at room temperature. The green color product formed was filtered, washed thoroughly with methanol followed by ether and dried over P_4O_{10} *in vacuo.*

[Cu(FPN)$_2$] (**7**): Yield: 60%, λ_m (DMF): 54 ohm^{-1} cm^2 mol^{-1}, μ_{eff} (B.M.): 1.67, Elemental Anal. Found (Calcd.) (%): C: 51.92 (52.41); H: 2.64 (2.93); N: 20.99 (20.37).

3.2.3.8. [Cu(FPN)(OAc)(H$_2$O)] (8)

Cu(CH$_3$COO)$_2$·H$_2$O (0.1990 g, 1 mmol) dissolved in ethanol was refluxed with ethanolic solution of HFPN·2H$_2$O (0.2802 g, 1 mmol) for 2 hours. The resulting solution was then chilled overnight and the green color product separated was filtered, washed thoroughly with methanol followed by ether and dried over P_4O_{10} *in vacuo.*

[Cu(FPN)(OAc)(H$_2$O)] (**8**): Yield: 59%, λ_m (DMSO): 2 ohm^{-1} cm^2 mol^{-1}, μ_{eff} (B.M.): 1.69, Elemental Anal. Found (Calcd.) (%): C: 43.22 (43.81); H: 3.16 (3.41); N: 15.11 (14.60).

3.3. Results and discussion

All the complexes except **1** and **5** were prepared by refluxing ethanolic solutions of the metal salt and the ligand in 1:1 or in 1:2 ratios. Complexes **1** and **5** were prepared by refluxing metal salt, ligand and pseudohalides in 1:1:1 ratio. In all the complexes except **2**, hydrazones deprotonate and chelate in the iminolate form as proven by IR spectral data. In complex **2**, the ligand coordinates to the metal center in the neutral amido form. The complexes prepared were either green or dark brown in color. They are air stable solids, soluble in DMSO, acetonitrile or DMF and insoluble in water, MeOH, ethanol, chloroform and dichloromethane. Complexes **2** and **8** contain coordinated or uncoordinated water molecules which are further confirmed from their thermogravimetric analyses. The X-ray crystal structure of the complex [Cu(FPB)(OAc)(H$_2$O)]·H$_2$O (**4a**) has been successfully determined and is found to possess a distorted square pyramidal coordination geometry. The thermal analyses (TG-DTG) of a few complexes show multi-step decomposition pattern of the bonded ligands. The synthesized compounds were characterized by the following physico-chemical methods.

3.3.1. Elemental analyses

Elemental (C, H, N) analyses of all the samples were carried out and the values are given in Section 3.2.3. The elemental analyses agree well with a 1:1 or 1:2 metal-to-ligand stoichiometry for most of the complexes.

3.3.2. Molar conductivity and magnetic susceptibility measurements

The molar conductivity values for 10^{-3} M DMF/DMSO solutions of the complexes indicate that they are probably non-electrolytic in nature.

Magnetic moments of the complexes were calculated from magnetic susceptibility measurements. Mononuclear copper(II) complexes exhibit magnetic moments in the range 1.63-1.81 B.M. which are close to their spin only value. The magnetic moment of binuclear Cu(II) complex $[Cu_2(FPB)_2(\mu\text{-}NCS)_2]$ (**1**) is 1.32 B.M. which was in the range of 1.15-1.40 B.M. found for binuclear complexes. This low magnetic moment may be attributed to the presence of a strong antiferromagnetic spin-spin interaction of two magnetic centers suggesting a dimeric nature for this complex [17,18].

### 3.3.3. Infrared spectral studies

The IR bands are most useful for the determination of the mode of coordination and are presented in Table 3.1 and Figs. 3.1-3.8. The coordination modes of the hydrazones in the Cu(II) complexes are confirmed by assigning the strong bands observed in the FT-IR spectra of complexes as suggested by Nakamoto [19].

Table 3.1. The important IR frequencies (cm^{-1}) of Cu(II) complexes

Compound	v(N–H)	v(C=O)/v(C–O)	v(C=N)	v(C=N)[a]
HFPB·H$_2$O	3059	1683	1597	--
$[Cu_2(FPB)_2(\mu\text{-}NCS)_2]$ (**1**)	--	1377	1551	1607
$[Cu(HFPB)(SO_4)]$·H$_2$O (**2**)	3050	1660	1590	--
$[Cu(FPB)(ClO_4)]$ (**3**)	--	1396	1572	1590
$[Cu(FPB)(OAc)(H_2O)]$ (**4**)	--	1337	1563	1593
$[Cu(FPB)(N_3)(H_2O)_2]$ (**5**)	--	1357	1564	1591
$[Cu(FPB)_2]$ (**6**)	--	1344	1550	1584
HFPN·2H$_2$O	3058	1682	1590	--
$[Cu(FPN)_2]$ (**7**)	--	1362	1574	1587
$[Cu(FPN)(OAc)(H_2O)]$ (**8**)	--	1365	1583	1594

[a]Newly formed C=N bond

The peak in the range 1590-1597 cm^{-1} corresponding to ν(C=N) band in the uncomplexed hydrazone shifts to lower frequency in all the complexes indicating the coordination of azomethine nitrogen to the central Cu(II) ion. The ν(C=O) and ν(N–H) stretching bands in the range 1682-1683 and 3058-3059 cm^{-1} respectively corresponding to free ligands are not observed in the spectra of complexes except for [Cu(HFPB)(SO$_4$)]·H$_2$O (**2**). This fact along with the appearance of a new medium band in the range assignable to ν(C–O) stretching vibration indicates that the hydrogen atom of the amide group is lost on complexation, supporting the ligand coordination around the Cu(II) ion in its deprotonated form in the complexes.
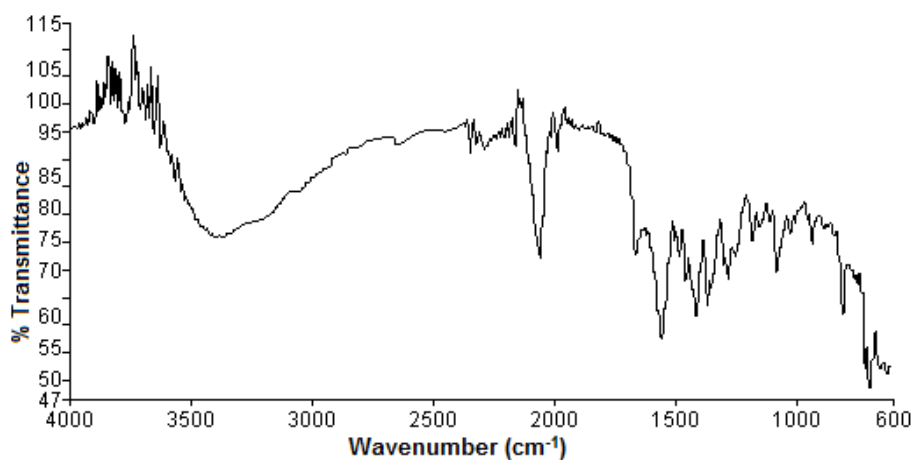
Fig. 3.1. IR spectrum of [Cu$_2$(FPB)$_2$(μ-NCS)$_2$] (1).

In the thiocyanato complex (Fig. 3.1), a single and strong sharp peak in the range 2078-2081 cm^{-1} is characteristic of bridging thiocyanate group in the compound. The intensity and the band position indicate the coordination of thiocyanate through the nitrogen atom [20,21]. The

newly formed C=N due to iminolization of the ligand resonates at 1607 cm^{-1} in the complex. The negative shift of the band corresponding to ν(C=N) at 1597 cm^{-1} in the free ligand to 1551 cm^{-1} in the complex is consistent with the coordination of the azomethine nitrogen to the central Cu(II) ion. A new band observed at 1377 cm^{-1} can be assigned to ν(C=O) stretch, newly formed as a result of deprotonation of the ligand for coordination. The pyridine ring vibrations are found in the usual range.
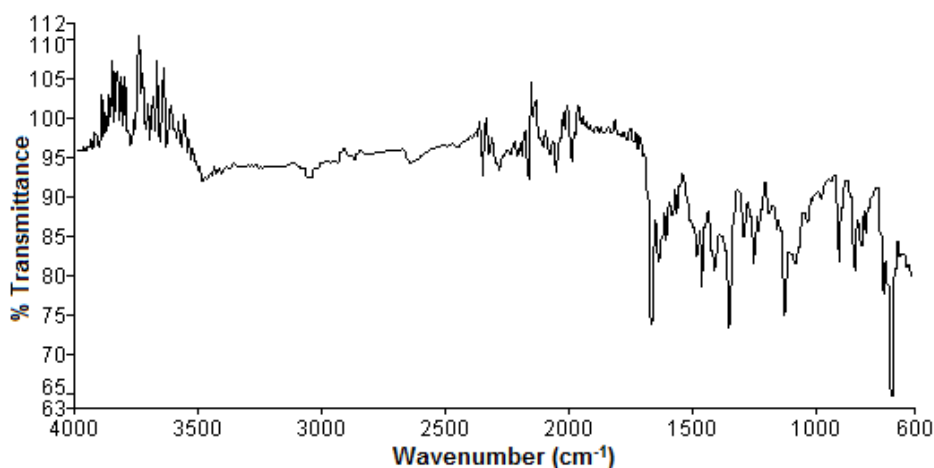
Fig. 3.2. IR spectrum of [Cu(HFPB)(SO$_4$)]·H$_2$O (2).

In the complex [Cu(HFPB)(SO$_4$)]·H$_2$O (**2**), the appearance of a medium band between 3362-3470 cm^{-1} is consistent with lattice water content in the sample, while a weak band around 3050 cm^{-1} can be assigned to the ν(NH) vibration. Coordination of the pyridine nitrogen is indicated by a positive shift of the in-plane ring deformation band. The free sulfate ion belongs to the high symmetry T$_d$ point group. Of the four fundamentals, only ν$_3$ and ν$_4$ are IR active; bands at ~ 1105 and ~ 615 cm^{-1}, assignable to ν$_3$ stretching [ν(SO)] and ν$_4$ bending [δ(OSO)] modes,

respectively [20]. The ν_1 stretching [ν(SO)] and ν_2 bending [δ(OSO)] fundamentals are not IR active. However, the coordination of SO_4^{2-} to metal ions in a bidentate fashion decreases the symmetry of the group and it reduces to C_{2v}, when it functions as a bidentate ligand in the complex and the ν_3 and ν_4 modes may be split [20,22,23]. For the sulfato complex **2** in this study, the chelating bidentate nature of the SO_4^{2-} group is indicated by the strong band at 1142 cm^{-1}; ν_3(S-O) as well as a medium band at 666 cm^{-1}; ν_4[δ(OSO)] characteristic for the tetrahedral (T_d) point group. These spectral features suggest a low symmetry for the sulfato ligand in the complex.
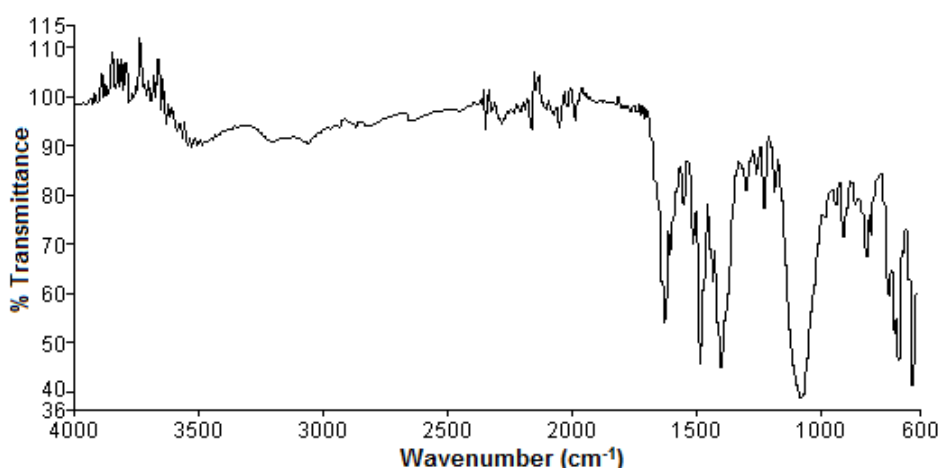
Fig. 3.3. IR spectrum of [Cu(FPB)(ClO$_4$)] (3).

The perchlorato complex (Fig. 3.3) shows a characteristic band at 1168 cm^{-1} indicating the presence of perchlorate bonded to the copper atom [24]. The appearance of a new peak at 1590 cm^{-1} in the complex [Cu(FPB)(ClO$_4$)] (**3**) is due to asymmetric stretching vibration of C=N bond as a result of the iminolization of the ligand. A medium band in the

3058-3059 cm^{-1} range due to ν(N–H) vibration disappears in the spectrum of complex providing strong evidence for ligand coordination to the Cu(II) ion in the deprotonated iminolate form. The out-of-plane pyridine ring deformation modes of free ligands are found to be shifted to higher energies in the spectrum of complex indicating the coordination *via* the nitrogen atom of the pyridine ring [25].
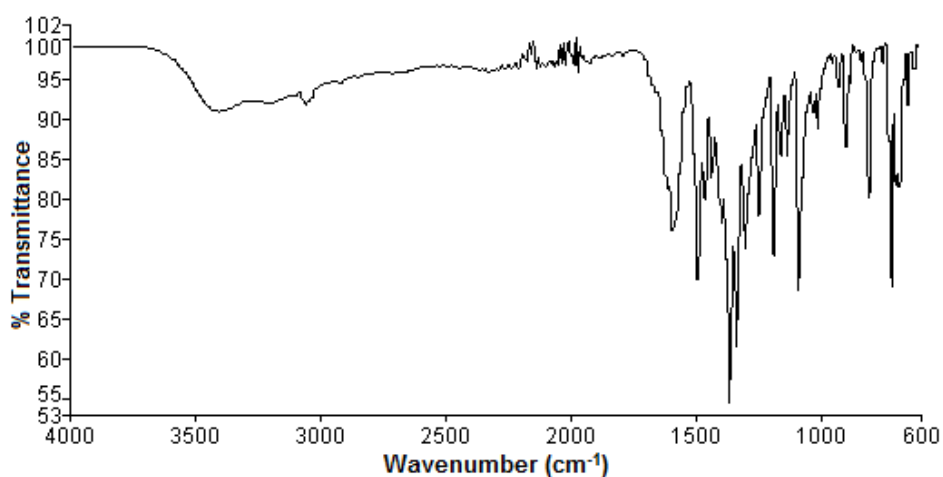
Fig. 3.4. IR spectrum of [Cu(FPB)(OAc)(H$_2$O)] (4).

Similar to complex **3** in the IR spectrum of [Cu(FPB)(OAc)(H$_2$O)] (**4**) (Fig 3.4), the bands due to ν(C=O) and ν(N–H) vibrations are absent in the complex but new band appears at 1337 cm^{-1} due to ν(C–O) stretching vibration, confirmed the deprotonation of the ligand upon complexation [25,26]. A positive shift corresponding to out-of-plane bending vibrations of the pyridine ring in the free ligands to higher frequencies in the complex is confirmative of pyridine nitrogen coordination to the metal center. The bands in the range 3467 and 923 cm^{-1} in the IR spectrum of

complex [Cu(FPB)(OAc)(H₂O)] (**4**) suggest the presence of coordinated water molecule in the compound. The bands at 1614 and 1389 cm⁻¹ indicates stretching vibrations of monodentate acetate ion [19].
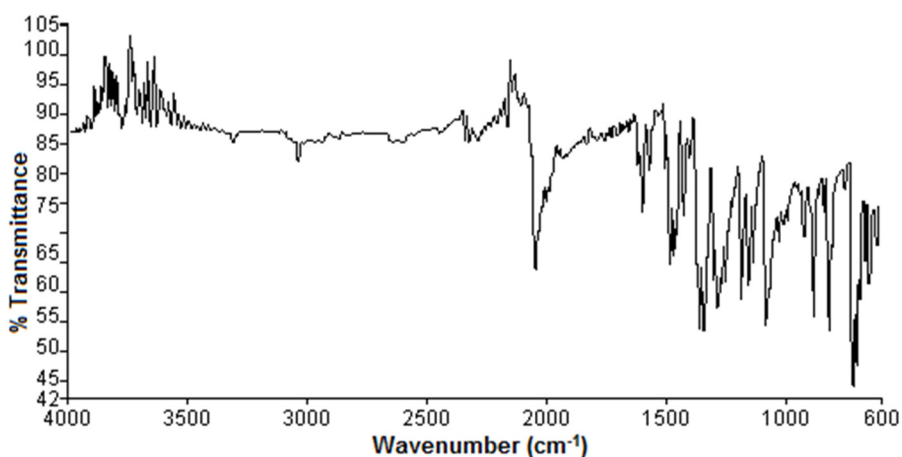
Fig. 3.5. IR spectrum of [Cu(FPB)(N₃)(H₂O)₂] (5).

The azido complex **5** (Fig. 3.5) shows a sharp band in the range 2000-2060 cm⁻¹ and strong bands at 1266 cm⁻¹ and 1306 cm⁻¹ respectively. These are assigned to ν_a and ν_s of the coordinated azido group [27]. The other vibrations are found in the usual range with bands due to iminolic stretch at 1357 cm⁻¹ and azomethine at 1564 cm⁻¹ (Fig. 3.5). The IR spectrum of the compound [Cu(FPB)(N₃)(H₂O)₂] (**5**) shows a sharp band at 1591 cm⁻¹ corresponding to –C=N–C=N– moiety. The out-of-plane bending vibrations of the pyridine ring in uncomplexed ligand are shifted to higher frequencies on complexation, confirming the coordination of the ligand to the metal *via* pyridine nitrogen [28,29]. The bands in the 3362-3470 and 901-924 cm⁻¹ domain, in the spectrum suggest the existence of coordinated water molecules.
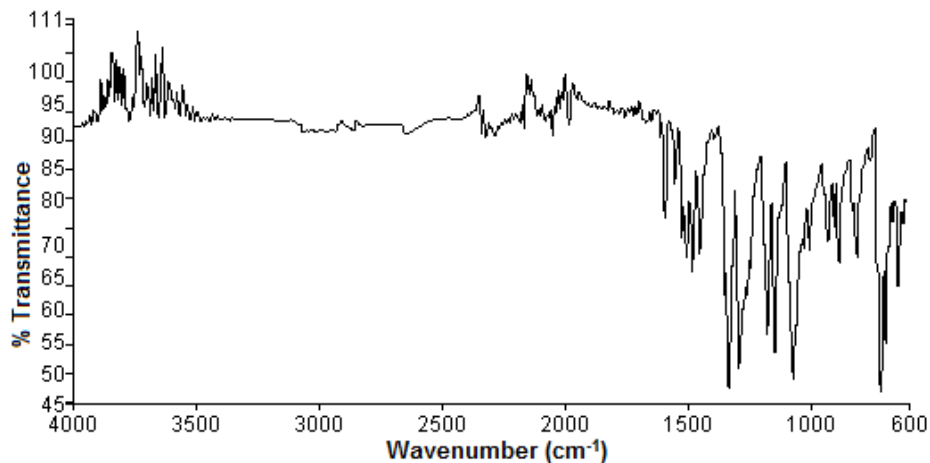
Fig. 3.6. IR spectrum of [Cu(FPB)₂] (6).
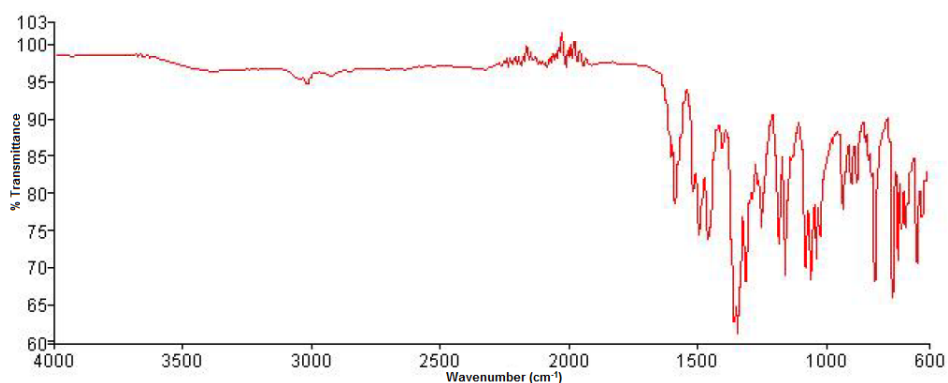
Fig. 3.7. IR spectrum of [Cu(FPN)₂] (7).

In the IR spectra of complexes **6** and **7** (Figs. 3.6 and 3.7), it is found that carbonyl band disappears and the azomethine band shifts due to coordination. The shifted azomethine bands are correspondingly assigned at 1550 and 1574 cm^{-1}. The bands obtained at 1584 and 1587 cm^{-1} are due to the newly formed –C=N–C=N– moiety. Further the appearance of two new bands at 1344 and 1362 cm^{-1} correspondingly in **6** and **7** are assigned for C–O band. The characteristic ring vibrations were found in the usual

region. Therefore six coordinated octahedral geometry is suggested for both the complexes based on magnetic susceptibility measurements and spectral studies.
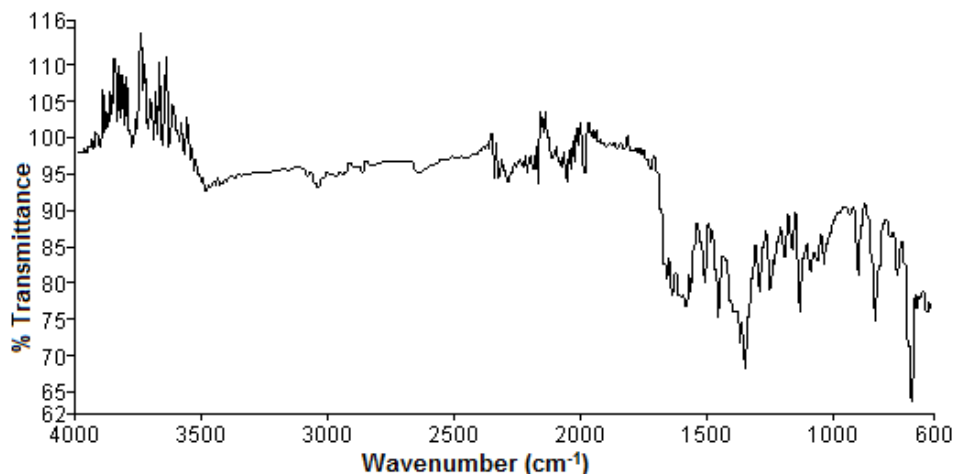
Fig. 3.8. IR spectrum of [Cu(FPN)(OAc)(H$_2$O)] (8).

In the case of complex **8** (Fig. 3.8), hydrazone coordinates to the metal center in the deprotonated anionic form. The azomethine band is observed at 1583 cm^{-1}. The band due to iminolic stretch was found at 1365 cm^{-1}. The aromatic ring vibrations are found in the usual range. The appearance of a new band at 1594 cm^{-1} in complex **8** due to newly formed ν(C=N) support the above observations.

3.3.4. Electronic spectral studies

Cu(II) complexes are known in a wide variety of structures. The electronic absorption spectra are very often helpful in the evaluation of results furnished by other methods of structural investigation. The electronic spectra of all the compounds were recorded in solution state by

dissolving in DMF/DMSO. The tentative assignments of the significant electronic spectral bands of the Cu(II) complexes are presented in Table 3.2 and shown in Figs. 3.9-3.15.

Table 3.2. Electronic spectral assignments (cm^{-1}) of Cu(II) complexes

Compound	n→π*/π→π*	LMCT	*d-d* transitions
[Cu$_2$(FPB)$_2$(μ-NCS)$_2$] (**1**)	36520, 33530	25230	--
[Cu(HFPB)(SO$_4$)]·H$_2$O (**2**)	33920	24980	--
[Cu(FPB)(ClO$_4$)] (**3**)	37060	28070	--
[Cu(FPB)(OAc)(H$_2$O)] (**4**)	36830	25270	14230
[Cu(FPB)(N$_3$)(H$_2$O)$_2$] (**5**)	33770	25080	14460
[Cu(FPB)$_2$] (**6**)	37320	25730	--
[Cu(FPN)$_2$] (**7**)	37510	25600	--
[Cu(FPN)(OAc)(H$_2$O)] (**8**)	37920	25610	--

Thus the electronic spectrum of Cu(II) is often of little value in structural assignment and the results obtained from electronic spectra do not permit a structural diagnosis free of uncertainity [27]. The bands in 38000-32000 cm^{-1} range are assigned as intraligand n→π* and π→π* transitions of complexes, suffered marginal shift from that of their corresponding free ligands. Strong bands in the range 24000-28100 cm^{-1} in the spectra of all Cu(II) complexes are mainly due to combination of O→Cu(II) and N→Cu(II) charge transfer transitions (Figs. 3.9-3.13) [30].
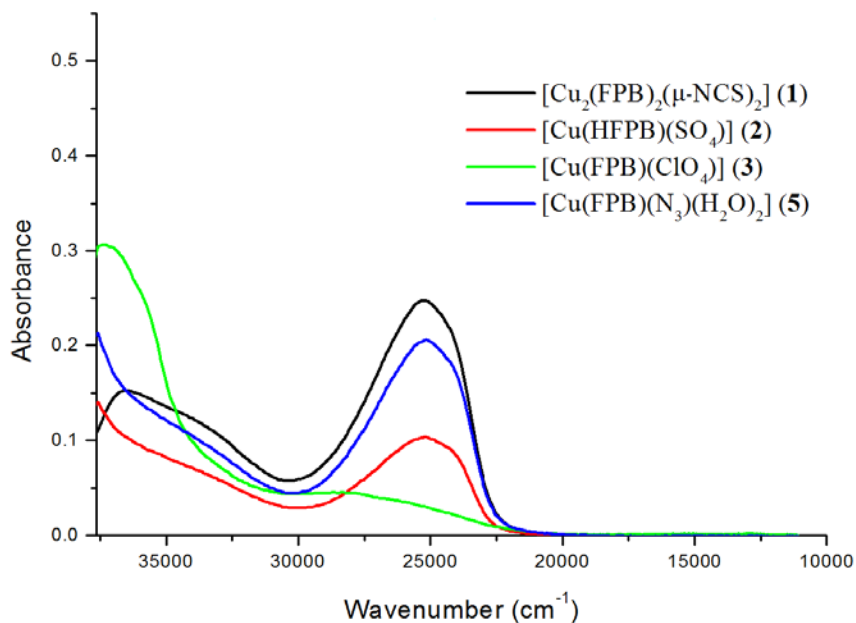
Fig. 3.9. Electronic spectra of copper(II) complexes.
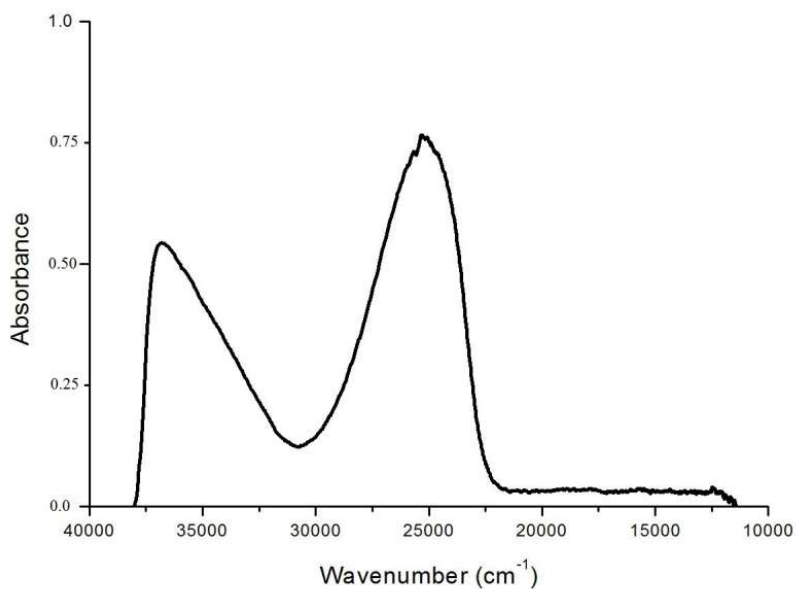
Fig. 3.10. Electronic spectrum of [Cu(FPB)(OAc)(H₂O)] (4).
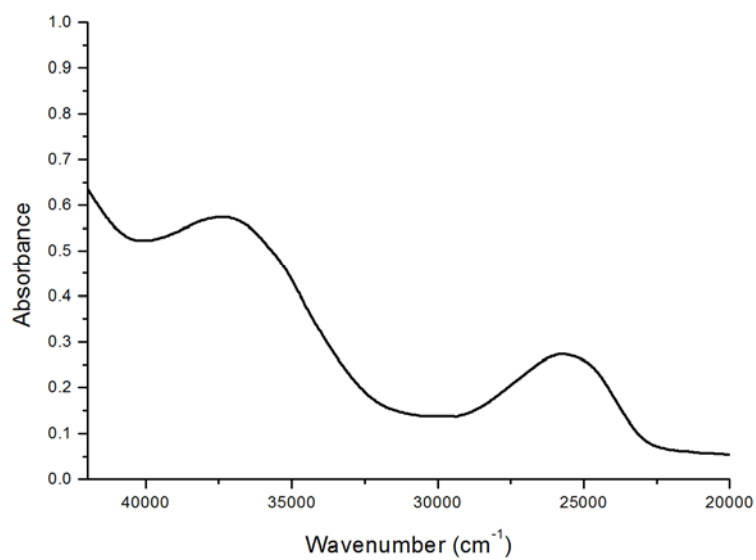
Fig. 3.11. Electronic spectrum of [Cu(FPB)$_2$] (6).
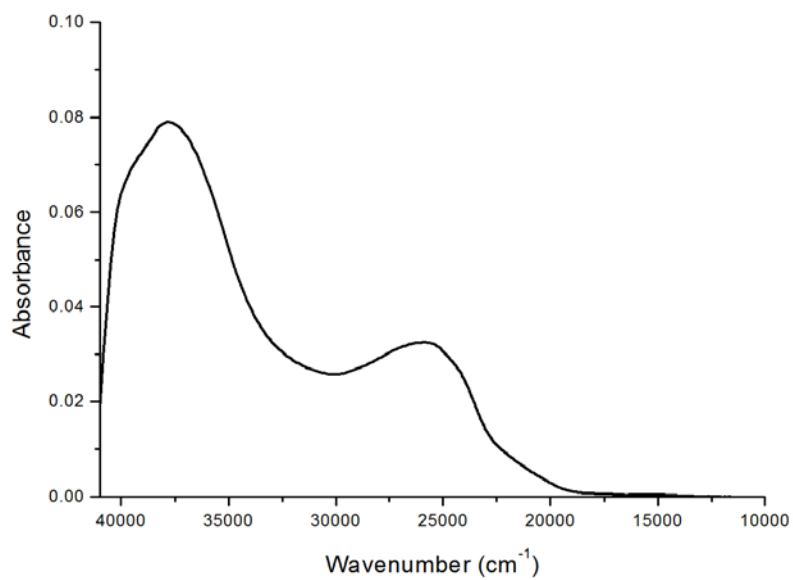
Fig. 3.12. Electronic spectrum of [Cu(FPN)$_2$] (7).
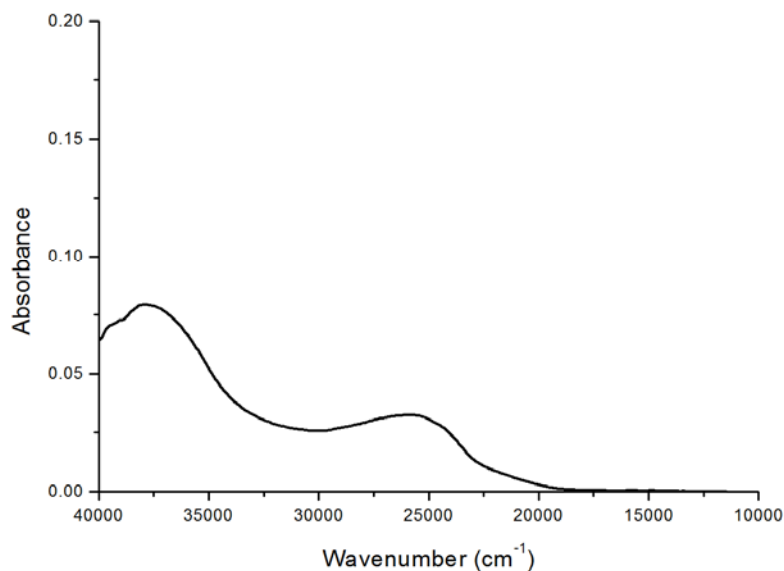
Fig. 3.13. Electronic spectrum of [Cu(FPN)(OAc)(H₂O)] (8).

The d^9 Cu²⁺ ion with a ^2D ground state free ion term is expected to experience Jahn-Teller distortion which leads to further splitting of $^2T_{2g}$ and ^2E_g levels and give rise to three spin allowed transitions *viz.* $^2B_{2g} \leftarrow ^2B_{1g}$, $^2A_{1g} \leftarrow ^2B_{1g}$ and $^2E_g \leftarrow ^2B_{1g}$. But often these theoretical expectations are overlooked in practice and these bands usually appear overlapped due to the very small energy difference between the d levels. A very broad band with a peak maximum in the range 14000-15000 cm⁻¹ assignable to the envelope of $^2B_{2g} \leftarrow ^2B_{1g}$, $^2A_{1g} \leftarrow ^2B_{1g}$ and $^2E_g \leftarrow ^2B_{1g}$ is observed for most of the geometries (Fig. 3.14) [31-33].
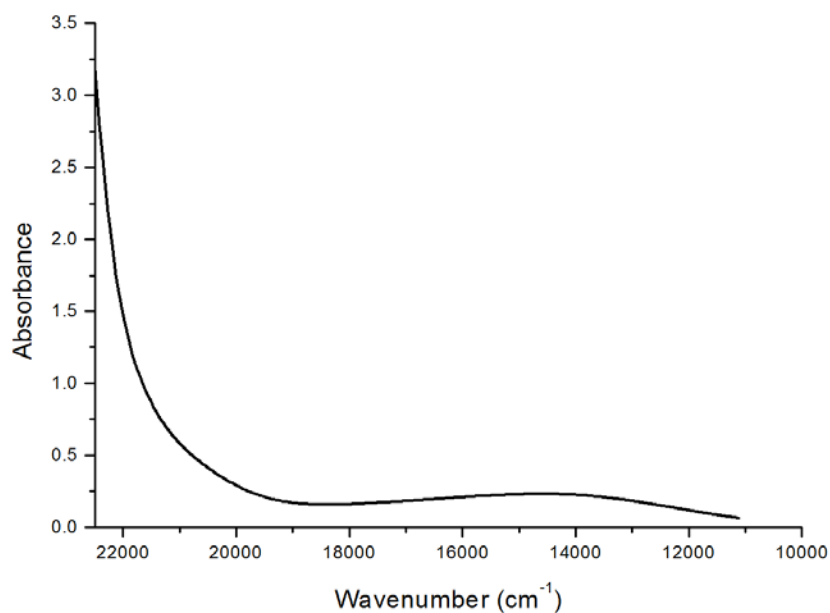
Fig. 3.14. Electronic spectrum of [Cu(FPB)(N$_3$)(H$_2$O)$_2$] (4) in visible region.

3.3.5. Thermogravimetric analyses

The thermogravimetric (TG/DTA) analysis is mainly used as a probe to prove the associated water or solvent molecules to be in coordination sphere or in crystalline form. TGA studies were carried out in the 50-800 °C range in nitrogen atmosphere at heating rate of 10 °C/min. TG curves are drawn as weight (mg) versus temperature (°C) and selected TG-DTG curves are shown in Figs. 3.15 and 3.16.
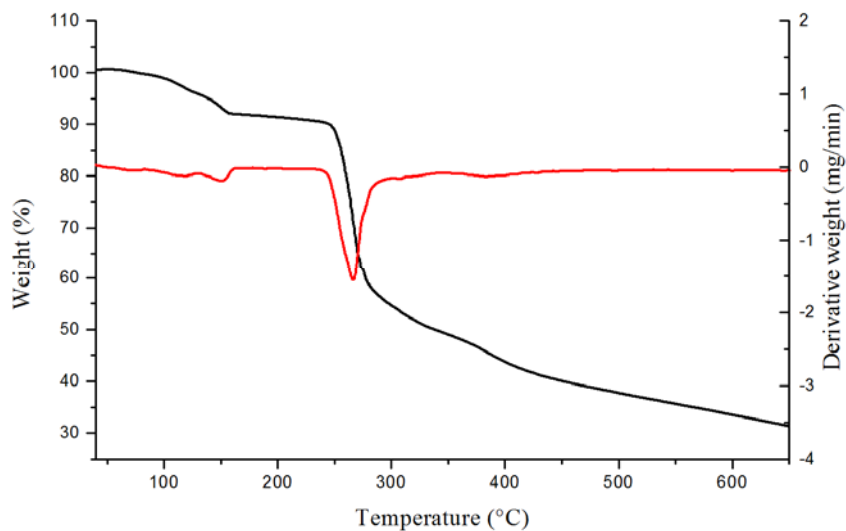
Fig. 3.15. Thermogram of [Cu(HFPB)(SO$_4$)]·H$_2$O (2).

In [Cu(HFPB)(SO$_4$)]·H$_2$O (**2**) (Fig. 3.15), the first weight loss of 4.60% (Calcd. 4.27%) is observed at 142 °C indicates that one water molecule is present in the lattice of the compound. A weight loss of 48.65% (Calcd. 47.69%) occurs in two steps at 200-390 °C range involves the removal of coordinated sulphate ion and C$_6$H$_4$FN fragment of the aroylhydrazone moiety from the compound. After 390 °C, compound decomposes continuously.
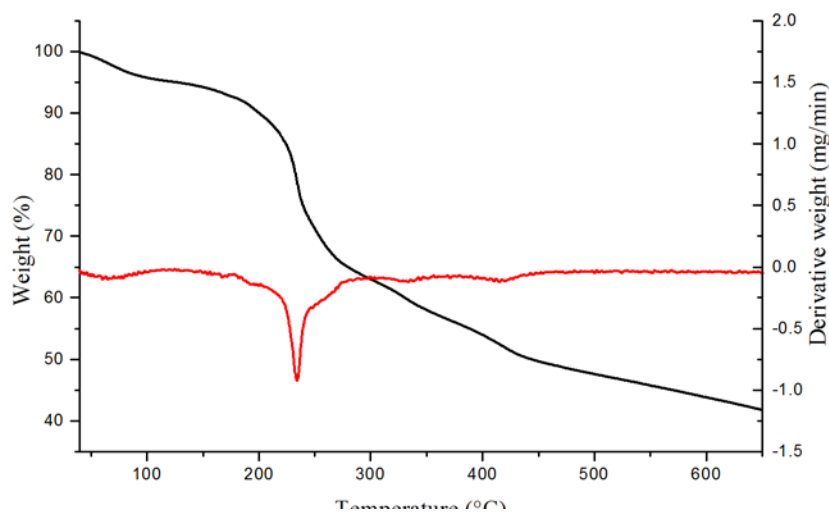
Fig. 3.16. Thermogram of [Cu(FPN)(OAc)(H₂O)] (8).

In [Cu(FPN)(OAc)(H$_2$O)] (**8**) (Fig. 3.16), a weight loss of 22.19% (Calcd. 21.06%) occurs continuously at 200-300 °C range involves the removal of coordinated monodentate acetate ion and water from the compound. After 300 °C, compound decomposes continuously.

3.3.6. EPR spectral studies

The EPR spectra of all the complexes were recorded in polycrystalline and solution state. All the EPR spectra are simulated using EasySpin 4.0.0 package [34] and the experimental (red) and simulated (blue) best fits are included. The observed EPR resonances and their computer simulated envelopes are shown in Figs. 3.17-3.30. EPR spectral parameters are presented in Table 3.3.

Table 3.3. EPR spectral parameters of copper complexes in polycrystalline state at 298 K and in DMF at 77 K

Compound	Polycrystalline state (298 K)				DMF (77 K)										
	g_{iso}	$g_\parallel/g_3$	$g_\perp/g_1, g_2$	G	$g_\parallel/g_3$	$g_\perp/g_1, g_2$	g_{av}	$A_\parallel^a$	$A_\perp^a$	α^2	β^2	γ^2	$K_\parallel$	$K_\perp$	f
[Cu₂(FPB)₂(μ-NCS)₂] (**1**)	2.110	--	--	--	2.250	2.083	2.138	168	20	0.7892	--	--	--	--	133.9
[Cu(HFPB)(SO₄)]·H₂O (**2**)	--	--	--	--	--	--	--	--	--	--	--	--	--	--	--
[Cu(FPB)(ClO₄)] (**3**)	--	2.231	2.070	3.3781	2.285	2.081	2.149	144	0	0.7565	--	--	--	--	158.7
[Cu(FPB)(OAc)(H₂O)] (**4**)	--	2.231	2.060	3.9636	2.255	2.077	2.136	184	19	0.8365	--	--	--	--	122.4
[Cu(FPB)(N₃)(H₂O)₂] (**5**)	--	2.241	2.070	3.5258	2.420	2.055, 2.230	2.235	--	--	--	--	--	0.9549	1.4101	--
[Cu(FPB)₂] (**6**)	--	2.240, 2.128	2.040, 2.128	2.9094	2.225	2.105	2.145	176	0	0.7973	--	--	--	--	126.0
[Cu(FPN)₂] (**7**)	2.130	--	--	--	2.25	2.10	2.150	--	--	--	--	--	--	--	--
[Cu(FPN)(OAc)(H₂O)] (**8**)	2.115	--	--	--	2.115	--	--	--	--	--	--	--	--	--	--

^{a}Expressed in units of cm^{-1} multiplied by a factor of 10^{-4}

Electron paramagnetic resonance is a branch of absorption spectroscopy in which radiation of microwave frequency is absorbed by a molecule or ion having unpaired electron(s). Thus it is a convenient and effective way to probe the electronic structure of paramagnetic molecules. The basic object of EPR studies in the transition metal complexes is to obtain as much information as possible about the metal-to-ligand bond, the unpaired electron distribution, coordination environment and the order of the energy levels. Generally, the greatest amount of information concerning nuclear or paramagnetic sites in complexes can be obtained from measurements in solution state. In frozen solutions, glasses, amorphous materials are inherently "powders" in the sense that they can be viewed as an ensemble of randomly oriented paramagnetic sites with respect to the applied magnetic field. Thus the "powder pattern" is an average over the resonance conditions for all possible orientations of the paramagnetic site.

For copper(II) in most environments, the ground state magnetism is essentially spin only and the orbital motion is said to be "quenched". Since copper(II) has one unpaired electron in its $3d^9$ configuration, the "effective" spin is equal to the actual spin of the free ion $S = 1/2$. The Zeeman splitting or g factors are shifted from the free-electron value of 2.0023 by spin-orbit coupling of the ground state to excited states.

The EPR spectra of the complexes in polycrystalline state at 298 K and solution state at 77 K were recorded in the X band, using 100 kHz field modulation. The copper(II) ion (S=1/2), is associated with a spin angular momentum, $m_s = \pm 1/2$, leading to a doubly degenerate spin state

in the absence of magnetic field. In a magnetic field the degeneracy is lifted between these states and the energy difference between them is given by $E = h\nu = g\beta B$, where h is Plank's constant, ν is the frequency, g is the Lande splitting factor (2.0023 for a free electron), β is Bohr magneton and B is the magnetic field.

The electronic properties of the Cu(II) ion are being affected by its geometry, establishes the order of the energy levels of the d orbitals, and accordingly, the ground state for a particular arrangement. ^{63}Cu ($I = 3/2$) gives rise to four ($2nI+1 = 4$) hyperfine lines. EPR spectroscopy plays an important role in determining the stereochemistry of copper complexes. For coordination geometries having an elongated octahedron or a square pyramid or square planar, the ground state is $d_{x^2-y^2}$ and when it is a compressed octahedron or a trigonal bipyramid, the ground state is d_{z^2}. EPR spectroscopy helps to differentiate the ground states on the basis of the principal values of the g tensor.

The complex $[Cu_2(FPB)_2(\mu\text{-}NCS)_2]$ (**1**) exhibited one broad signal at g_{iso}=2.11 in polycrystalline state (Fig. 3.17) arising from dipolar broadening and enhanced spin lattice relaxation. At 77 K, the compound shows an axial spectrum with four hyperfine lines ($g_\parallel$ =2.250, $g_\perp$=2.083) as expected due to the interaction of the electron spin with the nuclear spin (I=3/2) of the copper (Fig. 3.18).
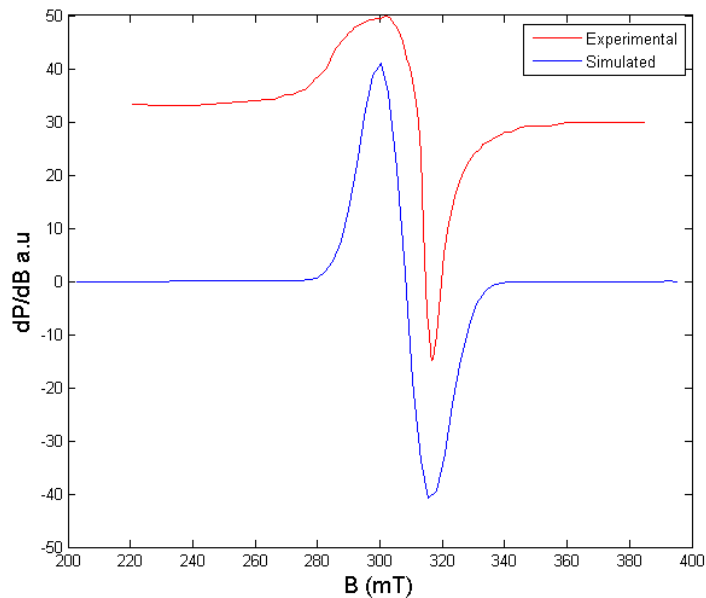
Fig. 3.17.   EPR spectrum of [Cu$_2$(FPB)$_2$(μ-NCS)$_2$] (1) in polycrystalline state at 298 K.
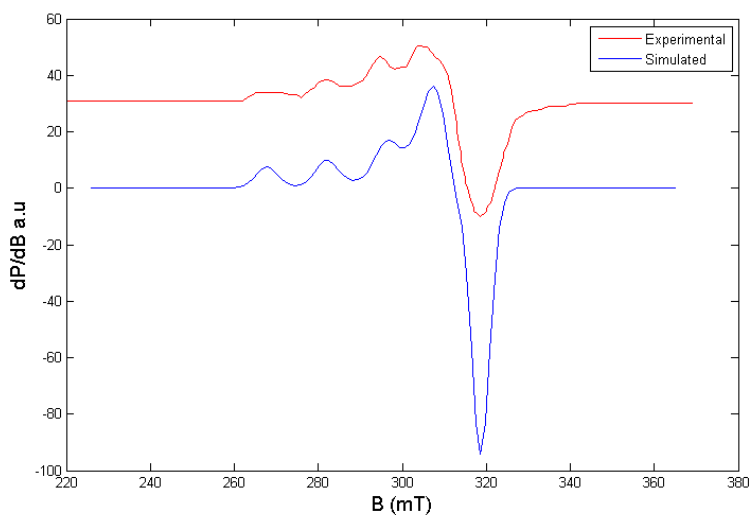
Fig. 3.18.   EPR spectrum of [Cu$_2$(FPB)$_2$(μ-NCS)$_2$] (1) in DMF at 77 K.

The EPR spectra of [Cu(HFPB)(SO$_4$)]·H$_2$O (**2**) were poorly resolved at 298 and 77 K and therefore not good to interpret.

The spectrum of [Cu(FPB)(ClO$_4$)] (**3**) is axial in the polycrystalline state (Fig. 3.19) and in frozen DMF. In solution state, the axial spectrum split into four lines in parallel region (Fig. 3.20).
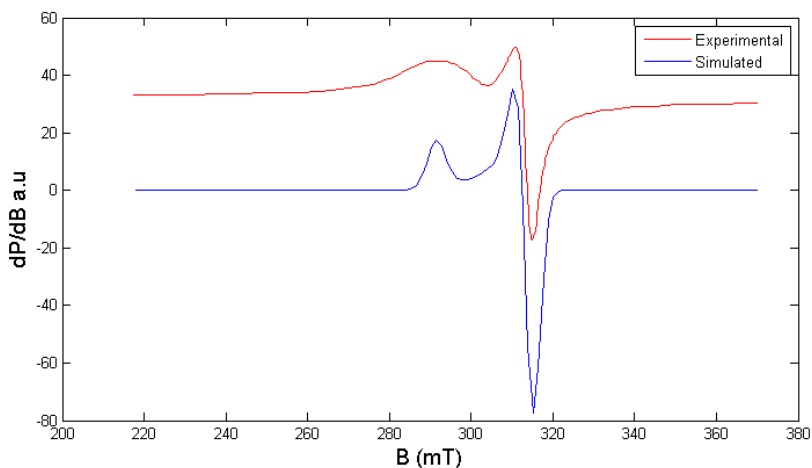
Fig. 3.19. EPR spectrum of [Cu(FPB)(ClO$_4$)] (3) in polycrystalline state at 298 K.
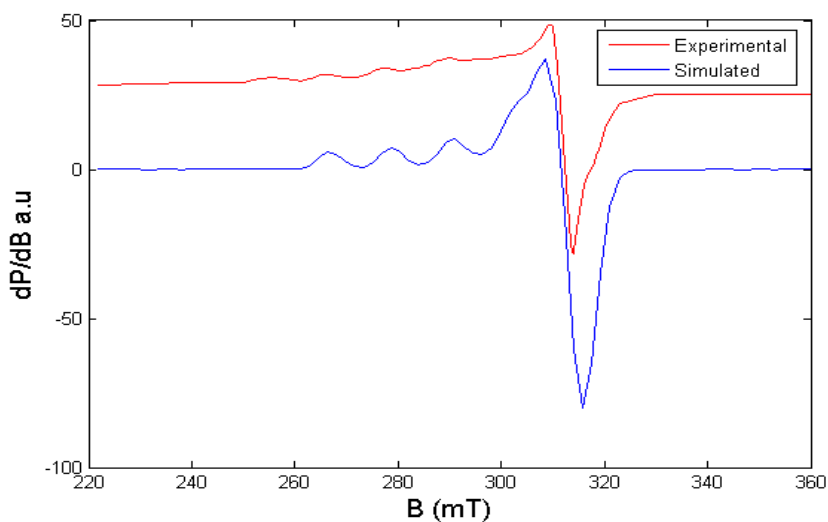
Fig. 3.20. EPR spectrum of [Cu(FPB)(ClO$_4$)] (3) in DMF at 77 K.
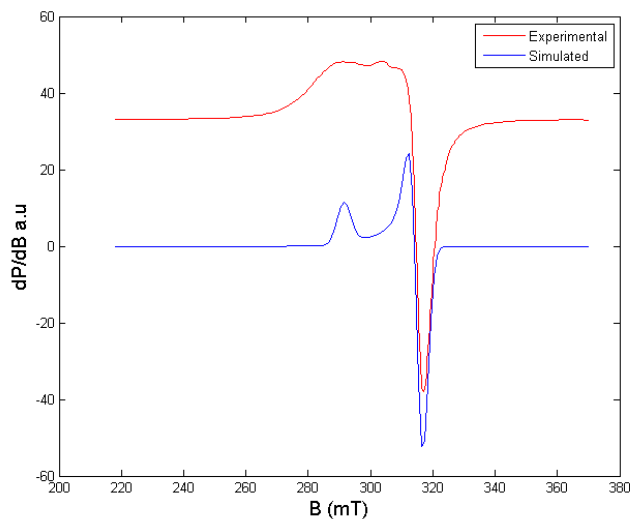
Fig. 3.21. EPR spectrum of [Cu(FPB)(OAc)(H₂O)]·H₂O (4) in polycrystalline state at 298 K.
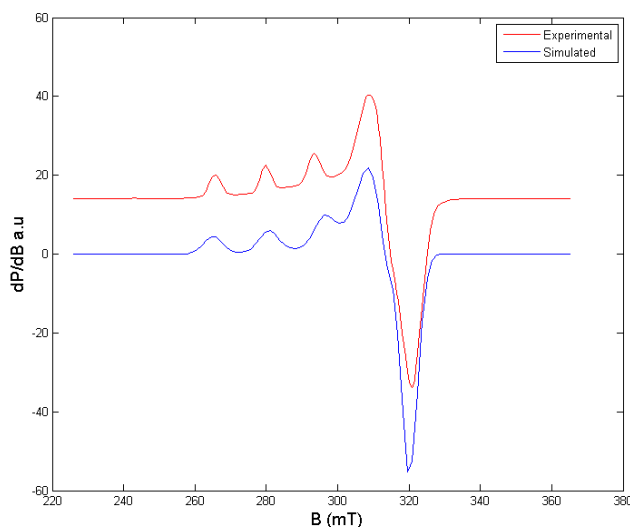
Fig. 3.22. EPR spectrum of [Cu(FPB)(OAc)(H₂O)]·H₂O (4) in DMF at 77 K.

For complex **4**, spectra for polycrystalline sample and in the solution exhibit absorptions typical for the mononuclear species with axial symmetry (Fig. 3.21) ($g_{\parallel}$ =2.231, $g_{\perp}$=2.060). The complex show a

well-defined hyperfine structure on the low field region (Fig. 3.22) to allow accurate calculations of *g* and *A* values indicating that the azomethine nitrogen dominates the bonding. However, such splittings in the *g* component in the high-field region are not clear, probably owing to poorly resolved ligand hyperfine interactions.
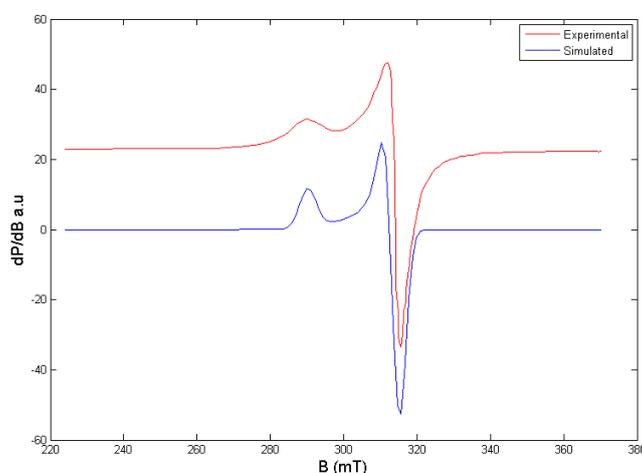
Fig. 3.23.   EPR spectrum of Cu(FPB)(N$_3$)(H$_2$O)$_2$] (5) in polycrystalline state at 298 K.
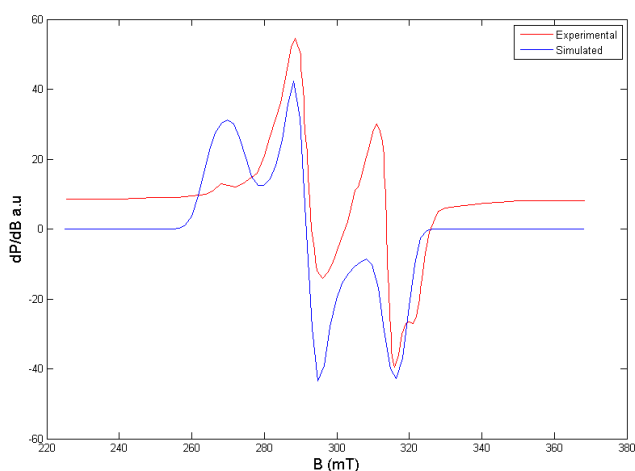
Fig. 3.24. EPR spectrum of [Cu(FPB)(N$_3$)(H$_2$O)$_2$] (5) in DMF at 77 K.

In polycrystalline state at 298 K [Cu(FPB)(N$_3$)(H$_2$O)$_2$] (**5**) displays a typical axial spectrum with g$_\parallel$ =2.241 and g$_\perp$=2.070. In polycrystalline state, since it is magnetically concentrated the anisotropy may be lost (Fig. 3.23). Dilution of the solid isolates the electron spin of the given complex from that of another paramagnetic molecule. In frozen DMF at 77 K, complex (**5**) displays a rhombic spectrum with three *g* values (Fig. 3.24). Since it is a six coordinated complex, the lowest g > 2.04 indicates copper(II) ion with all the axes aligned parallel and would be consistent with elongated rhombic octahedral stereochemistry [35].
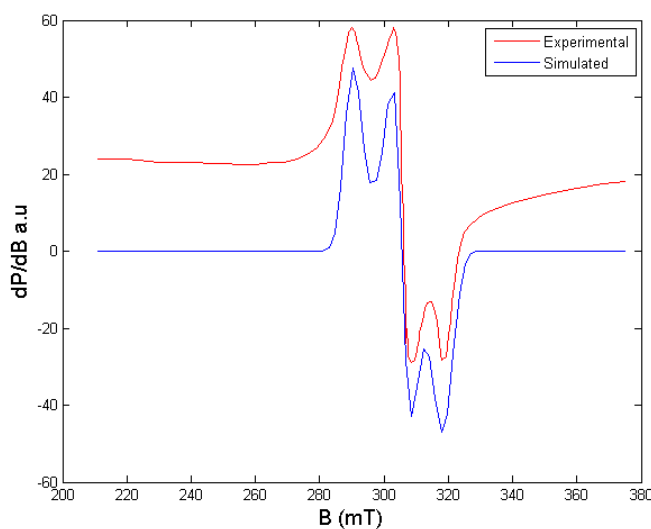
Fig. 3.25. EPR spectrum of [Cu(FPB)$_2$] (6) in polycrystalline state at 298 K.
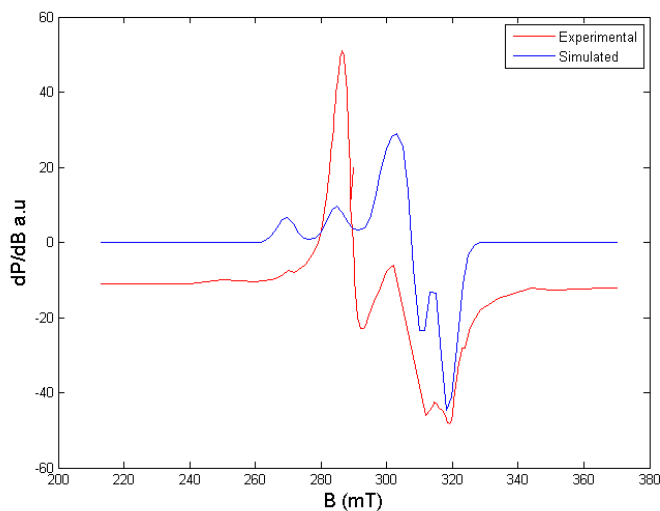
Fig. 3.26. EPR spectrum of [Cu(FPB)$_2$] (6) in DMF at 77 K.

The EPR spectrum of complex **6** at room temperature (Fig. 3.25) shows rhombic symmetry with g$_3$=2.240, g$_2$=2.218 and g$_1$=2.040. The value G < 4.4 indicates the presence of exchange interactions. The EPR spectrum of the [Cu(FPB)$_2$] (**6**) in solution state is presented in Fig. 3.26. The spectrum is resolved in parallel direction of the g-tensor and shows three of four well-resolved low-field parallel lines with a hyperfine splitting of 17 mT and g$_∥$=2.225 and g$_⊥$=2.105. The super-hyperfine splitting due to the directly bonded atoms is not seen in the low-temperature spectrum. In this case also, $g_∥ > g_⊥ > 2.0023$, which is consistent with $d_{x^2-y^2}$ ground state. EPR spectral data and the bonding parameters are summarized in Table 3.3.
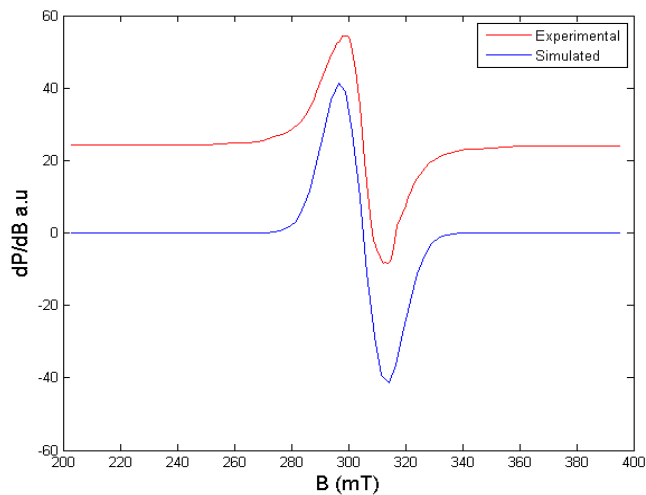
Fig. 3.27. EPR spectrum of [Cu(FPN)₂] (7) in polycrystalline state at 298 K.
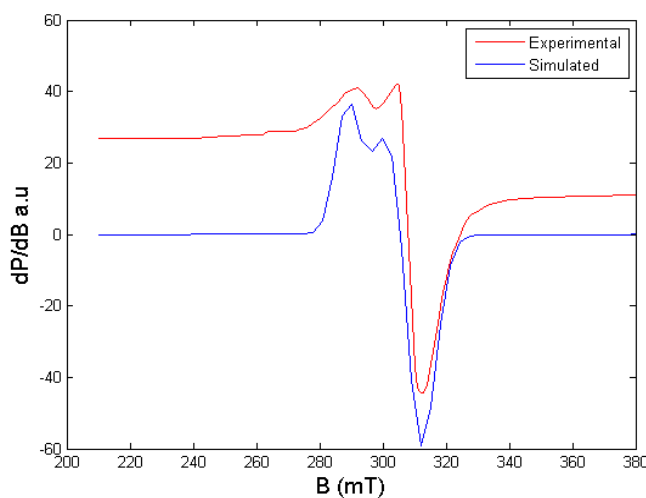
Fig. 3.28. EPR spectrum of [Cu(FPN)₂] (7) in DMF at 77 K.

Fig. 3.27 shows the EPR spectrum of [Cu(FPN)₂] (**7**) in polycrystalline state. Due to line broadening caused by the anisotropy of the g factors and hyperfine interactions, no hyperfine splitting was resolved in the undiluted powder samples. Compound **7** in DMF at 77 K (Fig. 3.28)

exhibit an axial spectrum with $g_{\parallel}$ = 2.250 and $g_{\perp}$= 2.100, resulting from coupling of the electron spin with the spin of the ^{63}Cu nucleus (I = 3/2).

The EPR spectra of complex **8** in the polycrystalline as well as DMF solution have similar features and same *g* value (g_{iso} 2.115) due to the tumbling motion of molecules (Figs. 3.29 and 3.30).
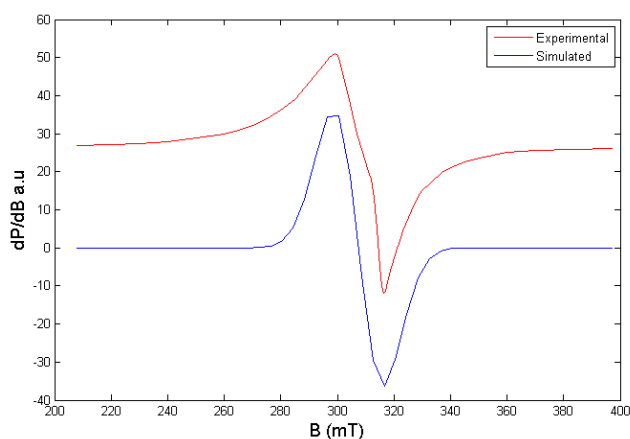
Fig. 3.29. EPR spectrum of [Cu(FPN)(OAc)(H$_2$O)] (8) in polycrystalline state at 298 K.
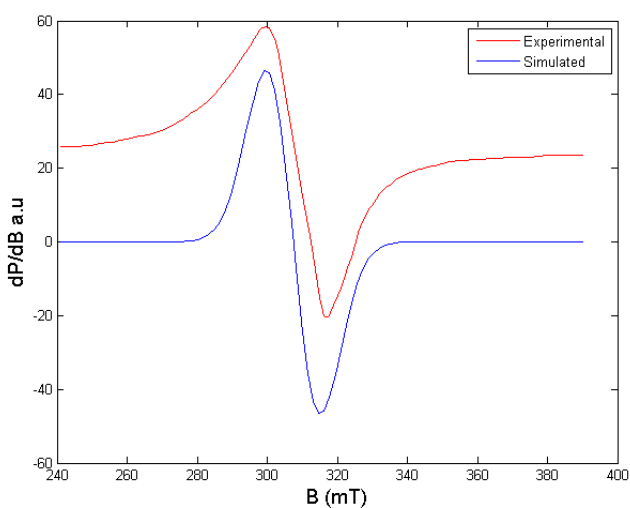
Fig. 3.30. EPR spectrum of [Cu(FPN)(OAc)(H$_2$O)] (8) in DMF at 77 K.

The geometric parameter G, represents the exchange interaction between copper centers in the polycrystalline compound and is calculated for each complexes using the equation, $G = (g_{\parallel}-2.0023)/(g_{\perp}-2.0023)$ for axial spectra and for rhombic spectra $G = (g_3-2.0023) / (g_{\perp}-2.0023)$, where $g_{\perp} = (g_1+g_2)/2$ [36,37]. If $G > 4$, exchange interaction is negligible and if it less than 4, considerable exchange interaction is indicated in the solid complex [37,38]. The calculated G values are less than 4 for complexes **3-6** which indicate that considerable exchange interaction is present in the polycrystalline state of the complexes. As $g_{\parallel}>g_{\perp}>2.0023$, a square pyramidal geometry consistent with $d_{x^2-y^2}$ ground state can be assigned to the copper(II) complexes, thereby ruling out the possibility of a trigonal bipyramidal structure (where $g_{\perp}>g_{\parallel}$). For rhombic systems with $g_3>g_2>g_1$, R is an significant parameter and can be calculated as $R = (g_2-g_1)/(g_3-g_2)$ [39]. If $R<1$, a distorted square pyramidal geometry consistent with $d_{x^2-y^2}$ ground state is predominated excluding the possibility a trigonal bipyramidal structure with d_{z^2} ground state where $R>1$. When R=1, the groung state is approximately an equal mixture of $d_{x^2-y^2}$ and d_{z^2} and the structure is obtained as an intermediate of square pyramidal and trigonal bipyramidal geometries [40,41]. For complex **6**, R value is found to be 0.785 suggesting the $d_{x^2-y^2}$ ground state for copper(II) ion.

The EPR parameters $g_{\parallel}$, $g_{\perp}$, $g_{av,}$ $A_{\parallel}$ (Cu) and $A_{\perp}$ (Cu) incorporated with the energies of *d-d* transition were used to evaluate the bonding parameters α^2, β^2 and γ^2 which is considered to be the measure of the

covalency of in-plane σ-bonds, in-plane π-bonds and out-of-plane π-bonds respectively.

The value of in-plane sigma bonding parameter α^2 was estimated from the expression [42]

$$\alpha^2 = -A_{\parallel} / 0.036 + (g_{\parallel}\text{-}2.0023) + 3/7\ (g_{\perp}\text{-}2.0023) + 0.04$$

The following simplified expression were used to calculate the bonding parameters

$$K_{\parallel}^2 = (g_{\parallel}\text{-}2.0023)\ E_{d\text{-}d}/8\lambda_o$$

$$K_{\perp}^2 = (g_{\perp}\text{-}2.0023)\ E_{d\text{-}d}/2\lambda_o$$

$$K_{\parallel}^2 = \alpha^2\beta^2$$

$$K_{\perp}^2 = \alpha^2\gamma^2$$

where $K_{\parallel}$ and $K_{\perp}$ are orbital reduction factors and λ_0 represents the one electron spin orbit coupling constant which equals -828 cm^{-1} for Cu(II) d^9 system.

For pure σ-bonding $K_{\parallel} \approx K_{\perp} \approx 0.77$ and for in-plane π-bonding $K_{\parallel} < K_{\perp}$, while for out-of-plane π-bonding $K_{\perp} < K_{\parallel}$ [43]. For compound **5**, $K_{\parallel} < K_{\perp}$ suggests that in-plane π-bonding is present in these complex. The value of in-plane sigma bonding parameter $\alpha^2 < 1$ confirms the covalent nature of complexes **1**, **3**, **4** and **6**. The nature of metal-ligand bond is also evaluated by comparing the value of in-plane sigma bonding parameter α^2 i.e., if the M–L bond is purely ionic, the value of α^2 is unity

and it is completely covalent, if α^2 =0.5 [43]. For complexes **1**, **3**, **4** and **6**, α^2 values calculated lie in between 0.5 and 1, which mean that the metal-ligand bonds in the complexes under study are partially ionic and partially covalent in nature.

The $g_{||}$ values also provide information regarding the nature of metal-ligand bond [44]. The $g_{||}$ value is normally 2.3 or larger for ionic and less than 2.3 for covalent metal-ligand bonds. The $g_{||}$ values obtained for complexes indicate a significant degree of covalency in the metal-ligand bonds [45]. The index of tetragonal distortion f is calculated as $f = g_{||}/A_{||}$, and depending on the nature of the coordinated atom and the value may vary from 105-135 for small to medium distortion [31,46]. High distortion is expected for perchlorate complex **3** evident from the value of 158 cm.

3.3.7. X-ray crystallography

Single crystal X-ray diffraction studies of [Cu(FPB)(OAc)(H$_2$O)]·H$_2$O (**4a**) were carried out using Bruker SMART APEXII CCD diffractometer equipped with graphite monochromated Mo Kα (λ = 0.71073 Å) radiation at the Sophisticated Analytical Instrument Facility, Cochin University of Science and Technology, Kochi-22, Kerala, India. Bruker SMART software was used for data acquisition and Bruker SAINT software for data integration [47]. Absorption corrections were carried out using SADABS based on Laue symmetry using equivalent reflections [47]. The cell refinement was done using APEX2 and SAINT [47]. The data was reduced using SAINT and XPREP [47]. The structure was solved by direct methods

using SHELXS97 [48] and refined by full-matrix least-squares refinement on F^2 using SHELXL97 [49]. The molecular and crystal structures were plotted using molecular graphics like ORTEP-3 for Windows [50] and DIAMOND version 3.2g [51].

In [Cu(FPB)(OAc)(H$_2$O)]·H$_2$O (**4a**), all the non-hydrogen atoms were refined anisotropically. The carbon bound hydrogen atoms were placed in geometrically idealized positions and constrained to ride on their parent atoms, with C–H distances of 0.93 Å, and with isotropic displacement parameters 1.2 times that of the parent carbon atoms. The hydrogen atoms attached H4A and H4B to the O4 of coordinated water molecule, were located from a difference maps and their distances were restrained using DFIX and DANG instructions. O–H distances of water were restrained to 0.86±0.02 Å and H···H distances to 1.36±0.02 Å.

During the refinement we were able to locate one water molecule in the lattice. But the position of hydrogen atoms associated with lattice water molecule were unable to locate or place in calculated position from Fourier difference map due to large thermal vibration of lattice water molecule. The difference map also shows the presence of severely disordered solvent molecules which could not be modelled. This was solved by using SQUEEZE option in *PLATON* [52]. It was found that unknown amount of solvent molecules having an electron count of 20 exists in three voids in the unit cell with void volume of 344, 344 and 342 Å^3. Crystal data and structural refinement for the complex **4** is tabulated in the Table 3.4.

Table 3.4. Crystal data and structure refinement parameters for [Cu(FPB)(OAc)(H₂O)]·H₂O (4a)

Parameters	[Cu(FPB)(OAc)(H₂O)]·H₂O (4a)
Empirical formula	$C_{15}H_{14}N_3O_5FCu$
Formula weight	398.84
Crystal system	Trigonal
Space group	$R\overline{3}$
Unit cell dimensions	
	a = 37.6927(18) Å α = 90°
	b = 37.6927(18) Å β = 90°
	c = 6.844(3) Å γ = 120°
Volume	8421(4) Å^3
Z	18
Density (calculated) (mgm^{-3})	1.416
Absorption coefficient (mm^{-1})	1.204
F(000)	3654
Crystal size	0.30 x 0.25 x 0.20 mm^3
θ range for data collection	2.86 to 24.99°
Limiting indices	$-44 \leq h \leq 21, 0 \leq k \leq 44, 0 \leq l \leq 8$
Reflections collected / unique	3016 / 3293 [R(int) = 0.0000]
Completeness to θ	24.99 91.5%
Absorption correction	Semi-empirical from equivalents
Max. and min. transmission	0.786 and 0.704
Refinement method	Full-matrix least-squares on F^2
Data / restraints / parameters	3016 / 3 / 247
Goodness-of-fit on F^2	0.747
Final R indices [I>2σ(I)]	R$_1$= 0.0411, wR$_2$= 0.0820
R indices (all data)	R$_1$= 0.1012, wR$_2$= 0.0904
Extinction coefficient	0.012(3)
Largest diff. peak and hole	0.296 and -0.254 e.A^{-3}

$R_1 = \Sigma||F_o| - |F_c|| / \Sigma|F_o|$ $wR_2 = [\Sigma w(F_o^2 - F_c^2)^2 / \Sigma w(F_o^2)^2]^{1/2}$

3.3.7.1. Crystal structure of [Cu(FPB)(OAc)(H$_2$O)]·H$_2$O (4a)

The molecular structure of mononuclear Cu(II) complex **4a** with atom numbering scheme is given in Fig. 3.31. An X-ray quality single crystal of compound **4a** of suitable dimensions was grown by slow evaporation from the mother liquor within one week. A summary of the key crystallographic information is given in Table 3.4. Relevant bond lengths and bond angles of the molecule are featured in Table 3.5.
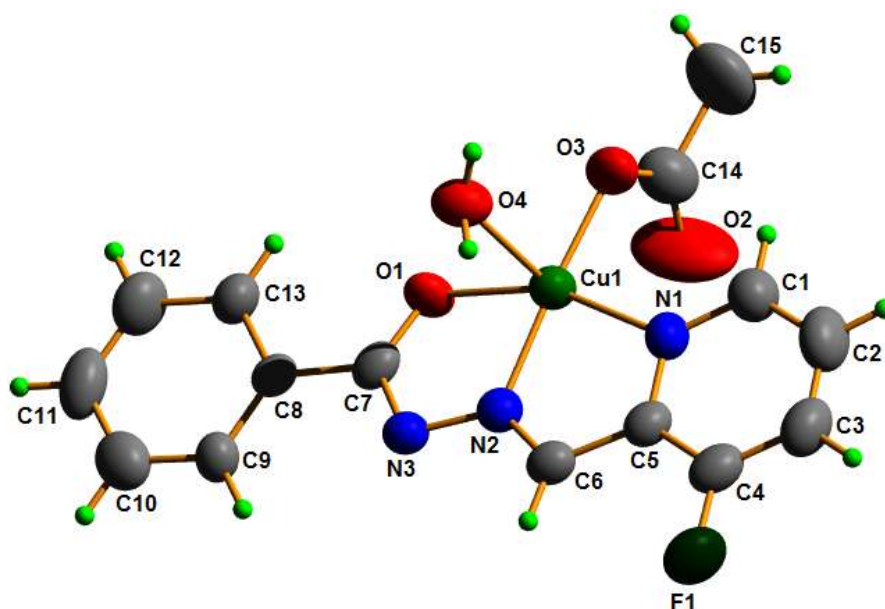
Fig. 3.31. Molecular structure of the [Cu(FPB)(OAc)(H$_2$O)]·H$_2$O (4a). The solvent molecule is omitted for clarity.

Table 3.5. Selected bond lengths (Å) and bond angles (°) for [Cu(FPB)(OAc)(H₂O)]·H₂O (4a).

Bond lengths (Å)		Bond angles (°)	
	HFPB·H₂O	[Cu(FPB)(OAc)(H₂O)]·H₂O (4a)	
C(6)–N(2)	1.2721 (18)	1.283(5)	O(2)–Cu(1)–N(2) 176.50(14)
N(2)–N(3)	1.3736 (16)	1.375(4)	O(1)–Cu(1)–N(1) 158.00(13)
C(7)–N(3)	1.3582 (18)	1.347(5)	O(2)–Cu(1)–O(1) 103.00(12)
C(7)–O(1)	1.2258 (17)	1.278(5)	N(1)–Cu(1)–O(4) 100.65(14)
N(1)–Cu(1)		2.044(3)	O(2)–Cu(1)–N(1) 97.42(14)
N(2)–Cu(1)		1.928(3)	O(2)–Cu(1)–O(4) 92.38(14)
O(1)–Cu(1)		1.997(3)	N(2)–Cu(1)–O(4) 90.51(13)
O(2)–Cu(1)		1.907(3)	O(1)–Cu(1)–O(4) 86.72(12)
O(4)–Cu(1)		2.344(4)	N(2)–Cu(1)–N(1) 80.11(14)
			N(2)–Cu(1)–O(1) 79.12(13)

Molecule crystallizes with one monomer per asymmetric unit in the trigonal space group, $R\bar{3}$ with Z = 18. In this complex, Cu(II) ion is in a pentacoordinated environment and the coordination sites are occupied by pyridyl N1, azomethine N2 and iminolate O1 from a monodeprotonated hydrazone moiety and the remaining positions are occupied by two oxygen atoms, one each from acetate ion O2 and water molecule O4. The oxygen atom of hydrazone ligand is coordinated to the metal atom in the iminolate form and it is confirmed by a decrease in bond length of C7–N3 and an increase in bond length of C7–O1 of the complex when compared to the corresponding values in free ligand. The relatively short C6=N2 and C7=N3 bond distances of 1.311(3) and 1.292(3) Å coupled with N2–N3 distance of 1.396(3) Å, indicate that there is conjugation along backbone of the tridentate ligand and it is coordinated to the copper ion in the iminolate form. The bond lengths, Cu–N$_{(py)}$, 2.358(4) Å and Cu–N$_{(azo)}$, 2.360(3) Å are very similar to other Cu(II) complexes of

hydrazones [25,53]. The bond distances to Cu are in the order $Cu-N_{(py)}$ $< Cu-N_{(azo)} < Cu-O_{(ketoxy)} < Cu-O(2) < Cu-O(1)$.

The Cu(II) center is surrounded by two fused five-membered chelate rings Cg(l) {Cu1,N1,C5,C6,N2} and Cg(2) {Cu1,O1,C7,N3,N2} with a dihedral angle of 5.45(17)° between them indicates deviation of the basal portion from planarity. The $Cu-N_{(azo)}$ bond length [1.9784 Å] is lesser by 0.0541 Å compared to $Cu-N_{(py)}$ indicates the strength of former bond than latter [27].

Selected torsion angles for the complex **4a** are given in Table 3.6. The torsion angle value of 178.6(3)° observed for C(5)–C(6)–N(2)–N(3) supports *E* configuration with respect to N(2)=C(6) bond. It is interesting to note that the Z configuration of the hydrazone (torsion angle of N(2)–N(3)–C(7)–O(1) (-0.4(2)°) about C7–N3 bond is retained in the complex (torsion angle of N(2)–N(3)–C(7)–O(1) (-1.4(6)°) to facilitate the coordination of iminolate oxygen to the copper center.

Table 3.6. Selected torsion angles [°] for HFPB·H₂O and [Cu(FPB)(OAc)(H₂O)]·H₂O (4a).

Torsion angles		
	HFPB·H₂O	[Cu(FPB)(OAc)(H₂O)]·H₂O (4a)
N(1)–C(5)–C(6)–N(2)	5.7(2)	-2.9(5)
C(4)–C(5)–C(6)–N(2)	-175.10(14)	177.4(4)
N(3)–N(2)–C(6)–C(5)	-179.18(11)	178.6(3)
C(6)–N(2)–N(3)–C(7)	176.10(12)	176.7(4)
N(2)–N(3)–C(7)–C(8)	177.81(11)	178.0(3)
N(2)–N(3)–C(7)–O(1)	-0.4(2)	-1.4(6)

For five coordinated complexes, the angular structural parameter (τ) is used to propose an index of trigonality suggested by Addison *et al.* [54]. The value of τ is defined by an equation represented by $\tau = (\beta-\alpha)/60$, where β is the greatest basal angle and α is the second greatest angle; τ is 0 for square pyramidal forms and 1 for trigonal bipyramidal forms [54,55]. However, in the case of the five coordinate systems, the structures vary from near regular trigonal bipyramidal (RTB) to near square based pyramidal (SBP). The value of τ for the complex **4a** is 0.308 indicating that the coordination geometry around Cu(II) is best described as distorted square based pyramidal geometry, where oxygen atom of acetate ion along with hydrazone moiety occupy the basal plane and the oxygen atom of water molecule occupies the axial position, Cu atom is displaced with a distance of 0.0928(6) Å above the basal plane along O4.

Ring puckering analysis and least square plane calculations [56] show that the ring Cg(2) comprising of atoms Cu(1), O(1), C(7), N(3) and N(2) is puckered with puckering amplitude Q(2) = 0.125(3) Å and ϕ(2) = 1(2)°. The puckering of five membered metallocycles was also calculated in terms of pseudorotation parameter P and τ_m [57] and it was found that the metallocycles adopt envelope on Cu(1) with P = 166.8(14)° and τ = 11.2(2)° for reference bond Cu(1)–O(1) in Cg(2). Conformational analyses [58] shows the five membered metallocycle Cg(1) adopts T-form (half chair) conformation.

The packing of the molecules is stabilized by intermolecular classical and non-classical hydrogen bonding, $\pi\cdots\pi$, O–H$\cdots\pi$ and C–F$\cdots\pi$

interactions. Table 3.6 represents the interaction parameters present in [Cu(FPB)(OAc)(H₂O)]·H₂O (**4a**).

Table 3.6. **Interaction parameters present in**
[Cu(FPB)(OAc)(H₂O)]·H₂O (4a)

Hydrogen bonding interactions				
D–H···A	**D–H (Å)**	**H···A (Å)**	**D···A (Å)**	**∠D–H···A (°)**
O(4)–H(4B)···N(3)[a]	0.87(2)	2.19(6)	2.869(5)	134(7)
O(4)–H(4A)···O(3)[b]	0.86(2)	1.90(3)	2.742(6)	165(5)
C(2)–H(2)···O(2)[c]	0.93	2.56	3.194(8)	126
π···π interactions				
Cg(I)···Cg(J)	**Cg···Cg**	**α**	**β**	**γ**
Cg(2)···Cg(2)[d]	3.772(3)	0	27.24	27.24
Cg(4)···Cg(5)[d]	3.612(3)	3.8(2)	19.85	21.80
Cg(4)···Cg(5)[a]	3.911(3)	3.8(2)	21.80	19.85
X–H···π interactions				
X–H···Cg	**H···Cg (Å)**	**X–H···Cg (°)**	**X···Cg (Å)**	
O(4)–H(4B)···Cg(2)[e]	2.80(7)	80(4)	2.775(4)	
O(4)–H(4B)···Cg(3)[e]	2.72(6)	105(5)	3.055(5)	
Y–X···π interactions				
Y–X···Cg	**X···Cg (Å)**	**Y–X···Cg (°)**	**Y···Cg (Å)**	
C(4)–F(1)···Cg(5)[d]	3.739(4)	65.9(2)	3.417(5)	
C(4)–F(1)···Cg(5)[a]	3.513(4)	77.1(2)	3.472(5)	

Symmetry code: a = -x+1,-y,-z+1; b = x,y,z+1; c = 1/3+y,2/3-x+y,2/3-z; d = 1-x,-y,-z; e = x,y,z
D = Donor, A = acceptor, Cg = Centroid of the ring
Cg(1) = Cu(1), O(2), C(14), O(3)
Cg(2) = Cu(1), O(1), C(7), N(3), N(2)
Cg(3) = Cu(1), N(1), C(5), C(6), N(2)
Cg(5) = C(8), C(9), C(10), C(11), C(12), C(13)
α(°) = Dihedral Angle between planes I and J
β(°) = Angle between Cg(I)···Cg(J) and Cg(J) perp.
γ(°) = Angle between Cg(I)···Cg(J) vector and Cg(I) perp.
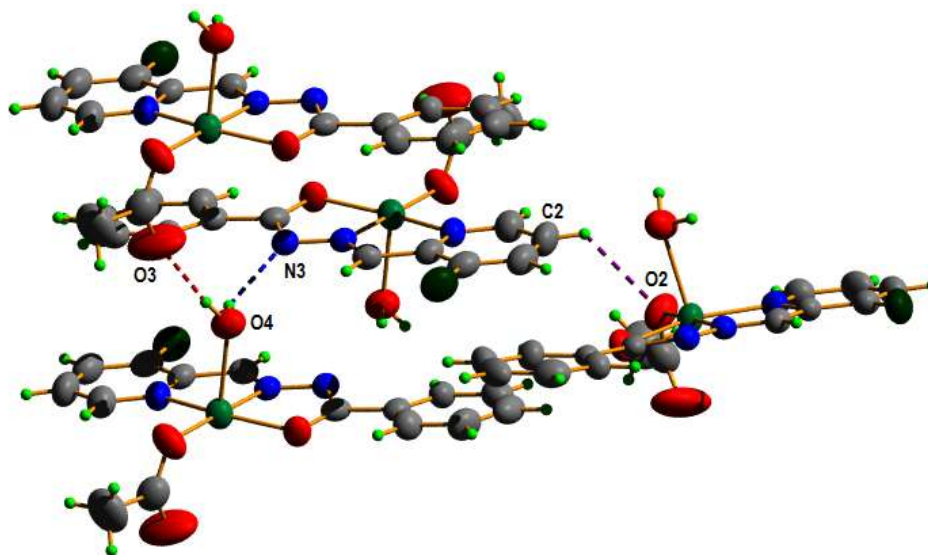
Fig. 3.32. Hydrogen bonding interactions in complex 4a.

There is extensive classical and non classical hydrogen bonding (Table 3.6 and Fig. 3.32) present in this molecule. Three different units in the crystal lattice are held together through two different intermolecular hydrogen bonding, $O(4)–H(4B)\cdots N(3)$ and $O(4)–H(4A)\cdots O(3)$ with the hydrogen atoms, H4A and H4B of coordinated water molecule of one of the unit. The non-classical intermolecular hydrogen bonding involving the hydrogen atom of the $C(2)$ and $O(2)$ with $H\cdots A$ distance of 2.53 Å and $\angle DHA$ bond angle of 126° connects two molecules in the crystal lattice (Fig. 3.32).
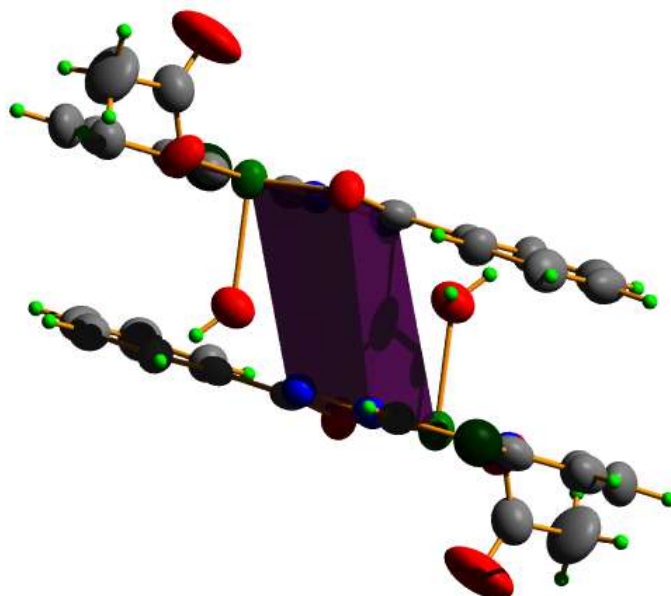
Fig. 3.33. The Cg(2)···Cg(2) interactions in
[Cu(FPB)(OAc)(H₂O)]·H₂O (4a).
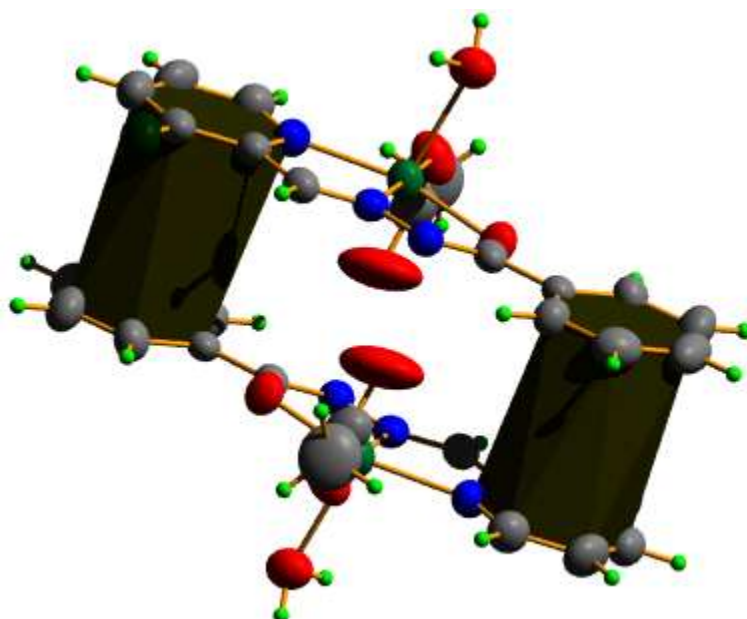
Fig. 3.34. The Cg(4)···Cg(5) interactions in
[Cu(FPB)(OAc)(H₂O)]·H₂O (4a).

There is $\pi\cdots\pi$, O–H$\cdots\pi$ and C–F$\cdots\pi$ interactions present in the crystal lattice leading to efficient packing in the crystalline state. The centroid Cg(2) is involved in $\pi\cdots\pi$ interaction with Cg(2) of the neighboring unit at a distance of 3.772(3) Å (Fig. 3.33). Rings Cg(4) and Cg(5) of adjacent molecules are also involved in $\pi\cdots\pi$ interaction at a distance of 3.612(3) and 3.911(3) Å (Fig. 3.34).
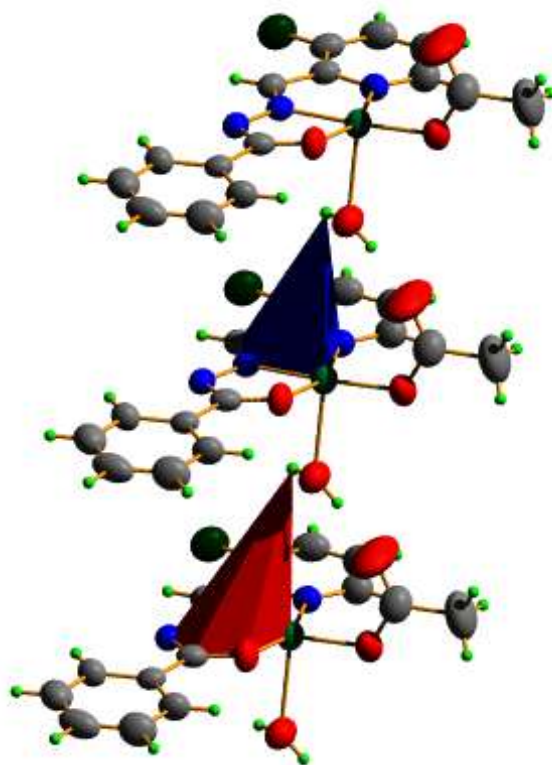
Fig. 3.35. O–H$\cdots\pi$ interactions in
[Cu(FPB)(OAc)(H$_2$O)]·H$_2$O (4a).

The complex motifs interact through two types of O–H$\cdots\pi$ interactions. The hydrogen atom H(4B) of the coordinated water molecule interacts with Cg(2) and Cg(3) of the adjacent molecules with

the H···Cg distance of 2.80(7) and 2.72(6) Å respectively (Fig. 3.35).

Weak C–F···Cg(5) interactions (Fig. 3.36 and Table 3.6) connects the adjacent monomeric complexes.

Fig. 3.36. C–F···π interactions connecting adjacent monomeric complexes.

Based on the elemental analyses and spectral studies, following tentative structures were assigned to the complexes.
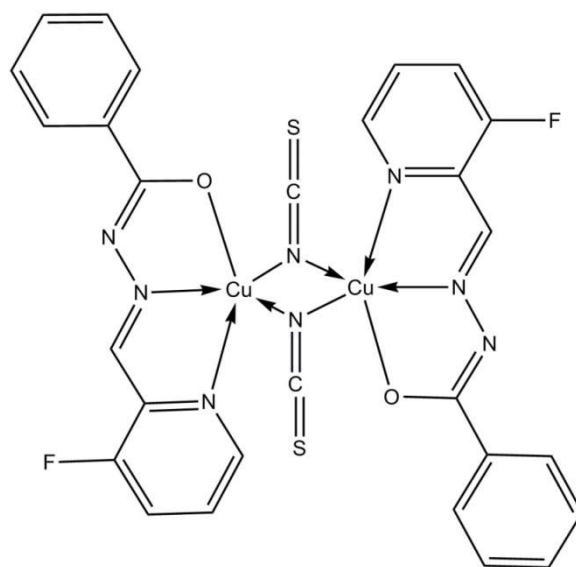
[Cu₂(FPB)₂(μ-NCS)₂] (1)
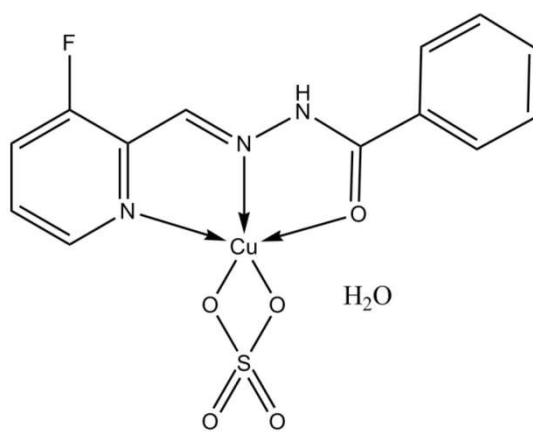
[Cu(HFPB)(SO₄)]·H₂O (2)
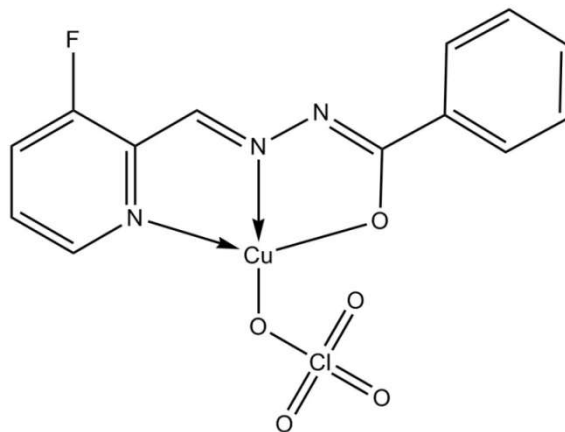
[Cu(FPB)(ClO₄)] (3)
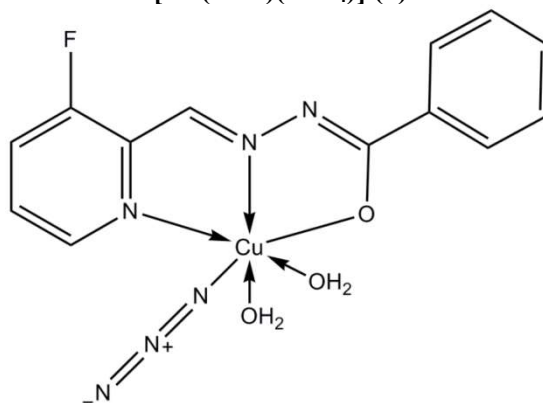
[Cu(FPB)(N₃)(H₂O)₂] (5)
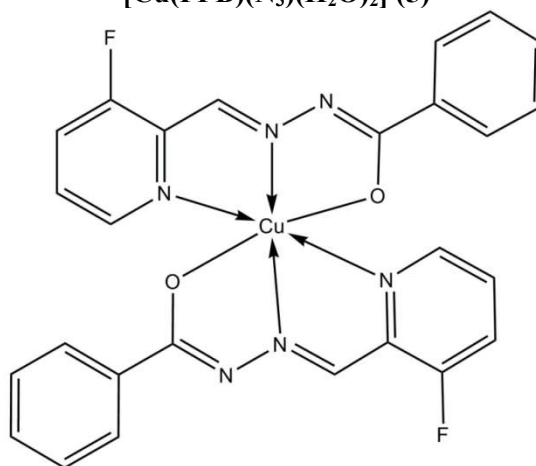
[Cu(FPB)₂] (6)
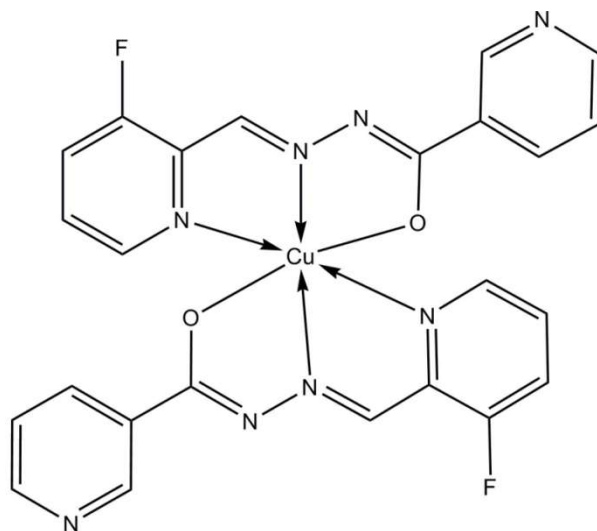
[Cu(FPN)₂] (7)

[Cu(FPN)₂] (7)
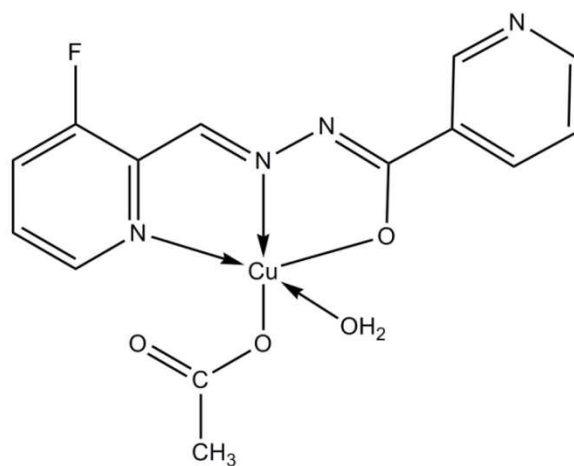
[Cu(FPN)(OAc)(H₂O)] (8)

[Cu(FPN)(OAc)(H₂O)] (8)

References

[1]   S. Mondal, S. Naskar, A.K. Dey, E. Sinn, C. Eribal, S.R. Herron, S.K. Chattopadhyay, Inorg. Chim. Acta 398 (2013) 98.

[2]   K. Roztocki, D. Matoga, J. Szklarzewicz, Inorg. Chem. Commun. 57 (2015) 22.

[3]   N.M.H. Salem, L. El Sayed, W. Haase, M.F. Iskander, Spectrochim. Acta 134A (2015) 257.

[4]   R. Csonka, C.V. -Barber, V. Psycharis, C.P. Raptopoulou, B.R. Steele, Polyhedron 34 (2012) 181.

[5]   M.V. Angelusiu, S.-F. Barbuceanu, C. Draghici, G.L. Almajan, Eur. J. Med. Chem. 45 (2010) 2055.

[6]   R.-Ş. Mezey, I. Máthé, S. Shova, M.-N. Grecu, T. Roşu, Polyhedron 102 (2015) 684.

[7]   R. Bhaskar, N. Salunkhe, A. Yaul, A. Aswar, Spectrochim. Acta 151A (2015) 621.

[8]   J.R. Anacona, M. Rincones, Spectrochim. Acta 141A (2015) 169.

[9]   D.S. Kalinowski, P.C. Sharpe, P.V. Bernhardt, D.R. Richardson, J. Med. Chem. 51 (2008) 331.

[10]   W.J. -Lin, Z.Y. -Qin, Y.B. -Sheng, Inorg. Chim. Acta 409 (2014) 484.

[11]   R. Gup, C. Gökçe, S. Aktürk, Spectrochim. Acta 134A (2015) 484.

[12]   S. Zhai, L. Yang, Q.C. Cui, Y. Sun, Q.P. Dou, B. Yan, J. Biol. Inorg. Chem. 15 (2010) 259.

[13]   S. Adsule, V. Barve, D. Chen, F. Ahmed, Q.P. Dou, S. Padhye, F.H. Sarkar, J. Med. Chem. 49 (2006) 7242.

[14]   N. Khadir, D.M. Boghaei, A. Assoud, O.R. Nascimento, A. Nicotina, L. Ghivelder, R. Calvo, Dalton Trans., 44 (2015) 2431.

[15] S. Chandra, X. Sangeetika, Spectrochim. Acta 60A (2004) 147.

[16] B. Graham, M.T.W. Hearn, P.C. Junk, C.M. Kepert, F.E. Mabbs, B. Moubaraki, K.S. Murray, L. Spiccia, Inorg. Chem. 40 (2001) 1536.

[17] S. Bootwala, M. Tariq, S. Somasundaran, K. Aruna, Int. J. Pharm. Bio. Sci. 3 (2013) 345.

[18] D. Matoga, J. Szklarzewicz, R. Grybos, K. Kurpiewska, W. Nitek, Inorg. Chem. 50 (2011) 3501.

[19] K. Nakamoto, Infrared and Raman spectra of Inorganic and Coordination compounds, 5th Edn., Wiley, New York, 1997.

[20] S.C. Chan, L.L. Koh, P.-H. Leung, J.D. Ranford, K.Y. Sim, Inorg. Chim. Acta 236 (1995) 101.

[21] C.G. Efthymiou, A.A. Kitos, C.P. Raptopoulou, S.P. Perlepes, A. Escuer, C. Papatriantafyllopoulou, Polyhedron 28 (2009) 3177.

[22] E. Bozkurt, A. Doner, I. Ucar, B. Karabulut, Chem. Phys. Lett. 502 (2011) 163.

[23] J.R. Anacona, V.E. Marquez, Transit. Met. Chem. 33 (2008) 579.

[24] M. Joseph, A. Sreekanth, V Suni, M. R. P. Kurup, Spectrochim. Acta 64A (2006) 637.

[25] H.H. -Monfared, H. Falakian, R. Bikas, P. Mayer, Inorg. Chim. Acta 394 (2013) 526.

[26] S.-P. Xu, F.-L. Yang, G.-Z. Zhu, H.-L. Shi, X.-L. Li, Polyhedron 68 (2014) 1.

[27] P.F. Raphael, E. Manoj, M.R.P. Kurup, Polyhedron 26 (2007) 818.

[28] S. Renjusha, M.R.P. Kurup, Polyhedron 27 (2008) 3294.

[29] B. Shaabani, A.A. Khandar, H. Mobaiyen, N. Ramazani, S.S. Balula, L.C. –Silva, Polyhedron 80 (2014) 166.

[30] L. Sacconi, M. Ciampolini, G.P. Speroni, J. Am. Chem. Soc. 87 (1965) 3102.

[31] R.P. John, A. Sreekanth, V. Rajakannan, T.A. Ajith, M.R.P. Kurup, Polyhedron 23 (2004) 2549.

[32] A.B.P. Lever, Inorganic Electronic Spectroscopy, 2nd Edn. Elsevier Amsterdam (1984).

[33] B.J. Hathaway, A.A.G. Tomlinson, Coord. Chem. Rev. 5 (1970) 24.

[34] S. Stoll, Spectral Simulations in Solid-State Electron Paramagnetic Resonance, Ph. D. thesis, ETH, Zurich, 2003.

[35] B.J. Hathaway, D.E. Billing, Coord. Chem. Rev. 5 (1970) 143.

[36] E.B. Seena, M.R.P. Kurup, Polyhedron 26 (2007) 829.

[37] I.M. Procter, B.J. Hathaway, P. Nicholis, J. Chem. Soc. A (1968) 1678.

[38] X. Wang, J. Ding, J.D. Ranford, J.J. Vittal, J. Appl. Phys. 93 (2003) 7819.

[39] V. Philip, V. Suni, M.R.P. Kurup, M. Nethaji, Polyhedron 24 (2005) 1133.

[40] S.S. Kandil, A. El-Dissouky, G.Y. Ali, J. Coord. Chem. 57 (2004) 105.

[41] M.F. El-Shazly, A. El-Dissouky, T.M. Salem, M.M. Osman, Inorg. Chim. Acta 40 (1980) 1.

[42] B.N. Figgis, Introduction to Ligand fields, Interscience, New York, 1996, p. 295.

[43] B.J. Hathaway, in: G. Wilkinson, R.D. Gillard, J.A. McCleverty (Eds.), Comprehensive Coordination Chemistry, Vol. 5, Pergamon, Oxford, 1987, p. 533.

[44] T.D. Smith, J. Pilbrow, Coord. Chem. Rev. 13 (1974) 173.

[45] D. Kivelson, R. Neiman, J. Chem. Phys. 35 (1961) 149.

[46]   L. Latheef, M.R.P Kurup, Spectrochim. Acta 70A (2008) 86.

[47]   Bruker, *APEX2, SAINT, XPREP and SADABS*, Bruker AXS Inc., Madison, Wisconsin, USA (2004).

[48]   G.M. Sheldrick, SHELXL97 and SHELXS97, University of Göttingen, Germany, 1997.

[49]   G.M. Sheldrick, Acta Cryst. A64 (2008) 112.

[50]   L.J. Farrugia, J. Appl. Cryst. 45 (2012) 849.

[51]   K. Brandenburg, Diamond Version 3.2g, Crystal Impact GbR, Bonn, Germany, (2010).

[52]   A.L. Spek, Acta Cryst. C71 (2015) 9.

[53]   H.H. -Monfared, R. Bikas, R. Szymczak, P. Aleshkevych, A.M. Owczarzak, M. Kubicki, Polyhedron 63 (2013)74.

[54]   A.W. Addison, T.N. Rao, J. Reedijk, J.V. Rijn, G.C. Verschoor, J. Chem. Soc., Dalton Trans. 7 (1984) 1349.

[55]   M. Vaidyanathan, R. Balamurugan, U. Sivagnanam, M. Palaniandavar, J. Chem. Soc., Dalton Trans. 23 (2001) 3498.

[56]   D. Cremer, J.A. Pople, J. Am. Chem. Soc. 97 (1975) 1354.

[57]   S.T. Rao, E. Westhof, M. Sundaralingam, Acta Cryst. A37 (1981) 421.

[58]   G.G. Evans, J.A. Boeyens, Acta Cryst. B45 (1989) 581.

.....ജ്ഞ.....

SYNTHESES, SPECTRAL CHARACTERIZATION AND CRYSTAL STRUCTURE OF NICKEL(II) CHELATES OF TRIDENTATE AROYLHYDRAZONES

Contents

4.1. Introduction
4.2. Experimental
4.3. Results and discussion

4.1. Introduction

Nickel is a naturally occurring, lustrous, silvery-white metallic element. It is the fifth most common element on earth and occurs extensively in the earth's crust. Nickel had been in use centuries before its actual discovery and isolation. The name comes from the German word *Kupfernickel,* meaning "Old Nick's copper," a term used by German miners. Swedish Axel Fredrik Cronstedt (1722-1765) was the first person to realize that nickel was a new element. Since then, nickel has become a very valuable metal. Nickel-containing materials play a major role in our everyday lives. Nickel is a hard, corrosion resistant metal. It can be electroplated onto other metals to form a protective coating. Finely divided nickel is used as a catalyst for the hydrogenation

of vegetable oils and adding nickel to glass gives it a green color. A single kilogram of nickel can be drawn into 300 kilometers of wire.

It has a melting point of 1453 °C, relatively low thermal and electrical conductivities, high resistance to corrosion and oxidation, excellent strength and toughness at elevated temperatures, and is capable of being magnetized. It is attractive and very durable as a pure metal, and alloys readily with many other metals. Reflecting these characteristics, nickel is widely used in over 300,000 products for consumer, industrial, military, transport, aerospace, marine and architectural applications. The biggest use is in alloying - particularly with chromium and other metals to produce stainless and heat-resisting steels. It is a key ingredient in many catalysts used to make chemical reactions more efficient. Nickel is a key part of several rechargeable battery systems used in electronics, power tools, transport and emergency power supply. Most nickel-containing products have long useful lives. Nickel is one of the most recycled materials globally. It is collected and recycled, mostly in the form of alloys. Nickel is also used to manufacture some types of coins and strong permanent magnets.

Nickel is both essential and toxic for animals and humans. A Ni-poor nutrition of <0.1 mg/kg leads to Ni deficiency symptoms. Nickel deficiency symptoms, however, have not yet been found in animals and humans since the nickel offer exceeds the nickel requirement. Enzymes known as hydrogenases in bacteria contain nickel. The enzyme urease present in the jack beans has been found to contain nickel protein and factor F_{430} isolated from methanogenic bacteria contain nickel tetrapyrrole [1]. All

metals and metal compounds have a certain level of toxicity and may cause adverse effects on living organisms. Nickel in certain forms and under particular circumstances, may generate detrimental environmental effects.

Nickel(II) has very rich coordination chemistry owing to its inherent ability to espouse various geometries. This versatile coordination chemistry of nickel has an area of considerable importance in inorganic chemistry with implications in other areas of chemistry and biology [2]. Nickel complexes are found to be stronger antioxidants than Vitamin E [3]. The Ni(II) ion forms many stable complexes as predicted by the Irving Williams series. While there are no other important oxidation states to consider, the Ni(II) ion can exist in a wide variety of coordination numbers which complicates its coordination chemistry and the phrase 'anomalous nickel' has been used to describe this behavior.

Metal chelates bear polar and nonpolar properties together; this makes them suitable for permeation to the cells and tissues. Transition metal complexes with pyridine-2-carboxaldehyde-benzoylhydrazone and its substituted derivatives are important members in this series and are well documented in the literature [4]. A large number of Ni(II) complexes of biological nature had already been reported [5-7]. Literature studies reveal that complexes of Ni(II) with Schiff bases derived from pyridine derived carbonyl compounds show antibacterial and antifungal activities against *Escherichia coli*, *Pseudomonas aeruginosa*, *Staphylococcus aureus*, *Bacillus subtilis*, *Enterococcus faecalis* and *Streptococcus pyogenes* and fungi *Candida albicans*, *Aspergillus niger* and *Aspergillus clavatus*. The activity data show that

the metal complexes have a promising biological activity comparable with the parent ligand against all bacterial and fungal species [4,8].

As DNA is primary target for most of the anticancer drugs, the discovery of small molecules which can interact, bind or cleave specifically and block DNA synthesis of cancer cells are of prime importance [9,10]. The first transition series metals are well known to bind specifically with the DNA molecule and possess a well defined geometry. These metals are quite economical than ruthenium, gold and platinum, comparatively very less toxic as they are required in small amount for the normal functioning of the biological systems and possess excellent complexation abilities [6,10,11]. The interaction of DNA with macrocyclic Schiff base nickel(II) complex have been reported in the literature [12]. Recently Jaydeep Adhikary and coworkers have studied the anticancer activity of octahedral and square planar Ni(II) complexes on Erhlich's ascites carcinoma cell and it has been reported that all the four complexes show excellent anticancer activity [2].

Nonlinear optics has received considerable attention due to its variety of applications in optoelectronic and photonic devices. There is a need to design and develop the nonlinear optical materials to meet the present demand due to their widespread applications such as high-speed information processing, optical communications, and optical data storage [13]. More recently, transition metal complexes have appeared as an important alternative for the design of NLO materials, since the metal center can impart important structural and electronic properties to the organic ligands, and consequently to the NLO responses. These types of

complexes have been vigorously explored in recent years and such studies have been the subject of many papers and reviews [14,15]. Metal complexes displayed better second-order NLO responses because the presence of metal ion changes the gaps between occupied and unoccupied orbitals thereby increasing the electron densities distribution of coordinated atoms and adjacent carbon atoms in the conjugated chain [14].

Aroylhydrazones with a variety of metals have been extensively used as efficient catalysts [16], sensors [17] and corrosion inhibitors [18]. The discovery of efficient method for catalytic oxidation of cyclohexane is an important goal in synthetic chemistry due to the importance of its products like cyclohexanol and cyclohexanone which have great values in the industry for the synthesis of nylon-6 and nylon-66. Higher catalytic activity has been observed for the nickel(II) complexes compared to the other complexes. Recently Antony *et al.* established the catalytic efficiency of few Ni(II) complexes in the cyclohexane oxidation reaction using H_2O_2 as oxidant at 70 °C [15]. Due to the presence of C=N group in the aroylhydrazone molecules, they are likely to be good corrosion inhibitors. The metal complexes of Ni(II) with different ligands have shown good corrosion inhibition property for steel in different acidic media at room as well as elevated temperatures [16].

Considering such a large number of applications of Ni(II) complexes in various fields, it is highly demandable to prepare and analyze the nickel(II) complexes with aroylhydrazones. Hence in this chapter we report the synthesis and characterization of some Ni(II) complexes of two novel aroylhydrazones.

4.2. Experimental

4.2.1. Materials

3-Fluoropyridine-2-carbaldehyde (Sigma-Aldrich), benzhydrazide (Sigma-Aldrich), nicotinic hydrazide (Sigma-Aldrich), nickel(II) acetate tetrahydrate (Merck), nickel(II) chloride hexahydrate (Merck), nickel(II) perchlorate hexahydrate (Aldrich) and nickel(II) nitrate hexahydrate (Alfa Aesar) were of Analar grade and were used as received. Solvents used were methanol, ethanol and DMF.

4.2.2. Syntheses of aroylhydrazones

Syntheses of aroylhydrazones, HFPB·H_2O and HFPN·$2H_2O$ were already discussed in Chapter 2.

4.2.3. Syntheses of Ni(II) complexes

4.2.3.1. [Ni(FPB)(NO₃)]·2H₂O (9)

Complex **9** has been prepared by mixing hot methanolic solution of HFPB·H_2O (0.2612 g, 1 mmol) with methanolic solution of nickel(II) nitrate hexahydrate (0.2908, 1 mmol). The resulting mixture was then refluxed for 5 hours. The solution was then cooled at room temperature and green color product obtained was filtered, washed with methanol followed by ether and dried over P_4O_{10} *in vacuo*.

[Ni(FPB)(NO₃)]·$2H_2O$ (**9**): Yield: 65%, λ_m (DMF): 12 ohm^{-1} cm^2 mol^{-1}, μ_{eff} (B.M.): 2.87, Elemental Anal. Found (Calcd.) (%): C: 39.68 (39.14); H: 3.71 (3.28); N: 14.53 (14.04).

4.2.3.2. [Ni(HFPB)(FPB)]Cl (10)

A solution of HFPB·H_2O (0.2612 g, 1 mmol) in methanol was treated with a methanolic solution of nickel(II) chloride hexahydrate (0.2377 g, 1 mmol). The resulting green color solution was then refluxed for 4 hours. The solution was cooled at room temperature and after slow evaporation, brown colored product separated out was filtered, washed with methanol followed by ether and dried over P_4O_{10} *in vacuo.*

[Ni(HFPB)(FPB)]Cl (**10**): Yield: 71%, λ_m (DMF): 87 ohm^{-1} cm^2 mol^{-1}, μ_{eff} (B.M.): 2.79, Elemental Anal. Found (Calcd.) (%): C: 54.50 (53.88); H: 3.77 (3.30); N: 15.08 (14.50).

4.2.3.3. [Ni(FPB)(OAc)(DMF)] (11)

A solution of HFPB·H_2O (0.2612 g, 1 mmol) in methanol was treated with a methanolic solution of Ni(OAc)$_2$·4H_2O (0.2480 g, 1 mmol). The resulting solution was then refluxed for about 4 hours. The precipitated complex was then recrystallized from DMF, brown colored product separated out was filtered, finally washed with ether and dried over P_4O_{10} *in vacuo.*

[Ni(FPB)(OAc)(DMF)] (**11**): Yield: 68%, λ_m (DMF): 6 ohm^{-1} cm^2 mol^{-1}, μ_{eff} (B.M.): 2.69, Elemental Anal. Found (Calcd.) (%): C: 50.49 (49.92); H: 4.83 (4.42); N: 13.33 (12.94).

4.2.3.4. [Ni(FPB)(ClO$_4$)]·DMF (12)

To a methanolic solution of HFPB·H_2O (0.2612 g, 1 mmol), nickel(II) perchlorate hexahydrate (0.3650 g, 1 mmol) dissolved in

methanol was added. The resulting green color solution was stirred for 1 hour followed by refluxing for about 5 hours. The solution was then allowed to stand at room temperature, green color needle shaped crystals were separated. It was then filtered, washed with methanol followed by ether and dried over P_4O_{10} *in vacuo.*

[Ni(FPB)(ClO$_4$)]·DMF (**12**): Yield: 72%, λ_m (DMF): 5 ohm^{-1} cm^2 mol^{-1}, μ_{eff} (B.M.): 2.92, Elemental Anal. Found (Calcd.) (%): C: 41.21 (40.59); H: 3.88 (3.41); N: 12.26 (11.83).

4.2.3.5. [Ni(FPB)$_2$] (13)

A methanolic solution of Ni(OAc)$_2$·4H$_2$O (0.1240 g, 0.5 mmol) was treated with a solution of HFPB·H$_2$O (0.2612 g, 1 mmol) in methanol. The resulting solution was then refluxed for 4 hours. The brown product formed immediately was filtered. The solution was cooled at room temperature and after slow evaporation, brown colored product separated out was filtered. It was then recrystallized from DMF solution, dark brown shining crystals separated were filtered, finally washed with ether and dried over P_4O_{10} *in vacuo.*

[Ni(FPB)$_2$] (**13**): Yield: 73%, λ_m (DMF): 11 ohm^{-1} cm^2 mol^{-1}, μ_{eff} (B.M.): 2.74, Elemental Anal. Found (Calcd.) (%): C: 57.70 (57.49); H: 3.46 (3.34); N: 15.61 (15.47).

4.2.3.6. [Ni(FPN)(ClO$_4$)] (14)

To a methanolic solution of nickel(II) perchlorate hexahydrate (0.3650 g, 1 mmol), HFPN·2H$_2$O (0.2802 g, 1 mmol) dissolved in

methanol was added. The resulting green color solution was stirred for 1 hour followed by refluxing for about 5 hours. The solution was then allowed to stand at room temperature, green product formed was separated, washed with methanol followed by ether and dried over P_4O_{10} *in vacuo*.

[Ni(FPN)(ClO$_4$)] (**14**): Yield: 60%, λ_m (DMF): 10 ohm^{-1} cm^2 mol^{-1}, μ_{eff} (B.M.): 3.14, Elemental Anal. Found (Calcd.) (%): C: 36.31 (35.91); H: 2.36 (2.01); N: 14.37 (13.96).

4.3. Results and discussion

The complexes were obtained from direct reaction between the metal salts and the ligand using methanol as solvent. The compounds showed different colors and were obtained with a moderate-good yields (50-70%). The composition, coordination mode and geometry of the complexes were established on the basis of elemental, spectral analyses, thermal analyses, molar conductivity measurements and magnetic properties which are discussed in detail in the following sections. Elemental analyses suggested a deprotonated iminolate form of the ligand in most of the complexes, however in few cases ligand is binding to the metal center in the neutral amido form, with the anions of the metal salt satisfying the Ni(II) valency. The complexes prepared were green or dark brown in color and are found to be readily soluble in solvents like DMF and DMSO but less soluble in solvents like ethanol, methanol and chloroform. All the isolated complexes were quite stable and could be stored for several weeks without any appreciable change. X-ray quality single crystals of one of the complexes, [Ni(FPB)$_2$] (**13**) were obtained by the recrystallization of the compound in DMF solution.

4.3.1. Elemental analyses

Elemental analyses data are in agreement with the general empirical formula and suggest a 1:2 metal to ligand stoichiometry for complexes **10** and **13** and all other complexes are found to have a 1:1 metal to ligand stoichiometry. The results are given in Section 4.2.3.

4.3.2. Molar conductivity and magnetic susceptibility measurements

Molar conductivity of the complexes were measured in the 10^{-3} M DMF solution and were found to be non-electrolytic in nature except complex **10** which is a 1:1 electrolyte [19]. The molar conductivity value of this complex is found to be in the range 87 ohm^{-1}cm^{2}mol^{-1}.

The magnetic properties of the complexes provide valuable information for distinguishing their stereochemistry. All the nickel complexes were found to be paramagnetic which excludes the possibility of a square planar configuration. The room temperature effective magnetic moments μ_{eff} of complexes **10**, **11** and **13** are found to be in the range 2.6-2.8 B.M., consistent with octahedral geometry for these complexes [20-22]. In regular octahedral complexes of Ni(II), consideration of spin-orbit coupling and contribution from the $^{3}A_{2g}$ and the next higher $^{3}T_{2g}$ states give a somewhat higher magnetic moment than the spin-only moment of 2.83 B.M. For complexes **9**, **12** and **14**, magnetic moments were found to be in the 2.8-3.2 B.M. range which is slightly greater than the spin only value which may be due to orbital contribution. This suggests a tetrahedral geometry for these complexes which are similar to the reports of other tetrahedral Ni(II) complexes [23-25].

4.3.3. Infrared spectral studies

The IR spectra of the hydrazones and their Ni(II) complexes were recorded in the solid state as KBr discs. The characteristic IR bands for the free ligands when compared with metal complexes provide meaningful information regarding the bonding sites of the ligands. The selected IR bands of the hydrazones and complexes are represented in Table 4.1. The IR spectra of the aroylhydrazones exhibit two bands in the range 3058-3059 and 1682-1683 cm^{-1} due to the v(NH) and v(C=O), respectively, and these bands are absent in the case of complexes. This indicates that the ligand coordinates to the metal in iminolate form [25]. The strong absorption bands for all the complexes in the region 1550-1570 cm^{-1} may be assigned to the coordination of Ni(II) ion by azomethine nitrogen atom.

Table 4.1. The important IR frequencies (cm^{-1}) of hydrazones and their Ni(II) complexes

Compound	v(N–H)	v(C=O)/v(C–O)	v(C=N)	v(C=N)[a]
HFPB·H$_2$O	3059	1683	1597	--
[Ni(FPB)(NO$_3$)]·2H$_2$O (**9**)	--	1353	1570	1590
[Ni(HFPB)(FPB)]Cl (**10**)	3020	1647, 1368	1550	1560
[Ni(FPB)(OAc)(DMF)] (**11**)	--	1328	1547	1570
[Ni(FPB)(ClO$_4$)]·DMF (**12**)		1341	1555	1587
[Ni(FPB)$_2$] (**13**)		1327	1567	1590
HFPN·2H$_2$O	3058	1682	1590	--
[Ni(FPN)(ClO$_4$)] (**14**)	--	1339	1581	1591

[a]Newly formed C=N bond
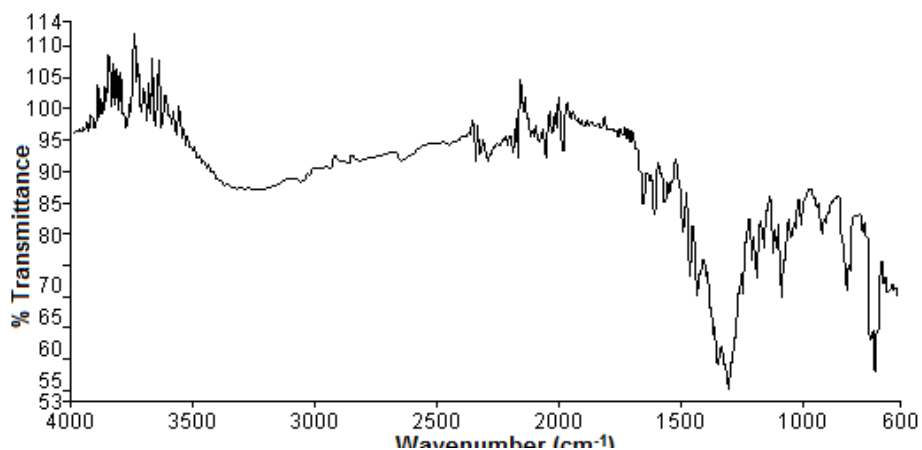
Fig. 4.1. IR spectrum of [Ni(FPB)(NO$_3$)]·2H$_2$O (9).

From the IR data, it was analyzed that in complex **9** (Fig. 4.1), the ligand HFPB·H$_2$O acts as a tridentate ligand coordinating through oxygen of the deprotonated –OH group formed due to iminolization, nitrogen of the azomethine group and nitrogen of the pyridyl ring. According to Stefov *et al.*, the broad band above 3200 cm^{-1} indicates the presence of lattice water in the complex [26]. The band in the region 1353 cm^{-1} may be assigned to ν(C–O) stretching vibration. The IR spectrum of [Ni(FPB)(NO$_3$)]·2H$_2$O (**9**) exhibits two bands at 1448 and 1325 cm^{-1} corresponding to N=O stretching vibrations of the nitrate ion. The separation of these bands by 120 cm^{-1} indicates the unidentate nature of the nitrate ion in the complex [27]. A positive shift corresponding to out-of-plane bending vibrations of the free ligand to higher frequencies in the complexes is confirmative of pyridine nitrogen coordination to the metal center.
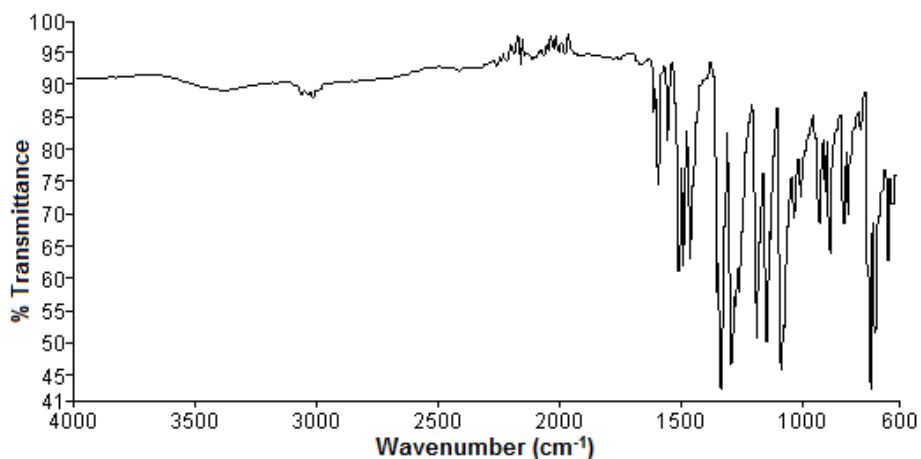
Fig. 4.2. IR spectrum of [Ni(HFPB)(FPB)]Cl (10).

The IR data of [Ni(HFPB)(FPB)]Cl (**10**) (Fig. 4.2) indicate that the ligand is bound as a uni-negative anion *via* the pyridine nitrogen, azomethine nitrogen and iminolate oxygen. The IR spectrum of compound **10** reveals a broad band around 3020 cm^{-1} corresponding to N–H vibration. This explains the fact that one of the ligands is not deprotonated. The negative shift of the bands corresponding to v(C=N) vibration from 1597 cm^{-1} to 1550 cm^{-1} in the complex is consistent with the coordination of the azomethine nitrogen to the central Ni(II) ion. The elemental analyses suggested the presence of chloride ion, however the conductivity measurements suggested the complex as 1:1 electrolyte which means that one of the ligands is deprotonated and coordinating to the metal ion in the anionic form. The appearance of a new band at 1560 cm^{-1} due to newly formed v(C=N) support the above observation. The coordination of pyridine nitrogen is indicated by the shift in the out-of-plane and in-plane modes of the pyridine ring.
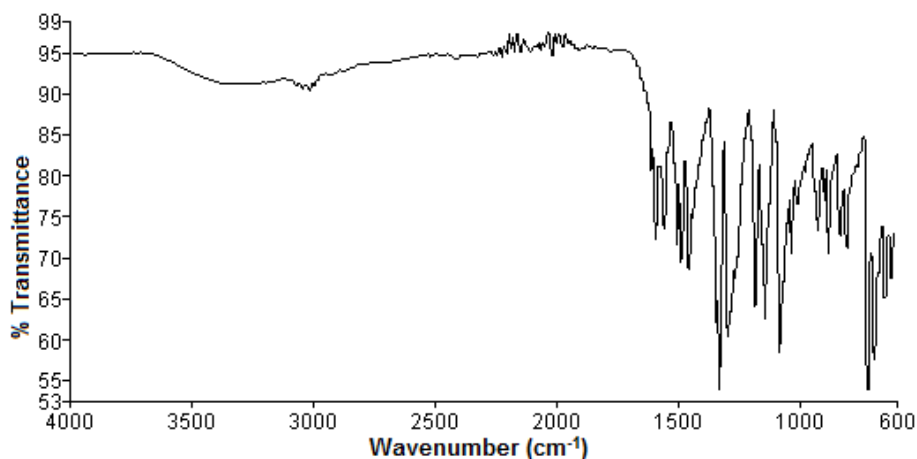
Fig. 4.3. IR spectrum of [Ni(FPB)(OAc)DMF](11).

In complex **11** (Fig. 4.3), the band corresponding to the newly formed C=N bond due to iminolization of the ligand is found at 1570 cm^{-1}. The disappearance of ν(N–H) and ν(C=O) peaks and the appearance of a new band at corresponding to ν(C–O) stretching vibration further support the coordination of the ligand in the iminolate form. The out-of-plane and in-plane bending vibrations of the pyridine ring found in the ligand shift to higher frequencies on complexation, confirming the coordination of the ligand to the metal *via* the pyridine nitrogen [28]. The ν(C=N) band of the hydrazone is found to be shifted to lower frequency in the complex indicating the coordination *via* azomethine nitrogen. The complex **11** displays bands at 1570-1600 and 1415-1425 cm^{-1} regions due to the asymmetric and symmetric modes of vibration characteristic of acetate group, respectively. The frequency difference $\Delta\nu$ of acetate group is found at ~150 cm^{-1} which is consistent with the bidentate nature of the acetate group [29].
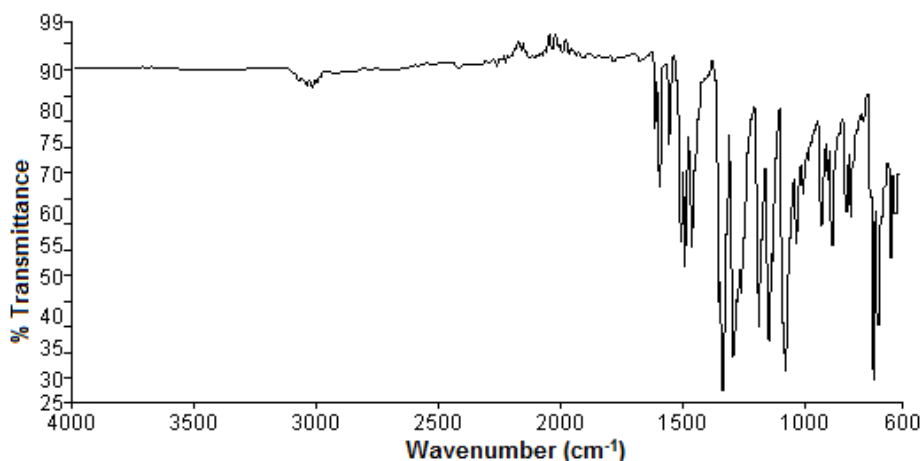
Fig. 4.4.   IR spectrum of [Ni(FPB)(ClO₄)]·DMF (12).

In complex **12** (Fig. 4.4), the band at 1597 cm^{-1} assignable to ν(C=N) in the free ligand was shifted to lower values indicating its participation in the chelation with π-electron delocalization.   The absence of C=O stretching band and the appearance of new band around 1587 cm^{-1}, assigned to –C=N–N=C– stretching vibration indicates that the ligand coordinates to Ni(II) metal ion *via* iminolization followed by deprotonation.   The perchlorate assignments were made by comparison to known values.   Although regarded as weakly coordinating anion, perchlorate is known to coordinate under special conditions.   Such interactions normally manifest themselves by a splitting of the antisymmetric (Cl–O) stretching mode due to a reduced symmetry of the coordinated species.   The absorption bands occuring in the IR spectrum of the complex **12** (Fig. 4.4) at 1095 and 649 cm^{-1} are assignable to ν_3(ClO₄) and ν_4(ClO₄) respectively [30].   Both show considerable splitting due to a reduced symmetry of the perchlorate species

suggesting some interaction of perchlorate anion ClO_4^- with the metal. The pyridyl in-plane ring deformation and out-of-plane ring deformation are found at higher frequencies compared to that of the ligand suggesting the coordination of pyridyl nitrogen [31,32].
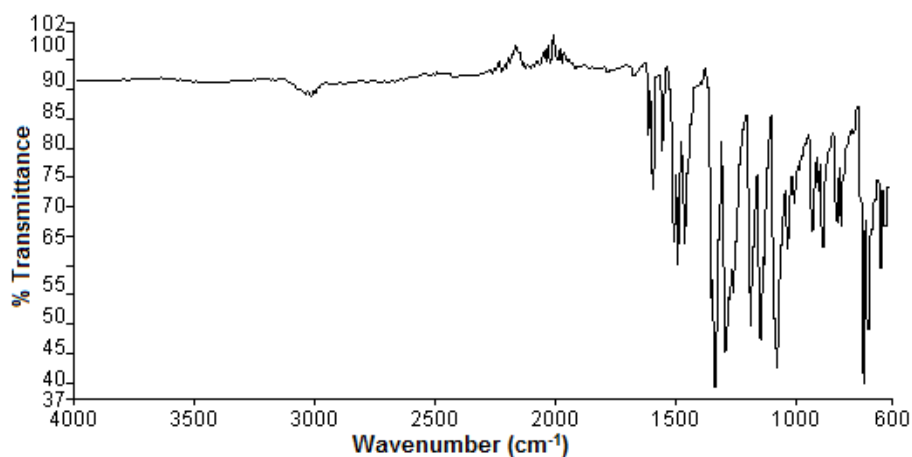
Fig. 4.5.   IR spectrum of [Ni(FPB)$_2$] (13).

In complex **13** (Fig. 4.5), the ligand coordinates the metal center with nitrogen atoms from the pyridine and imino moieties and one oxygen atom coming from its iminolic counterpart. The IR spectrum of the ligand exhibits two bands at 3059 and 1683 cm^{-1} due to the ν(N–H) and ν(C=O), respectively, and these bands are absent in complex **13**. This indicates that the ligand coordinates to the metal in the iminolate form. A new band appearing at 1384 is assigned to the ν(C–O) band. The band due to ν(C=N) of the free ligand has been shifted to lower frequency by 27-30 cm^{-1} respectively on complexation, indicating the involvement of azomethine nitrogen in coordination. The coordination of the nitrogen atom of the pyridine ring to the metal center in the

complex is indicated by shifting of the pyridine ring vibrations of the ligand to higher frequencies. The absence of the band corresponding to $\nu(N–H)$ vibration in the expected region of the complex confirm the deprotonation of the ligand during complex formation.
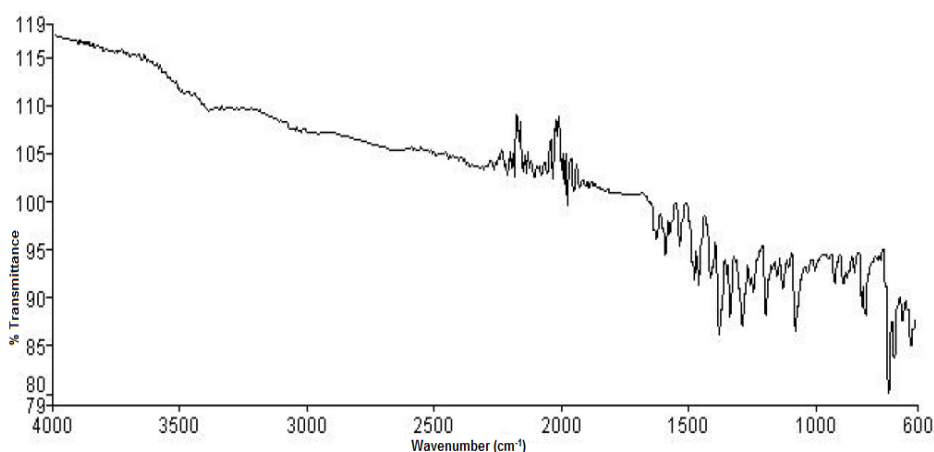
Fig. 4.6.   IR spectrum of [Ni(FPN)(ClO$_4$)] (14).

The IR data of complex **14** (Fig. 4.6) suggest a similar structure to that proposed for compound **12**. The absence of $\nu(C=O)$ stretching band and the appearance of new band around 1591 cm^{-1}, assigned to –C=N–N=C– stretching vibration, indicates that the ligand coordinates to Ni(II) ion *via* iminolization followed by deprotonation. The lowering of $\nu(C=N)$ on complexation may be attributed to a lowering of bond order as a result of coordination of ligand to metal ion via azomethine nitrogen which was indicative of the involvement of ring nitrogen of pyridine in chelation. The out-of-plane bending modes of vibrations of the free ligands are found to be shifted to higher energies in the spectra of complexes indicating the coordination *via* pyridine nitrogen.

4.3.4. Electronic spectral studies

The electronic spectral assignments of the complexes in DMF solutions are summarized in Table 4.2 and shown in Figs. 4.7 and 4.8. The absorption spectrum exhibits a charge transfer transition (CT) at 22000-29500 cm^{-1} region which may be assigned to the ligand-to-metal charge transfer from the coordinated unsaturated ligand to the metal ion. The absorption bands due to n$\rightarrow\pi^*$ and $\pi\rightarrow\pi^*$ transitions of free hydrazones suffered considerable shift upon complexation and the bands at ~ 36100 cm^{-1} can be assigned to shifted intraligand transitions. This is due to the weakening of the C=O bond and the extension of conjugation upon complexation [33].

Table 4.2. Electronic spectral assignments (cm^{-1}) of Ni(II) complexes

Compound	n$\rightarrow\pi^*$/$\pi\rightarrow\pi^*$	LMCT
[Ni(FPB)(NO$_3$)]·2H$_2$O (**9**)	34800	24610
[Ni(HFPB)(FPB)]Cl (**10**)	34380	24840, 23850 (sh)
[Ni(FPB)(OAc)(DMF)] (**11**)	34520	24800, 23940
[Ni(FPB)(ClO$_4$)]·DMF (**12**)	34620	24800
[Ni(FPB)$_2$] (**13**)	34660	24800, 23800
[Ni(FPN)(ClO$_4$)] (**14**)	36060	29210 (sh), 25340, 22410 (sh)

The electronic spectra of Ni(II) complexes of regular O_h symmetry have the following assignments for *d-d* bands: $^3T_{2g}(F)\leftarrow^3A_{2g}(F)$ (ν_1), $^3T_{1g}(F)\leftarrow^3A_{2g}(F)$ (ν_2) and $^3T_{1g}(P)\leftarrow^3A_{2g}(F)$ (ν_3) [34,35], but unfortunately these *d-d* bands are masked by the stronger CT absorption bands in these complexes and hence we did not observe any d-d bands for such transitions. In Ni(II) complexes with tetrahedral stereochemistry also three transitions

are expected ie. $^3T_2$(F)←$^3T_1$(F), $^3A_2$(F) ←$^3T_1$(F), $^3T_1$(P)←$^3T_1$(F); however we could not locate any of these bands, probably due to masking by the high-intensity charge transfer bands [36]. The electronic spectra of the complexes in DMF solution are not well resolved owing to very intense charge transfer bands extending into visible portion of spectra.
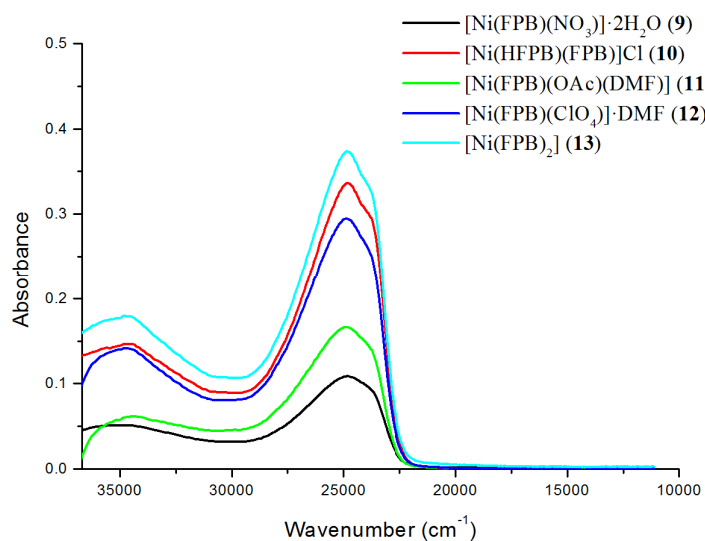
Fig. 4.7.   Electronic spectra of nickel(II) complexes.
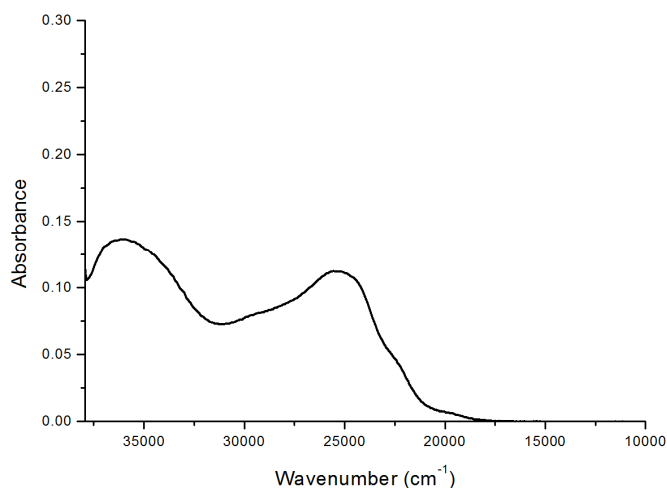
Fig. 4.8.   Electronic spectrum of [Ni(FPN)(ClO$_4$)] (14).

4.3.5. Thermogravimetric analyses

TG-DTG curve for the complex [Ni(FPB)(NO$_3$)]·2H$_2$O (**9**) (Fig. 4.9) shows a three step weight loss. At 150-230 °C, a weight loss of 25.93% (Calcd. 24.57%) occurs due to loss of two lattice water and nitrate ion. The weight loss of 36.105% (Calcd. 36.25%) at 410 °C is due to loss of C$_6$H$_4$FN fragment of the aroylhydrazone moiety. After 410 °C, compound decomposes continuously and yields NiO as final product [37].
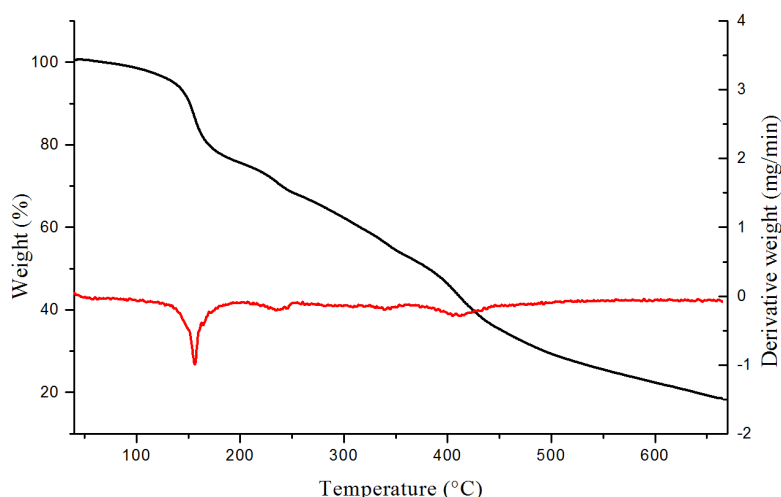
Fig. 4.9.   Thermogram of [Ni(FPB)(NO$_3$)]·2H$_2$O (9).

4.3.6. X-ray crystallography

Single crystals of compound **13** of X-ray diffraction quality were grown from its DMF solution by slow evaporation at room temperature in air. Single crystals of suitable dimensions of the complex **13** were selected and mounted on a Bruker SMART APEXII CCD diffractometer with graphite-monochromated MoKα (λ = 0.71073 Å) radiation at the

Sophisticated Analytical Instruments Facility (SAIF), Cochin University of Science and Technology, Kochi-22, Kerala, India. The crystallographic data and structure refinement parameters are given in Table 4.3. Bruker SMART software was used for data acquisition and Bruker SAINT software for data integration [38]. Absorption corrections were carried out using SADABS based on Laue symmetry using equivalent reflections [38]. The cell refinement was done using APEX2 and SAINT [38]. The data was reduced using SAINT and XPREP [38]. The structure was solved by direct methods using SHELXS97 [39] and refined by full-matrix least-squares refinement on F^2 using SHELXL97 [40]. The molecular and crystal structures were plotted using molecular graphics like ORTEP-3 for Windows [41] and DIAMOND version 3.2g [42].

In [Ni(FPB)$_2$] (**13**), all the non-hydrogen atoms were refined anisotropically and the hydrogen atom attached to the carbon atom were placed in geometrically idealized positions and constrained to ride on their parent atoms, with C–H distances of 0.93 Å, and with isotropic displacement parameters 1.2 times that of the parent carbon atoms. Crystal data and structural refinement for the complex **13** is tabulated in the Table 4.3.

Table 4.3. Crystal data and structure refinement parameters for [Ni(FPB)$_2$] (13)

Parameters	[Ni(FPB)$_2$] (13)
Empirical formula	C$_{26}$H$_{18}$F$_2$N$_6$O$_2$Ni
Formula weight	543.15
Temperature	293(2) K
Wavelength	0.71073 Å
Crystal system	Monoclinic
Space group	*P*2$_1$/c
Unit cell dimensions	
	a = 11.8775(8) Å α = 90°
	b = 8.6363(6) Å β = 90.230(3)°
	c = 22.8725(17) Å γ = 90°
Volume (Å^3)	2346.2(3)
Z	4
Density (calculated) mgm^{-3}	1.538
Absorption coefficient (mm^{-1})	0.881
F(000)	1112
Crystal size	0.30 x 0.25 x 0.20 mm^3
θ range for data collection	2.92 to 28.00°
Limiting indices	-15≤h≤15, -7≤k≤11, -30≤l≤30
Reflections collected / unique	16698 / 5673 [R(int) = 0.0340]
Completeness to θ	28.00 99.6%
Absorption correction	Semi-empirical from equivalents
Max. and min. transmission	0.825 and 0.755
Refinement method	Full-matrix least-squares on F^2
Data / restraints / parameters	5651 / 0 / 334
Goodness-of-fit on F^2	0.993
Final R indices [I>2σ(I)]	R$_1$ = 0.0441, wR$_2$= 0.0981
R indices (all data)	R$_1$= 0.0681, wR$_2$= 0.1107
Largest diff. peak and hole	0.325 and -0.309 e.A^{-3}

$R_1 = \Sigma||F_o| - |F_c|| / \Sigma|F_o|$ $wR_2 = [\Sigma w(F_o^2 - F_c^2)^2 / \Sigma w(F_o^2)^2]^{1/2}$

4.3.6.1. Crystal structure of [Ni(FPB)$_2$] (13)

Single crystals of the complex [Ni(FPB)$_2$] (13) suitable for X-ray analysis were obtained by recrystallization of compound from dimethylformamide. The molecular structure of compound 13 along with atom numbering scheme is given in Fig. 4.10 and selected bond lengths and bond angles are summarized in Table 4.4. The ligands with their donor atoms are arranged around the nickel ion in a meridional fashion. The complex crystallizes with one monomer per asymmetric unit into a monoclinic space group $P2_1$/c with Z = 4. In complex 13, Ni(II) is in a distorted octahedral N$_4$O$_2$ coordination environment, with each of the two ligands coordinating through the pyridine nitrogen, imino-hydrazone nitrogen and the deprotonated oxygen of the hydrazone moiety [43].
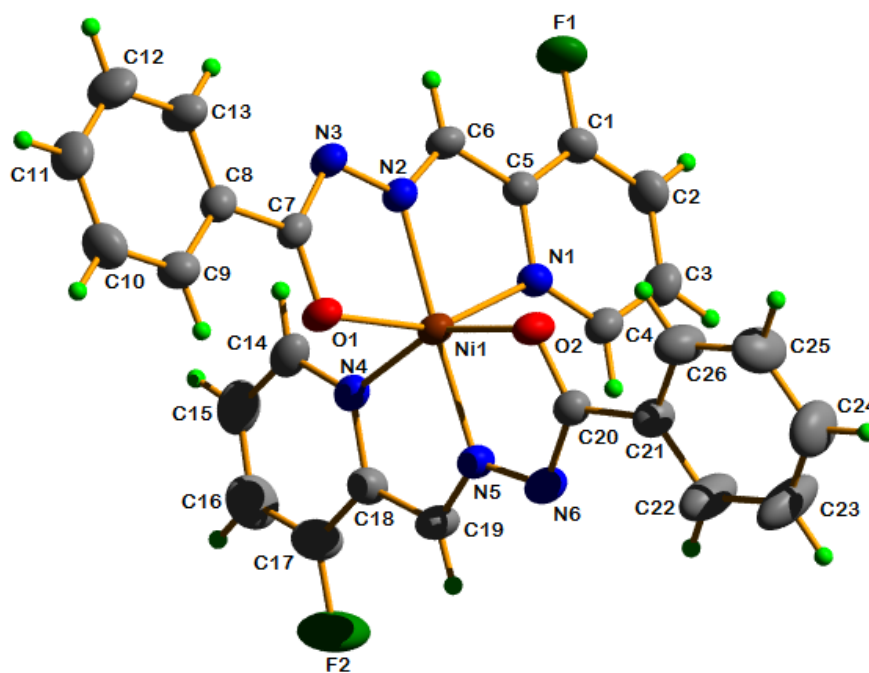

Fig. 4.10. Molecular structure of [Ni(FPB)$_2$] (13).

Table 4.4. Selected bond lengths (Å) and bond angles (°) for [Ni(FPB)₂] (13)

Bond lengths (Å)			Bond angles (°)	
	HFPB·H₂O	[Ni(FPB)₂] (13)		
C(6)–N(2)	1.2721 (18)	1.283(3)	N(5)–Ni(1)–N(2)	177.27(9)
C(19)–N(5)		1.283(3)	O(2)–Ni(1)–N(4)	154.50(8)
N(2)–N(3)	1.3736 (16)	1.362(3)	O(1)–Ni(1)–N(1)	154.46(8)
N(5)–N(6)		1.360(3)	N(5)–Ni(1)–O(1)	106.55(8)
C(7)–N(3)	1.3582 (18)	1.345(3)	N(2)–Ni(1)–O(1)	103.67(8)
C(20)–N(6)		1.349(3)	N(2)–Ni(1)–N(4)	101.82(8)
C(7)–O(1)	1.2258 (17)	1.266(3)	N(5)–Ni(1)–N(1)	98.99(9)
C(20)–O(2)		1.266(3)	O(2)–Ni(1)–O(1)	94.06(8)
N(1)–Ni(1)		2.128(2)	O(1)–Ni(1)–N(4)	92.57(8)
N(2)–Ni(1)		1.992(2)	N(1)–Ni(1)–N(4)	92.41(8)
N(4)–Ni(1)		2.139(2)	O(2)–Ni(1)–N(1)	92.14(8)
N(5)–Ni(1)		1.989(2)	N(2)–Ni(1)–N(1)	78.28(9)
O(1)–Ni(1)		2.0925(19)	N(5)–Ni(1)–N(4)	78.06(8)
O(2)–Ni(1)		2.0698(19)	N(5)–Ni(1)–O(2)	76.45(8)
			N(2)–Ni(1)–O(1)	76.18(8)

The C(6)–N(2) and C(7)–N(3) bond lengths are comparable to that for C=N bond length [44]. The *cis* angles, O1–Ni1–N4 (92.57(8)°) and O2–Ni1–N1 (92.41(8)°) and *trans* angles N5–Ni1–N2 (177.27(9)°), O2–Ni1–N4 (154.5(8)°) and O1–Ni1–N1 (154.46(8)°) indicating that complex has a large distortion from octahedral geometry. All the angles subtended at the Ni(II) ion by donor atoms show marked deviation from that expected for an ideal octahedral geometry. While O1, O2, N1 and N4 lie in the equatorial plane, N2 and N5 occupy the axial positions. The torsion angle of 178.7(2)° observed for C(5)–C(6)–N(2)–N(3) supports *E* configuration with respect to N(2)=C(6) bond (Table 4.5).

The Ni–N(py), Ni–N(imine) and Ni–O bond lengths observed here are within the range reported for other similar complexes of divalent metal ions [45] The Ni–N(azo) bond lengths are less compared to Ni–N(py) indicating the strength of former bond than the latter.   Coordination lengthens the hydrazone moiety's C(7)–O(1) bond length by 0.0402 Å and shortens the C(7)–N(3) bond by 0.0132 Å, suggesting a deprotonation after iminolization.

Table 4.5. Selected torsion angles [°] for [Ni(FPB)₂] (13).

Torsion angles	
	[Ni(FPB)₂] **(13)**
N1–C5–C6–N2	-1.2(4)
C1–C5–C6–N2	179.8(3)
N4–C18–C19–N5	0.8(4)
C17–C18–C19–N5	-178.8(3)
N3–N2–C6–C5	178.7(2)
C18–C19–N5–N6	-176.8(3)
C6–N2–N3–C7	179.9(2)
C19–N5–N6–C20	180.0(3)
N2–N3–C7–C8	177.8(2)
C21–C20–N6–N5	-175.0(2)
N2–N3–C7–O1	-2.0(4)
O2–C20–N6–N5	3.7(4)

Non-classical hydrogen bonding interactions and other non-covalent interactions like $\pi \cdots \pi$, C–H$\cdots \pi$ and C–F$\cdots \pi$ interactions were present in the compound and is shown in Table 4.6.

Table 4.6. Interaction parameters present in [Ni(FPB)$_2$] (13)

Hydrogen bonding interactions				
D–H···A	**D–H (Å)**	**H···A (Å)**	**D···A (Å)**	**∠D–H···A (°)**
C(10)–H(10)···O(2)[a]	0.93	2.47	3.271(4)	145
C(15)–H(15)···N(3)[b]	0.93	2.55	3.455(4)	163
C(25)–H(25)···F(2)[c]	0.93	2.53	3.296(4)	140
π···π interactions				
Cg(I)···Cg(J)	**Cg···Cg (Å)**	**α (°)**	**β (°)**	**γ (°)**
Cg(5)···Cg(7)[d]	3.7048(17)	3.18(14)	23.47	26.49
Cg(7)···Cg(5)[a]	3.7047(17)	3.18(14)	26.49	23.47
C–H···π interactions				
C–H···Cg	**H···Cg (Å)**	**C–H···Cg (°)**	**C···Cg (Å)**	
C(3)–H(3)···Cg(6)[d]	2.99	152	3.834(3)	
C–F···π interactions				
C–F···Cg	**F···Cg (Å)**	**C–F···Cg (°)**	**C···Cg (Å)**	
C(1)–F(1)···Cg(5)[e]	3.313(2)	99.72(15)	3.783(3)	
C(1)–F(1)···Cg(7)[d]	3.666(2)	69.19(14)	3.427(3)	
C(17)–F(2)···Cg(2)[f]	3.317(3)	98.7(2)	3.758(4)	

Symmetry code: a = x,-1+y,z; b = 1-x,-y,-z; c = x,1/2-y,1/2+z; d = x,1+y,z; e = 1-x,1-y,-z; f = 2-x,-y,-z

D = Donor, A = acceptor, Cg = Centroid

Cg(2) = Ni(1), O(2), C(20), N(6), N(5)

Cg(5) = N(1), C(4), C(3), C(2), C(1), C(5)

Cg(6) = N(4), C(14), C(15), C(16), C(17), C(18)

Cg(7) = C(8), C(9), C(10), C(11), C(12), C(13)

α(°) = Dihedral Angle between planes I and J

β(°) = Angle between Cg(I)···Cg(J) and Cg(J) perp

γ(°) = Angle between Cg(I)···Cg(J) vector and Cg(I) perp

In this complex, no classical hydrogen bonds were present. Non-coventional hydrogen bonding interactions play a significant role in the crystal packing. The C–H···N hydrogen bonding interactions connects two complex units along *b* axis (Fig. 4.11).
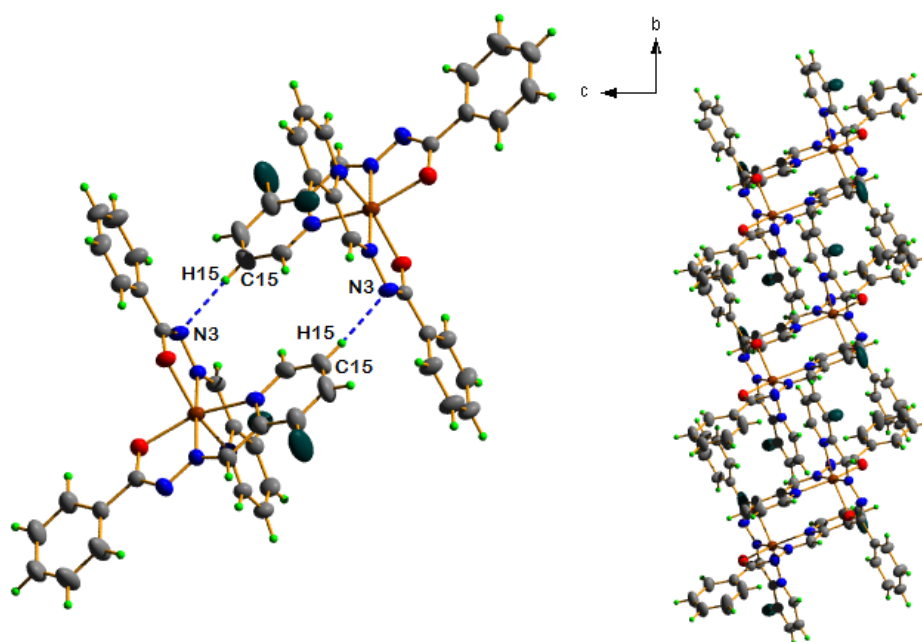
Fig. 4.11. C–H···N hydrogen bonding interactions in the complex along *b* axis.

The remaining intermolecular hydrogen bonding interactions connects the complex entities to form three dimensional supramolecular structures. The weak intermolecular hydrogen bonding interactions such as C–H···O (Fig. 4.12) and C–H···F (Fig. 4.13) connects each other which propagate like a chain along *b* axis.
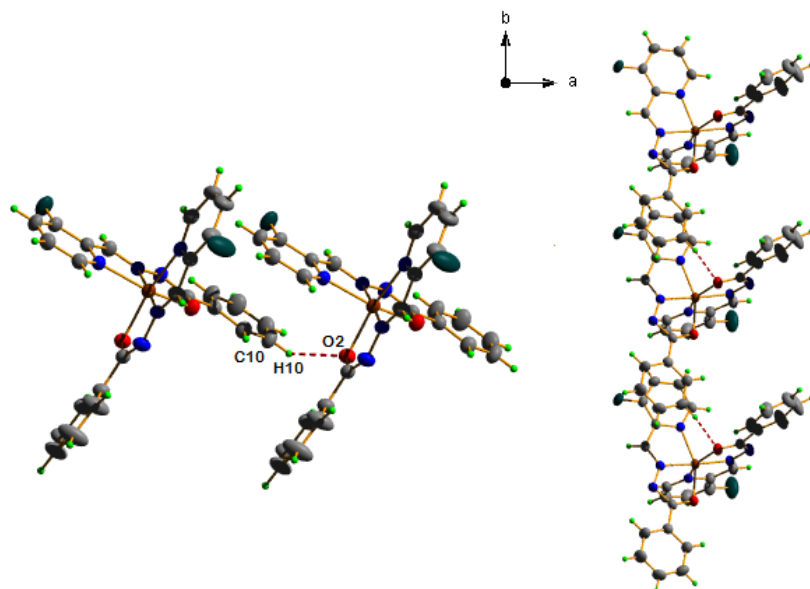
Fig. 4.12. C–H···O hydrogen bonding interactions connecting adjacent molecules and propagating along *b* axis.
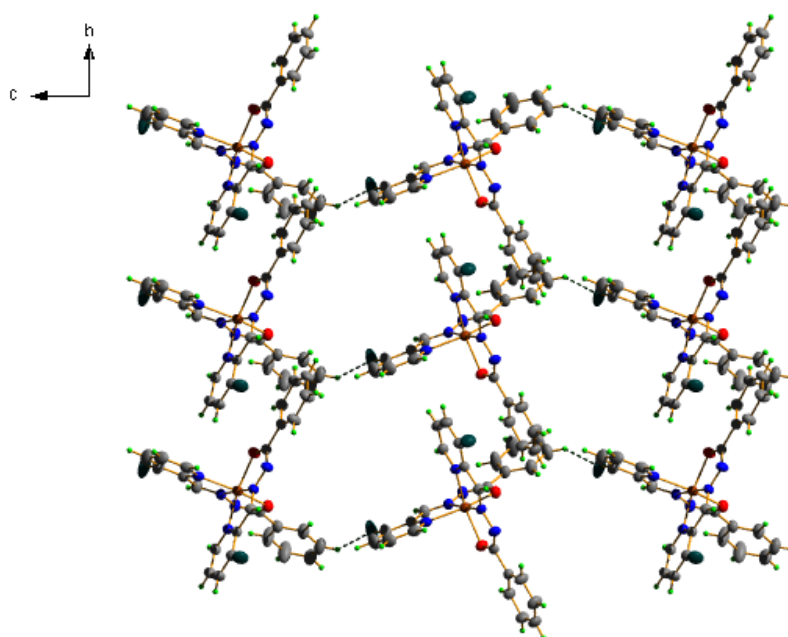
Fig. 4.13. C–H···F hydrogen bonding interactions connecting adjacent molecules and propagate along *b* axis.

The unit cell is viewed along the *a* axis along with weak intermolecular hydrogen bonding interactions is shown in Fig. 4.14.
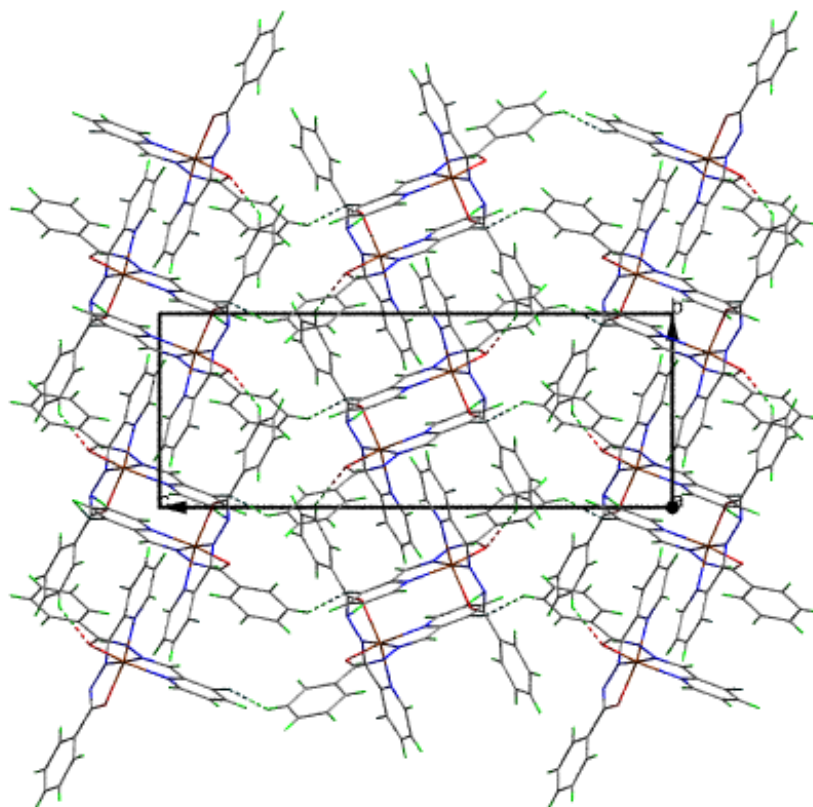
Fig. 4.14. Packing diagram of the complex in unit cell viewed along *a* axis.

The packing of the molecules is also stabilized by other weak non-conventional interactions like C–H···π, C–F···π and π···π interactions. These interactions are given in Table 4.6. The centroid Cg(5) is involved in π···π interaction with Cg(7) of the neighboring unit at a distance of 3.7048(17) Å (Fig. 4.15).
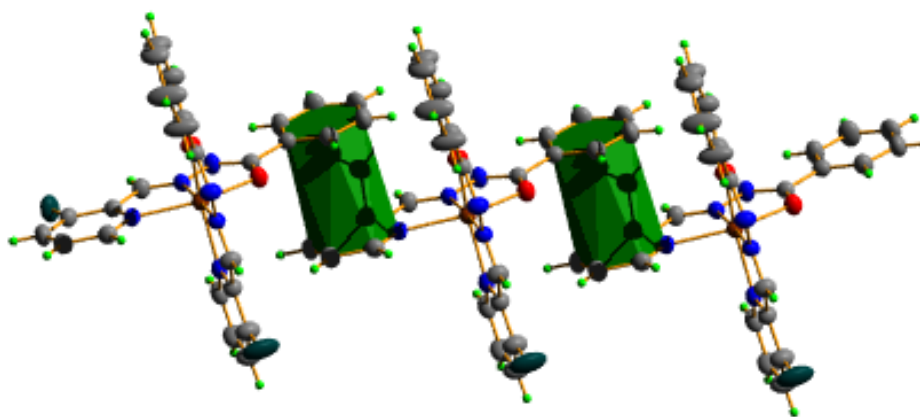
Fig. 4.15. The π···π interactions in complex 13.

In addition to the weak π···π stacking, significant C–F···π (Fig. 4.16 and 4.17) and C–H···π (Fig. 4.18) contributes to the stability of the unit cell packing.
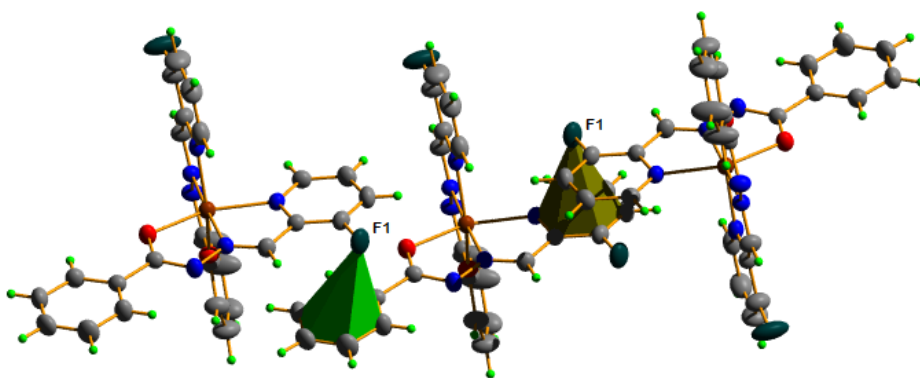
Fig. 4.16. C–F···π interactions in complex 13.
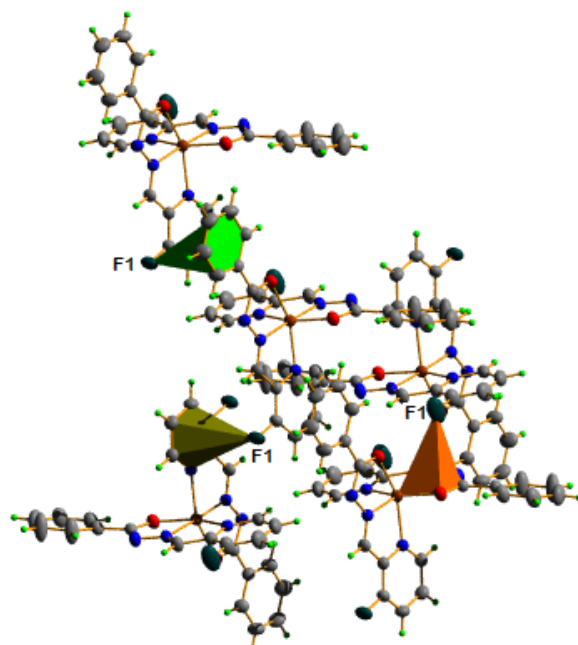
Fig. 4.17. C–F···π interactions present in complex 13.
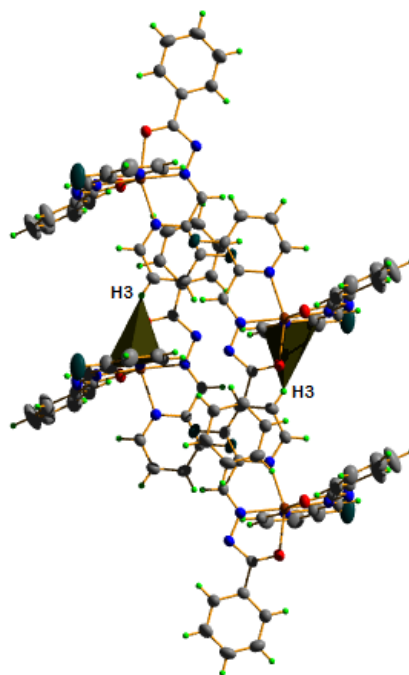
Fig. 4.18. C–H···π interactions present in complex 13.

Based on the elemental analyses and spectral studies, following tentative structures were assigned to the nickel(II) complexes.
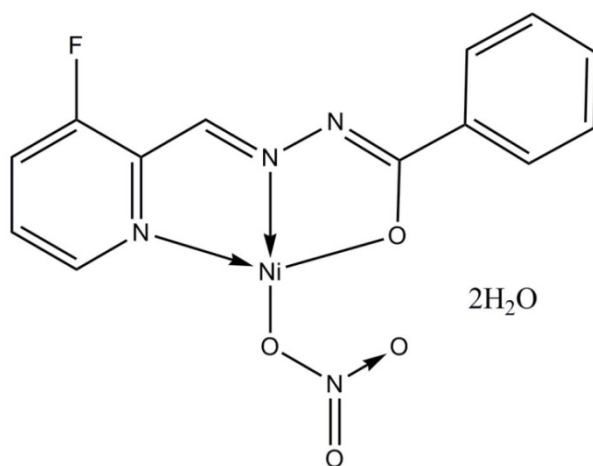
[Ni(FPB)(NO₃)]·2H₂O (9)

[Ni(HFPB)(FPB)]Cl (10)

[Ni(FPB)(OAc)(DMF)] (11)

[Ni(FPB)(ClO₄)]·DMF (12)

[Ni(FPN)(ClO₄)] (14)
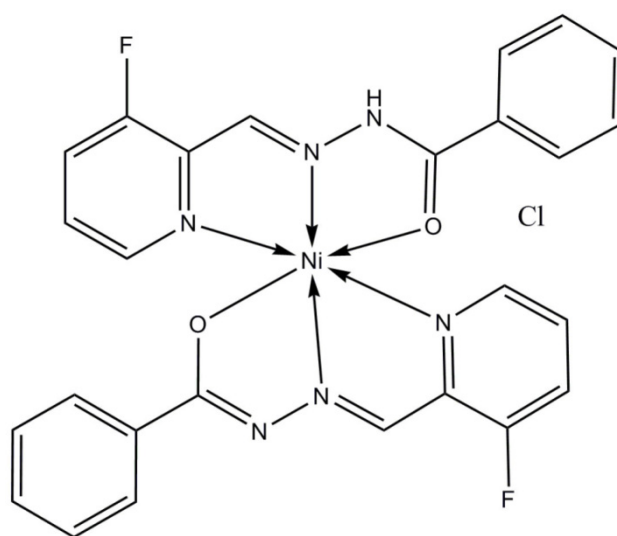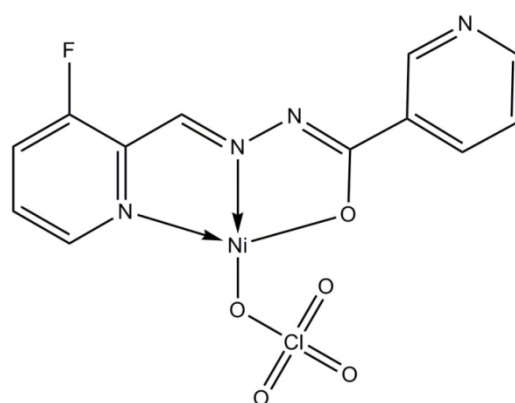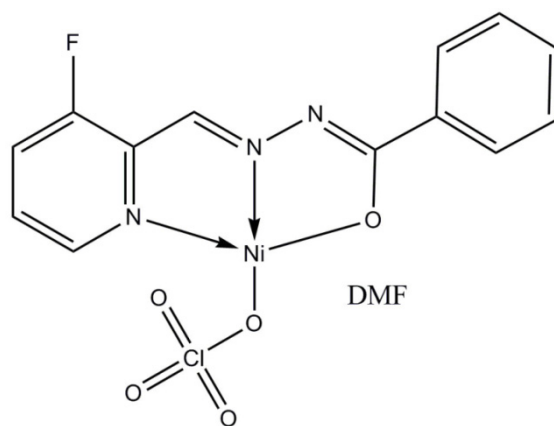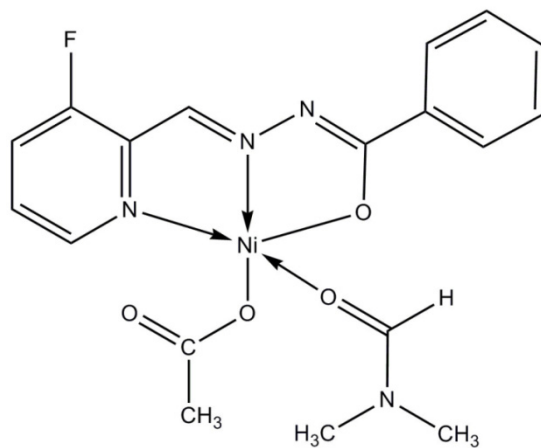
References

[1] R.K. Thauer, G. Diekert, P. Schönheit, Trends in Biochemical Sciences 5 (1980) 304.

[2] J. Adhikary, P. Kundu, S. Dasgupta, S. Mukherjee, S. Chattopadhyay, G. Aullón, D. Das, Polyhedron 101 (2015) 93.

[3] M.T.H. Tarafder, N. Saravanan, K.A. Crouse, A.M. Ali, Transit. Metal Chem. 26 (2001) 613.

[4] M.V. Angelusiu, S.-F. Barbuceanu, C. Draghici, G.L. Almajan, Eur. J. Med. Chem. 45 (2010) 2055.

[5] P. Krishnamoorthy, P. Sathyadevi, R.R. Butorac, A.H. Cowley, N.S.P. Bhuvanesh, N. Dharmaraj, Dalton Trans. 41 (2012) 6842.

[6] P. Sathyadevi, P. Krishnamoorthy, M. Alagesan, K. Thanigaimani, P.T. Muthiah, N. Dharmaraj, Polyhedron 31 (2012) 294.

[7] P. Sathyadevi, P. Krishnamoorthy, R.R. Butorac, A.H. Cowley, N.S.P. Bhuvanesh, N. Dharmaraj, Dalton Trans. 40 (2011) 9690.

[8] J. Devi, N. Batra, R. Malhotra, Spectrochim. Acta 97A (2012) 397.

[9] K.J. Davis, C. Richardson, J.L. Beck, B.M. Knowles, A. Guédin, J.-L. Mergny, A.C. Willis, S.F. Ralph, Dalton Trans. 44 (2015) 3136.

[10] G.S. Kurdekar, S.M. Puttanagouda, N.V. Kulkarni, S. Budagumpi, V.K. Revankar, Med. Chem. Res. 20 (2011) 421.

[11] S. Mondal, C. Das, B. Ghosh, B. Pakhira, A.J. Blake, M.G.B. Drew, S.K. Chattopadhyay, Polyhedron 80 (2014) 272.

[12] M. Shakir, S. Khanam, M. Azam, M. Aatif, F. Firdaus, J. Coord. Chem. 64 (2011) 3158.

[13] S. Sumathi, P. Tharmaraj, C.D. Sheela, R. Ebenezer, J. Coord. Chem. 64 (2011) 1707.

[14] C.-G. Liu, Y.-Q. Qiu, S.-L. Sun, N. Li, G.-C. Yang, Z.-M. Su, Chem. Phys. Lett. 443 (2007) 163.

[15] R. Shanmuga kala, P Tharmaraj, C.D. Sheela, Synth. React. Inorg. Met.-Org. Nano-Met. Chem. 44 (2014) 1487.

[16] D.P. Singh, B.K. Allam, K.N. Singh, V.P. Singh, RSC Adv. 4 (2014) 1155.

[17] K. Tiwari, M. Mishra, V.P. Singh, RSC Adv. 3 (2013) 12124.

[18] M. Mishra, K. Tiwari, A.K. Singh, V.P. Singh, Inorg. Chim. Acta 425 (2015) 36.

[19] W.J. Geary, Coord. Chem. Rev. 7 (1971) 81.

[20] J.R. Anacona, V. Marquez, Transit. Met. Chem. 33 (2008) 579.

[21] M.P. Teotia, J.N. Gurtu, V.B. Rana, J. Inorg. Nucl. Chem. 42 (1980) 821.

[22] K.M. Ibrahim, M.M. Bekheit, G.M. Abu El Reash, M.M. Mostafa, Polyhedron 5 (1986) 1635.

[23] A. Cukurovali, İ. Yilmaz, S. Kirbag, Transit. Met. Chem. 31 (2006) 207.

[24] F.A. Cotton, O.D. Faut, D.M.L. Goodgame, J. Am. Chem. Soc. 83 (1961) 344.

[25] N. Nawar, N.M. Hosny, Chem. Pharm. Bull. 47 (1999) 944.

[26] V. Stefov, V.M. Petruševski, B. Šoptajanov, J. Mol. Struct. 293 (1993) 97.

[27] S.K. Jain, B.S. Garg, Y.K. Bhoon, Transit. Met. Chem. 11 (1986) 89.

[28] M. Joseph, A. Sreekanth, V. Suni, M.R.P. Kurup, Spectrochim. Acta 64A (2006) 637.

[29] V.T. Yilmaz, S. Hamamcia, O. Andaca, K. Guven, Z. Anorg. Allg. Chem. 629 (2003) 172.

[30] K. Nakamoto, Infrared and Raman Spectra of Inorganic and Coordination compounds, Part B, 5th Edn. Wiley, New York, 1997.

[31]   P.F. Raphael, E. Manoj, M.R.P. Kurup, Pilyhedron 26 (2007) 5088.

[32]   A. Ray, S. Banerjee, R.J. Butcher, C. Desplanches, S. Mitra, Polyhedron 27 (2008) 2409.

[33]   T.A. Reena, M.R.P. Kurup, Spectrochim. Acta 76A (2010) 322.

[34]   N. Chitrapriya, V. Mahalingam, M. Zeller, K. Natarajan, Inorg. Chim. Acta 363 (2010) 3685.

[35]   M. Calinescu, E. Ion, A.M. Stadler, Rev. Roum. Chim. 53 (2008) 903.

[36]   P. Mukherjee, M.G.B. Drew, C.J. Gomez-Garc, A. Ghosh, Inorg. Chem. 48 (2009) 5848.

[37]   P.K. Singh, D.N. Kumar, Spectrochim. Acta 64A (2006) 853.

[38]   Bruker, *APEX2, SAINT, XPREP and SADABS*, Bruker AXS Inc., Madison, Wisconsin, USA (2004).

[39]   G.M. Sheldrick, SHELXL97 and SHELXS97, University of Göttingen, Germany, 1997.

[40]   G.M. Sheldrick, Acta Cryst. A64 (2008) 112.

[41]   L.J. Farrugia, J. Appl. Cryst. 45 (2012) 849.

[42]   K. Brandenburg, Diamond Version 3.2g, Crystal Impact GbR, Bonn, Germany, (2010).

[43]   S. Naskar, S. Naskar, R.J. Butcher, S.K. Chattopadhyay, Inorg. Chim. Acta 363 (2010) 3641.

[44]   L. Latheef, M.R.P. Kurup, Spectrochim. Acta 70A (2008) 86.

[45]   A.S. Pedrares, N. Camina, J. Romero, M.L. Duran, J.A.G. Vazquez, Polyhedron 27 (2008) 3391.

.....ೞೞ.....

SYNTHESES, SPECTRAL CHARACTERIZATION AND CRYSTAL STRUCTURE OF COBALT(II) CHELATES OF TRIDENTATE AROYLHYDRAZONES

5.1. Introduction

The coordination chemistry was pioneered by Nobel Prize winner Alfred Werner and his studies on the metal-amine complexes such as [Co(NH$_3$)$_6$Cl$_3$] had brought him the Nobel Prize in Chemistry. The experiments by Werner and his associates on cobalt coordination compounds accomplished two things: they increased the chemical knowledge in this extensive area (more than 700 compounds) and helped Werner develop his ideas on coordination theory and stereochemistry. Since ancient times cobalt compounds have been used to produce blue glass and ceramics. The element was first isolated by Swedish chemist George Brandt in 1735. He showed, it was the presence of the element cobalt that caused the blue color in glass, not bismuth as previously thought. The word cobalt is derived from the German 'kobold', meaning *goblin* or

elf. Cobalt is a brittle, hard, silver-grey transition metal with magnetic properties similar to those of iron (ferromagnetic). Cobalt stays magnetic to the highest temperature of all the magnetic elements (it has a Curie point of 1121 ^{o}C). Radioactive ^{60}Co is used in the treatment of cancer. A growing use of cobalt-60 is in food irradiation. Cobalt is used in alloys for aircraft engine parts and in alloys with corrosion/wear resistant uses. It is also widely used in batteries and in electroplating. Cobalt is also used in samarium-cobalt permanent magnets. Cobalt compounds are important catalysts in a number of industrial processes. Cobalt molybdate ($CoMoO_4$) is used in the petroleum industry to convert crude oil to gasoline and other petroleum products. It is also used to remove sulfur from crude oil. Common oxidation states of cobalt include +2 and +3, although compounds with oxidation states ranging from -3 to +4 are also known.

Cobalt is required in small amounts for life and is the only metal found in vitamins, cobalt is the active center of coenzymes called cobalamins, the most common example of which is Vitamin B_{12}. Electronic properties of cobalt(II) complexes have received substantial attention due to the fact that many of these complexes bind oxygen reversibly and are model systems for vitamin B_{12}. Cobalt is a necessary trace element in mammals and has many uses in medicine, magnetic resonance imaging, and drug delivery. Cobalt ethylenediamine complexes are potent antimicrobial agents. Low-spin cobalt porphyrins are of interest since cobalt-substituted hemoglobin, "coboglobin," binds oxygen in a cooperative fashion. Cobalt(II) compounds have interesting

magnetochemistry, several examples of high-nuclear complexes with six-coordinate cobalt(II) behaving as single molecule magnets and single chain magnets have been reported [1-4]. It has been reported that some of the cobalt(II) complexes of Schiff bases show potent antibacterial activity against *Escherichia coli*, *Streptococcus pyogenes*, *Staphylococcus aureus*, *Salmonella typhi* and *Pseudomonas aeruginosa* and antifungal activity against *Aspergillus flavus*, *Aspergillus niger* and *Cladosporium*. Investigations on the interactions of DNA with transition metal complexes provide leads for rational drug design, as well as means for the development of sensitive chemical probes for DNA [5]. It has been reported that the cobalt(II) complexes of salicylaldehyde-2-phenylquinoline-4-carboylhydrazone interact with calf-thymus DNA *via* a groove binding mode [6].

Transition metal catalyzed reactions have had a large impact on the human progress for the last century. Several extremely important areas, such as the agricultural industry and the plastic industry, have benefited from this development. It is reported that binucleating complexes of cobalt with Schiff bases act as catalysts in the oligomerisation of ethylene [7]. In general, the cobalt(II) complexes have a very high activity for alkane oxidation reactions [8,9]. Nonlinear optics has received considerable attention due to its variety of applications in optoelectronic and photonic devices. A comparison between complexes of different metals with the same ligand indicated that the NLO response strongly depends upon the electronic configuration of the metal center [10]. The literature studies reveal that

many metal Schiff base complexes containing cobalt exhibit good second order NLO properties [10].

Heteroaroylhydrazones are an important group of multidentate ligands with potential binding sites available for a wide variety of metal ions. Aroylhydrazones and their metal complexes are very promising compounds and act as bidentate ligand coordinating to the metal through azomethine nitrogen and oxygen atom. Hydrazone Schiff bases and their cobalt complexes have a variety of applications in biological, clinical and analytical fields. There has been a considerable interest in the coordination chemistry of transition metals especially cobalt with NNO donor hydrazone ligands because of their potential biological and pharmacological applications, several of these molecules display significant biological activity [11,12]. In view of growing importance of aroylhydrazones and their cobalt complexes here we report six mononuclear cobalt(II) complexes of two NNO donor heteroaroylhydrazones. These complexes were characterized by various physicochemical techniques like elemental analysis, infrared and electronic spectra, molar conductivity and magnetic susceptibility measurements and single crystal XRD measurements.

5.2. Experimental

5.2.1. Materials

3-Fluoropyridine-2-carbaldehyde (Sigma-Aldrich), benzhydrazide (Sigma-Aldrich), nicotinic hydrazide (Sigma-Aldrich), cobalt (II) acetate tetrahydrate (Merck), cobalt(II) bromide (Aldrich) were of Analar grade

and were used as received. Solvents used were methanol, ethanol, DMF and DMSO.

5.2.2. Syntheses of aroylhydrazones

3-Fluoropyridine-2-carbaldehyde benzoylhydrazone monohydrate ($HFPB \cdot H_2O$) and 3-fluoropyridine-2-carbaldehyde nicotinoylhydrazone dihydrate ($HFPN \cdot 2H_2O$) were synthesized as discussed previously in Chapter 2.

5.2.3. Syntheses of Co(II) complexes

5.2.3.1. [Co(HFPB)₂]Br₂·2H₂O (15)

To the methanolic solution of $HFPB \cdot H_2O$ (0.2612 g, 1 mmol), cobalt(II) bromide (0.2180 g, 1 mmol) dissolved in methanol was added. The resulting dark brown color solution was stirred for 1 hour followed by refluxing for 3 hours. The solution was then allowed to stand at room temperature for cooling, dark brown shining crystals separated were filtered, washed with methanol followed by ether and dried over P_4O_{10} *in vacuo*.

[Co(HFPB)₂]Br₂·2H₂O (**15**): Yield: 65%, λ_m (DMF): 114 ohm^{-1} cm^2 mol^{-1}, μ_{eff} (B.M.): 5.9, Elemental Anal. Found (Calcd.) (%): C: 42.69 (42.13); H: 3.67 (3.26); N: 11.73 (11.34).

5.2.3.2. [Co(HFPB)(FPB)](OAc)·DMF (16)

A solution of $HFPB \cdot H_2O$ (0.2612 g, 1 mmol) in methanol was treated with a methanolic solution of cobalt(II) acetate tetrahydrate (0.2490 g, 1 mmol). The resulting solution was refluxed for 4 hours.

The solution was cooled at room temperature and after slow evaporation, brown colored product separated out was filtered, washed with methanol followed by ether and dried over P_4O_{10} *in vacuo.*

[Co(HFPB)(FPB)](OAc)·DMF (**16**): Yield: 67%, λ_m (DMF): 87 ohm^{-1} cm^2 mol^{-1}, μ_{eff} (B.M.): 5.79, Elemental Anal. Found (Calcd.) (%): C: 55.64 (55.04); H: 4.68 (4.32); N: 13.98 (14.49).

5.2.3.3. [Co(FPB)₂] (17)

A solution of HFPB·H_2O (0.2612 g, 1 mmol) in methanol was treated with a methanolic solution of cobalt(II) acetate tetrahydrate (0.1230 g, 0.5 mmol). The resulting solution was then refluxed for 4 hours. The solution was cooled at room temperature and after slow evaporation, brown colored product separated out was filtered, washed with methanol followed by ether and dried over P_4O_{10} *in vacuo.*

[Co(FPB)₂] (**17**): Yield: 71%, λ_m (DMF): 6 ohm^{-1} cm^2 mol^{-1}, μ_{eff} (B.M.): 5.73, Elemental Anal. Found (Calcd.) (%): C: 56.85 (57.47); H: 3.06 (3.34); N: 15.95 (15.47).

5.2.3.4. [Co(HFPN)Br₂] (18)

To the methanolic solution of HFPN·$2H_2O$ (0.2802 g, 1 mmol), cobalt(II) bromide (0.2180 g, 1 mmol) dissolved in methanol was added. The resulting dark brown color solution was stirred for 1 hour followed by refluxing for 3 hours. After cooling the reaction mixture to ambient temperature, dark brown shining crystals separated were filtered, washed with methanol followed by ether and dried over P_4O_{10} *in vacuo.*

[Co(HFPN)Br$_2$] (**18**): Yield: 68%, λ_m (DMF): 14 ohm^{-1} cm^2 mol^{-1}, μ_{eff} (B.M.): 4.68, Elemental Anal. Found (Calcd.) (%): C: 31.62 (31.13); H: 2.66 (1.96); N: 12.49 (12.10).

5.2.3.5. [Co(FPN)$_2$] (19)

A solution of HFPN·2H$_2$O (0.2802 g, 1 mmol) in methanol was treated with a methanolic solution of cobalt(II) acetate tetrahydrate (0.1230 g, 0.5 mmol). The resulting solution was then refluxed for 4 hours. The solution was cooled at room temperature and after slow evaporation, brown colored product separated out was filtered, washed with methanol followed by ether and dried over P$_4$O$_{10}$ *in vacuo.*

[Co(FPN)$_2$] (**19**): Yield: 73%, λ_m (DMSO): 7 ohm^{-1} cm^2 mol^{-1}, μ_{eff} (B.M.): 5.82, Elemental Anal. Found (Calcd.) (%): C: 52.21 (52.86); H: 3.28 (2.96); N: 21.16 (20.55).

5.2.3.6 [Co(FPN)(OAc)] (20)

A solution of HFPN·2H$_2$O (0.2802 g, 1 mmol) in methanol was treated with a methanolic solution of cobalt(II) acetate tetrahydrate (0.2490 g, 1 mmol). The resulting solution was then refluxed for 3 hours. The solution was cooled at room temperature and after slow evaporation, brown colored product separated out was filtered, washed with methanol followed by ether and dried over P$_4$O$_{10}$ *in vacuo.*

[Co(FPN)(OAc)] (**20**): Yield: 72%, λ_m (DMSO): 5 ohm^{-1} cm^2 mol^{-1}, μ_{eff} (B.M.): 4.6, Elemental Anal. Found (Calcd.) (%): C: 47.16 (46.55); H: 3.44 (3.07); N: 16.13 (15.51).

5.3. Results and discussion

Reactions of equimolar ratios of corresponding ligands and metal salts yielded complexes under neutral conditions in which ligand to metal ratio is 1:1. However in few cases, reactions done by mixing the ligand and the corresponding metal salt in 2:1 ratio resulted in compounds of stoichiometry $[ML_2]$ or $[M(HL)_2]X_2$. Thus the monobasic ligands are deprotonated under neutral conditions itself coordinating through iminolic oxygen except in few cases, this may be due to peculiarity of the metal salt chosen and in such cases carbonyl oxygen may bind to the metal salt in the neutral amido form and the two anions of the metal salt satisfy the cobalt(II) valency. The stoichiometry of all the complexes was confirmed by elemental analysis. All the complexes prepared were dark brown in color. The complexes were quite stable and could be stored for several weeks without any appreciable change. The complexes are found to be readily soluble in coordinating solvents like DMF and DMSO but less soluble in solvents like ethanol, methanol and chloroform. X-ray quality single crystals of one of the complexes, $[Co(HFPB)_2]Br_2 \cdot 2H_2O$ (**15**) were obtained by recrystallization of the compound from DMF solution.

5.3.1. Elemental analyses

Quantitative elemental analysis of carbon, hydrogen and nitrogen were carried out in order to determine the elemental content of the synthesized compounds. The results were found to be in acceptable range compared with calculated values and are given in Section 5.2.3.

5.3.2. Molar conductivity and magnetic susceptibility measurements

The molar conductance of the solutions of complexes **17-20** in DMF/DMSO is in the range 5-20 ohm^{-1} cm^2 mol^{-1}. These observations suggest that these complexes are non-electrolytes. The conductance value of complex **15** is found to be 114 ohm^{-1} cm^2 mol^{-1} indicating that it is a 2:1 electrolyte. Complex **16** is a 1:1 electrolyte with molar conductance value of 87 ohm^{-1} cm^2 mol^{-1} [13].

The magnetic susceptibility which characterizes the extent of paramagnetism for metal complexes was measured in order to determine the spin properties of the complexes. The complex can either appear in the high spin state or low spin state. The measurement is crucial to identify the number of unpaired electrons and therefore to determine their geometric structure. Magnetic moments of tetrahedral Co(II) complexes are found in the range 4.2-4.7 B.M., while octahedral Co(II) complexes exhibit μ_{eff} in the range 4.8-5.6 B.M. because of large contribution from its ^4T_g ground term [14,15]. The observed magnetic moments for all the octahedral complexes were found to be in the range 5.7 - 6.1 B.M., which is slightly higher than that calculated by spin only formula and it may be due to orbital contribution [16]. The room temperature magnetic moment values of all other complexes are found to be in the range 4.3-5.2 B.M. and are within the range of tetrahedral or octahedral Co(II) complexes. High spin five-coordinate Co(II) complexes also show magnetic moment values in this range. Therefore no definite conclusion regarding the structure can be drawn on the basis of magnetic moment values alone [17].

5.3.3. Infrared spectral studies

The IR spectra of the hydrazones and their Co(II) complexes were recorded in the solid state as KBr discs. IR spectral analyses provide significant indications regarding the bonding sites of the ligands. The infrared frequencies in the free ligand associated with amide group (carbonyl-oxygen), azomethine-nitrogen (C=N), and heterocyclic nitrogen are expected to be influenced on complex formation with cobalt(II) [18]. A summary of the most important IR absorption bands corresponding to the ligand and the complexes, together with their proposed assignments, are given in the Table 5.1.

The ν(C=N) bands of the hydrazones are found to be shifted to higher frequencies in all the complexes, indicating the coordination *via* azomethine nitrogen. A medium band at 3050-3060 cm^{-1} region in the free ligands due to ν(N–H) vibration disappears in the spectra of complexes **16**, **17**, **19** and **20** providing strong evidence for ligand coordination around Co(II) ion in the deprotonated form. Moreover, in the IR spectra of these complexes, the hydrazidic C=O band disappears. In all the above complexes, another strong band is found at 1590-1605 cm^{-1} region which may be due to newly formed (C=N) bond formed as a result of iminolization. All these data clearly indicate that the tautomeric form of the ligand in the complexes is iminolic form. However for complexes **15** and **18**, ν(C=O) stretching vibration is retained but is shifted to a lower wave number suggesting that ligand is binding to the metal center in the neutral amido form. A positive shift corresponding to out-of-plane bending vibrations of free ligands to higher frequencies in

the complexes is confirmative of pyridine nitrogen coordination to the cobalt center [19].

Table 5.1. The important IR frequencies (cm^{-1}) of hydrazones and their Co(II) complexes

| Compound	ν(N–H)	ν(C=O)/ν(C–O)	ν(C=N)	ν(C=N)[a]
HFPB·H$_2$O	3059	1683	1597	--
[Co(HFPB)$_2$]Br$_2$·2H$_2$O (**15**)	--	1640	1587	--
[Co(HFPB)(FPB)](OAc)· DMF (**16**)	3040	1672, 1334	1548	1602
[Co(FPB)$_2$] (**17**)	--	1330	1541	1592
HFPN·2H$_2$O	3058	1682	1590	--
[Co(HFPN)Br$_2$] (**18**)	3056	1677	1553	--
[Co(FPN)$_2$] (**19**)	3024	1335	1552	1597
[Co(FPN)(OAc)] (**20**)		1385	1580	1590

[a]Newly formed C=N bond
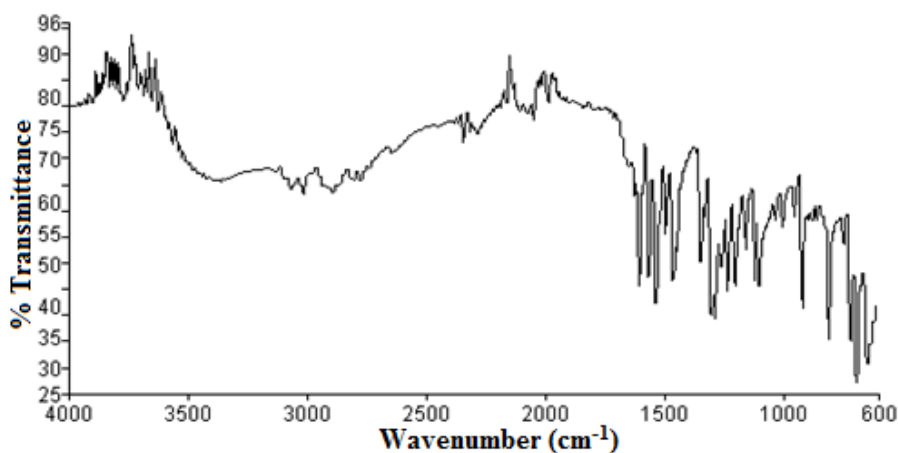
Fig. 5.1. IR spectrum of [Co(HFPB)$_2$]Br$_2$·2H$_2$O (15).

In complex **15** (Fig. 5.1), a broad band in the range 3450-3500 cm^{-1} and a medium band at 3070 cm^{-1} correspond to lattice water and N–H

vibration [20] respectively, this shows that ligand is not deprotonated and is coordinated in the neutral amido form and the Co(II) valency is satisfied by the two bromide ions of the metal salt. The crystal structure also supports these findings. However a negative shift of carbonyl moiety to 1640 cm^{-1} suggests its involvement in coordination. The band due to azomethine stretching vibration is shifted to a lower number suggesting the coordination through azomethine nitrogen but a band due to the formation of new C=N bond is absent in complex **15** as the ligand is coordinated in the neutral amido form. The low energy pyridine ring in-plane and out-of-plane vibrations are shifted to higher energies in the spectrum of complex indicating the coordination *via* pyridine nitrogen.
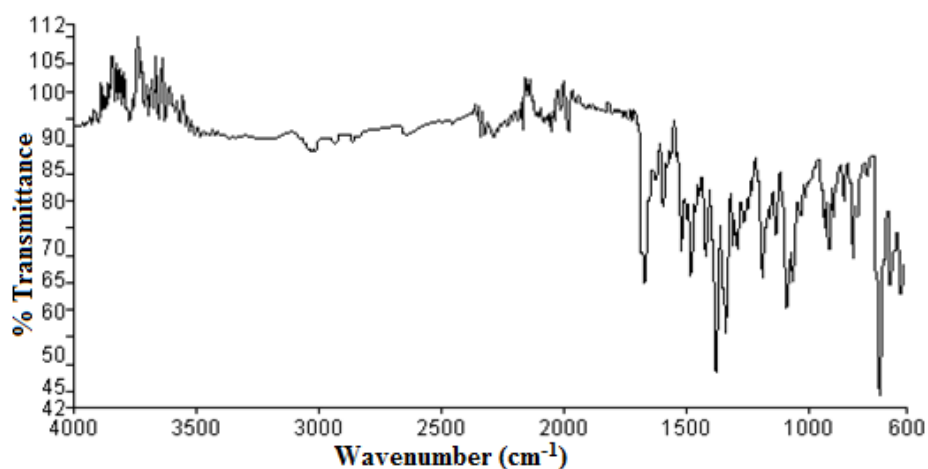
Fig. 5.2. IR spectrum of [Co(HFPB)(FPB)](OAc)·DMF (16).

In complex **16** (Fig. 5.2), elemental analyses suggested the presence of acetate ion, however conductivity measurements suggested that compound is nearly a 1:1 electrolyte which means that acetate ion outside the coordination sphere. This along with the observation that ν(C=O)

stretching vibration is only slightly shifted to a lower wave number confirm the fact that one of the coordinated ligands is not deprotonated. On the other hand, the band corresponding to azomethine stretching vibration is shifted to 1547 cm^{-1} in the IR spectrum of complex indicating the coordination of azomethine nitrogen to the central metal ion.   The presence of a new band at 1334 cm^{-1} corresponds to –C=N–C=N– moiety formed due to deprotonation of the ligand.   From this observation it appears that second ligand is coordinated in the iminolic form [21].
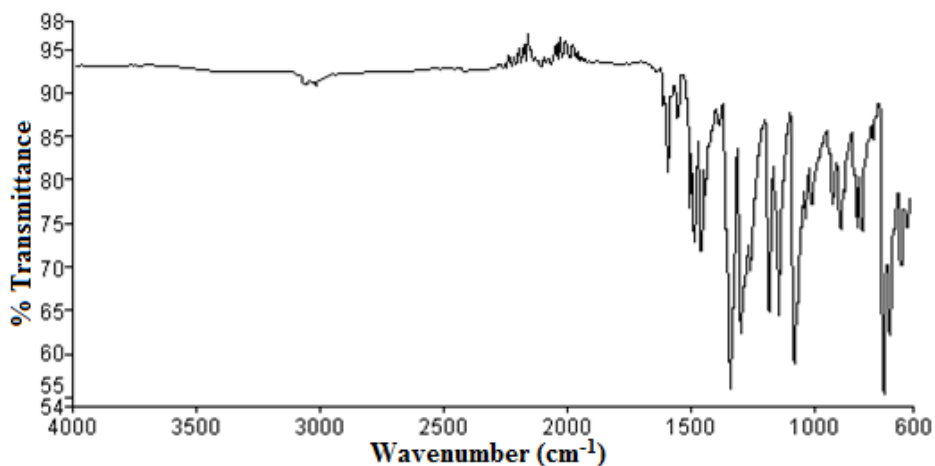
Fig. 5.3. IR spectrum of [Co(FPB)$_2$] (17).

The band at 1597 cm^{-1} due to the stretching mode of the –C=N– group in the spectrum of the free ligand shows a remarkable negative shift with splitting at 1541 cm^{-1} for complex **17** (Fig. 5.3) suggesting that the azomethine nitrogen atom is involved in the complex formation [21].   In the IR spectrum of complex **17**, the bands due to ν(C=O) and ν(N–H) stretching vibrations are absent and the presence of a new band at 1330 cm^{-1} assignable to ν(C–O) stretching vibration suggest that the frame –

NH–C=O is transformed to –N=C–OH form coordinating to metal ion in iminolate form [22]. Further the appearance of a new band at 1592 cm^{-1} due to newly formed ν(C=N) confirm the iminolization of the ligand during the complex formation. The pyridyl in-plane ring deformation and out-of-plane ring deformation are found at higher frequencies compared to that of the ligand, suggesting the coordination of the ligand *via* pyridyl nitrogen.
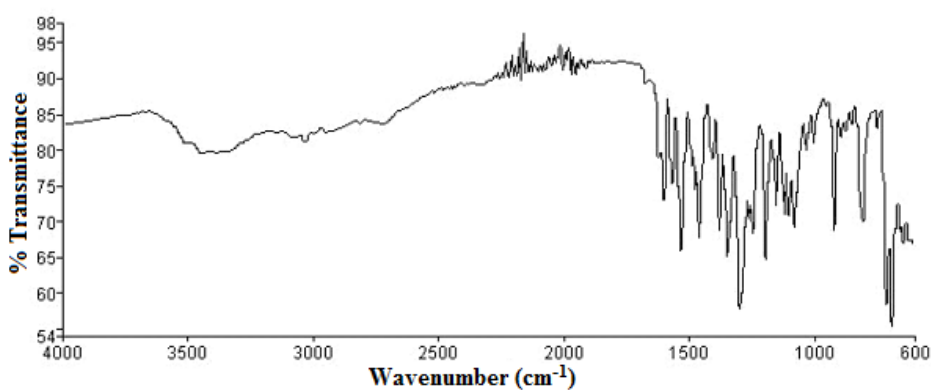
Fig. 5.4. IR spectrum of [Co(HFPN)Br$_2$] (18).

In the infrared spectrum of the complex **18** (Fig. 5.4), a considerable negative shift in ν(C=O) was observed indicating a decrease in the stretching force constant of –C=O as a consequence of coordination through the carbonyl oxygen atom of the ligand. Another important band in the free ligand is found at 1590 cm^{-1} attributed to ν(C=N) (azomethine) mode. In the spectrum of the complex **18**, this band is shifted to lower wave number and appears at 1553 cm^{-1} indicating the involvement of nitrogen atom of the azomethine group in coordination. The overall infrared spectral evidences suggest that the present ligand acts as a

tridentate ligand and coordinates through amide oxygen, azomethine nitrogen and pyridyl nitrogen atoms in the neutral amide form. The elemental analyses of complex **18** suggests the presence of two bromide ions, but the molar conductance values lie in the range 12 ohm^{-1} cm^{2} mol^{-1} indicating the non-electrolytic nature of the complex. This along with the observation that band due to the formation of a new C=N bond is absent in complex **18** confirm the proposed stoichiometry that the two bromide ions are inside the coordination sphere.
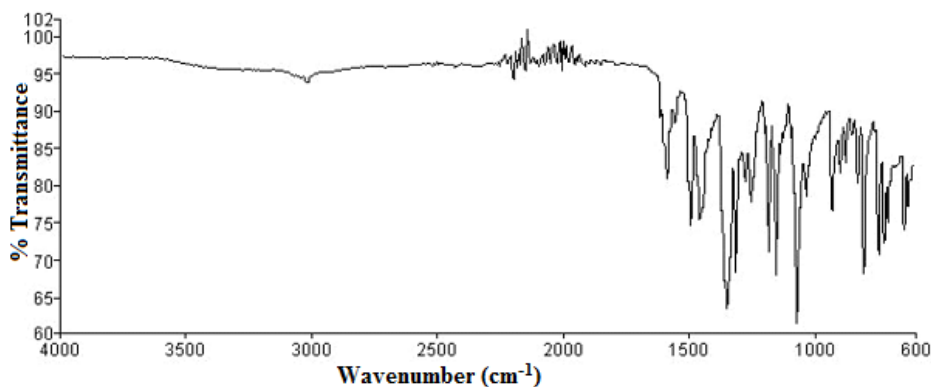
Fig. 5.5. IR spectrum of [Co(FPN)$_2$] (19).

The IR spectrum of complex **19** (Fig. 5.5) is very similar to that of complex **17** and it is found that carbonyl band disappears and azomethine band shifts to a lower wave number due to coordination. Further the appearance of a new band at 1355 cm^{-1} assignable to ν(C–O) band confirm the iminolization of the ligand, indicating the loss of proton upon complexation along with the formation of metal-oxygen bond. This finding was further supported by the appearance of a new band due to newly formed C=N bond at 1597 cm^{-1}. The low energy pyridine ring out-

of-plane vibrations observed in the spectrum of hydrazone is shifted to higher frequencies in the spectrum of complex suggesting the coordination through pyridine nitrogen.
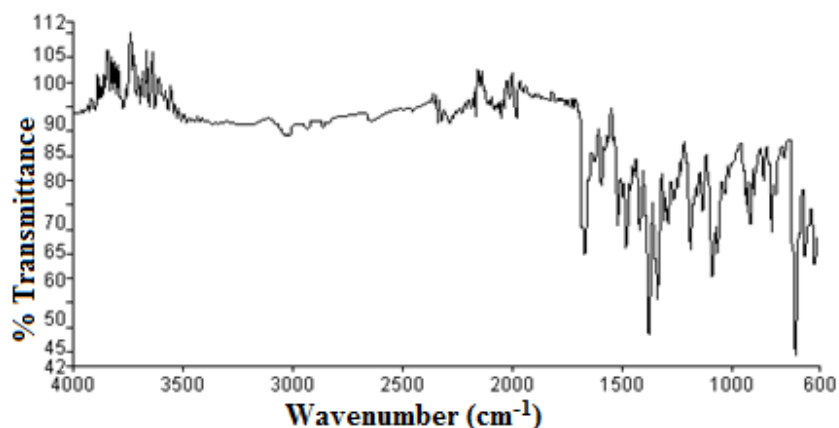

Fig. 5.6. IR spectrum of [Co(FPN)(OAc)] (20).

In complex **20** (Fig. 5.6), elemental analyses suggested the presence of acetate ion with a stoichiometry of [ML(OAc)]. IR spectral data support the coordination of hydrazone to the metal center through azomethine and pyridyl nitrogens and iminolate oxygen. The most interesting part of complex **20** is the region where strong absorption band due to acetate group is visible. The free acetate ion CH_3COO^- exhibits the $\nu_{as}(COO)$ and $\nu_s(COO)$ at 1578 and 1414 cm^{-1} respectively. It is reported that if it is covalently bonded to a metal as a unidentate ligand the ν_{as} and ν_s get shifted to higher and lower frequencies respectively. Further the complex displays a band at 1365 cm^{-1} which was seen in other complexes also, but when compared to the corresponding peak in other complexes, this was found to be significantly stronger. Thus it may be due to the symmetric stretching vibration of acetate ion [23].

5.3.4. Electronic spectral studies

The electronic spectra of cobalt(II) complexes of aroylhydrazones were recorded in DMF and DMSO solutions. The electronic absorption spectral data (cm^{-1}) of the cobalt(II) complexes are tabulated in Table 5.2 and shown in Figs. 5.7-5.10. In all the complexes, intraligand transitions like $n{\rightarrow}\pi^*$ and $\pi{\rightarrow}\pi^*$ transitions are found between 33000-45600 cm^{-1} and shifted as compared with aroylhydrazone due to complexation. The ligand to metal charge transfer transitions are observed in the 23000-28000 cm^{-1} region.

The terms arising for a Co^{2+} (d^7 system) are the ground state ^3F and the excited states ^3P, ^1G, ^1D, ^1S. The transitions from the ground state to the three singlet states (^1G, ^1D, ^1S) are spin forbidden and will be very weak and can be ignored. The two remaining states ^3F and ^3P can have spin permitted transitions. The F state split into $A_{2g}+T_{1g}+T_{2g}$ and P state is transformed into a T_{1g} state. Hence three peaks should appear in the spectrum corresponding to $^4T_{2g}(F){\leftarrow}^4T_{1g}(F)$, $^4A_{2g}(F){\leftarrow}^4T_{1g}(F)$ and $^4T_{1g}(P){\leftarrow}^4T_{1g}(F)$. There are two T_{1g} states and since they are of same symmetry, they interact with one another and this interelectronic repulsion is much more marked in d^7 T_d case. Due to this they may cross each other but it is impossible because states of same symmetry cannot cross each other. But this occurs in O_h case and thus $^4A_{2g}(F){\leftarrow}^4T_{2g}$ transition is very weak. The weak broad *d-d* band observed at 18630 cm^{-1} for complex [Co(FPB)$_2$] (**17**) can be assigned to $^4T_{1g}(P){\leftarrow}^4T_{1g}(F)$ transition [24]. The *d-d* bands were not observed in other complexes due to the masking of high intense charge transfer transitions [25,26].

Table 5.2. Electronic spectral assignments (cm^{-1}) of Co(II) complexes

Compound	n→π*/π→π*	LMCT	*d-d* transitions
[Co(HFPB)$_2$]Br$_2$·2H$_2$O (**15**)	36400, 32030	25070	--
[Co(HFPB)(FPB)](OAc)· DMF (**16**)	33680	24610, 25790(sh), 23330(sh)	--
[Co(FPB)$_2$] (**17**)	34700	25790	18630
[Co(HFPN)Br$_2$] (**18**)	34330	25790	--
[Co(FPN)$_2$] (**19**)	36770	26140	--
[Co(FPN)(OAc)] (**20**)	36440	25870	--
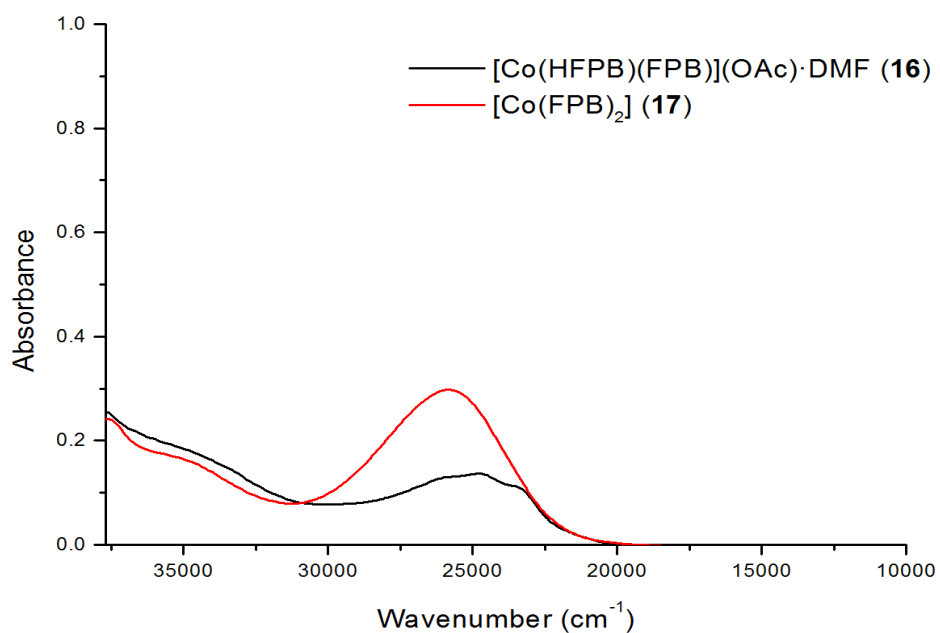
Fig. 5.7. Electronic spectra of complexes 16 and 17.
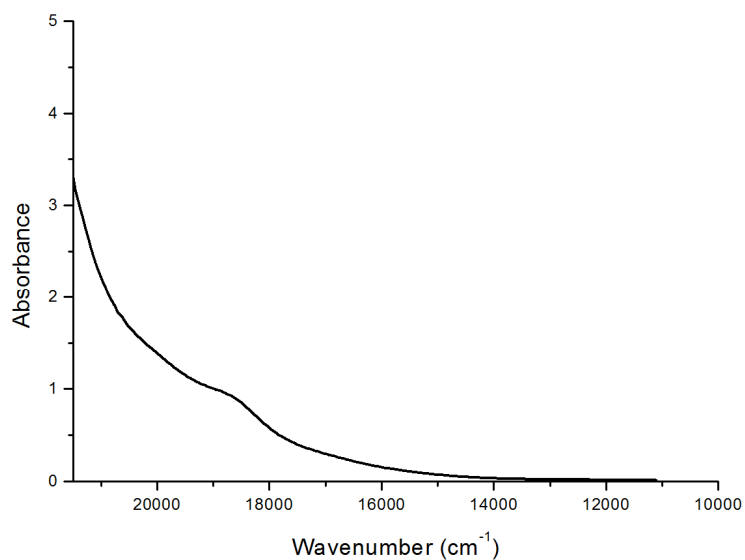
Fig. 5.8. Electronic spectrum of [Co(FPB)₂] (17) in the 20000-10000 cm⁻¹ region.
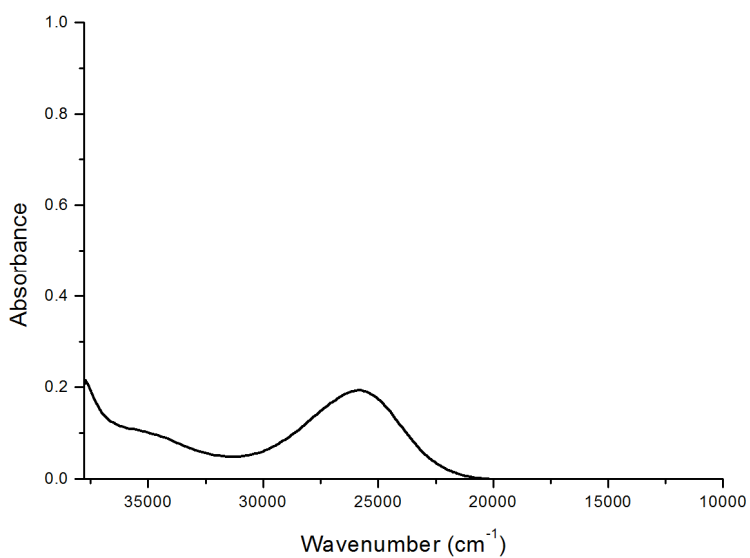
Fig. 5.9. Electronic spectrum of [Co(HFPN)Br₂] (18).
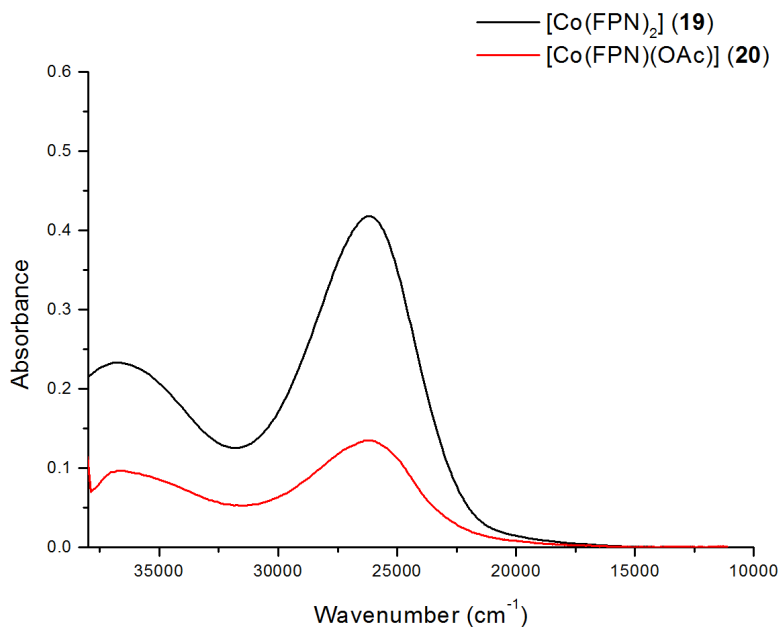
Fig. 5.10. Electronic spectra of complexes 19 and 20.

5.3.5. X-ray crystallography

Although the existence of chelate rings and the general features of the structure of metal chelates have been established by chemical methods of investigation, our knowledge of chelation was greatly strengthened by the confirmation of the correctness of their structures by X-ray crystal analysis. X-ray crystal analysis introduced a metrical element into the understanding of coordination by revealing the lengths and angles of chemical bonds and other structural details that could not be ascertained by other physical and chemical methods.

Single crystal X-ray diffraction studies of $[Co(HFPB)_2]Br_2 \cdot 2H_2O$ (**15**) were carried out at 293(2) K using a Bruker SMART APEXII CCD

diffractometer equipped with graphite monochromated Mo Kα (λ = 0.71073 Å) radiation at the Sophisticated Analytical Instrument Facility, Cochin University of Science and Technology, Kochi-22, Kerala, India. Bruker SMART software was used for data acquisition and Bruker SAINT software for data integration [27]. Absorption corrections were carried out using SADABS based on Laue symmetry using equivalent reflections [27]. The cell refinement was done using APEX2 and SAINT [27]. The data was reduced using SAINT and XPREP [27]. The structure was solved by direct methods using SHELXS97 [28] and refined by full-matrix least-squares refinement on F^2 using SHELXL97 [29]. The molecular and crystal structures were plotted using molecular graphics like ORTEP-3 for Windows [30] and DIAMOND version 3.2g [31].

In [Co(HFPB)$_2$]Br$_2$·2H$_2$O (**15**), all the non-hydrogen atoms were refined anisotropically and the hydrogen atom attached to the carbon atom were placed in geometrically idealized positions and constrained to ride on their parent atoms, with C–H distances of 0.93 Å, and with isotropic displacement parameters 1.2 times that of the parent carbon atoms. The hydrogen atom attached to the nitrogen atoms, N3 and N5 were located from difference maps and refined isotropically. Hydrogen atoms of the solvent water molecules could not be located from the difference Fourier map. Crystal data and structural refinement for the complex **15** is tabulated in the Table 5.3.

Table 5.3. Crystal data and structure refinement parameters for [Co(HFPB)₂] Br₂·2H₂O (15)

Parameters	[Co(HFPB)₂]Br₂·2H₂O (15)
Empirical formula	$C_{26}H_{20}N_6O_4Br_2F_2Co$
Formula weight	737.21
Crystal system	Monoclinic
Space group	$P2_1/c$
Unit cell dimensions	
	a = 12.4395(13) Å α = 90°
	b = 20.710(2) Å β = 93.675(6)°
	c = 10.8272(9) Å γ = 90°
Volume	2783.5(5) Å³
Z	4
Density (calculated) (mgm⁻³)	1.759
Absorption coefficient (mm⁻¹)	3.545
F(000)	1460
Crystal size	0.30 x 0.25 x 0.20 mm³
θ range for data collection	1.64 to 25.10°
Limiting indices	-14 ≤ h ≤ 13, -24 ≤ k ≤ 24, -12 ≤ l ≤ 12
Reflections collected / unique	17686 / 4949 [R(int) = 0.0405]
Completeness to θ	25.10 99.7%
Absorption correction	Semi-empirical from equivalents
Max. and min. transmission	0.4820 and 0.3490
Refinement method	Full-matrix least-squares on F²
Data / restraints / parameters	4932 / 0 / 371
Goodness-of-fit on F²	1.611
Final R indices [I>2σ(I)]	R₁= 0.1275, wR₂= 0.3693
R indices (all data)	R₁= 0.1604, wR₂= 0.3973
Extinction coefficient	0.012(3)
Largest diff. peak and hole	2.985 and -2.304 e.A⁻³

$R_1 = \Sigma||F_o| - |F_c||\,/\,\Sigma|F_o|$ $wR_2 = [\Sigma w(F_o^2 - F_c^2)^2\,/\,\Sigma w(F_o^2)^2]^{1/2}$

5.3.5.1. Crystal structure of [Co(HFPB)$_2$]Br$_2$·2H$_2$O (15)

Single crystals of the complex [Co(HFPB)$_2$]Br$_2$·2H$_2$O (**15**) suitable for X-ray analysis were obtained by recrystallization of compound from a mixture of methanol and dimethylformamide (1:1 *v/v*). The molecular structure along with atom numbering scheme for the [Co(HFPB)$_2$]Br$_2$·2H$_2$O (**15**) are depicted in Fig. 5.11. Selected bond lengths and bond angles for the complex are given in Table 5.4. Compound crystallizes in the monoclinic space group, *P*2$_1$/c with Z = 4. The asymmetric unit consists of only one molecule of Co(II) complex with two water molecules as solvate and two bromide ions as counter ions.
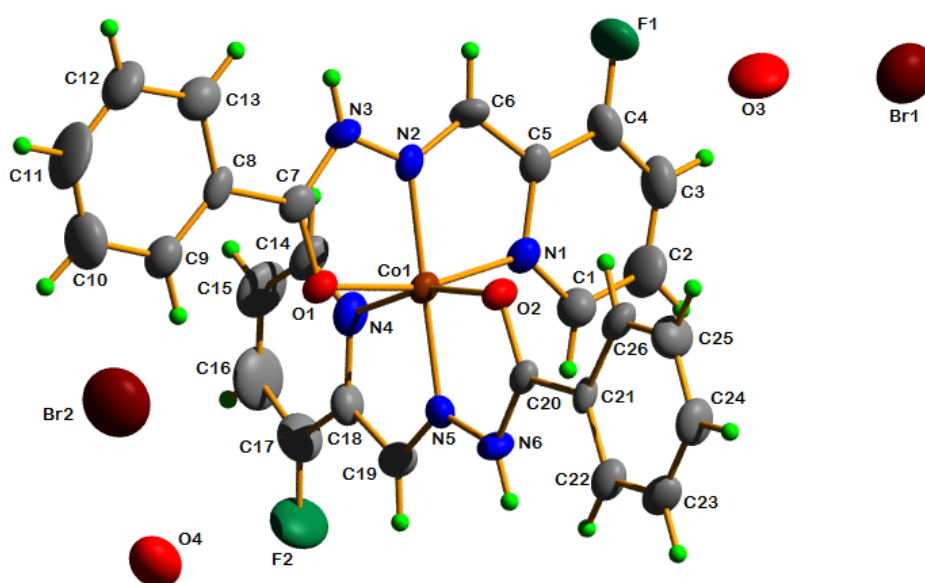
Fig. 5.11. Molecular structure of [Co(HFPB)$_2$]Br$_2$·2H$_2$O (15).

Table 5.4. Selected bond lengths (Å) and bond angles (°) for [Co(HFPB)$_2$] Br$_2$·2H$_2$O (15).

Bond lengths (Å)			Bond angles (°)	
	HFPB·H$_2$O	[Co(HFPB)$_2$]Br$_2$· 2H$_2$O (15)		
C(6)–N(2)	1.2721 (18)	1.289(12)	N(5)–Co(1)–N(2)	174.4(3)
C(19)–N(5)		1.293(12)	O(2)–Co(1)–N(4)	165.4(3)
N(2)–N(3)	1.3736 (16)	1.322(10)	O(1)–Co(1)–N(1)	165.1(3)
N(5)–N(6)		1.360(10)	N(2)–Co(1)–N(4)	101.0(3)
C(7)–N(3)	1.3582 (18)	1.330(11)	N(5)–Co(1)–N(1)	99.4(3)
C(20)–N(6)		1.319(11)	N(5)–Co(1)–O(1)	95.5(3)
C(7)–O(1)	1.2258 (17)	1.300(11)	N(2)–Co(1)–O(2)	93.6(3)
C(20)–O(2)		1.300(10)	O(2)–Co(1)–N(1)	91.5(3)
N(1)–Co(1)		1.923(7)	O(2)–Co(1)–O(1)	91.0(3)
N(2)–Co(1)		1.872(7)	O(1)–Co(1)–N(4)	90.7(3)
N(4)–Co(1)		1.937(8)	N(1)–Co(1)–N(4)	90.6(3)
N(5)–Co(1)		1.856(7)	N(5)–Co(1)–N(4)	83.8(3)
O(1)–Co(1)		1.907(6)	N(2)–Co(1)–N(1)	83.5(3)
O(2)–Co(1)		1.875(6)	N(2)–Co(1)–O(1)	81.7(3)
			N(5)–Co(1)–O(2)	81.6(3)

The molecular structure of the bis-ligated complex [Co(HFPB)$_2$] Br$_2$·2H$_2$O (**15**), shows that, it is monomeric with each tridentate ligand coordinating to the metal atom in the neutral amido form in a meridional fashion. This is confirmed by single bond nature of C7–N3 and C20–N6 bonds and double bond nature C7–O1 and C20–O2 bonds in the complex. The metal is octahedrally surrounded by two hydrazone moieties through

two pyridyl nitrogen atoms N1 and N4, two azomethine nitrogen atoms, N2 and N5 and two amido oxygen atoms O1 and O2. The coordinated ligands form a pair of five membered metal chelates by imposing intraligand bite angles, N(2)–Co(1)–N(1) (83.5(3)°), N(2)–Co(1)–O(1) (81.7(3)°), N(5)–Co(1)–N(4) (83.8(3)°) and N(5)–Co(1)–O(2) (81.6(3)°). The *cis* angles, N(5)–Co(1)–N(1) (99.4(3)º), N(5)–Co(1)–O(1) (95.5(3)º) and N(5)–Co(1)–O(2) (93.6(3)º) and *trans* angles N(5)–Co(1)–N(2) (174.4(3)º), O(1)–Co(1)–N(1) (165.1(3)º) and O(2)–Co(1)–N(4) (165.4(3)º) gives clear evidence that complex has a large distortion from octahedral geometry. The Co–$N_{azomethine}$, Co–N_{py} and Co–O bond lengths observed in the complex are comparable with the previously reported similar complexes of divalent metal ions [19]. The Co–$N_{azomethine}$, bond lengths are shorter compared to Co–N_{py} bond lengths, indicating the greater strength of the former bonds compared to the latter [19]. It is interesting to note that the azomethine bond distances are slightly decreased in the complex and amido bond distances are slightly increased in the complex when compared to the corresponding values in the free ligand and this supports coordination. A significant amount of metal-to-ligand π back bonding generates a delocalized conjugating effect along the metal-chelate rings which imparts partial single and double bond nature to C7–O1, C7–N3, N2–N3 and C6–N2 bonds in the hydrazone moiety owing to the extensive delocalization over the entire coordination frame work.

Table 5.5. Selected torsion angles [°] for HFPB·H₂O and [Co(HFPB)₂] Br₂·2H₂O (15).

Torsion angles		
	HFPB·H₂O	**[Co(HFPB)₂]Br₂·2H₂O (15)**
N1–C5–C6–N2	5.7(2)	0.2(12)
C4–C5–C6–N2	-175.10(14)	176.1(9)
N4–C18–C19–N5		-0.9(12)
C17–C18–C19–N5		176.1(10)
N3–N2–C6–C5	-179.18(11)	177.4(8)
C18–C19–N5–N6		-177.4(7)
C6–N2–N3–C7	176.10(12)	-176.9(9)
C19–N5–N6–C20		-178.4(8)
N2–N3–C7–C8	177.81(11)	-178.0(7)
C21–C20–N6–N5		179.2(6)
N2–N3–C7–O1	-0.4(2)	2.5(12)
O2–C20–N6–N5		0.0(11)

Selected torsion angles for the complex **15** are given in Table 5.5. The torsion angle value of -179.18(11)° observed for C(5)–C(6)–N(2)–N(3) supports *E* configuration with respect to N(2)=C(6) bond. It is interesting to note that the Z configuration of the hydrazone (torsion angle of N(2)–N(3)–C(7)–O(1) (-0.4(2)°) about C7–N3 bond is retained in the complex (torsion angle of N(2)–N(3)–C(7)–O(1) (2.5(12)°) to facilitate the coordination of amido oxygen to the cobalt center. This reveals that no rotation has occurred about the azomethine bond for coordination [32].

Table 5.6. Interaction parameters present in complex 15

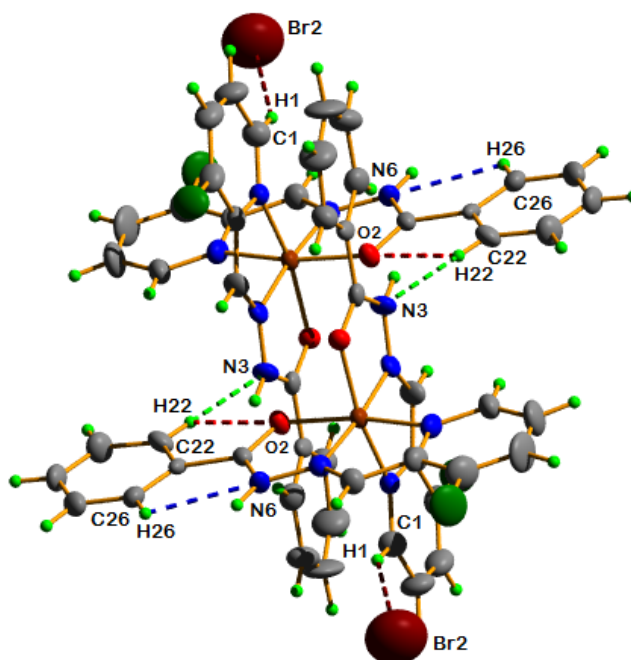| Hydrogen bonding interactions				
D–H···A	**D–H (Å)**	**H···A (Å)**	**D···A (Å)**	**∠D–H···A (°)**
C(1)–H(1)···Br(2)	0.93	2.74	3.562(11)	148
C(22)–H(22)···O(2)	0.93	2.46	2.771(12)	100
C(22)–H(22)···N(3)[a]	0.93	2.51	3.439(12)	176
C(26)–H(26)···N(6)	0.93	2.55	2.859(12)	100
C–F···π interactions				
C–F···Cg	**F···Cg (Å)**	**C–F···Cg (°)**	**C···Cg (Å)**	
C(4)–F(1)···Cg(3)[a]	3.526(9)	89.3(6)	3.748(12)	

Symmetry code: a = 2-x,-y,2-z

D = Donor, A = acceptor, Cg = Centroid of the ring

Cg(3) = C(8), C(9), C(10), C(11), C(12), C(13)

α(°) = Dihedral Angle between planes I and J

β(°) = Angle between Cg(I)···Cg(J) and Cg(J) perp.

γ(°) = Angle between Cg(I)···Cg(J) vector and Cg(I) perp.

Fig. 5.12. Hydrogen bonding interactions for compound 15.

There is extensive non classical hydrogen bonding (Table 5.6 and Fig. 5.12) in this molecule. There is bifurcated hydrogen bond formed between hydrogen atom of C(22) with iminolate oxygen O(2) and imine nitrogen N(3) of which one is intramolecular and other is intermolecular in nature. The non-classical intermolecular hydrogen bonding involving the hydrogen atom of the C(22) and N(3) with H···A distance of 2.51 Å and ∠DHA bond angle of 176° connects two molecules in the crystal lattice and extends through crystallographic *b* axis (Fig. 5.13).
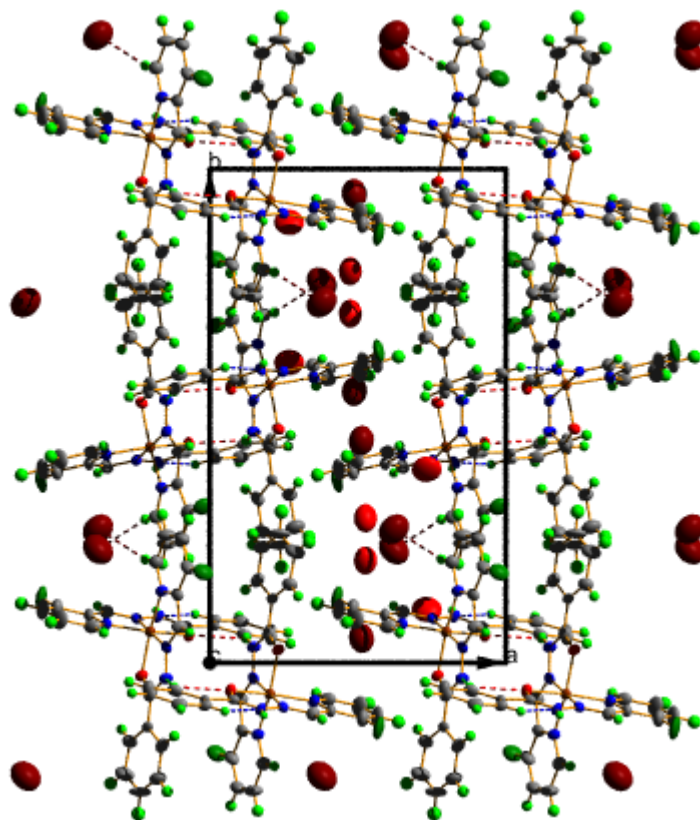
Fig. 5.13. Packing diagram showing the hydrogen bonded dimers extending along *b* axis.
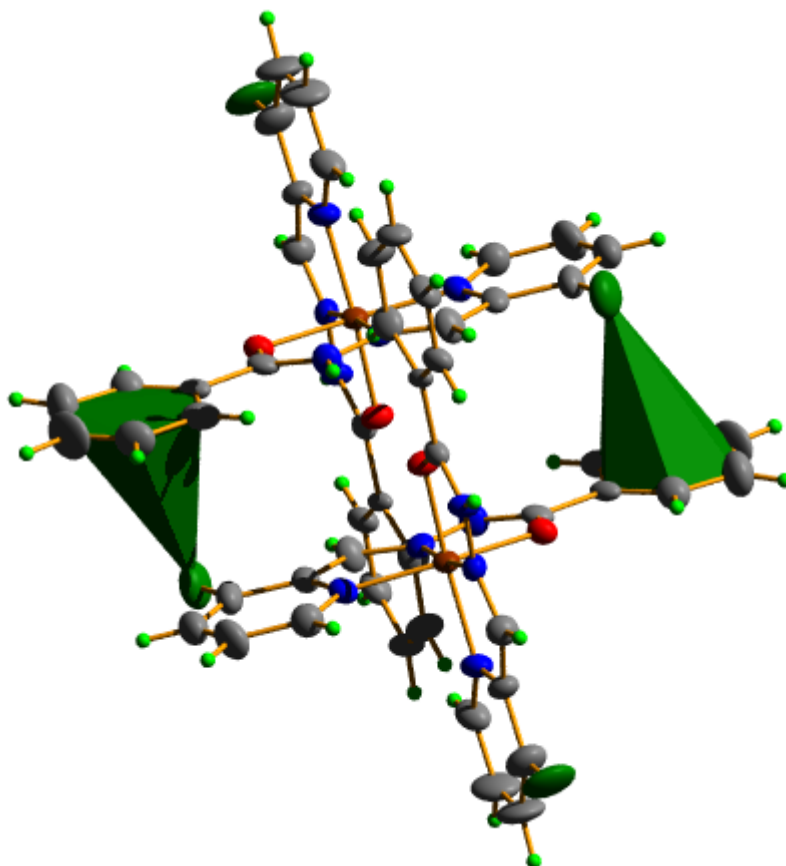
Fig. 5.14. C–F⋯π interactions connecting adjacent monomeric complexes.

There is one C–F⋯π interaction present in the crystal lattice leading to efficient packing in the crystalline state. Weak C–F⋯Cg(3) interactions (Fig. 5.14 and Table 5.6) along with non classical intermolecular hydrogen bonding connect the adjacent monomeric complexes to form dimers.

Based on the elemental analyses and spectral studies, following tentative structures were assigned to the complexes.

[Co(HFPB)(FPB)](OAc)·DMF (16)

OAc

DMF

[Co(FPB)₂] (17)

[Co(HFPN)Br₂] (18)
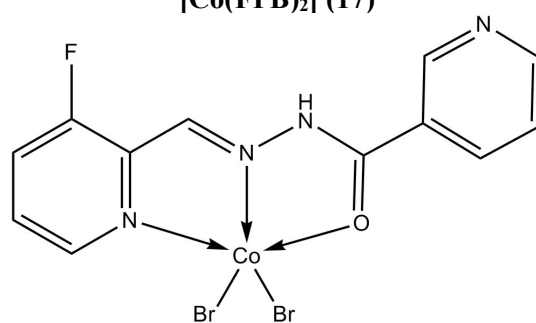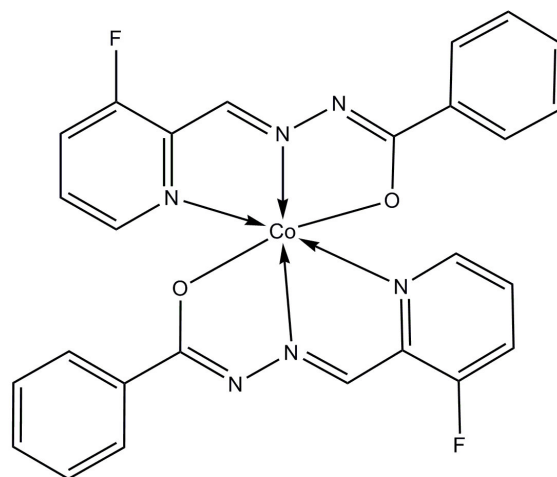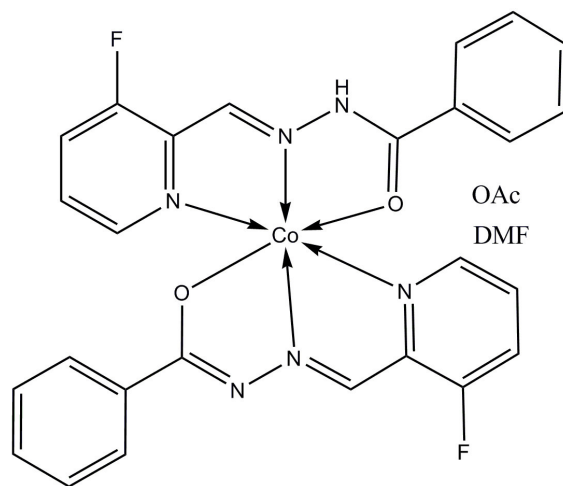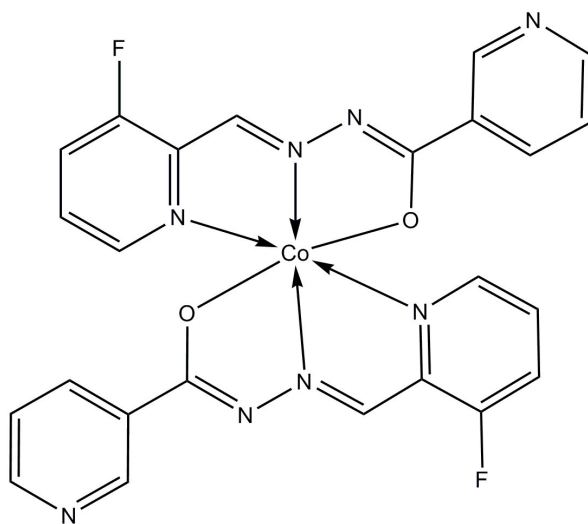
[Co(FPN)₂] (19)
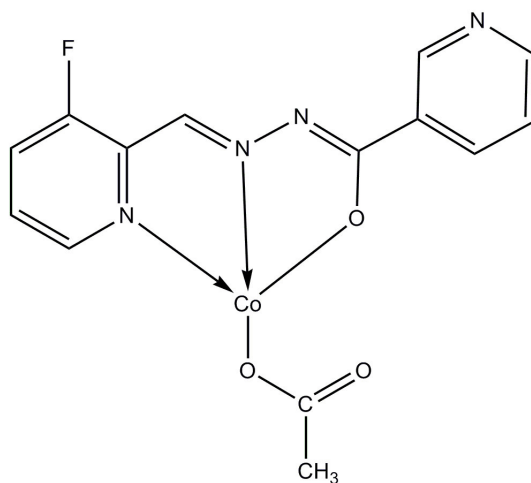
[Co(FPN)(OAc)] (20)

References

1. C. Lydon, M.M. Sabi, M.D. Symes, D.-L. Long, M. Murrie, S. Yoshii, H. Nojiri, L. Cronin, Chem. Commun. 48 (2012) 9819.

2. A. Ferguson, M. Schmidtmann, E.K. Brechin, M. Murrie, Dalton Trans. 40 (2011) 334.

3. M. Murrie, Chem. Soc. Rev. 9 (2010) 1986.

4. H. Miyasaka, M. Julve, M. Yamashita, R. Clérac, Inorg. Chem. 48 (2009) 3420.

5. A.T. Chaviara, E.E. Kioseoglou, A.A. Pantazaki, A.C. Tsipis, P.A. Karipidis, D.A. Kyriakidis, C.A. Bolos, J. Inorg. Biochem. 102 (2008) 1749.

6. Z.-H. Xu, F.-J. Chen, P.-X. Xi, X.-H. Liu, Z.-Z. Zeng, J. Photochem. Photobiol. 196A (2008) 77.

7. Y.D.M. Champouret, J. Fawcett, W.J. Nodes, K. Singh, G.A. Solan, Inorg. Chem. 45 (2006) 9890.

8. M. Tümer, E. Akgün, S. Toroğlu, A. Kayraldiz, L. Dönbak, J. Coord. Chem. 61 (2008) 2935.

9. A.A.A. Emara, A.M. Ali, A.F. El-Asmy, El-Sayed M. Ragab, J. Saudi Chem. Soc. 18 (2014) 762.

10. S. Di Bella, I. Fragalà, I. Ledoux, T.J. Marks, J. Am. Chem. Soc. 117 (1995) 9481.

11. M.V. Angelusiu, S.-F. Barbuceanu, C. Draghici, G.L. Almajan, Eur. J. Med. Chem. 45 (2010) 2055.

12. P. Sathyadevi, P. Krishnamoorthy, M. Alagesan, K. Thanigaimani, P. Thomas Muthiah, N. Dharmaraj, Polyhedron 31 (2012) 294.

13. W.J. Geary, Coord. Chem. Rev. 7 (1971) 81.

14. S. Yamada, Coord. Chem. Rev. 1 (1966) 415.

15. S.M. Devi, A.M. Singh, Int. J. Res. Chem. Environ. 2 (2012) 290.

16. E.C. Sañudo, V.A. Grillo, M.J. Knapp, J.C. Bollinger, J.C. Huffman, D.N. Hendrickson, G. Christou, Inorg. Chem. 41 (2002) 2441.

17. K. Dey, K. Chakraborty, P.K. Bhattacharya, D. Bandyopadhyay, S.K. Nag, R. Bhowmick, Ind. J. Chem. 38A (1999) 1139.

18. B. Samanta, J. Chakraborty, S. Shit, S.R. Batten, P. Jensen, J.D. Masuda, S Mitra, Inorg. Chim. Acta 360 (2007) 2471.

19. P.F. Rapheal, E. Manoj, M.R.P. Kurup, E. Suresh, Polyhedron 26 (2007) 607.

20. P.F. Rapheal, E. Manoj, M. R.P. Kurup, Polyhedron 26 (2007) 5088.

21. X.-H. Chen, Q.-J. Wu, Z.-Y. Liang, C.-R. Zhang, J.-B. Liu, Acta Cryst. C65 (2009) 190.

22. C.-Y. Meng, X.-S. Wan, X.-F. Zheng, L.-Y. Meng, H.-Y. Zhang, R. Yang, H.-W. Hou, Synth. React. Inorg. Met. -Org. and Nano Met. Chem. 37 (2007) 97.

23. K. Nakamoto, Infrared and Raman spectra of Inorganic and Coordination compounds, 5th ed., Wiley, New York, 1997.

24. M.M. Omar, G.G. Mohamed, Spectrochim. Acta 61A (2005) 929.

25. N. Nawar, N.M. Hosny, Transit. Met. Chem. 25 (2000) 1.

26. A.B.P. Lever, Inorganic Electronic Spectroscopy, 2nd Edn., Elsevier, Amsterdam, 1984.

27. Bruker, *APEX2, SAINT, XPREP and SADABS*, Bruker AXS Inc., Madison, Wisconsin, USA (2004).

28. G.M. Sheldrick, SHELXL97 and SHELXS97, University of Göttingen, Germany, 1997.

29. G.M. Sheldrick, Acta Cryst. A64 (2008) 112.

30. L.J. Farrugia, J. Appl. Cryst. 45 (2012) 849.

31. K. Brandenburg, Diamond Version 3.2g, Crystal Impact GbR, Bonn, Germany, (2010).

32. L. Latheef, M.R.P. Kurup, Polyhedron 27 (2008) 35.

.....౬౧.....

Chapter 6

SYNTHESES AND SPECTRAL CHARACTERIZATION OF MANGANESE(II) AND IRON(III) CHELATES OF TRIDENTATE AROYLHYDRAZONES

Contents
6.1. *Introduction*
6.2. *Experimental*
6.3. *Results and discussion*

6.1. Introduction

Iron, the most abundant transition element in the biosphere, is essential in higher forms of life and its compounds have numerous industrial applications. The element has catalytic properties. Several simple iron compounds are industrially important, for example, large amounts of iron oxides are produced for pigment and magnetic recording media applications. Oxidation states ranging from −2 to +6 are known, the most familiar are +2 (ferrous iron) and +3 (ferric iron). Most common complexes are octahedral, although examples of higher (e.g. seven coordinate) and lower (e.g. tetrahedral and square planar) geometries are well known. Depending on ligands involved high-spin and low-spin complexes can be formed, and temperature-dependent spin-state crossover complexes are well documented [1-4].

The principle of the molecular switching is a change of the spin state of a transition metal ion that is located in the center of complex molecules and coordinated to ligand atoms or molecules. Depending on the strength of the ligand field, i.e., the electrostatic field exerted at the central metal ion, the valence electron configuration of the metal can switch between two stable electron arrangements, one with maximum spin multiplicity, known as the high spin (HS) state, and one with minimum spin multiplicity, the low spin (LS) state. This switching can be stimulated by variation of temperature, application of pressure, light irradiation, and other external stimuli. The two phases involved have drastically different magnetic and optical properties, which provide the means for detection of the spin state phases. The spin crossover phenomenon occurs in numerous classes of coordination compounds; by far the majority of them are coordination compounds containing iron(II) or iron(III) [5-7]. Spin crossover compounds, though known for more than eight decades, have become most attractive in recent years and are extensively studied by chemists and physicists. The switching properties make such materials potential candidates for practical applications in thermal and pressure sensors as well as optical devices [8].

Even though iron is a potentially required element for bacterial growth, it is usually present in the environment as insoluble iron(III) oxide minerals and thus is not readily available for living organisms. To acquire iron, sideropores are produced by aerobically growing bacteria. Sideropores are low molecular weight compounds that help in acquisition of iron. Siderophores have greater affinity towards iron(III) and are

biosynthesized in response to low iron levels [9,10]. As compared to other naturally abundant metal ions such as Zn^{2+}, Cu^{2+}, Ca^{2+}, Mg^{2+} and Al^{3+} siderophores forms hexadentate, octahedral complexes with iron(III). The greater affinity of siderophore to iron(III) can be explained by HSAB (hard and soft acids and bases) principle, originally proposed by Pearson [11], that is, preferential coordination between the hard iron(III) Lewis acid and the hard anionic oxygen Lewis base donor ligand [12].

Nature uses nitrogenase enzymes to convert atmospheric N_2 to NH_3. These enzymes are limited to certain bacterial species (100-200 species), are responsible for all biologically fixed nitrogen. Nitrogenase enzymes catalyze the reduction and protonation of dinitrogen, and although the breaking of the dinitrogen bond is extremely energy intensive, these enzymes are able to perform the conversion at biological temperatures and atmospheric pressure. Because of the growing biochemical evidence suggesting that iron is responsible for the reduction of N_2 to ammonia in nitrogenase, understanding the coordination chemistry of iron with dinitrogen and reduced dinitrogen species, such as diazene and hydrazine, is becoming increasingly important [13].

Many transition metals have been applied as catalysts for organic reactions. Organoiron chemistry was started by the discovery of pentacarbonyliron in 1891, independently by Mond and Berthelot. A further milestone was the report of ferrocene in 1951. Iron catalysis came into focus by the Reppe synthesis. Iron-catalyzed cross-coupling reactions of Grignard reagents with organic halides have been studied [14]. More recently, increasing number of reactions using catalytic

amounts of iron complexes indicates the importance of this metal in catalysis [15,16].

Manganese is the third most abundant transition metal in Earth's crust considerably less abundant than iron. Manganese is a silvery-gray metal that resembles iron. It is hard and very brittle, difficult to fuse, but easy to oxidize. Manganese metal and its common ions are paramagnetic. The most common oxidation states of manganese are 2+, 3+, 4+, 6+, and 7+. Mn^{2+} often competes with Mg^{2+} in biological systems. Manganese compounds where manganese is in oxidation state of 7+ are powerful oxidizing agents. Compounds with oxidation states 5+ (blue) and 6+ (green) are strong oxidizing agents. Manganese is an essential element in living systems with some 20 identified functions in enzymes and proteins. The major biological roles of manganese are in making O_2 (photosystem II) and disposing of superoxide radicals (superoxide dismutase). The geochemical distribution of manganese in the hydrosphere, lithosphere and atmosphere involves oxidation states Mn(II), Mn(III) and Mn(IV) which show a wide range of strength as Lewis acids. Mn^{2+} has a high spin d^5 configuration. It has no coordination geometry preferences and forms relatively weak complexes with the ligands in general stronger than Mg^{2+} and Ca^{2+} but weaker than other transition metal ions. The coordination chemistry of manganese has continued to attract attention in recent years due to its presence in several biological systems. The coordination chemistry of manganese covers wide fields, as shown by a survey covering the crystallographic and structural parameters of over 700 examples [17-19].

Manganese and its compounds are widely used in analytical chemistry, metallurgical processes, paint and pigments industry and alloy industry, particularly in stainless steels. Schiff base complexes of manganese(II) have an excellent catalytic property [20]. The common ligands for manganese compounds involve the donor atoms nitrogen, oxygen, and the halogens while only few are known with other group V and group VI donors. One of the major areas of expansion has been the multinuclear complexes that are relevant to diverse fields such as metalloenzymes and single-molecule magnets. Besides the small clusters, comprising two to four metal ions synthesized to model the structures and functions of manganese metalloenzymes, a lot of interest has been invested in larger clusters, not only for their biological relevance, but also for the development of materials with novel magnetic properties [21]. Significant advances have been also been made in the chemistry of higher oxidation state manganese complexes (III), (V), (VI), and (VII) [22].

In view of the growing importance of iron and manganese complexes, we present here the synthesis and spectroscopic characterization of two iron(III) and two manganese(II) complexes of the tridentate aroylhydrazones.

6.2. Experimental

6.2.1. Materials

All reagents for the synthesis were commercially available and were used as received without further purification. 3-Fluoropyridine-2-

carbaldehyde (Sigma-Aldrich), benzhydrazide (Sigma-Aldrich), nicotinic hydrazide (Sigma-Aldrich), manganese(II) acetate tetrahydrate (Merck), and ferric(III) chloride (Himedia) were of Analar grade and were used as received. Solvents used were methanol, ethanol and DMF.

6.2.2 Syntheses of aroylhydrazones

3-Fluoropyridine-2-carbaldehyde benzoylhydrazone monohydrate (HFPB·H_2O) and 3-fluoropyridine-2-carbaldehyde nicotinoylhydrazone dihydrate (HFPN·$2H_2O$) were synthesized as discussed in Chapter 2.

6.2.3. Syntheses of Mn(II) and Fe(III) complexes
6.2.3.1. [Mn(FPB)₂] (21)

A methanolic solution of Mn(CH₃COO)₂·$4H_2O$ (0.1230 g, 0.5 mmol) was added to a solution of HFPB·H_2O (0.2612 g, 1 mmol) in methanol. The mixture was refluxed for 4 hours and cooled. Dark brown colored product separated out was collected, washed with methanol followed by ether and dried over P_4O_{10} *in vacuo*.

[Mn(FPB)₂] (21): Yield: 68%, λ_m (DMF): 12 ohm^{-1} cm^2 mol^{-1}, μ_{eff} (B.M.): 5.98, Elemental Anal. Found (Calcd.) (%): C: 58.26 (57.89); H: 2.95(3.36); N: 15.26 (15.58).

6.2.3.2. [Mn(FPB)(OAc)(H_2O)₂]·H_2O (22)

A methanolic solution of HFPB·H_2O (0.2612 g, 1 mmol) was treated with methanolic solution of Mn(CH₃COO)₂·$4H_2O$ (0.2450 g, 1 mmol). The resulting solution was refluxed for about 4 hours and then allowed to stand at room temperature. The brown colored product formed

was filtered, washed with methanol followed by ether and then dried over P_4O_{10} *in vacuo*.

[Mn(FPB)(OAc)(H$_2$O)$_2$]·H$_2$O (**22**): Yield: 61%, λ_m (DMF): 14 ohm^{-1} cm^2 mol^{-1}, μ_{eff} (B.M.): 6.02, Elemental Anal. Found (Calcd.) (%): C: 43.38 (43.91); H: 4.27 (4.42); N: 10.74 (10.24).

6.2.3.3. [Fe(FPB)$_2$]FeCl$_4$·H$_2$O (23)

Complex **23** was prepared by refluxing methanolic solutions of HFPB·H$_2$O (0.2612 g, 1 mmol) and iron(III) chloride (0.1620 g, 1 mmol) for about 6 hours. The black colored product obtained was filtered, washed with methanol followed by ether and dried over P_4O_{10} *in vacuo*.

[Fe(FPB)$_2$]FeCl$_4$·H$_2$O (**23**): Yield: 59%, λ_m (DMF): 88 ohm^{-1} cm^2 mol^{-1}, μ_{eff} (B.M.): 4.32, Elemental Anal. Found (Calcd.) (%): C: 40.18 (40.35); H: 3.16 (2.86); N: 10.61 (10.86).

6.2.3.4. [Fe(FPN)$_2$]FeCl$_4$ (24)

The complex was prepared by refluxing a methanolic solutions of HFPN·2H$_2$O (0.2802 g, 1 mmol) and iron(III) chloride (0.1620 g, 1 mmol) for 6 hours. The product separated was black colored solid and it was then filtered, washed with methanol followed by ether and dried over P_4O_{10} *in vacuo*.

[Fe(FPN)$_2$]FeCl$_4$ (**24**): Yield: 72%, λ_m (DMF): 92 ohm^{-1} cm^2 mol^{-1}, μ_{eff} (B.M.): 4.28, Elemental Anal. Found (Calcd.) (%): C: 39.34 (38.96); H: 1.98 (2.18); N: 15.40 (15.14).

6.3. Results and discussion

From the analytical data, the iron complexes can be formulated as either [FeLCl$_2$] or [FeL$_2$]FeCl$_4$ (where L is the monodeprotonated hydrazone) but the conductivity measurements clearly indicate that FeCl$_4^-$ anion is formed in the reaction. The compound is found to be a 1:1 electrolyte in DMF with values near to 88 ohm^{-1} cm^2 mol^{-1}. The metal center of the iron(III) complexes is expected to contain two deprotonated ligands attached to low-spin iron(III). The Mn(II) complexes are found to be readily soluble in polar organic solvents. Out of the two manganese(II) complexes synthesized, compound **21** has a stoichiometry [MnL$_2$] with two anionic ligands coordinated to the Mn(II) ion. The complexes were characterized by the following physico-chemical methods.

6.3.1. Elemental analyses

The analytical data indicate that the observed C, H, N values of the complexes were in close agreement with that of the formula suggested and are given in section 6.2.3.

6.3.2 Molar conductivity and magnetic susceptibility measurements

The molar conductivity of the complexes in 10^{-3} M DMF solutions was measured at 298 K with a Systronic model 303 direct-reading conductivity bridge. Both the iron complexes are found to be 1:1 electrolytes in DMF with λ_m values in the range 85-100 ohm^{-1} cm^2 mol^{-1} [23]. These observations along with elemental analyses data strongly support the finding that both the complexes are associated with FeCl$_4^-$ anion outside the coordination sphere. In general high spin Fe(III)

complexes have magnetic moments very close to the spin only value of 5.9 B.M. since the ground state (derived from the ^6S state of the free ion) has no orbital angular momentum and no coupling is found with the excited state [24]. The low spin complexes with t_{2g} configuration usually have magnetic moment value is ~ 2.3 B.M. at room temperature due to the considerable orbital contributions to their magnetic moments [24,25]. Magnetic moments have been calculated for the iron complexes at room temperature and found to be in the range 4.2-4.4 B.M. This is consistent with one high-spin iron and one low spin iron centers in the complexes **23** and **24** [26,27].

The molar conductivity measurements of manganese complexes in DMF (10^{-3} M) give values 10-24 ohm^{-1} cm^2 mol^{-1} and confirm that they are neutral and probably non-electrolytes [28]. The magnetic moments of the two Mn(II) complexes, **21** and **22** were calculated from the magnetic susceptibility measurements. The magnetic moments of the two compounds are found to be in the range 5.9-6.1 B.M., indicating that these complexes are high spin in nature with five unpaired electrons [29].

6.3.3. Infrared spectral studies

The IR spectra of the Mn(II) and Fe(III) complexes were recorded in the solid state as KBr discs. Table 6.1 lists the assignments of IR bands most useful for the establishment of the mode of coordination of the hydrazone ligands in their iron(III) coordination and Mn(II) complexes.

The azomethine stretching vibration is observed in the range 1590-1597 cm^{-1} in the case of free ligands. However in the complexes this band is shifted to the 1550-1585 cm^{-1} range suggesting that the azomethine

nitrogen is coordinated to the metal center. The stretching vibrations of the newly formed C=N, due to coordination through deprotonation, appear as sharp bands in the region near 1595 cm^{-1}. The spectra of the complexes showed an increase in pyridyl ring in-plane and out-of-plane bending mode of vibrations. The ν(N–H) broad band at 3000-3500 cm^{-1} in the ligand disappears in the complex, suggesting the coordination through deprotonated iminolate oxygen substantiating the iminolization of the ligand at the time of complexation.

**Table 6.1. The important IR frequencies (cm^{-1}) of Mn(II) and Fe(III) complexes**

Compound	ν(N–H)	ν(C=O)/ν(C–O)	ν(C=N)	ν(C=N)[a]
HFPB·H$_2$O	3059	1683	1597	--
[Mn(FPB)$_2$] (**21**)	--	1341	1572	1597
[Mn(FPB)(OAc)(H$_2$O)$_2$]·H$_2$O (**22**)	--	1340	1565	1593
[Fe(FPB)$_2$]FeCl$_4$·H$_2$O (**23**)	--	1354	1552	1595
HFPN·2H$_2$O	3058	1682	1590	--
[Fe(FPN)$_2$]FeCl$_4$ (**24**)	--	1375	1584	1598

[a]Newly formed C=N bond
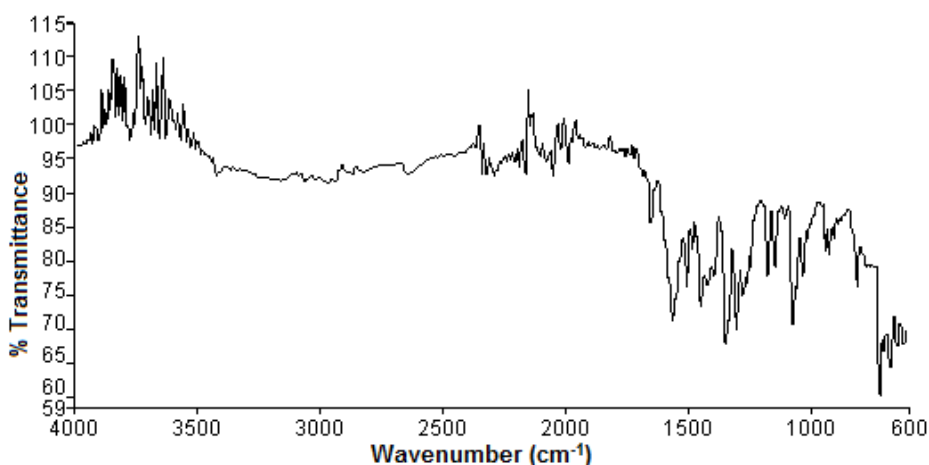
**Fig. 6.1. IR spectrum of [Mn(FPB)$_2$] (21).**

In complex **21** (Fig. 6.1), the pattern of coordination is similar to that observed in similar types of complexes [29,30]. The two monodeprotonated ligand molecules coordinate to the metal center *via* pyridyl nitrogen, azomethine nitrogen and iminolate oxygen atoms and coordination of azomethine nitrogen is indicated by lowering of the band at 1597 to 1572 cm^{-1}. The newly formed C=N bond due to deprotonation of the ligand is also observed at 1593 cm^{-1}. The coordination of the nitrogen atom of the pyridine ring to the Mn(II) ion in the complexes is indicated by the shifting of the pyridine ring vibrations of the ligands to higher frequencies in their manganese complexes [29]. A new band observed at 1341 cm^{-1} is assigned to (C–O) stretch suggesting change of bond order and strong delocalization.
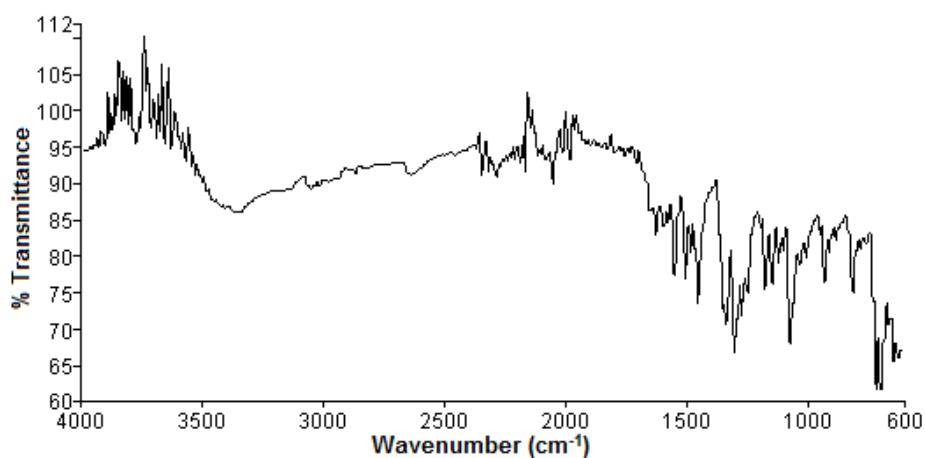
Fig. 6.2. IR spectrum of [Mn(FPB)(OAc)(H$_2$O)$_2$]·H$_2$O (22).

The broad band at 3467 cm^{-1} in the IR spectrum of complex [Mn(FPB)(OAc)(H$_2$O)$_2$]·H$_2$O (**22**) (Fig. 6.2) suggest the presence of coordinated as well as lattice water molecules [31] in the compound

which was also confirmed by thermal analysis. The most interesting part of complex **22** is the region where strong absorption band due to acetate group is visible. The free acetate ion CH_3COO^- exhibits the $\nu_{as}(COO)$ and $\nu_s(COO)$ at 1578 cm^{-1} and 1414 cm^{-1} respectively. It is reported that if it is covalently bonded to a metal as a unidentate ligand where the ν_{as} and ν_s get shifted to higher and lower frequencies respectively [32]. The present acetato complex shows a peak near 1620 cm^{-1} possibly due to ν_{as} stretch of the unidentate acetate group [33]. Further the complex display a band at 1338 cm^{-1} which was seen in other complexes also, but when compared to the corresponding peak in other complexes, this was found to be significantly stronger. Thus it may be due to the symmetric stretching vibration of acetate ion.
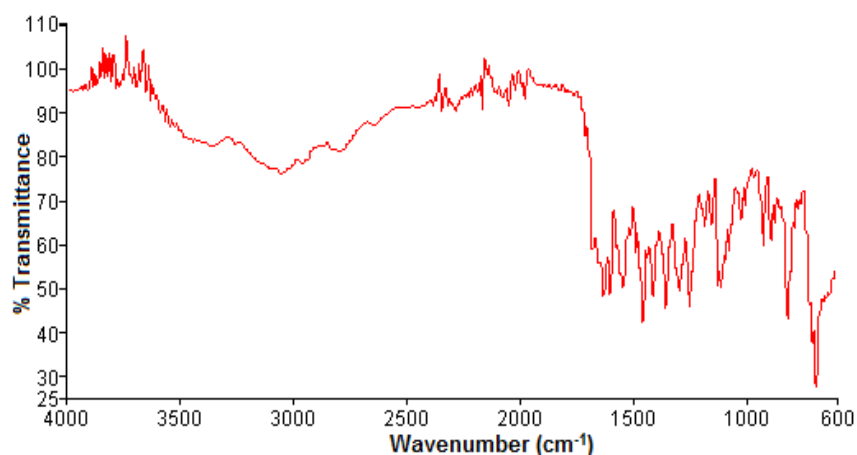
Fig. 6.3. IR spectrum of [Fe(FPB)₂]FeCl₄·H₂O (23).

The band $\nu(C=N)$ of HFPB·H$_2$O is found at 1597 cm^{-1}. This strong band is shifted after coordination to lower energies by 40-50 cm^{-1} indicating the coordination *via* azomethine nitrogen. The coordination of

pyridine ring nitrogen to the Fe(III) ion in the complexes is indicated by shifting of the pyridine ring vibrations of the ligand to higher frequencies. The newly formed C=N bond due to deprotonation of the ligand is also observed at $\sim$ 1595 cm^{-1}. A broad band around 3000-3500 cm^{-1} in the IR spectrum of the complex **23** (Fig. 6.3) is assigned to the –OH stretching vibrations of lattice water which is further confirmed from its thermogravimetric analysis.
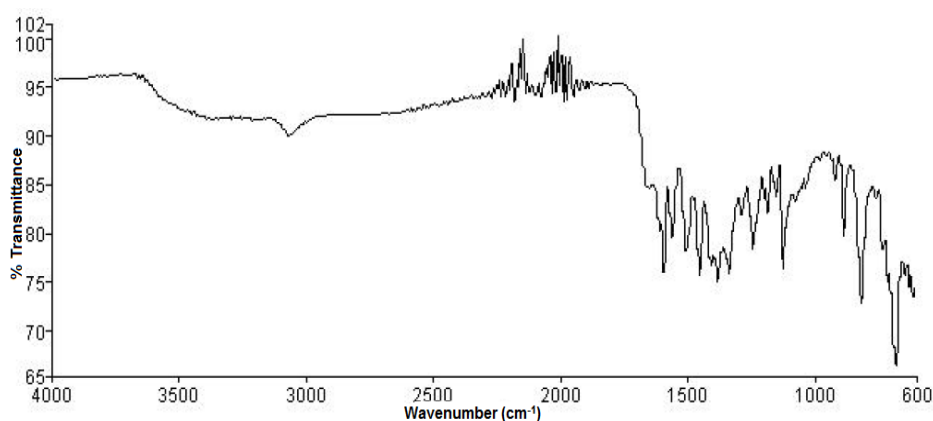
Fig. 6.4. IR spectrum of [Fe(FPN)$_2$]FeCl$_4$ (24).

In complex **24** (Fig. 6.4), the band ν(C=N) of free hydrazone is found to be shifted to lower frequency indicating the coordination *via* azomethine nitrogen. The appearance of a new band at $\sim$ 1375 cm^{-1} due to iminolic stretch substantiates the coordination of the ligand *via* iminolate oxygen. The appearance of a new band at 1598 cm^{-1} due to the newly formed supports the above observation. The out-of-plane pyridine ring deformation modes of free ligand are found to be shifted to higher energies in the spectrum of the complex indicating the coordination *via* nitrogen atom of the pyridine ring.

6.3.4. Electronic spectral studies

The electronic spectra of the complexes were recorded in DMF solutions on an Evolution 220 model, UV-Vis Double Beam Spectrophotometer. The significant electronic absorption spectral data of the complexes in DMF with their possible assignments are summarized in Table 6.2 and the spectra are shown in Figs. 6.5 and 6.6.

Table 6.2. Electronic spectral assignments (cm^{-1}) of Mn(II) and Fe(III) complexes

| Compound	$n{\to}\pi^*/\pi{\to}\pi^*$	LMCT	*d-d*
[Mn(FPB)$_2$] (**21**)	36660, 32720	25460	
[Mn(FPB)(OAc)(H$_2$O)$_2$]·H$_2$O (**22**)	36520, 32860	25310	
[Fe(FPB)$_2$]FeCl$_4$·H$_2$O (**23**)	32330	24720	
[Fe(FPN)$_2$]FeCl$_4$ (**24**)	32720	25020	14990
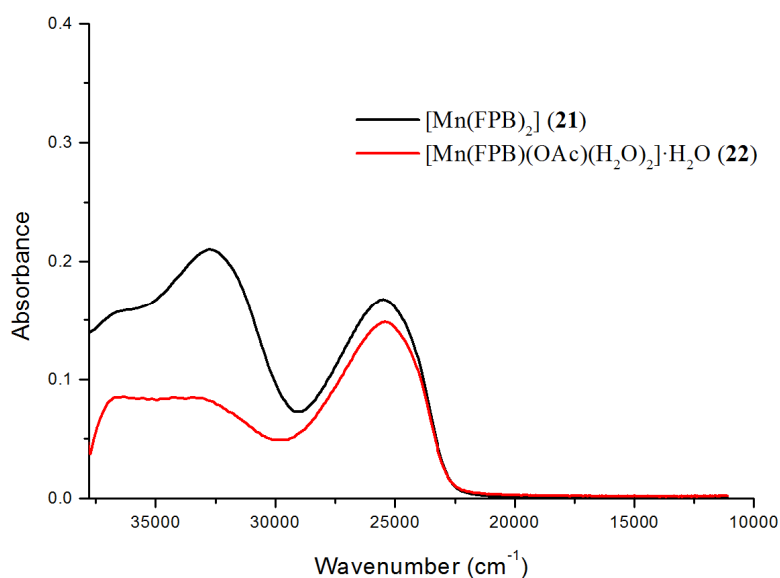
Fig. 6.5. Electronic spectra of manganese(II) complexes.

The electronic spectra of all Mn(II) complexes (Fig. 6.5) dominated by two intraligand bands in the range 36700-32000 cm^{-1} assigned to n→π* and π→π* transitions of the aroylhydrazone moiety. Electronic transition intensities of octahedral manganese(II) complexes are very low since the transitions from the ground state are doubly forbidden. The ground state of the high spin octahedrally coordinated manganese(II) ion is d^5. Since there are no other terms of sextet spin multiplicity, all the *d-d* transitions in high spin complexes are not only Laporte forbidden but also spin forbidden [30]. The high intense charge transitions tailing into the visible region obscure the very weak *d-d* absorption bands of the Mn(II) complexes.
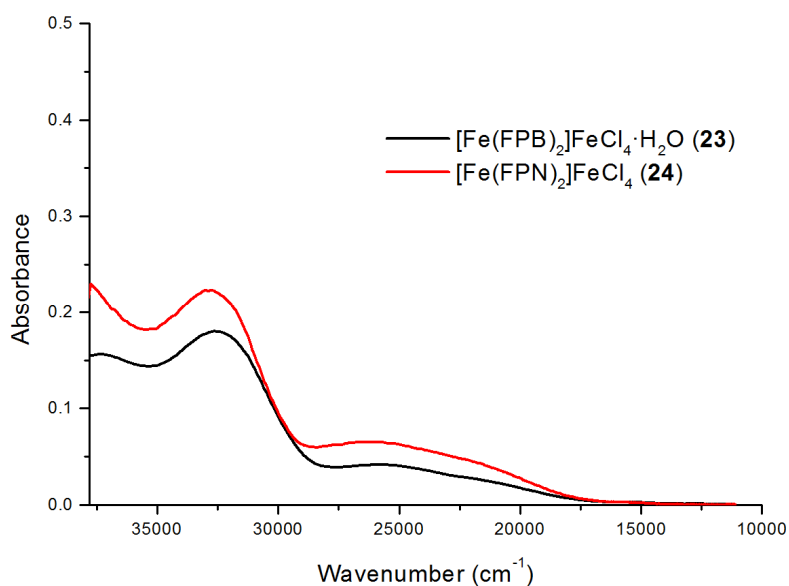
Fig. 6.6. Electronic spectra of iron(III) complexes.

The electronic spectra of iron(III) complexes were taken in DMF solutions and shown in Fig. 6.6. A broad band at 32000-33000 cm^{-1}

corresponds to the intraligand transitions. Due to the greater oxidising power of Fe(III) as compared with Mn(II), ligand-metal charge transfer bands often obscure the very low intensity, spin forbidden, *d-d* absorption bands. The band obtained at 14990 cm^{-1} (Fig. 6.7) can be assigned to the *d-d* transitions of the spin-paired d^5 iron(III) metal centers [34]. The bands obtained between 15000-26000 cm^{-1} are due to the $d \rightarrow \pi^*$ metal-to-ligand transitions [34].
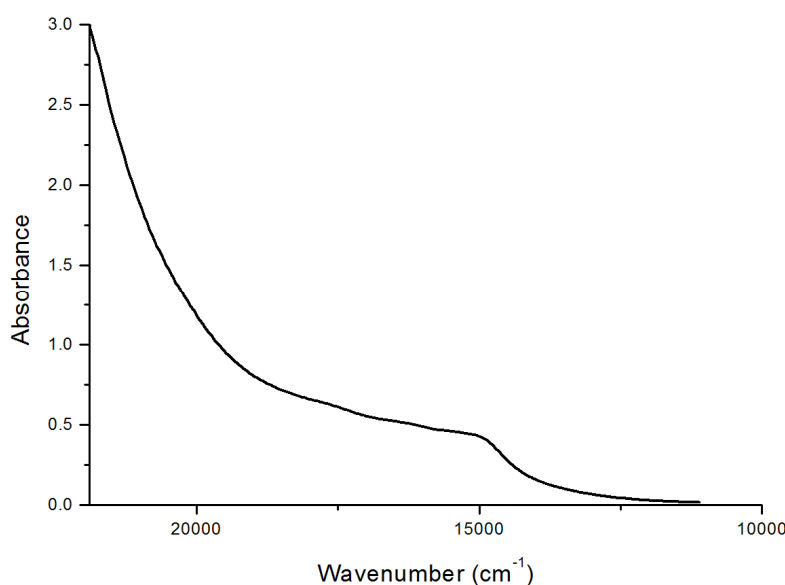
**Fig. 6.7. Electronic spectra of [Fe(FPN)$_2$]FeCl$_4$ (24) in 22000-10000 cm^{-1} region.**

6.3.5. Thermogravimetric analyses

Thermal behavior of the complexes **22** and **23** was analyzed by TG-DTA measurements starting from room temperature to 700 °C. Thermogravimetric analyses of the complexes gave information concerning the thermal stability and the nature of water molecules in the

complexes [35,36]. It was observed that the hydrated complexes lose water of hydration in the first step, followed by decomposition of the rest of the compound in the subsequent steps.
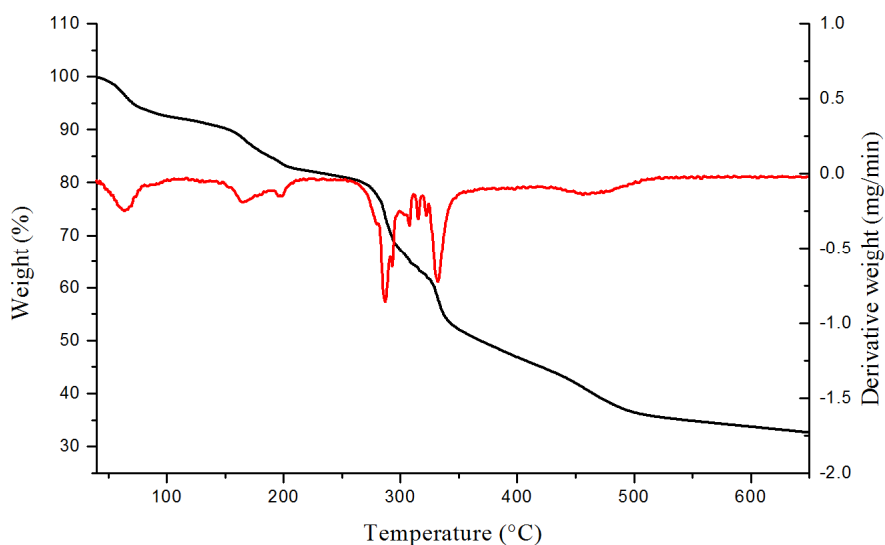
Fig. 6.8. Thermogram of [Mn(FPB)(OAc)(H₂O)₂]·H₂O (22).

In $[Mn(FPB)(OAc)(H_2O)_2]\cdot H_2O$ (**22**) (Fig. 6.8), the first weight loss of 4.85% (Calcd. 4.38%) is observed at 65 °C range indicates that one water molecule is present in the lattice of the compound. A weight loss of 25.32% (Calcd. 24.71%) occurs in two steps at 150-300 °C range involves the removal of two coordinated water molecules and acetate ion from the compound. The compound again decomposes with weight loss of 37.38% (Calcd. 36.83%) due to the loss of C_6H_4FN fragment of the aroylhydrazone moiety. After 350 °C, compound decomposes continuously.
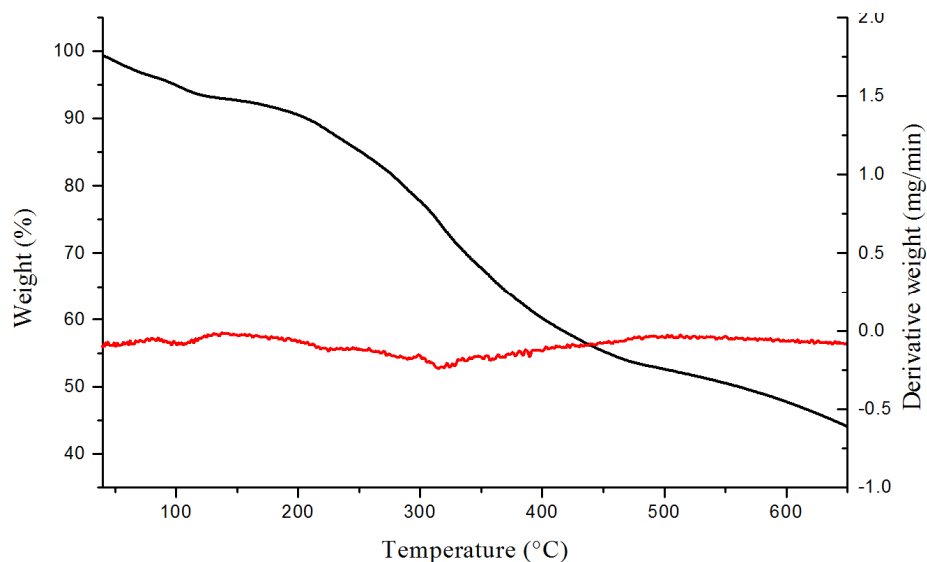
Fig. 6.9. Thermogram of [Fe(FPB)$_2$]FeCl$_4$·H$_2$O (23).

For the complex [Fe(FPB)$_2$]FeCl$_4$·H$_2$O (**23**) (Fig. 6.9), the first step in the decomposition sequence within the temperature range of 100-110 °C corresponds to the loss of one molecule of lattice water present in the complex. The observed weight loss of 2.35% is in good agreement with the calculated value of 2.38%. The decomposition of the ligands take place in the 210-601 °C range and after this temperature a plateau is obtained, which indicates the formation of stable metal oxide.

6.3.6. EPR spectral studies

The EPR spectra of the iron(III) and manganese(II) complexes in polycrystalline state at 298 K and in DMF at 77 K were recorded in the X-band, using 100-kHz modulation frequency and 9.5 GHz microwave frequency. The EPR spectra are simulated using EasySpin 4.0.0 package

[37] and the experimental (red) and simulated (blue) best fits are included (Figs. 6.10-6.13).

EPR spectroscopy is an important tool to probe the manganese centers in manganese proteins. Kramers' ground-state doublets and zero-field splitting are the two interesting features of Mn(II) systems. Mn^{2+} (d^5) is an odd electron system which causes the zero-field splitting to produce three doubly degenerate spin states M_s = ±5/2, ±3/2, ±1/2 (Kramers' degeneracy). Each of these spin states splits into two singlets on application of the applied field, producing six levels. As a result of this splitting, five transitions (-5/2→-3/2, -3/2→-1/2, -1/2→-1/2, 1/2→3/2, 3/2→5/2) are expected. Generally in practice usually only one signal is observed since they are of equal energy. This signal will further split by nuclear hyperfine interaction with the Mn nucleus ($I = 5/2$) giving rise to thirty peaks in the spectrum. For high spin Mn(II) complexes, *g* value lie very close to the free electron *g* value due to the negligible spin orbit coupling.

The spin Hamiltonian $\hat{H}$ used to represent the EPR spectra of Mn(II) is given by

$$\hat{H} = g\beta HS + D[S_z^2 - S(S+1)/3] + E(S_x^2 - S_y^2)$$

where *H* is the magnetic field vector, *g* is the Lande's splitting factor, *β* is the Bohr magneton, *D* is the axial zero field splitting term, *E* is rhombic zero field splitting parameter and *S* is the electron spin vector [38]. Five EPR transitions are expected corresponding to Δm_s ±1 provided *D* and *E* are very small compared to *gβHS* [38].

The EPR spectrum of compound **21** at polycrystalline state at 298 K (Fig. 6.10) exhibits a broad signal with g_{iso} value of 2.023. The broadening of the signal is due to the dipolar interactions and random orientations of Mn^{2+} ions.
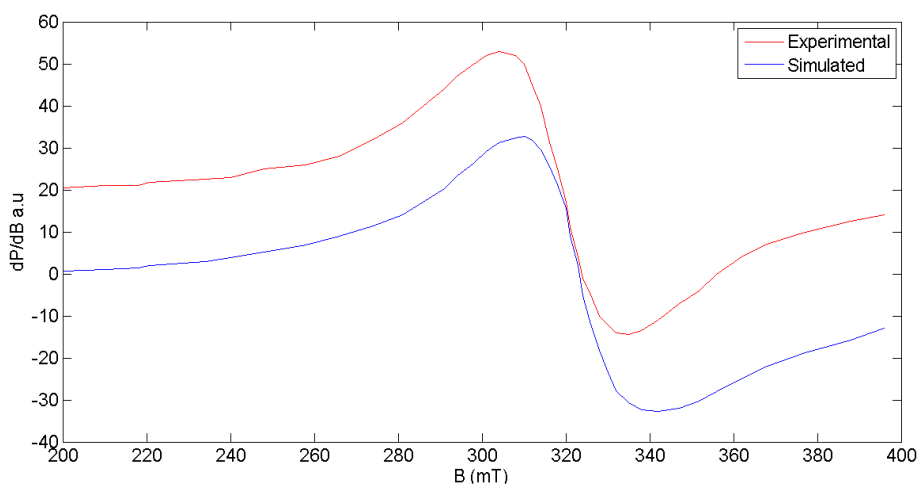
Fig. 6.10. EPR spectrum of [Mn(FPB)₂] (21) in polycrystalline state at 298 K.
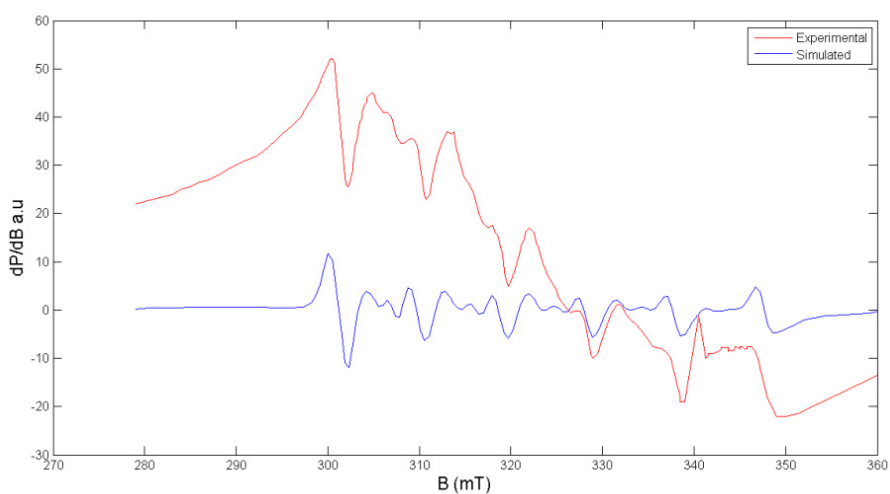
Fig. 6.11. EPR spectrum of [Mn(FPB)₂] (21) in DMF at 77 K.

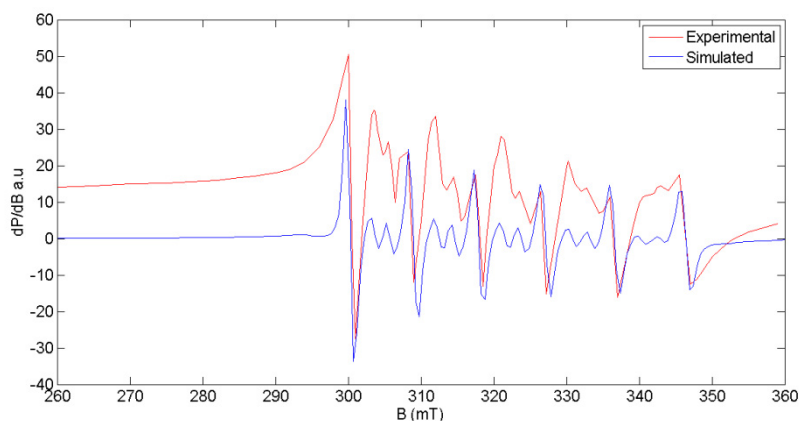For [Mn(FPB)$_2$] (**21**) in DMF at 77 K, a hyperfine sextet is obtained substantiating the hyperfine interaction of the unpaired electron and ^{55}Mn nucleus (*I*=5/2) in the complex. The observed g value, 2.001 is very close to the free electron value and is consistent with the typical Mn(II) complexes suggesting the absence of spin orbit coupling in the ground state $^6A_{1g}$ without another sextet term of higher energy. In addition to this, a pair of lines with low intensity is found between each of the two main hyperfine lines. This low intensity lines were found to be forbidden transitions arise from the arising due to the mixing of hyperfine lines with zero-field splitting [39]. Axial splitting factor D, rhombic splitting factor E and E/D ratio calculated for the complex **21** are found to be that were found to be 320 MHz, 160 MHz and 0.500, respectively.
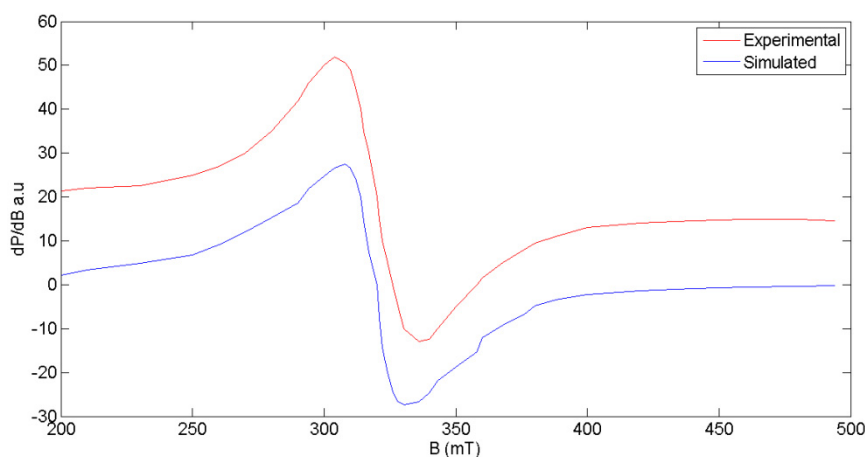
Fig. 6.12. EPR spectrum of [Mn(FPB)(OAc)(H$_2$O)$_2$]·H$_2$O (22) at polycrystalline state 298 K.

For [Mn(FPB)(OAc)(H$_2$O)$_2$]·H$_2$O (**22**) at polycrystalline state 298 K (Fig. 6.12), exhibits a broad signal with g$_{iso}$ value of 1.98 without hyperfine splittings.

Fig. 6.13. EPR spectrum of [Mn(FPB)(OAc)(H₂O)₂]·H₂O (22) in DMF at 77 K.

For [Mn(FPB)(OAc)(H_2O)$_2$]·H_2O (**22**) (Fig. 6.13) in DMF at 77 K a sextet is observed due to the hyperfine interaction of the unpaired electron and ^{55}Mn nucleus (I=5/2) in the complex. The low intensity forbidden lines are also visible in the spectrum and arise due to the mixing of hyperfine lines with zero-field splitting. Axial splitting factor D, rhombic splitting factor E and E/D ratio calculated for the complex **22** are found to be that were found to be 220 MHz, 90 MHz and 0.409, respectively.

The geometry and coordination number of the complex influence the E/D ratio. It varies from pure axial systems (E/D = 0) to close rhombic ones (E/D = 1/3) and mostly it depends on the nature of neutral ligands [40]. The E/D ratio obtained for Mn(II) complexes deviate significantly [40] and hence no conclusion can be drawn for these complexes [40,41].

The EPR spectra of iron(III) complexes were poorly resolved at 298 and 77 K and therefore not good to interpret.

Based on the elemental analyses and spectral studies, following tentative structures were assigned to the complexes.
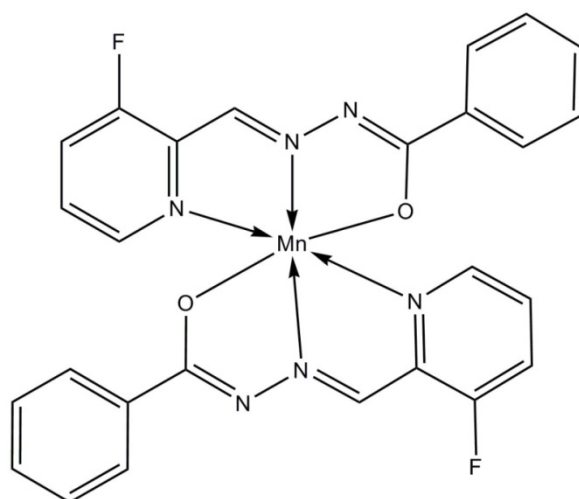
[Mn(FPB)₂] (21)
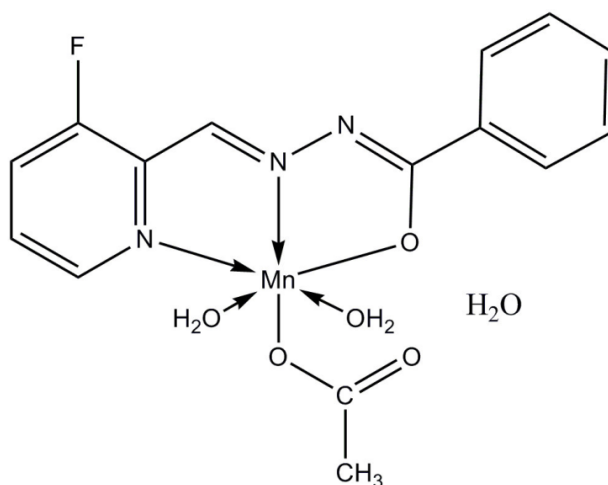
[Mn(FPB)(OAc)(H₂O)₂]·H₂O (22)
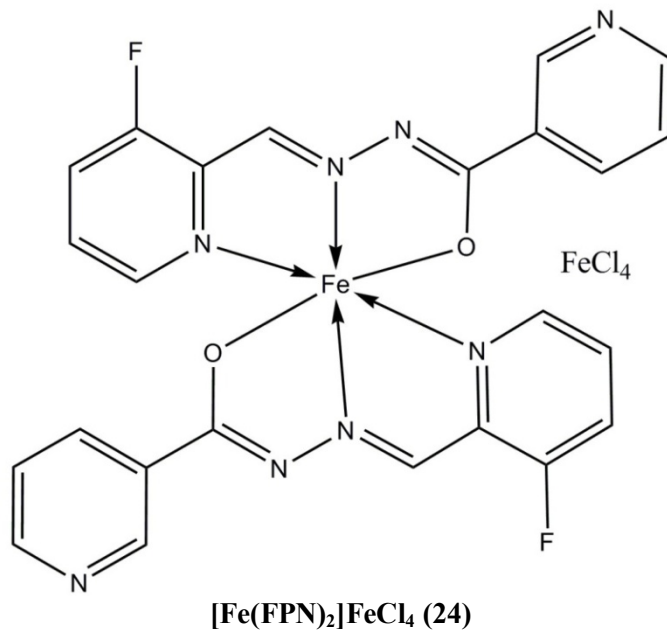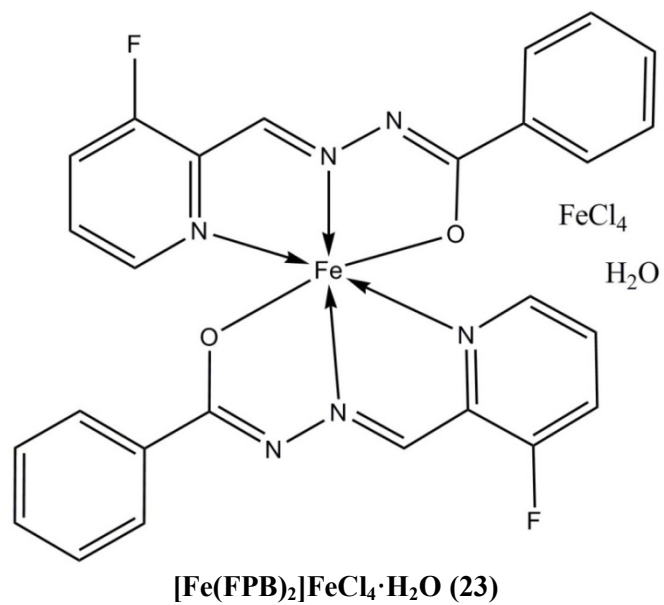
[Fe(FPB)₂]FeCl₄·H₂O (23)

[Fe(FPN)₂]FeCl₄ (24)

References

[1] C. Lydon, M.M. Sabi, M.D. Symes, D.-L. Long, M. Murrie, S. Yoshii, H. Nojiri, L. Cronin, Chem. Commun. 48 *(*2012) 9819.

[2] A. Ferguson, M. Schmidtmann, E.K. Brechin, M. Murrie, Dalton Trans. 40 (2011) 334.

[3] M. Murrie, Chem. Soc. Rev. 9 (2010) 1986.

[4] H. Miyasaka, M. Julve, M. Yamashita, R. Clérac, Inorg. Chem. 48 (2009) 3420.

[5] T. Kawakami, Y. Tsujimoto, H. Kageyama, X.-Q. Chen, C.L. Fu, C. Tassel, A. Kitada, S. Suto, K. Hirama, Y. Sekiya, Y. Makino, T. Okada, T. Yagi, N. Hayashi, K. Yoshimura, S. Nasu, R. Podloucky, M. Takano, Nature Chemistry 1 (2009) 371.

[6] M. Seredyuk, K.O. Znovjyak, J. Kusz, M. Nowak, M. C. Muñoz, J. A. Real, DaltonTrans. 43 (2014) 16387.

[7] Y.D.M. Champouret, J. Fawcett, W.J. Nodes, K. Singh, G.A. Solan, Inorg. Chem. 45 (2006) 9890.

[8] M. Tümer, E. Akgün, S. Toroğlu, A. Kayraldiz, L. Dönbak, J. Coord. Chem. 61 (2008) 2935.

[9] A.M. Albrecht-Gary, A.L. Crumbliss, Metal Ions in Biological Systems, Marcel Dekker, New York, (1998) 239.

[10] H. Boukhalfa, A.L. Crumbliss, Biometals 15 (2002) 325.

[11] R.G. Pearson, J. Am. Chem. Soc. 85 (1963) 3533.

[12] A. Butler, R. M. Theisen, Coord. Chem. Rev. 254 (2010) 288.

[13] J.L. Crossland, D.R. Tyler, Coord. Chem. Rev. 254 (2010) 1883.

[14] M. Tamura, J. Kochi, J. Am. Chem. Soc. 93 (1971) 1487.

[15] J.W. Kück, R. M. Reich, F.E. Kühn, Chem. Rec. 16 (2016) 349.

[16]   S. Chakraborty, G. Leitus, D. Milstein, Chem. Commun. 52 (2016) 1812.

[17]   H.N. Tang, L.F. Wang, R.D. Yang, Transit. Met. Chem. 28 (2003) 395.

[18]   H.H. -Monfared, R. Bikas, S. Mohammadi, T. M. Percino, S. Demeshko, F. Meyer, M.A.L. Ramírez, Z. Anorg. Allg. Chem. 640 (2014) 405.

[19]   E.C. Sañudo, V.A. Grillo, M.J. Knapp, J.C. Bollinger, J.C. Huffman, D.N. Hendrickson, G. Christou, Inorg. Chem. 41 (2002) 2441.

[20]   R.I. Kureshy, N.H. Khan, S.H.R. Abdi, P. Iyer, S.T. Patel, Polyhedron 18 (1999) 1773.

[21]   K. Fegy, D. Luneau, E. Belorizky, M. Novac, J.-L. Tholence, C. Paulsen, T. Ohm, P. Rey, Inorg. Chem. 37 (1998) 4524.

[22]   J.B. Vincent, G. Christou, Advances in Inorganic Chemistry, 33 (1989) 197.

[23]   W.J. Geary, Coord. Chem. Rev. 7 (1971) 81.

[24]   M. Joseph, A. Sreekanth, V. Suni, M.R.P. Kurup, Spectrochim. Acta 64A (2006) 637.

[25]   R.L. Dutta, A. Syamal, Elements of Magnetochemistry, 2nd Edn., East-West Press, New Delhi, 1993.

[26]   A. Sreekanth, H.-K. Fun, M.R.P. Kurup, J. Mol. Struct. 737 (2005) 61.

[27]   A. Sreekanth, M.R.P. Kurup, Polyhedron 23 (2004) 969.

[28]   O. Pouralimardan, A.-C. Chamayou, C. Janiak, H.H. -Monfared, Inorg. Chim. Acta 360 (2007) 1599.

[29]   A Sreekanth, M. Joseph, H.-K. Fun, M.R.P. Kurup, Polyhedron 25 (2006) 1408.

[30]   N.A. Mangalam, S.R. Sheeja, M.R.P. Kurup, Polyhedron 29 (2010) 3318.

[31]   V. Stefov, V.M. Petruševski, B. Šoptajanov, J. Mol. Struct. 293 (1993) 97.

[32]   K. Nakamoto, Infrared and Raman Spectra of Inorganic and Coordination compounds, Part B, 5th Edn., Wiley, New York, 1997.

[33] N.R. Sangeetha, S. Pal, Polyhedron 19 (2000) 1593.

[34] B.S. Garg, M.R.P. Kurup, S.K. Jain, Y.K. Bhoon, Transit. Met. Chem. 13 (1988) 247.

[35] A.A.A. Emara, B.A.E. Sayed, E.A.E. Ahmed, Spectrochim. Acta 69A (2008) 757.

[36] B. Hollo, J. Magyari, V.Z. Radovanovic, G. Vuckovic, Z.D. Tomic, I.M. Szilagyi, G. Pokol, K.M. Szecsenyi, Polyhedron 80 (2014) 142.

[37] S. Stoll, Spectral Simulations in Solid-State Electron Paramagnetic Resonance, Ph. D. thesis, ETH, Zurich, 2003.

[38] D.J.E. Ingram, Spectroscopy at Radio and Microwave frequencies, 2nd ed., Butterworth, London, 1967.

[39] T.H. Bennur, D. Srinivas, P. Ratnasamy, Micro. Meso. Mater. 48 (2001) 111.

[40] C. Mantel, C. Baffert, I. Romero, A. Deronzier, J. Pecaut, M. Collomb, C. Duboc, Inorg. Chem. 43 (2004) 6455.

[41] S. Sasi, M. Sithambaresan, M.R.P. Kurup, H.-K. Fun, Polyhedron 29 (2010) 2643.

.....ೞ೦ೞ.....

SYNTHESES AND SPECTRAL CHARACTERIZATION OF ZINC(II) AND CADMIUM(II) CHELATES OF TRIDENTATE AROYLHYDRAZONES

7.1. Introduction

Zinc is a moderately reactive bluish grey metal and is an essential element, necessary for sustaining all life. The dietary necessity of zinc for humans has only become established since the 1980s. Biologically it is the second most important transition metal. Zinc in the form of Zn^{2+} ions is essential for the functioning of several hundred enzymes, including those that catalyze the breaking of P–O–P bonds in ATP. Based on the functions of many of its enzymes, it can be speculated that the popularity of Zn(II) is due to its ability to act as a Lewis acid without engaging in either oxidation or reduction. The most studied of all zinc enzymes are carbonic anhydrase and carboxypeptidases.

Zinc and cadmium complexes are often yellow in color because of metal to ligand charge transfer transitions. Eventhough the coordination

numbers from 2 to 8 are known, Zn(II) and Cd(II) occurs largely in four-coordination as tetrahedral complexes. The octahedral complexes of Zn(II) are not very stable, but Cd(II) forms octahedral complexes more readily and they are more stable than those of zinc. Among the less common five-coordinate complexes, trigonal bipyramidal (tbp) geometry occurs more frequently than square-pyramidal. It is strange that zinc is an essential element for life, but cadmium in the same group is extremely toxic. It causes the malfunctioning of kidneys and also replaces zinc in some enzymes, thus preventing them from working.

Zinc plays an important role in biochemical and nutritional processes. It is estimated that 3,000 of the proteins in the human body contain zinc prosthetic groups. In the field of coordination chemistry also, zinc has its own importance. The zinc metal complexes are reported to have emerging applications in the field of medicines and as active catalysts. The catalytic role of zinc comprises Lewis acid activation of the substrate, generation of a reactive nucleophile (Zn–OH) and stabilization of the leaving group [1]. Zn(II) complexes of ONO donor ligands are reported to possess several biological applications [2-6]. There are several reports in literature based on the Zn(ll) and Cd(II) complexes of aroylhydrazones [7-11].

Zinc complexes are of great interest in organic synthesis and bioinorganic chemistry. In the former, zinc complexes are used in stereospecific organic reactions. In bioinorganic chemistry, it is well known that zinc plays an important role in many biological processes, and Zn(II) coordinated by a strategic ligand can thus lead to a structural and/or

functional model for zinc metalloenzymes [12]. The chemical similarity of zinc(II) and cadmium(II) suggests that the latter may displace the former from the active site in enzymes containing zinc(II). Cadmium is a known carcinogen that inactivates the DNA mismatch repair pathway. Many literature studies reveal that cadmium(II) complexes show antimicrobial activity against pathogenic fungus *Candida albicans* and pathogenic Gram-negative *(Escherichia coli, Pseudomonas aeruginosa)* and Gram-positive (*Staphylococcus aureus, Enterococcus faccalis*) [13-18]. Zn(II) and Cd(II) complexes have also attracted considerable interest due to potential applications of their fluorescence properties [19,20]. Schiff base complexes, especially those of Zn(II), are nowadays used as electroluminescent materials. It has been reported that zinc(II) complexes with Schiff bases type chelating ligands can be used as an effective emitting layer [21,22].

Complexes of group 12 metals mainly zinc and cadmium can provide an interesting range of stoichiometries depending on the preparative salt and in the light of this interest, we here describe the syntheses, characterization and spectroscopic studies of some metal(II) complexes obtained from the reaction of aroylhydrazones with Zn(II) and Cd(II) ions.

7.2. Experimental

7.2.1. Materials

3-Fluoropyridine-2-carbaldehyde, benzhydrazide (Sigma-Aldrich), nicotinic hydrazide (Sigma-Aldrich), zinc(II) chloride (Sigma-Aldrich), zinc(II) sulfate heptahydrate (Sigma-Aldrich), zinc(II) perchlorate hexahydrate (Sigma-Aldrich), cadmium(II) perchlorate hexahydrate (Sigma-Aldrich)

were of Analar grade and were used as received. Solvents used were ethanol, methanol and DMF.

7.2.2. Syntheses of aroylhydrazones

3-Fluoropyridine-2-carbaldehyde benzoylhydrazone monohydrate (HFPB·H_2O) and 3-fluoropyridine-2-carbaldehyde nicotinoylhydrazone dihydrate (HFPN·$2H_2O$) were synthesized as discussed in Chapter 2.

7.2.3. Syntheses of Zn(II) complexes

All the complexes were prepared by refluxing methanolic solutions of the respective metal salts and the corresponding hydrazone in 1:1 or in 1:2 ratio.

7.2.3.1. [Zn(HFPB)$_2$](ClO$_4$)$_2$ (25)

To the hot methanolic solution of HFPB·H_2O (0.5220 g, 2 mmol), methanolic solution of zinc(II) perchlorate hexahydrate (0.3723 g, 1 mmol) was added dropwise. The mixture was refluxed for 4 hours and the yellow colored complex separated out was collected, washed with methanol followed by ether and dried over P_4O_{10} *in vacuo*.

[Zn(HFPB)$_2$](ClO$_4$)$_2$ (**25**): Yield: 60%, λ_m(DMF): 116 ohm^{-1} cm^2 mol^{-1}, Elemental Anal. Found (Calcd.) (%): C: 42.01 (41.59); H: 2.72(2.69); N: 11.10 (11.19).

7.2.3.2. [Zn(HFPB)(SO$_4$)] (26)

A methanolic solution of HFPB·H_2O (0.2612 g, 1 mmol) was treated with methanolic solution of zinc(II) sulfate heptahydrate (0.3830

g, 1 mmol). The resulting solution was refluxed for about 3 hours. The yellow colored product formed was filtered, washed with methanol followed by ether and then dried over P_4O_{10} *in vacuo.*

[Zn(HFPB)(SO$_4$)] (**26**): Yield: 66%, λ_m(DMF): 9 ohm^{-1} cm^2 mol^{-1}, Elemental Anal. Found (Calcd.) (%): C: 39.10 (38.58); H: 2.70 (2.49); N: 10.17 (10.38).

7.2.3.3. [Zn(HFPB)Cl$_2$] (27)

Complex **27** was prepared by refluxing methanolic solutions of HFPB·H$_2$O (0.261 g, 1 mmol) and ZnCl$_2$ (0.1363 g, 1 mmol) for about 3 hours. The resulting yellow colored solution on slow evaporation yielded a yellow crystalline product. It was then was filtered, washed with methanol followed by ether and dried over P_4O_{10} *in vacuo.*

[Zn(HFPB)Cl$_2$] (**27**): Yield: 59%, λ_m(DMF): 8 ohm^{-1} cm^2 mol^{-1}, Elemental Anal. Found (Calcd.) (%): C: 40.82 (41.14); H: 2.88 (2.66); N: 11.31 (11.07).

7.2.3.4. [Zn(HFPN)Cl$_2$] (28)

The complex was prepared by refluxing a methanolic solutions of HFPN·2H$_2$O (0.280 g, 1 mmol) and ZnCl$_2$ (0.136 g, 1 mmol) for 4 hours. The resulting yellow colored solution was kept for evaporation. The yellow colored product obtained on cooling the reaction mixture to room temperature, was filtered, washed with methanol followed by ether and dried over P_4O_{10} *in vacuo.*

[Zn(HFPN)Cl$_2$] (**28**): Yield: 63%, λ_m (DMF): 10 ohm^{-1} cm^2 mol^{-1}, Elemental Anal. Found (Calcd.) (%): C: 37.51 (37.87); H: 2.21 (2.38); N: 14.49 (14.72).

7.2.3.5. [Cd(FPB)(ClO$_4$)]·DMF (29)

The aroylhydrazone, HFPB·H$_2$O (0.2612 g, 1 mmol) and cadmium(II) perchlorate hexahydrate (0.4194 g, 1 mmol) were dissolved in a 1:1 mixture of methanol and DMF and refluxed for about two hours. Light yellow colored product obtained was filtered, washed with methanol followed by ether and dried over P$_4$O$_{10}$ *in vacuo*.

[Cd(FPB)(ClO$_4$)]·DMF (**29**): Yield: 71%, λ_m (DMF): 12 ohm^{-1} cm^2 mol^{-1}, Elemental Anal. Found (Calcd.) (%): C: 36.74 (36.45); H: 2.93 (3.06); N: 10.42 (10.63).

7.3. Results and discussion

Reactions of equimolar ratios of the corresponding aroylhydrazone and the metal salts yielded metal complexes in which ligand to metal ratio is 1:1. However reaction done with perchlorate salt results a metal complex [Zn(HFPB)$_2$](ClO$_4$)$_2$ (**25**) in which ligand to metal ratio is 2:1. All the zinc(II) and cadmium(II) complexes were found to be yellow in color and soluble in solvents like methanol, ethanol and DMF. These were all obtained in 60-70% yields by the procedure described in detail above under section 7.2.3. Based on the elemental analyses, conductivity and spectral investigations, the complexes were formulated. All zinc(II) complexes appear to have preserved the ligands in their neutral form and the hydrazones coordinate to the metal centre *via* azomethine nitrogen, pyridyl nitrogen and amido oxygen. In complex [Cd(FPB)(ClO$_4$)]·DMF (**29**), hydrazone coordinates in the iminolate form and elemental analyses data suggest one molecule of DMF in the lattice. The complexes were characterized by the following physico-chemical methods.

7.3.1. Elemental analyses

The partial elemental analyses data are consistent with the general formulation of the complexes and are given in section 7.2.3.

7.3.2. Molar conductivity measurements

The molar conductances of the complexes in 10^{-3} M DMF solutions were measured at 298 K with a Systronic model 303 direct-reading conductivity bridge. The molar conductivity values of all the complexes except complex $[Zn(HFPB)_2](ClO_4)_2$ (**25**) are found to be in the range 4-12 ohm^{-1} cm^2 mol^{-1} range which is much less than the value of 65-90 ohm^{-1} cm^2 mol^{-1} obtained for uni-univalent electrolytes in the same solvent [23-26] indicating their non-electrolytic nature. The conductance value of complex **25** is found to be 116 ohm^{-1} cm^2 mol^{-1} indicating that it is a 2:1 electrolyte.

7.3.3. Infrared spectral studies

The IR spectra of the aroylhydrazones and their Zn(II) and Cd(II) complexes were recorded in the solid state as KBr discs. The most characteristic IR bands (Table 7.1) have been assigned following the literature [27-30].

Table 7.1. The important IR frequencies (cm^{-1}) of aroylhydrazones and their Zn(II) and Cd(II) complexes

| Compound	v(N–H)	v(C=O)/v(C–O)	v(C=N)	v(C=N)[a]
HFPB·H$_2$O	3059	1683	1597	--
[Zn(HFPB)$_2$](ClO$_4$)$_2$ (**25**)	3061	1663	1583	--
[Zn(HFPB)(SO$_4$)] (**26**)	3045	1672	1574	--
[Zn(HFPB)Cl$_2$] (**27**)	3052	1675	1586	--
HFPN·2H$_2$O	3058	1682	1590	--
[Zn(HFPN)Cl$_2$] (**28**)	--	1670	1560	--
[Cd(FPB)(ClO$_4$)]·DMF (**29**)	--	1324	1557	1594

[a]Newly formed C=N bond

It has been observed that IR spectra of all the complexes show significant differences from free ligand indicating the binding of the ligand to the metal center. In principle, the hydrazones exhibit amido-iminol tautomerism since it contains –NH–C=O functional group. In all the complexes which we have synthesized for our present work except in complex [Cd(FPB)(ClO$_4$)]·DMF (**29**), hydrazone coordinates to the metal centre in the amido form whereas in complex **29** it is in the deprotonated iminolate form. The ν(C=O) stretching vibrations observed in 1660-1684 cm^{-1} region in the spectra of the free hydrazones are retained but are shifted to lower frequencies in complexes **25-28**. This fact along with the observation that the band due to formation of new –C=N– bond is absent in the spectra of all the complexes except [Cd(FPB)(ClO$_4$)]·DMF (**29**) confirm the binding of the aroylhydrazone in the neutral amido form rather than the iminolate form to the central metal ion. On the other hand the stretching frequencies of azomethine –C=N– group found near 1590 cm^{-1} in free ligands are shifted to lower wave numbers upon complexation by 20-40 cm^{-1} suggesting the coordination *via* azomethine nitrogen in all the complexes [31]. Upon complexation, the stretching vibrations of azomethine bond are found to be weakened and this results a negative shift in the azomethine stretching frequencies in comparison with the free hydrazones. The low energy pyridine ring-in-plane and out-of-plane vibrations are shifted to higher frequencies when compared with the corresponding bands in free ligands indicating the involvement of pyridyl nitrogen in the complex formation [32,33].
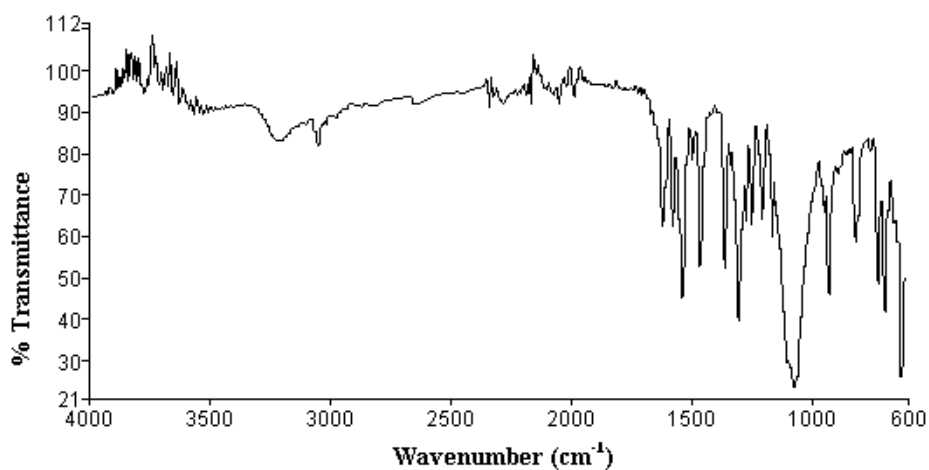
Fig. 7.1. FT-IR spectrum of [Zn(HFPB)₂](ClO₄)₂ (25).

The strong bands at 1089 and 639 cm^{-1} found in the spectrum of complex **25** (Fig. 7.1), assignable to $\nu_3(ClO_4)$ and $\nu_4(ClO_4)$ respectively indicates the presence of ionic perchlorate [34].
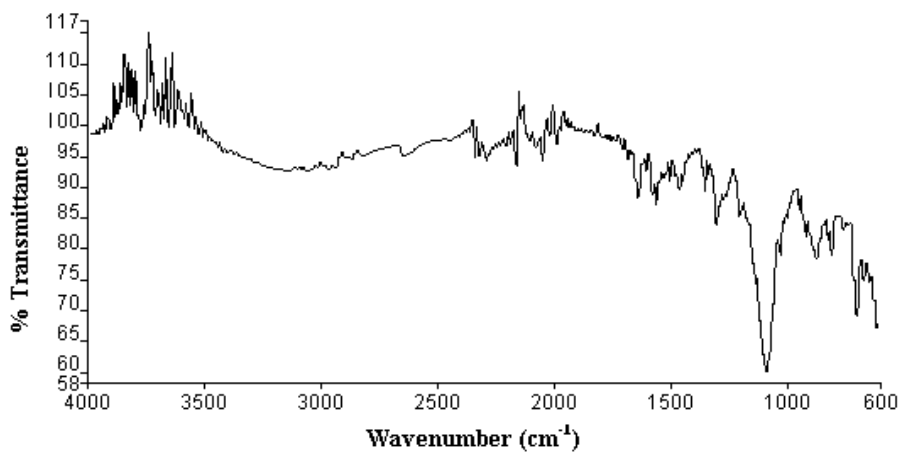
Fig. 7.2. FT-IR spectrum of [Zn(HFPB)(SO₄)] (26).

The infrared spectrum of [Zn(HFPB)(SO$_4$)] (**26**) (Fig. 7.2) displayed a band at 1574 cm^{-1} which can be assigned to –C=N– stretching frequency of the coordinated hydrazone [35] whereas for the free ligand same band is observed at 1597 cm^{-1}. The shift of this band on complexation towards lower wave number indicates the coordination of azomethine to the central metal ion [33]. In the case of complex **26** aroylhydrazone is coordinated in the neutral form as the decrease in the –C=O– stretching is less (1672 cm^{-1}) when compared to the free ligand (1683 cm^{-1}). The presence of SO$_4$$^{2-}$ anion in the coordination sphere of the complex **26** is supported by the appearance of three bands in the range of 969-983, 1042-1065 and 1209-1215 cm^{-1} respectively, which can be assigned to the bidentately coordinated sulfato group [36].

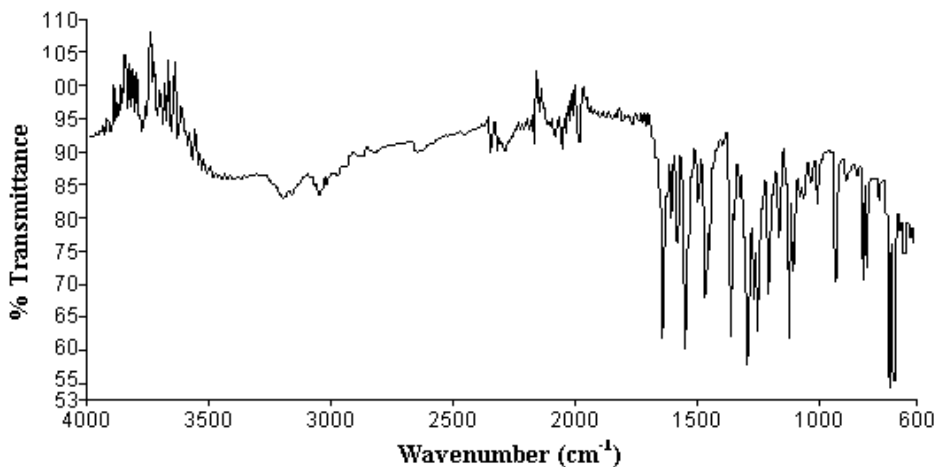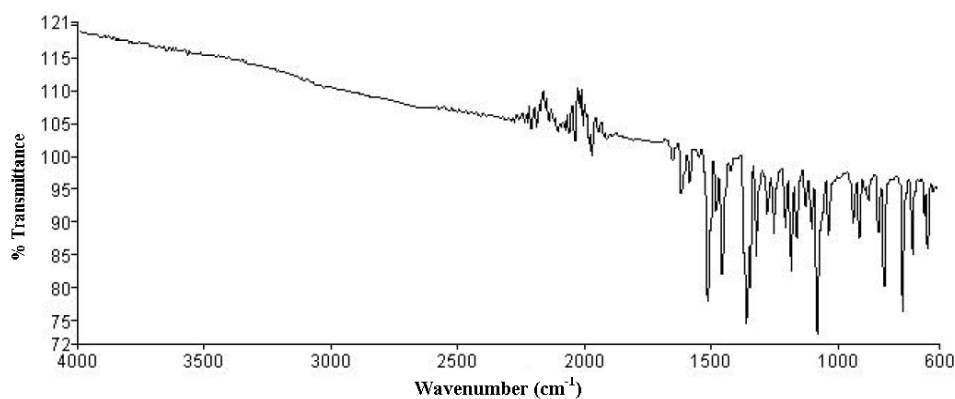**Fig. 7.3. FT-IR spectrum of [Zn(HFPB)Cl$_2$] (27).**

The IR spectrum of compound **27** (Fig. 7.3) show a medium band at 3052 cm^{-1} corresponding to N–H vibration indicating that ligand is not

deprotonated during coordination and Zn(II) valency is satisfied by the two coordinated chloride ions. This is further supported by a negative shift of the carbonyl moiety by only 5 cm^{-1}. The azomethine band is showing a negative shift and is observed at 1586 cm^{-1}. The shifting of azomethine band to a lower frequency can be attributed to the conjugation of p-orbital on the double bond with the *d*-orbital on the metal ion with a reduction in force constant [37]. The low energy pyridine ring in-plane and out-of-plane vibrations are shifted to higher energies in the case of complex which is a clear indication of coordination *via* pyridine nitrogen.

Fig. 7.4. FT-IR spectrum of [Zn(HFPN)Cl$_2$] (28).

In the case of complex **28** (Fig. 7.4), like other complexes aroylhydrazone coordinates to the metal center in the neutral amido form as the decrease in v(C=O) stretching is less (1670 cm^{-1}) when compared to the corresponding band in the free ligand (1682 cm^{-1}). Coordination of carbonyl oxygen reduces the electron density in the (C=O) bond resulting a shift in the (C=O) band. The azomethine band is observed at 1560 cm^{-1}.
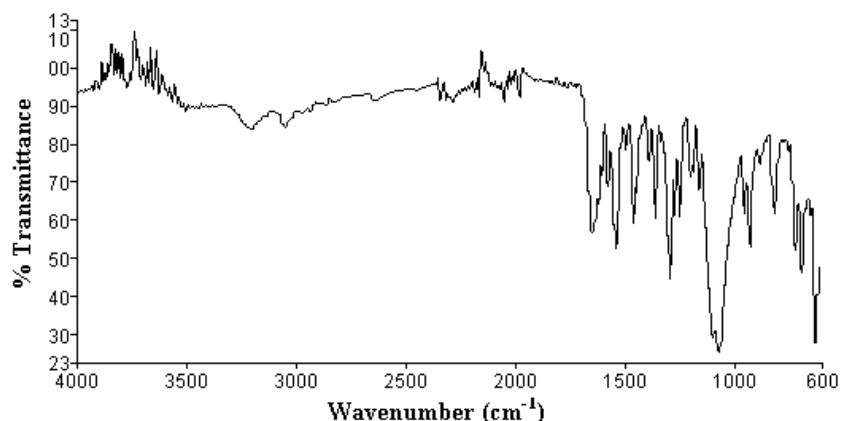
Fig. 7.5. FT-IR spectrum of [Cd(FPB)(ClO₄)]·DMF (29).

Unlike in other complexes, the bands due to v(C=O) and v(NH) stretching vibrations are absent in the IR spectrum of complex **29** (Fig. 7.5), but two new bands appeared at 1594 and 1324 cm^{-1} respectively probably due to –C=N–N=C– and C–O stretching respectively, suggesting that the NH proton is likely lost *via* deprotonation induced by the metal and the resulting iminolic oxygen coordinates with the metal ion [38-40] during the complex formation. The band due to the azomethine group of the ligand underwent a shift to lower frequency (by 1597-1557 cm^{-1}) after complexation, indicating the coordination of azomethine nitrogen to metal ion. The complex **29** shows a characteristic band at 1081 cm^{-1} for the perchlorate bonded to the zinc(II) atom [41]. The coordination through pyridyl nitrogen was evident from the shifting of out-of-plane bending modes of vibrations of the free ligand to higher frequency.

7.3.3. Electronic spectral studies

Because of the d^{10} electronic configuration of the Zn(II) and Cd(II) ions, the diffuse electronic spectra of the complexes have a very small

relevance. But, the weak modification of the bands frequencies of the ligand in the UV-Vis spectra of the complexes indicates the coordination of the ligand and the formation of the complexes. The electronic spectra of the ligands and complexes were recorded in DMF solutions. The significant electronic absorption spectral data of the complexes in DMF solution with their possible assignments are summarized in Table 7.2 and the spectra are shown in Figs. 7.6-7.8.

Table 7.2. Electronic spectral assignments (cm^{-1}) of Zn(II) and Cd(II) complexes

Compound	n→π*/π→π*	MLCT
[Zn(HFPB)$_2$](ClO$_4$)$_2$ (**25**)	33450	25550
[Zn(HFPB)(SO$_4$)] (**26**)	33350	25500
[Zn(HFPB)Cl$_2$] (**27**)	33150	25400
[Zn(HFPN)Cl$_2$] (**28**)	37560, 33240	25780
[Cd(FPB)(ClO$_4$)]·DMF (**29**)	33420	25330
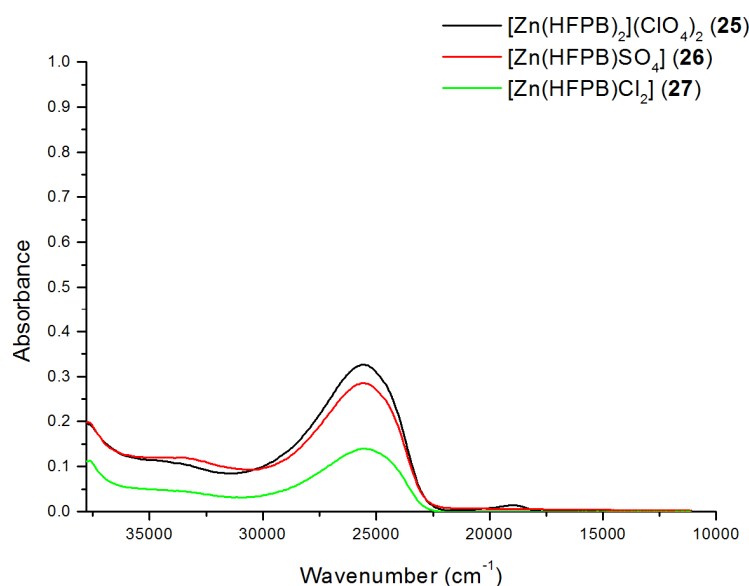
Fig. 7.6. Electronic spectra of zinc(II) complexes 25-27.
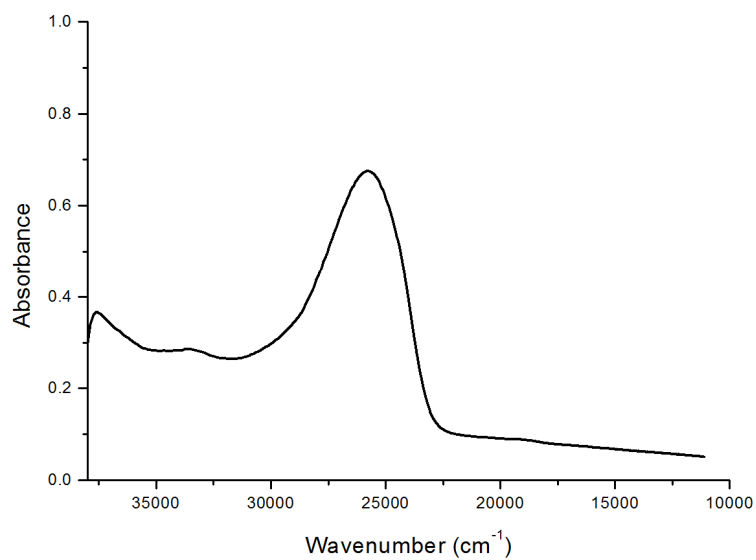
Fig. 7.7. Electronic spectrum of [Zn(HFPN)Cl$_2$] (28).
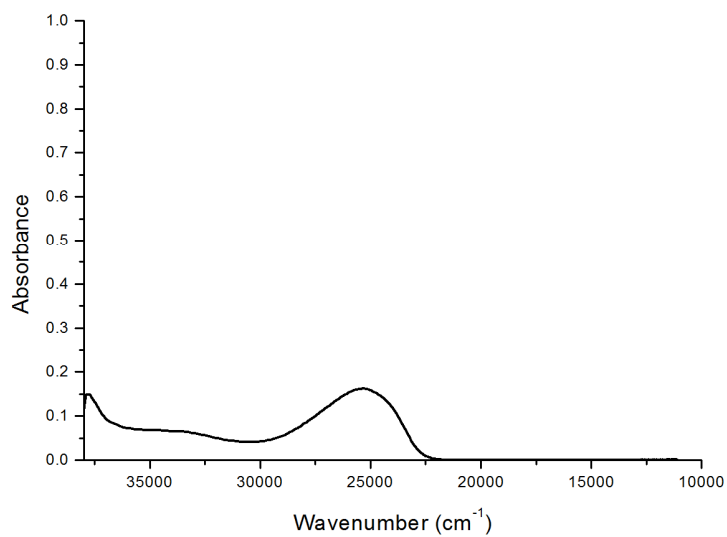
Fig. 7.8. Electronic spectrum of [Cd(FPB)ClO$_4$]·DMF (29).

The electronic absorption spectra are often very helpful in the evaluation of results furnished by other methods of structural investigation. The electronic spectral measurements are used for assigning the stereochemistries of metal ions in the complexes based on the positions and number of *d-d* transition peaks. But in the case of Zn(II) and Cd(II) complexes, no *d-d* transitions are expected since it is a d^{10} system and is completely filled. The intraligand transitions are slightly shifted in all the complexes as a result of extensive conjugation in the ligand part of the molecule on complexation. All the presently studied Zn(II) and Cd(II) complexes were bright yellow in color even though there were no *d-d* transitions in the molecule. This may be due to the new bands observed for complexes in the 22060-24820 cm^{-1} region and can be assigned to the metal to ligand charge transfer transitions. The bands observed in the UV-Vis spectra of Zn(lI) and Cd(II) complexes are due to the intraligand n→π* and π→π* transitions (weak bands) and also due to the charge transfer transitions (strong broad band) from the filled metal orbital to the ligand orbital. No appreciable absorptions occurred below 20000 cm^{-1} indicating the absence of *d-d* bands which is in accordance with d^{10} configuration of Zn(II) and Cd(II) ions [42].

Based on the elemental analyses and spectral studies, following tentative structures were assigned to the complexes.

[Zn(HFPB)₂](ClO₄)₂ (25)

(ClO₄)₂

[Zn(HFPB)(SO₄)] (26)

[Zn(HFPB)Cl₂] (27)

[Zn(HFPN)Cl₂] (28)

[Cd(FPB)(ClO₄)]·DMF (29)
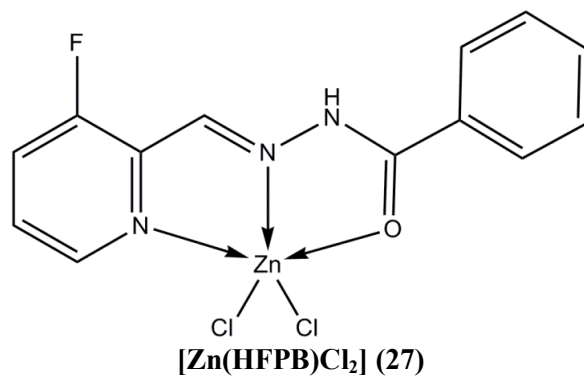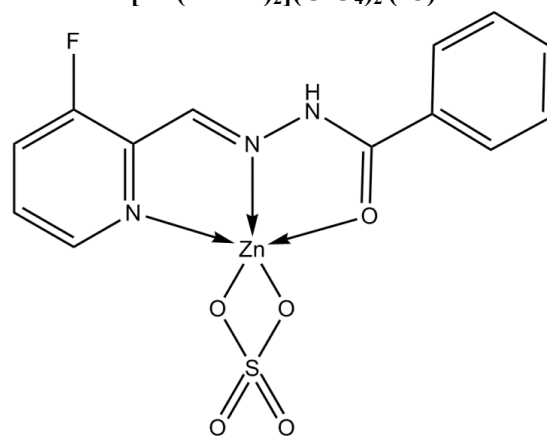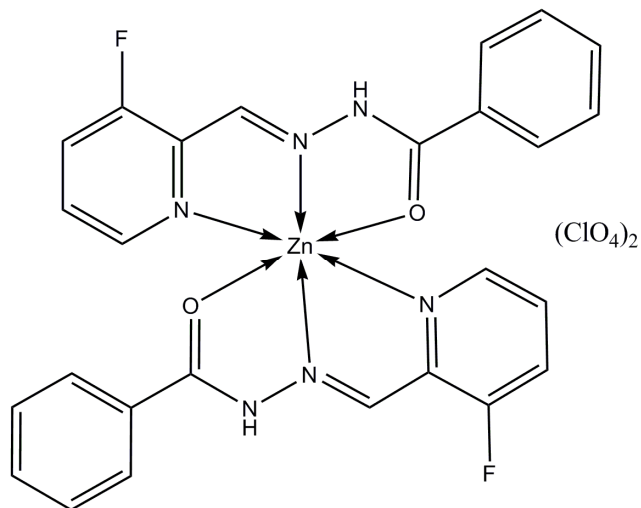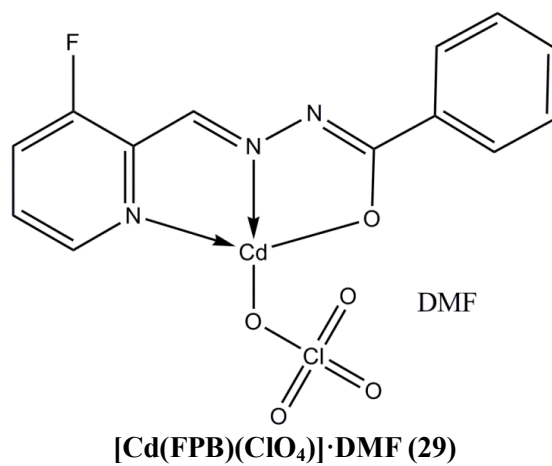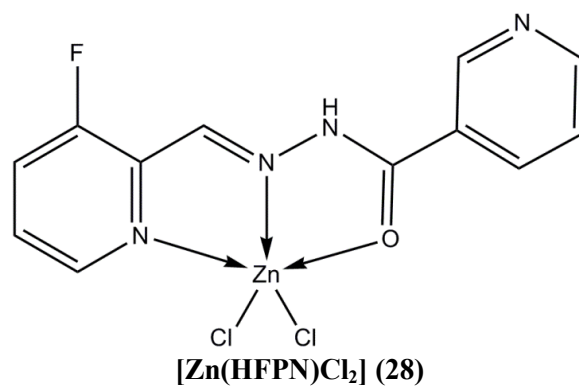
References

[1]   A. Erxleben, J. Hermann, J. Chem. Soc. Dalton Trans. (2000) 569.

[2]   H.-Q. Chang, L. Jia, J. Xu, Z.-Q. Xu, R.-H. Chen, W.-N. Wu, H.-Y. Bie, T.-F. Zhu, T.-L. Ma, Y. Wang, Inorg. Chem. Commun. 57 (2015) 8.

[3]   O.A. El-Gammal, T.H. Rakha, H.M. Metwally, G.M. Abu El-Reash, Spectrochim. Acta 127A (2014) 144.

[4]   R. Bhaskar, N. Salunkhe, A. Yaul, A. Aswar, Spectrochim. Acta 151A (2015) 621.

[5]   B.K. Singh, A. Prakash, H.K. Rajour, N. Bhojak, D. Adhikari, Spectrochim. Acta 76A (2010) 376.

[6]   J.R. Anacona, V. Rangel, M. Loroño, J. Camus, Spectrochim. Acta 149A (2015) 23.

[7]   A.-M. Stadler, J. Harrowfield, Inorg. Chim. Acta 362 (2009) 4298.

[8]   S. Konar, A. Jana, K. Das, S. Ray, S. Chatterjee, J.A. Golen, A.L. Rheingold, S.K. Kar, Polyhedron 30 (2011) 2801.

[9]   P. Singh, A.K. Singh, V.P. Singh, Polyhedron 65 (2013) 73.

[10]   M.N. Abd El-Hady, R.R. Zaky, K.M. Ibrahim, E.A. Gomaa, J. Mol. Struct. 1016 (2012) 169.

[11]   M. Mohan, A. Kumar, M. Kumar, N.K. Jha, Inorg. Chim. Acta 136 (1987) 65.

[12]   N. Mitić, S.J. Smith, A. Neves, L.W. Guddat, L.R. Gahan, G. Schenk, Chem. Rev. 106 (2006) 3338.

[13]   R. Sanyal, P. Chakraborty, E. Zangrando, D. Das, Polyhedron 97 (2015) 55.

[14]   M.-F. Zaltariov, M. Cazacu, M. Avadanei, S. Shova, M. Balan, N. Vornicu, A. Vlad, A. Dobrov, C.-D. Varganici, Polyhedron 100 (2015) 121.

[15]   V.P. Singh, S. Singh, D.P. Singh, K. Tiwari, M. Mishra, J. Mol. Struct. 1058 (2014) 71.

[16] C.W. Tang, S.A. VanSlyke, Appl. Phys. Lett. 51 (1987) 913.

[17] T. Yu, W. Su, W. Li, Z. Hong, R. Hua, B. Li, Thin Solid Films 515 (2007) 4080.

[18] J. Devi, N. Batra, R. Malhotra, Spectrochim. Acta 97A (2012) 397.

[19] A. Ray, S. Banerjee, S. Sen, R.J. Butcher, G.M. Rosair, M.T. Garland, S. Mitra, Struct. Chem. 19 (2008) 209.

[20] F. Liu, W.P. Zhang, S.Y. He, Russ. J. Coord. Chem. 36 (2010) 105.

[21] Y. Hamada, T. Sano, M. Fujita, T. Fujii, Y. Nishio, K. Shibata, Jpn. J. Appl. Phys. 32 (1993) L511.

[22] T. Kawamoto, M. Nishiwaki, Y. Tsunekawa, K. Nozaki, T. Konno, Inorg. Chem. 47 (2008) 3095.

[23] W.J. Geary, Coord. Chem. Rev. 7 (1971) 81.

[24] Z.H. Chohan, K.M. Khan, C.T. Supuran, Appl. Organometal. Chem. 18 (2004) 305.

[25] N.A. Mangalam, M.R.P. Kurup, Spectrochim. Acta 71A (2009) 2040.

[26] J. Chakraborty, S. Thakurta, G. Pilet, D. Luneau, S. Mitra, Polyhedron 28 (2009) 819.

[27] S. Naskar, D. Mishra, R.J. Butcher, S.K. Chattopadhyay, Polyhedron 26 (2007) 3703.

[28] M.K. Prasanna, K. Pradeepkumar, Int. J. Pharm. Biomed. Sci. 4 (2013) 24.

[29] V.K. Sharma, S. Srivastava, Synth. React. Inorg. Met.-Org. Nano-Met. Chem. 35 (2005) 311.

[30] P.F. Rapheal, E. Manoj, M.R.P. Kurup, Polyhedron 26 (2007) 607.

[31] M. Joseph, A. Sreekanth, V. Suni, M.R.P. Kurup, Spectrochim. Acta 64A (2006) 637.

[32] F. Hueso-Ureña, A.L. Peñas-Chamorro, M.N. Moreno-Carretero, J.M. Amigó, V. Esteve, T. Debaerdemaeker, Polyhedron 18 (1999) 2205.

[33] K. Nakamoto, Infrared and Raman spectra of Inorganic and Coordination compounds, 5th Edn., Wiley, New York, 1997.

[34] B.S. Garg, M.R.P. Kurup, S.K. Jain, Y.K. Bhoon, Transit. Met. Chem. 13 (1988) 247.

[35] B. Singh, K.K. Narang, R. Srivastava, Synth. React. Inorg. Met.-Org. Chem. 32 (2002) 1577.

[36] V. Philip, V. Suni, M.R.P. Kurup, M. Nethaji, Polyhedron 25 (2006) 1931.

[37] R. Dinda, P. Sengupta, S. Ghosh, T.C.W. Mak, Inorg. Chem. 41 (2002) 1684.

[38] R. Gup, B. Kirkan, Spectrochim. Acta 62A (2005) 1188.

[39] K.Z. Ismail, Transit. Metal Chem. 25 (2000) 522.

[40] A.B.P. Lever, Inorganic Electronic Spectroscopy, Elsevier, Amsterdam (1968).

[41] J.R. Anacona, V.E. Marquez, Transit. Met. Chem. 33 (2008) 579.

[42] M.M. Al-Ne'aimi, M.M. Al- Khuder, Spectrochim. Acta 105A (2013) 365.

..... හα.....

SUMMARY AND CONCLUSIONS

The coordination chemistry and biochemistry of aroylhydrazones, R–CO–NH–N=CH–R′, have attracted increasing interest due to their chelating ability and their pharmacological applications. Hydrazone ligands create environment similar to biological systems coordinating through oxygen and nitrogen atoms. Hydrazone nucleus is found in natural and synthetic products of biological interest. Furthermore, hydrazones have wide spread applications in fields such as coordination chemistry, analytical chemistry and bioinorganic chemistry. Literature studies revealed that hydrazones and various substituted hydrazones are associated with a broad spectrum of biological activities such as antioxidant, antibacterial, antiviral, analgesic, antiplatelet, antimicrobial, and anticancer activities etc. The ease of preparation, increased hydrolytic stability and tendency toward crystallinity are all desirable characteristics of hydrazones. Compared to the simple hydrazone, aroyl or heteroaroyl schiff bases have additional donor sites. This introduces a wider range of properties for these substances.

Hydrazones are formed by the condenzation between a carbonyl compound and a hydrazide which is a derivative of hydrazine. The expected donor atoms in a hydrazone are azomethine nitrogen and

amide/iminolate oxygen atoms. The number of donor atoms can be increased by substitution on carbonyl part or on hydrazide part leading to a tridentate ligand system with NNO or ONO activity. In hydrazones, a proton transfer can occur between the nitrogen atom and amido group of the hydrazide part. Due to this intramolecular proton transfer, they exhibit amido-iminol tautomerism and are found in two different forms i.e., amido and iminol forms. In solid state, hydrazones predominantly exist in the amido form and in the solution, iminol form predominates.

Interest in coordination chemistry of benzohydrazide has been a subject of enthusiastic research since their complexes show a wide range of applications in different areas such as catalysis, bioinorganic, biomimetic and medicinal chemistry. Benzohydrazone derivatives are also important due to their wide spectrum of biological activities. The above mentioned facts guided us for the development of some transition metal complexes using aroylhydrazones as the ligand system. As a part of our research in the study of coordinating capabilities of aroylhydrazones and their coordination compounds, we have selected 3-fluoropyridine-2-carbaldehyde benzoylhydrazone and 3-fluoropyridine-2-carbaldehyde nicotinoylhydrazone as ligands to synthesize and characterize some transition metal complexes. The choice of nicotinoyl hydrazide in one of the ligand systems is mainly due to the fact that this heteroatomic moiety can provide a further binding site for metal cations. These aroylhydrazones of HL type (H represents dissociable amide proton) can coordinate a given metal ion *via* pyridine nitrogen, azomethine nitrogen and amido/iminolate oxygen atoms.

The synthesized ligand systems consisting of NNO donor aroylhydrazones are given below.

- 3-Fluoropyridine-2-carbaldehyde benzoylhydrazone monohydrate (HFPB·H_2O)

- 3-Fluoropyridine-2-carbaldehyde nicotinoylhydrazone dihydrate (HFPN·$2H_2O$)

Summary of the thesis:

The thesis is divided into seven chapters.

Chapter 1

Chapter 1 involves a brief prologue to aroylhydrazones and their metal complexes, bonding and coordination strategy of aroylhydrazones and their various applications. The objectives of the present work and the various physicochemical methods adopted for the characterization of the aroylhydrazones and their complexes are also discussed in this chapter.

Chapter 2

Chapter 2 describes the syntheses of two new aldehyde based NNO donor aroylhydrazones and their characterization by elemental analyses, FT-IR, UV-Vis and ^{1}H-NMR spectral studies. X-ray quality single crystals of these two ligands were grown and their molecular structures were established by single crystal X-ray diffraction studies.

Chapter 3

This chapter discusses the syntheses and characterization of eight copper(II) complexes with the synthesized aroylhydrazones. All the

complexes are characterized by various techniques such as elemental analyses, molar conductivity studies, magnetic susceptibility measurements, FT-IR, UV-Vis, EPR spectral studies and single crystal X-ray diffraction studies. Molar conductances of the complexes in DMF/DMSO solution were measured at 298 K and found to be in the 1-9 ohm^{-1} cm^2 mol^{-1} range. These low values indicate their non-electrolytic nature. Magnetic moment values of mononuclear Cu(II) complexes were found to be very close to their spin only value corresponding to a single unpaired electron. The low magnetic moment for dinuclear complexes can be assigned to the coupling of two magnetic centers. In all the complexes except one, hydrazones are coordinated to the metal centre in the deprotonated iminolate form and act as a monoanionic tridentate ligand as evidenced from the infrared spectra. EPR spectra in polycrystalline state at 298 K show that some of the compounds are isotropic and some are axial and others are rhombic in nature. In DMF at 77 K, some complexes are found to be axial with hyperfine lines in the parallel region. We could isolate X-ray quality single crystals of one of the complexes by the slow evaporation from the mother liquor. Molecule crystallizes in the trigonal space group $R\bar{3}$. In this complex Cu(II) ion is in a pentacoordinated environment and the coordination sites are occupied by azomethine nitrogen, pyridyl nitrogen and iminolate oxygen from a monodeprotonated hydrazone moiety and the remaining positions are occupied by two oxygen atoms, one each from acetate ion and water molecule.

Chapter 4

Chapter 4 deals with the syntheses and characterization of six nickel(II) complexes of the aroylhydrazones by CHN analyses, molar conductivity and magnetic susceptibility measurements, infrared and electronic spectral studies and single crystal X-ray diffraction studies. All the complexes, except one are found to be non-electrolytic in nature. Effective magnetic moments of the complexes were calculated from magnetic susceptibility measurements at room temperature. All nickel(II) complexes were found to be paramagnetic excluding the possibility of a square planar configuration. IR spectral data support the binding of the ligand to the metal center in the deprotonated iminolate form through azomethine and pyridyl nitrogens and iminolate oxygen atom. The structure of one of the complexes has been resolved using single crystal X-ray diffraction studies. The complex crystallizes in monoclinic space group $P2_1/c$. In this complex, metal center is hexacoordinated and the coordination around Ni(II) ion can be described as distorted octahedron. Each nickel(II) is coordinated by azomethine N, iminolate O and pyridyl N from the two monodeprotonated hydrazone ligands.

Chapter 5

This chapter describes the syntheses and characterization of six cobalt(II) complexes. The characterization techniques include elemental analyses, molar conductivity and magnetic susceptibility measurements, FT-IR, UV-Vis and single crystal X-ray diffraction studies. The molar conductivity values obtained for all the complexes except two confirmed their non-electrolytic nature. Out of six complexes prepared, in two

complexes IR data support the coordination of the hydrazone to the metal center through azomethine and pyridyl nitrogens and iminolate oxygen. In the remaining complexes ν(C=O) stretching mode is retained but is shifted to a lower wave number indicating that ligand is not deprotonated and binding with the metal center in the neutral amido form. The effective magnetic moments for octahedral complexes are found to be in the range 5.7-6.1 B.M. which is slightly higher than their spin only value, this suggests that there is an orbital contribution. For all other complexes, magnetic moments are found to be in the range 4.3-5.2 B.M. We could isolate X-ray quality single crystals of one of the complexes by recrystallization of DMF solution. The complex crystallizes in monoclinic space group $P2_1$/c. In this complex, metal center is hexacordinated and the coordination around Co(II) ion can be described as a distorted octahedron. Each Co atom is coordinated by azomethine N, pyridyl N and amido O from two hydrazone moieties.

Chapter 6

Chapter 6 explains the syntheses of two Mn(II) and two Fe(III) complexes of the hydrazones and characterization by CHN analyses, molar conductivity and magnetic susceptibility measurements, infrared, electronic and EPR spectral studies. Molar conductivity measurements in DMF solutions indicated that all Mn(II) complexes are non-electrolytic in nature which is in accordance with their proposed formulations. Magnetic moment values of Mn(II) complexes are found to be in the range 5.6-6.6 B.M. which are consistent with high spin d^5 system. Magnetic moment values of iron(III) complexes are found to be in the range 5.5-5.7 B.M. which are very close to their spin only value. The

tridentate character of the hydrazones is inferred from IR spectra. EPR spectra of all Mn(II) complexes in polycrystalline state at 298 K exhibited an isotropic spectra, while solution spectra in DMF at 77 K displayed a central hyperfine sextet with definite g value.

Chapter 7

Four zinc(II) and one cadmium(II) complexes have been synthesized and physico-chemically characterized by CHN analyses, conductivity measurements, infrared and electronic spectral studies. The molar conductivity measurements in DMF (10^{-3} M) indicates that all complexes except one are non-electrolytic in nature. In two complexes, IR spectral data support the binding of the ligand to the metal center in the deprotonated iminolate form and in all other complexes $\nu(C=O)$ stretching mode is retained but shifted to a lower wave number indicating that ligand is coordinating to the metal center in the neutral amido form.

.....ജ്യാ.....

<div align="center">

▕▏▏▏ Curriculum Vitae ▕▏▏▏

</div>

Yamuna S. Nair
Dwaraka
Amalagiri P.O.
Kottayam-686061
Kerala, India
Email: yamunanair@christuniversity.in

Areas of Interest: Teaching and Research

Academic Profile

Pursuing Ph.D. (Inorganic Chemistry)
(2010 December - present)
Area of research - Coordination Chemistry

Supervising guide - Prof. M.R. Prathapachandra Kurup
Department of Applied Chemistry
Cochin University of Science & Technology, Kochi-22

Co-guide - Prof. S. Muraleedharan Nair
Department of Chemical Oceanography, School of Marine Sciences
Cochin University of Science & Technology, Kochi-16

Educational Qualifications

M.Phil. Chemistry
Percentage of marks - 63 %
Year: 2010
Vinayaka Mission University, Tamil Nadu

B.Ed. Physical Science
Percentage of marks – 55 %
Year: 1999
St. Joseph Training College, Mannanam
MG University

Post Graduate Diploma in Computer Application
Percentage of marks – 71%
Year: 1998
IHRD, Kerala

M.Sc. Pure Chemistry
Year: 1994-96
Baselious College, Kottayam
University - Mahatma Gandhi University, Kerala
Percentage of marks - 57 %

B.Sc. Pure Chemistry
Year: 1991-94
KE College, Kottayam
University - Mahatma Gandhi University, Kerala
Percentage of marks - 81.5 %

Pre-Degree
Year: 1989-91
KE College, Kottayam
University - Mahatma Gandhi University, Kerala
Percentage of marks - 74 %

S.S.L.C
St. Mary's High School, Athirampuzha, Kottayam
Percentage of marks - 81%

Research Experience

- Nearly four years of research experience in the field of coordination chemistry

1. Professional Skills

- Familiar with MS Office
- Familiar with chemistry software packages like ChemSketch, Origin, EPR simulation packages
- Familiar with crystallographic softwares

Personal Profile

Father's name	:	K.N. Sudhakaran Nair
Date of Birth	:	08th April 1974
Nationality	:	Indian
Gender	:	Female
Marital Status	:	Married
Husband's Name	:	Gopakumar K.

Papers published

[1]. N'-[(E)-(3-Fluoropyridin-2-yl)methylidene]pyridine-3-carbohydrazide dihydrate, Yamuna Nair, M. Sithambaresan, S. Muraleedharan Nair and M. R. Prathapachandra Kurup, Acta Cryst. E70 (2014) o483–o484.

[2]. N'-[(E)-(3-Fluoropyridin-2-yl)methylidene]benzohydrazide monohydrate, Yamuna Nair, M. Sithambaresan and M.R. Prathapachandra Kurup, Acta Cryst. E68 (2012) o2709.

Papers presented in symposia

[1]. Participated in the National Conference on 'Advances in nano science and technology" held at Department of Basic Sciences, Amal Jyothi College of Engineering, Kanjirappally, Kerala during 22 and 23rd April 2010.

[2]. Participated in a workshop on "Recent Advances in Organic Synthesis and Biosciences" held at Department of Chemistry, Christ University, Bangalore, on 18th February 2010.

[3]. Participated in the National Seminar on "Modern methods in Organic chemistry" held at the Department of Chemistry, Christ University, Bangalore, during 18 and 19th February 2011.

[4]. Participated in a workshop on "Advances in Chemical Science" organized by Christ University in association with KSTA during 12 and 13th September 2013.

[5]. Participated and presented a paper in the National Seminar "Science and Technology Challenges for promoting Innovative Research and Development" (KSTA) held at the Department of Chemistry, Christ University, Bangalore, during 20 and 21st December 2013.

[6]. Participated and presented a poster in the National Conference "Current Trends in Chemistry" (CTriC-2014) held at the Department of Applied Chemistry, Cochin University of Science and Technology, Kochi during 17 and 18th January 2014.

[7]. Participated in Science Academies' Lecture Workshop on Spectroscopy held at the Department of Chemistry, Christ University, Bangalore, during 28th February-1st March, 2014.

[8]. Participated in a workshop on "Advances in Material Science" organized by JNCASR held at the Department of Chemistry, Christ University, Bangalore, during 27 and 28th August 2014.

[9]. Participated in a workshop on "Modern Trends in Chemistry" organized by Indian Academy of Science, Bangalore held at the Department of Chemistry, Christ University, Bangalore, during 13 and 14th February 2015.

[10]. Participated and presented a poster in the International Conference on Materials for the Millennium (MatCon 2016) held at the Department of Applied Chemistry, Cochin University of Science and Technology, Kochi during 14-16th January, 2016.

.....ജയ.....